ADVANCED SPREADSHEET BASED METHODOLOGY FOR THE DYNAMIC THERMAL MODELLING OF BUILDINGS

A thesis submitted for the degree of Doctor of Philosophy

by

Louis Demetriou

School of Engineering and Design

March 2006

ABSTRACT

Thermal analysis of buildings was carried out using simplified design tools, prior to the widespread use of computers. Since the early 1980's, the rapid growth of computational power has lead to the introduction of many building dynamic thermal simulation software programs. The accurate performance of many of these programs has lead to the view that manual calculation methods should only be used as indicative design tools. The CIBSE admittance method is based on the fundamentals of building heat transfer, its calculations procedures being simplified for use on hand held calculators. Manual calculation methods must be developed for use on more powerful calculators, if greater accuracy is required. Such calculators are available in the form of computer spreadsheet programs. The computational power of the computer spreadsheet program, combined with suitable mathematical thermal modelling techniques, has thus far, remained unexploited.

This thesis describes the development of a powerful manual thermal design method, for application on a computer spreadsheet program. All the modes of building heat transfer are accurately modelled. Free-running or plant-controlled spaces can be simulated. In the case of a single zone, the accuracy of the new manual dynamic thermal model is comparable with commercially available software programs. The level of mathematical modelling complexity is limited only by computer power and user ability.

The Iterative Frequency Domain Method (IFDM) and the Adiabatic Iterative Frequency Domain Method (AIFDM) are alternative mathematical simulation techniques developed to form the core of the Thermal Analysis Design Method. In the IFDM and AIFDM, the frequency domain and numerical iteration techniques have been integrated to produce a thermal simulation method that can model all non-linear heat transfer processes. A more accurate formulation of sol-air temperature, a window sol-air temperature and an accurate reduced internal long-wave radiant exchange model is a sample of further innovations in the thesis.

Many of the developments described in the thesis, although designed for the computer spreadsheet environment, may also be employed to enhance the performance of some of the current dynamic thermal models of buildings.

ACKNOWLEDGEMENTS

I would like to express my gratitude to my supervisor Professor Savvas A. Tassou for his expert guidance, encouragement and support during the period of this research thesis.

I wish to express my deep appreciation to my wife Ellen, for understanding, encouragement and patience.

I would like to thank my children, Lara, Michael, Matthew and Anna for their support and for the sacrifices they had to make in keeping the number of house parties to a minimum.

I acknowledge and appreciate the financial support afforded me, during this thesis, by the Dublin Institute of Technology.

Finally I wish to acknowledge the many useful discussions I had with colleagues, Michael Crowley and Ben Costelloe, in particular.

NOMENCLATURE

General symbols

A	Surface area (m^2)
a	Solar altitude angle (°)
c	Constant
C	Air flow or pressure coefficient or fractional cloud cover
d	Declination angle (°)
D	Diurnal range
E	Illuminance (Lux)
F	View factor between surfaces
H, z *or* Z	Height (m)
I	Solar radiation (W m^{-2})
$I_G(\delta\gamma)$	Global solar irradiance (W m^{-2}) for a plane of slope δ (°) and orientation γ (°)
k	Air flow coefficient (L s^{-1} m^{-1} Pa^{-n})
h	Surface heat transfer coefficient (W m^{-2} K^{-1}) or hour angle (Degrees)
L	Latitude (°)
LF	Lamp luminous flux (Lumens)
l	Perimeter length or element thickness (m)
MF	Maintenance factor of lighting system
N	Number of lamps
m	Coefficient
n	Wall-solar azimuth angle (°)
p	Pressure (Pa)
q	Surface heat flow (W m^{-2})
Q	Total surface heat flow (W)
R	Long-wave radiation (W)
T	Temperature (K)
t	Time (s) or temperature in Celsius (°C)
$\tilde{t}$ or $\tilde{q}$ etc.	Fluctuating thermal component or thermal complex quantity
$\bar{t}$ or $\bar{q}$ etc.	Mean thermal component

ΔT *or* Δt	Temperature difference (K)
UF	Utilisation factor of luminaire
v	Velocity (m s^{-1})

Subscripts

ai	Inside air
ao	Outside air
bld	Building
eo	Sol-air
c	Convective
ci	Internal convection
co	External convection
d	Direct
g or grd	Ground
G	Global
h	Horizontal
i	Identification number of surface being evaluated
j	Designating room surfaces 1 to *N*
m	Mean value
pf	Parallel flow
r	Reflected
s or sur	Surface
v	Vertical surface

Superscripts

n	Air flow exponent

Greek letters

α	Thermal diffusivity (m^2/s)
ε	Surface emissivity
σ	Stepfan-Boltzmann constant = 5.67×10^{-8} W m^{-2} K^{-4}
δ	Tilt angle of surface (°)
ρ	Ground reflectance
ρ	Density (kg m^{-2})
θ	Temperature amplitude or time
η	Solar azimuth angle (°)
μ	Dynamic viscosity (N s m^{-2})
λ	Thermal conductivity (W m^{-1} K^{-1})

TABLE OF CONTENTS

Chapter IV

Chapter V

Chapter VI

Chapter VII

Chapter VIII

LIST OF TABLES

LIST OF FIGURES

Chapter I

1.0 INTRODUCTION

1.1 An alternative approach to dynamic thermal modelling of buildings

The integrated thermal design of a building and its mechanical thermal systems is a complex subject involving the interaction of many physical variables and probabilistic influences. Minimising energy consumption in buildings and maintaining the health and safety of its occupants are important sustainability issues. Optimising building thermal design is a prerequisite and should always form an important part of the design solution. Smaller mechanical thermal systems, less raw and manufactured materials, less transportation and all the associated energy consumption, are some of the benefits. The subsequent positive impact on the external environment is a further beneficial result. Conservation of energy and raw materials is not the only area of concern. The analysis of thermal comfort to ensure the wellbeing of the building's occupants is a further important factor concerning the optimum thermal design of the building systems. The nature of the related costs and benefits are not as apparent as those relating to the energy and environmental issues. To date, only dynamic thermal models of buildings, developed for coding into computer software programs, have the capability to analyse the building thermal problem with an acceptable degree of precision.

The primary aim of the thesis is to develop an advanced spreadsheet based methodology for the dynamic thermal modelling of buildings. The method should accurately model all the modes of heat transfer and thermal excitations. The methodology should allow the creation of dynamic building thermal models, based on the fundamentals of building heat transfer, within the spreadsheet environment, using its basic mathematical and logical functions, without resorting to the formulations of macros. The primary application of the method is intended for practical design-day calculations and building thermal analysis.

The scope of application of the Thermal Analysis Design Method is wider than the traditional thermal design tools intended for cooling load calculations. Building thermal design, investigating passive and mechanical design solutions, creating network ventilation models, analysis of thermal comfort, as well as the traditional cooling load and peak

temperature calculations is a sample of its scope. The method is ideally suited to the thermal analysis of a single space during a single 24-hour period using representative weather data. Longer simulation periods and multi-zone analysis are also possible, subject to computer computational speed and memory.

The salient idea of the thesis is that the application of Thermal Analysis Design Method is totally under the control of the user. It is a powerful, manual, dynamic thermal simulation method in contrast to the dynamic thermal models that are implemented via computer software programs. The competence of the user and the computational power of the calculation tool are the only factors limiting its application. Manual method should not be construed as a simplified thermal calculation method such as the well-known CIBSE Admittance procedure. The proposed manual method is designed to simulate all modes of heat transfer by employing accurate mathematical models describing each process.

1.2 Scope of application

The Thermal Analysis Design Method should find application in postgraduate research work. The method is modular in design allowing the addition and integration of building thermal sub-models. The development of a new solar diffuse model or an internal convection model can be formulated, in the spreadsheet program, by the user and linked to the core thermal model. The replaced modules may remain as alternative sub-models, disconnected from the core thermal model via *software switches* created by logic statements. The addition or replacement of modules, by the user, is usually not possible when employing a commercial software program. The computer spreadsheet is a powerful computational environment. A new module can be added, at will, once the mathematical model describing the physical processes involved is known or derived. Complex mathematical models of particular thermal processes can be formulated and analysed in great detail. Integrated ventilation and thermal models can be created with relative ease within the spreadsheet environment. The important mathematical functions essential to modelling heat transfer processes, such as trigonometric, hyperbolic, complex numbers, matrices, numerical iteration and logic, are included in a suitable spreadsheet program. Hand-held calculators contain approximately eighty mathematical functions. A single spreadsheet cell has approximately 330 functions available to it. Each spreadsheet file contains over 15 million cells; i.e., 15 million calculators linked together. This arsenal of

computational power has the potential for creating complex dynamic thermal models, which can be utilised as virtual laboratory test rigs on research projects.

The Thermal Analysis Design Method would be an ideal teaching and learning aid on building services engineering degree courses. A major difficulty concerning the subject of building heat transfer is that its practical demonstration, in a realistic manner, requires the use of a building simulation software program. Although experience of these software programs is beneficial to the postgraduate student, their use does not fully test a student's understanding and application of the subject matter. The proposed method allows the student to create building thermal models utilising the fundamentals of heat transfer. Hands-on practical experience of dynamic thermal modelling is beneficial when using the commercial building simulation programs. The quality of a building thermal analysis requires a clear understanding of the physical processes involved.

The method should appeal to those engineers who prefer to use a manual building thermal simulation method but have been drawn towards commercial simulation programs due to the indicative performance of current simplified manual methods. Engineers who use a computer spreadsheet program for many of their design calculations should also benefit from the introduction of the new manual method. Many associated design calculations can be arranged on the spreadsheet and linked to the building thermal model. At first glance, the level of mathematical complexity involved in the application of the proposed new manual method may not appeal to all practising engineers. A learning curve is always associated with the introduction of a new method. An innate feature of the new manual method is *levels of complexity*, which allows the method to be used at ascending levels of thermal modelling difficulty.

1.3 Salient features of the method

Developing the criteria, on which the proposed method is designed, is the initial focus of the thesis. The essential components of a building thermal analysis method are the mathematical models describing the internal and external physical processes taking place. These mathematical models are defined as physical models in the thesis. The performance of the thermal simulation model depends on the accuracy of these physical models. An important feature of the new manual method is the ability to update, replace or include a number of model options of a particular physical model. Chapter II, Mathematical Modelling of Building Thermal Behaviour, describes typical physical models that are used

in dynamic thermal models of buildings. Mathematical simulation techniques are required to provide solutions to the differential equations describing the conduction of heat in solids. Chapter III provides an overview of the major mathematical simulation techniques employed in computer software programs, the response factor, frequency domain and finite difference methods. This comparison study enables one to decide on which mathematical simulation technique is suitable for computer spreadsheet application. Reduced simulation design methods are developed for modelling the thermal behaviour of a single zone over a 24-hour period. Chapter IV investigates the ASHRAE and CIBSE design methods in order to establish the advantages and deficiencies of each method. Chapter V analyses the findings of the previous three chapters in order to define the design criteria for developing the new manual thermal simulation method and the assumptions underlying its application.

Chapter VI describes, in detail, the development of the Thermal Analysis Design Method. The Iterative Frequency Domain Method (IFDM) and the Adiabatic Iterative Frequency Domain Method (AIFDM) are alternative thermal simulation techniques that have been specifically developed for computer spreadsheet application. A notable structural feature of the Thermal Analysis Design Method is that it is composed of three thermal models, an internal and an external environmental model, and a window model.

The external environmental model includes a solar model, a solar shadow model, long-wave and convection models. The external long-wave model incorporates a radiation view factor sub-model. Neighbouring façades, ground surface and sky temperatures are also simulated. An important feature of the external environmental model is the development of a new and accurate sol-air temperature formulation that combines all the external thermal excitations into a single thermal driving force.

A window sol-air temperature, which accounts for all the thermal influences of the external and internal environments, is an innovative development. The window sol-air temperature is employed to obtain an accurate inner window, surface temperature profile for simulating the subsequent internal convective and long-wave radiant exchange processes. The thermal modelling of a window system incorporating internal operable blinds is another important addition to the window model. A daily schedule for operating the internal blinds can be set-up to simulate the appropriate surface temperature, i.e., blind or inner glazing, which is

exposed to the internal environment at a particular time of the day. The model simulates the airflow between the inner glazing pane and blind during the times when the blinds are closed. This airflow can produce significant convective heat transfers in an air-conditioned space. An implicit finite difference scheme was found to be the most computationally efficient technique for simulating, on a computer spreadsheet program, the complex heat transfer processes taking place. A subsequent innovation is the thermal/temporal linking of a finite difference sub-model with the core iterative frequency domain model.

The Iterative Frequency Domain Method (IFDM) and the Adiabatic Iterative Frequency Domain Method (AIFDM) are alternative core simulation methods of the internal environmental model. Each method combines numerical iteration techniques with the frequency domain technique to produce simulation methods that can model all non-linear heat transfers. The traditional frequency domain method is limited to modelling linear heat transfers. The IFDM employs the traditional thermal transmission matrices that incorporate surface convective coefficients. The AIFDM is a more elegant method that excludes the surface heat transfer coefficients from the thermal transmission matrices, allowing variable convective heat transfer coefficients to be determined by a sub-model, resulting in the accurate modelling of the conductive and convective heat transfer processes. The AIFDM option also allows the space air node to be modelled by an implicit finite difference scheme. The IFDM simulates variable convective heat transfer coefficients but employs a convective flux correction technique that minimises the error due to using constant convective coefficients in the thermal transmission matrices. Both methods produce identical results.

An exact long-wave radiant exchange model, incorporating a radiant view factor sub-model is used. It was found, when examining the long-wave radiant exchange process, that the emissive power is reasonably linear over the range of surface temperatures normally experienced in rooms. As a result, the derivation of an accurate linearised correlation expression for calculating a surface's emissive power is presented. The development of a new reduced long-wave radiant exchange model that is sensitive to the dominant radiant exchange processes taking place is also described.

A numerical iteration technique, for simulating ventilation network models, has been developed for implementation on a computer spreadsheet program. The ventilation network model can be linked to the space's thermal model.

A number of examples detailing the simulation of plant on a computer spreadsheet program are presented. Mechanical ventilation with night-time sub-cooling, air- conditioning convective cooling, chilled ceiling with displacement ventilation, are practical design solutions that can be simulated on the spreadsheet program. The modelling of single sided natural ventilation via windows is also described. These examples employ numerical iteration simulation techniques. The derivation of an exact solution method for determining the space cooling load is an alternative development. The method is based on determining the thermal response function of the space being modelled. The thermal response function is utilised to derive a set of simultaneous response factor equations, which may be solved by the spreadsheet's matrix inversion functions to give the space's cooling load profile. Computational efficiency is an important issue concerning all computer simulation programs. A number of the physical models were examined in order to establish if simpler mathematical expressions could be derived without significantly compromising accuracy. The thesis contains a number of examples where intricate mathematical models, describing particular physical processes, have been reduced to simpler expressions that give almost identical results.

Chapter II

2.0 MATHEMATICAL MODELLING OF BUILDING THERMAL BEHAVIOUR

2.1 Physical Models

Modelling realistic building thermal behaviour requires using accurate mathematical models of the modes of heat transfer and thermal driving forces. Conduction, convection and long-wave radiant exchange are the main modes of building heat transfer, while the thermal driving forces can be divided into external sources, i.e., solar irradiation and outside air temperature, and internal sources such as heat gains due to electrical lighting and occupants. The mathematical models describing these building heat transfer processes shall be called physical models, for the purpose of the thesis. Dynamic thermal models of buildings also require mathematical simulation techniques, such as response factor, frequency domain or finite difference methods, to simulate the dynamic energy flows defined by some of the physical models. Hence the essential components of the dynamic thermal model of a building are illustrated in Figure 2.1.

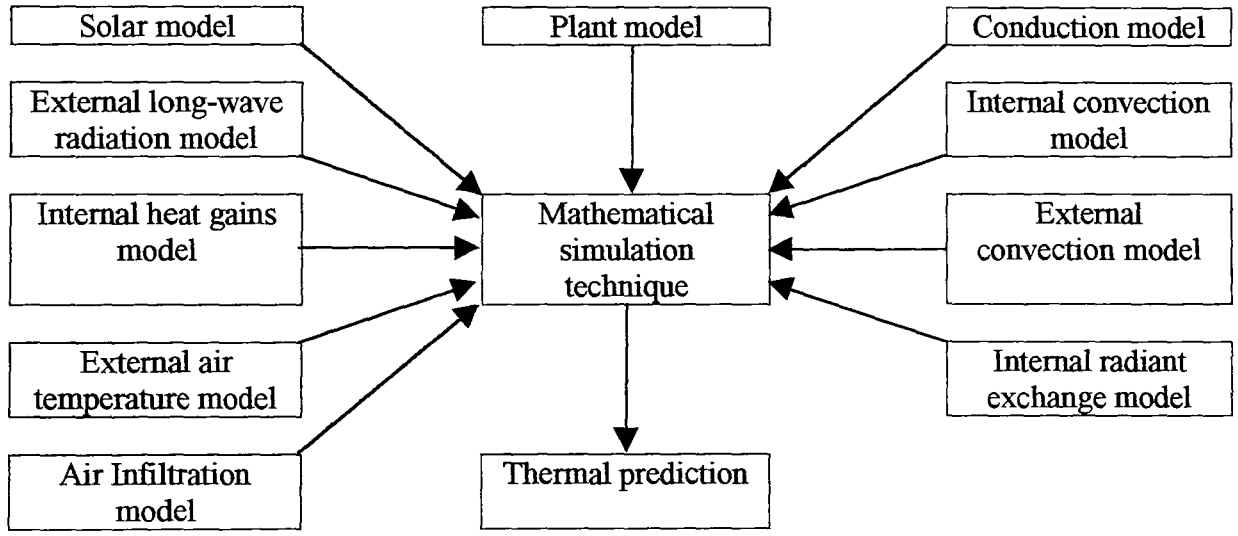

Figure 2.1 Dynamic thermal model of a Building

The thermal relationship between these sub-models requires the constant exchange of simulated results. Errors will also be exchanged. Accurate performance of the dynamic thermal model requires minimising two types of error; errors due to the correctness of the physical models adopted and errors associated with the type of mathematical simulation technique employed. Prior to the widespread use of computers, it was necessary to reduce

the complexity of some of the physical models and the mathematical simulation techniques in order to produce results within a reasonable time frame. The computational power of modern computers allows mathematical simulation techniques to compute more precisely the heat transfer processes. As a consequence, preciseness in the mathematical modelling of the thermal processes becomes a prerequisite and the correctness of the resulting physical models adopted may be used to rank the performance of the building dynamic thermal model.

2.1.1 The conduction model

One-dimensional heat flow through the building fabric elements is normally assumed. Each layer of a multilayered building element is assumed a homogeneous material with constant thermophysical properties. Transient heat conduction is defined by Fourier's thermal diffusion equation (For one-dimensional heat conduction), described by equation (2.1).

$$\frac{\partial T}{\partial t} = \alpha \frac{\partial^2 T}{\partial x^2}, \tag{2.1}$$

where α is the thermal diffusivity.

The diffusion equation combined with suitable initial and boundary conditions is used to model heat conduction processes through solid materials. Mathematical simulation techniques, mainly numerical finite difference, periodic heat transfer and response factor methods provide solutions to the diffusion equation and can be employed to simulate one-dimensional heat conduction through building structural elements. One-dimensional heat conduction is assumed a linear process and the cited mathematical simulation techniques can accurately model linear heat transfer processes. However, the assumption of constant thermophysical properties used to define the thermal diffusion coefficient, α, in equation (2.1) may lead to some error. Values of thermophysical properties of building materials may be prone to measurement error [1a] and variation with moisture content [2]. Further errors can occur due to thermal bridging and airflow through gaps and cracks [3].

2.1.2 The internal convection model

In building heat transfer, convective heat flux at structural surfaces is usually evaluated using the expression:

$$q_c = A_s h_c (T_{ai} - T_s) \tag{2.2}$$

Equation (2.2) is non-linear due to the convective heat transfer coefficient h_c being also a function of the surface to air temperature difference, $T_{ai} - T_s$. For accurate work, the convective heat transfer coefficient is treated as a variable, requiring that the mathematical simulation technique adopted is capable of assimilating revised convective coefficient values at each successive time step. It is generally assumed that the convective coefficient represents a surface-average value. Due to the convective heat transfer coefficient being a complex function of the local fluid dynamics, time varying thermophysical properties and surface geometry, it is difficult to evaluate in order to produce a concise analytical formulation similar to the diffusion equation. In practice, expressions developed from empirical studies are employed. The following expressions, by Alamdari and Hammond [4], valid over the range of flow conditions found within buildings, are used in a number of computer dynamic simulation programs.

Vertical surface
H = space height

$$h_c = \left\{ \left[1.5 \left(\frac{|(T_{ai} - T_s)|}{H} \right)^{1/4} \right]^6 + \left[1.23 \left(|(T_{ai} - T_s)| \right)^{1/3} \right]^6 \right\}^{1/6} \qquad (2.3)$$

Horizontal surface
Upward heat flow
A = surface area
P = surface perimeter

$$h_c = \left\{ \left[1.4 \left(\frac{|(T_{ai} - T_s)|}{4A/P} \right)^{1/4} \right]^6 + \left[1.63 \left(|(T_{ai} - T_s)| \right)^{1/3} \right]^6 \right\}^{1/6} \qquad (2.4)$$

Horizontal surface
Downward heat flow

$$h_c = 0.6 \left(\frac{|(T_{ai} - T_s)|}{(4A/P)^2} \right)^{1/5} \qquad (2.5)$$

In the case of horizontal surfaces such as ceilings and floors, the direction of heat flow normally changes as the space air temperature swings above and below the surface temperature. Evaluation of equations (2.4) and (2.5) will show that upward convective heat transfer coefficients can be about four times the value of corresponding downward coefficients. The convection sub-model of the dynamic thermal model must be programmed to switch appropriately between equations (2.4) and (2.5) to avoid significant errors occurring.

2.1.3 The external convection model

The magnitude of the external convective coefficient is mainly influenced by wind speed and surface roughness with surface-to-air temperature difference having a relatively smaller influence. Similar to internal convection, the external convection coefficient is a complex function and empirical type correlations are found to give reasonable results.

For example, the following empirical correlation with the parallel wind speed, v_{pf}, is from McAdams [5].

$$h_c = 5.678\left[a + b\left(\frac{v_{pf}}{0.3048}\right)^n\right] \tag{2.6}$$

Table 2.1 Values of coefficient for equation (2.6)

Nature of surface	v_{pf}<4.88 m s^{-1}			4.88≤v_{pf}<30.48 m s^{-1}		
	a	b	n	a	b	n
Smooth	0.99	0.21	1	0	0.5	0.78
Rough	1.09	0.23	1	0	0.53	0.78

A simpler expression [6], relating the external convective coefficient to wind velocity is:

$$h_c = 4 + 4v \tag{2.7}$$

If the parallel wind velocity is used, equation (2.7) gives comparable values to equation (2.6).

Heat transfer at the external surface is then determined using equation (2.2) and the external surface to outside air temperature difference. In the case of insulated external cavity wall constructions and roofs, fluctuations in external thermal excitations have an insignificant influence on the internal environment. In contrast, the mean value of the external thermal disturbance and the thermal transmittance value (U-value) of the structural element have a greater influence on the daily mean internal air temperature. Table 2.2 demonstrates that the external convective heat transfer coefficient has little influence on the U-value of a typical external wall construction. The use of a constant external convective heat transfer coefficient may not incur significant errors. In the case of solar irradiation, parallel heat paths are created and as the external convective heat transfer coefficient increases, heat flow to the external air will increase with a consequential decrease in heat flow to the

internal environment. For thin lightweight constructions, such as window systems, the external heat transfer coefficient has a much greater influence on the heat transfer processes due to the insignificant thermal resistance and mass of such constructions. The use of a constant convective heat transfer coefficient for lightweight constructions would incur significant errors.

Table 2.2 Correlation between external convective heat transfer coefficient and U-value

v_{pf} ($m\ s^{-1}$)	h_c ($W\ m^{-2}\ K^{-1}$)		Corresponding U-value ($W\ m^{-2}\ K^{-1}$)	
	Smooth surface	Rough surface	Smooth surface	Rough surface
0.5	7.58	8.33	0.356	0.357
1	9.53	10.47	0.359	0.360
3	17.36	19.04	0.365	0.366
5	25.17	26.68	0.368	0.368
10	43.21	45.81	0.370	0.370
20	74.21	78.66	0.371	0.372
30	101.81	107.92	0.372	0.372

2.1.4 Internal long-wave radiant exchange model

Long-wave radiant exchange takes place between all surfaces in view of each other. The main thermal driving force is the emissive power of the surface, $\varepsilon\sigma T^4$. The room surfaces are assumed to act as radiative grey surfaces with long-wave inter reflection also taking place between the emitting surfaces. Each room surface is assumed isothermal and is represented by a single temperature. Sub-division of a surface into a suitable number of isothermal temperature patches is required for a more precise analysis. Only the major room surfaces are included in the radiant exchange process to minimise the amount of computation. The net surface heat flux, for surface i, due to long-wave radiant exchange between surface i and the other major room surfaces j is given by equation (2.8).

$$q_i = \varepsilon_i \left[\sigma \sum_{j=1}^{N} F_{ij} \left(T_i^4 - T_j^4 \right) + \sum_{j=1}^{N} F_{ij} \left(\frac{1}{\varepsilon_j} - 1 \right) q_j \right] \tag{2.8}$$

where ε and F are the surface emissivity and radiant view factor respectively. Equation (2.8) and versions of it are well documented in the literature. For a rectangular room with a single window, a set of seven equations are generated from equation (2.8) and solved simultaneously (or by an iterative technique) to give the net radiant heat flux for each surface at each successive time step. The temperatures to the forth power indicate that the equations are non-linear requiring a suitable mathematical simulation technique to be employed. The inter-reflected flux is small compared to the emissive power component and equation (2.8) is usually reduced to:

$$q_i = \varepsilon_i \sigma \sum_{j=1}^{N} F_{ij} \left(T_i^4 - T_j^4 \right) \tag{2.9}$$

A further simplification is to linearize equation (2.9) to the form:

$$q_i = \varepsilon_i \sigma \sum_{j=1}^{N} F_{ij} T_{\mathrm{m}}^3 \left(T_i - T_j \right) \tag{2.10}$$

T_{m} is the average of the temperatures of the two exchanging surfaces and because the temperature variation, on an absolute scale, is relatively small, a constant value of T_{m} is sometimes used. The error is small when room surface temperatures are close in value, which is usually the case, the exception being surfaces at significantly different temperatures to the major room surfaces such as windows, chilled-ceilings and radiators. Some of the less rigorous mathematical simulation techniques model the radiant exchange process by transforming it into a conductive star network in which the major room surfaces exchange energy with a central hypothetical mean radiant index temperature. In the CIBSE admittance method [7], the radiant star temperature T_{rs} is used as the index temperature and a further simplification is formulated by combining T_{rs} with the mean space air temperature to produce the environmental index temperature. Davies [8] gives an informative review of the derivation of environmental temperature and the derivation of a more rigorously defined room index temperature: the rad-air temperature. A major disadvantage of adopting this level of simplicity is the inability to compute surface temperatures, thereby limiting the assessment of thermal comfort within a space.

2.1.5 The air infiltration model

Air infiltration is a difficult process to model due to the flow characteristics of the building's air leakage paths and the complex characteristics of the driving forces, wind

pressure and 'stack effect' in particular. Air infiltration is well known to constitute a significant proportion of the plant thermal load, in many cases about 50% of the winter heating load. Although complex, there are theoretical calculation techniques and supporting data available [9,10] for predicting air infiltration for single and multi-zone applications. Accordingly, the CIBSE has updated its air infiltration section [11] of the CIBSE guide by including appropriate formulae, supporting data, and prediction techniques. ASHRAE's Cooling and Heating Load Calculation Manual also includes a comprehensive section on estimating air infiltration rates [12]. Modelling building air infiltration is analogous to modelling building heat transfer. The temperature difference across a building element is replaced by the pressure difference. Thermal conductances are replaced by airflow conductances (flow coefficient C), characterising the airflow paths created by cracks around doors and windows as well as cracks and joints in the building fabric. A network ventilation model defining all the infiltration airflow paths connecting the outside pressure nodes p_{oj} to the single indoor pressure node p_i can be constructed for a single zone. The summation of the flow equations, defining all the branches of the flow network, must equal zero, as defined by equation (2.11) [11].

$$\sum_{j=1}^{N}\left[C_j\left(p_{oj}-p_i\right)^{n_j}\right]=0 \qquad (2.11)$$

The flow exponent of the path j, n_j, is typically 0.5 to 0.65 in value. The value of the flow coefficient, C_j, depends on the airflow characteristics of the leakage path. Note the similarity with a space's steady state heat balance equation as described by a thermal conductance and temperature difference. Equation (2.11) is non-linear requiring the unknown inside pressure p_i to be determined by iteration, subject to an assumed p_i as the initial condition. The iteration process is terminated when equation (2.11) sums to approximately zero. The external driving force, p_{oj}, combines the influences of wind and stack pressures. The stack pressure, being a function of space air temperature, imposes a further level of non-linearity on equation (2.11). In the case of multi-zone models, the flow network will include additional airflow conduction paths connecting internal zone pressure nodes. Airflow balance equations are generated for each space and the equation set is solved by iteration to obtain the internal pressure of each zone. For an internal airflow leakage path connecting two spaces, the corresponding expression defined by equation (2.11), will include the pressures of each neighbouring space rather than an internal and

external pressure. The influence of the stack effect between the two spaces must also be accounted for in the equation.

External pressures are determined for each building external surface. The external pressure is influenced by wind pressure and stack effects. Typical equations [11] for determining wind and stack effect pressures are:

$$p_{\mathrm{w}} = 0.5\rho C_{\mathrm{p}} v_{\mathrm{z}}^2 \tag{2.12}$$

$$\Delta p_{\mathrm{s}} = \rho_{\mathrm{o}} g 273 (z_2 - z_1)(1/T_{\mathrm{o}} - 1/T_i) \tag{2.13}$$

The mean wind speed v_z is a function of the reference regional wind speed, local topography, ground roughness and nearby obstacles. The wind pressure coefficient C_p is a function of the wind direction and location on the building surface. Equation (2.13) shows that the stack effect pressure drop Δp_s is a function of inside and outside air temperatures, and height between the lower and upper airflow paths quantified by $(z_2 - z_1)$. A typical equation for the airflow rate through a crack of length L_c due to a total pressure difference Δp is given by [11]:

$$Q_{\mathrm{c}} = L_{\mathrm{c}} k_1 (\Delta p)^n \tag{2.14}$$

Note that equation (2.14) could form one or more of the set of equations defined by equation (2.11), with $C = L_c k_1$. The CIBSE guide [11] provides information regarding the determination of v_z and obtaining values for C_p. Crack flow coefficients k_1 and flow exponent n for doors and windows are provided as well as references to obtain further data and formulae for other types of air infiltration paths.

The CIBSE guide does not include a procedure for determining air infiltration due to the quality of construction of external walls. Considering the magnitude of surface area involved, this component may be considerable and should be accounted for. An ASHRAE publication [12] includes a procedure for determining this component.

The complex nature of air infiltration has resulted in prediction methods relying on a relatively small quantity of empirical data that cannot fully cover the range of possibilities encountered in buildings. Due to the significant influence air infiltration has on building thermal loads, large errors associated with the air infiltration model, should be expected.

2.1.6 Internal heat gains model

Similar to air infiltration in winter, the internal heat gains can form the largest component of the building cooling load in summer. The sources of the heat gains are difficult to model

due to being functions of many variables and probabilistic influences relating to occupancy patterns and diversity in the operation of electric lighting and equipment throughout the day. These complexities have lead to a more pragmatic approach in which statistical type assessment techniques have been developed rather than the derivation of precise physical models for predicting the internal heat gains. The accuracy of an assessment technique relies significantly on a suitable quantity of good quality up to-date data, thus avoiding an overestimate of the internal gain [13]. The CIBSE has revised its section on internal heat gains [14], providing much data and guidance. The ASHRAE Fundamentals Handbook [15] also includes good supporting heat gain data, of which the data on restaurant/cooking equipment is included in the appendices of the CIBSE guide [14].

Occupants, electric lighting and electric office machines are typical sources of the internal gains in office buildings. Cooking appliances in kitchens and, manufacturing and process equipment/plant in industry are other sources of internal heat gains. Convective and radiant energy are the main components of electrical sources of internal gains. In addition to these components, people, the majority of kitchen appliances and many industrial processes produce latent heat. Convective and radiant heat gains are accounted for in the prediction of peak temperatures, heating and cooling loads. Latent heat gains are considered at a later stage when sizing air conditioning plant. Occupants are stationary for only a fraction of the working day and office equipment is frequently relocated. The level of activity and gender significantly influences heat gains from people. Due to these factors, convective and radiant heat gains are not determined in the traditional manner, using the convective and long-wave radiant exchange models. The CIBSE guide [14] provides sensible and latent heat gains from people based on activity level and gender. Assessment of the electrical lighting heat gain is based on the installed electrical power with factors applied to obtain the fractional gain to the space and to account for diversity of operation. The CIBSE guide [14] provides installed power densities per 100 lux maintained illuminance for different types of lamp. If the luminaire model is known, a more precise estimate is obtained by using the Lumen Method Equation to determine the total number of lamps N.

$$N = \frac{E \times A}{LF \times UF \times MF} \tag{2.15}$$

The illuminance level, lamp flux, utilisation and maintenance factor, and floor area are given by E, LF, UF, MF and A respectively. The total power demand is then given by:

$$Total\ Power\ Demand = (1 + \%\ power\ of\ control\ gear/100) \times N \times Lamp\ wattage \tag{2.16}$$

Heat gains from electrical office machines are based on applying appropriate statistical factors to manufacturer's nameplate power ratings. The CIBSE guide [14] provides calculation methods, supporting data such as usage and diversity factors. In the absence of manufacture's data, representative nameplate power ratings are provided.

The split of the heat gains into their convective and radiant components is usually achieved by applying a radiant fraction; typically, 30% for electrical lighting and office machines, and 70% for people. The convective component is assumed a direct gain to the air node, while the radiant component is applied to the room surfaces.

The convective and radiant components of a particular source are assumed to remain constant, although in reality, the convective and radiant outputs are influenced by changes in source and space surface temperatures, and air temperature. There are no precise guidelines regarding the distribution of the radiant gains over the room surfaces. Usually the radiant flux is simply distributed uniformly over the major room surfaces. It would seem that these assumptions are compatible with the current level of accuracy adopted in modelling the internal gains.

2.1.7 Solar model

The analysis of solar irradiation of external vertical surfaces is performed in terms of direct, sky-diffused and ground reflected components. For horizontal surfaces, only direct and sky diffused are relevant. Theoretical solar models for direct solar radiation have been developed [16]. Basing the calculation on meteorological measurements of direct horizontal solar radiation I_d, which takes into account the local climatic and atmospheric conditions, is a more precise method. Accurate solar trigonometric formulae may then be used to calculate the direct normal solar radiation incident on any inclined surface. The intensity of direct solar radiation I incident on a surface normal to the rays of the sun is given by:

$$I = I_d / \sin a \tag{2.17}$$

The direct solar radiation I_δ normally incident on a tilted surface inclined at an angle δ with the ground is given by:

$$I_\delta = I \sin a \cos\delta \pm I \cos a \cos n \sin\delta \tag{2.18}$$

For solar radiation I_v normally incident on a vertical wall, equation (2.18) reduces to

$$I_v = I \cos a \cos n \tag{2.19}$$

Trigonometric formulae for calculating solar altitude and azimuth angles are available in various texts [17] and are presented here for completeness.

$$\text{Solar altitude } a = \sin^{-1}(\sin d \sin L + \cos d \cos L \cos h) \tag{2.20}$$

$$\text{Solar azimuth } \eta = \tan^{-1}[\sin h / (\sin L \cos h - \cos L \tan d)] \tag{2.21}$$

Where:

L = Latitude of the location on the surface of the earth.

The hour angle h, equal to$15 \times$ (Sun time), represents the angular displacement of the sun from noon. The sun declination angle is given by:

$$d = 23.45 \sin [360\ (284 + \text{Day No. counting from 1 on 1}^{st}\ \text{Jan.})/365] \tag{2.22}$$

It is more difficult to model sky diffuse radiation. Scattered atmospheric radiation, horizon brightening, solar position and cloud cover are some of the phenomena influencing the magnitude of diffuse radiation incident on vertical surfaces. Because of these factors, diffuse radiation exhibits a mix of pure diffuse and directional behaviour, the mix varying between an isotropic (fully overcast sky) and an anisotropic sky (clear sky). Various formulations for modelling sky diffuse radiation have been developed [18,19,20] but the different treatments of the subject can result in significantly different predictions. However, validation trials [21] have shown that the Perez *et al* model [20] gave the best performance when applied to a wide range of locations. The Perez model is based on a sky hemisphere superimposing a circumsolar disc (modelling the directional component) and horizon band (modelling the horizon brightening component) on an isotropic background. The reasonable performance of this model is probably due to the circumsolar and horizon brightness coefficients (F_1' and F_2' respectively) that were correlated from a comprehensive range of climatic measurements. The original model was more complex to use compared to other practical models and in response, Perez *et al* developed the following reduced model.

$$I_c = I_h \left[0.5(1+\cos\delta)\left(1-F_1'\right)+F_1' a/c+F_2' \sin\delta\right] \tag{2.23}$$

The diffuse horizontal irradiation I_h is usually available from meteorological measurements. The solid angles a and c relate the circumsolar region to the tilted and horizontal surfaces respectively. Further information required to evaluate these solid angles and, the circumsolar and horizon brightness coefficients are provided in reference [20].

A fraction of the direct irradiance I_d and diffused irradiance I_h incident on the ground is reflected to tilted surfaces and this component is generally evaluated using an expression of the form [16]

$$I_r = 0.5(1-\cos\delta)(I_d + I_h)\rho \tag{2.24}$$

$0.5(1-\cos\delta)$ defines the view factor between the surface and the ground, and ρ is the ground reflectance. For a vertical surface, the expression simplifies to

$$I_r = 0.5(I_d + I_h)\rho \tag{2.25}$$

Although this simple treatment incurs some error, typical ground reflectance values of about 0.2 ensure that this component is small compared with the direct and diffuse components.

In summary, the modelling of the direct irradiation component is relatively uncomplicated and may be defined fully and accurately by trigonometric expressions, while the more difficult treatment of the problematic sky diffuse and ground reflected components have resulted in less accurate physical models. Large errors may occur when predicting solar irradiation for cloudy and fully overcast skies, when the sky diffuse component is the dominant or sole component. The modelling of the direct component is not completely free of error due to its reliance on measurements of horizontal irradiation. Typical and worst accuracies of ±3% and ±5% respectively have been quoted for solar irradiation sensors [22].

Of the total incident solar irradiation, a fraction is absorbed by the surface and the remainder reflected. The same value of solar absorption coefficient is usually assumed for the direct and diffuse irradiation, typically 0.9 and 0.5 for dark and light coloured surfaces respectively. In the case of transparent materials some of the solar energy is transmitted, some absorbed and the remainder reflected. The transmitted solar radiation is treated as a gain to the space surfaces while the absorbed component heats up the glass resulting in convective and long-wave heat exchanges with the internal and external environments. Accurate modelling requires tracking the movement of the transmitted beam's sunlit patch around the room surfaces. Tracking of the insolation patch can be modelled successfully by trigonometric expressions. The transmitted diffuse component is usually distributed uniformly over the room surfaces 'seen by the window'. In simpler models, the transmitted direct and diffuse solar radiation is uniformly distributed over all the room surfaces. In multi-layer window systems, for instance double-glazed with internal blinds, multiple

reflections take place between adjacent layers. The amount of solar energy absorbed by each layer and the resulting transmitted radiation can be determined by means of sketching a trace of the reflected and transmitted rays [23].

A sun shadow sub-model determines the extent of shading of building facades and selfshading of glazing due to window recesses and frames. The geometry of shadows is well presented in the literature [24,25], its treatment is relatively straightforward and the model can be fully defined by trigonometric expressions. Tracking of the window transmitted insolation patch is also an appropriate task for this model.

Some building dynamic thermal models use a combined solar, external long-wave radiation and outside air temperature model called the sol-air temperature. The CIBSE guide [26] defines sol-air temperature as follows

$$T_{eo} = \left[\alpha I_G(\delta\gamma) + L^*(\delta)\right] / h_c + T_{ao} \qquad (2.26)$$

$I_G(\delta\gamma)$ is the global solar irradiation for a plane of tilt angle δ and orientation γ. $L^*(\delta)$ is the long-wave radiation balance and h_c the external convective surface heat transfer coefficient. $L^*(\delta)$ depends on the external surface temperature which is unknown prior to calculation. Simpler simulation programs assume values for $L^*(\delta)$ or tabulated values of sol-air temperature for particular global locations. The advantage of the sol-air temperature concept is the combination of the external environmental thermal influences into a single thermal excitation, which is computationally more efficient.

2.1.8 External long-wave radiation exchange model

Similar to research into the subject of sky diffuse radiation, the study of external long-wave radiation exchange is complex leading to different treatments, formulations and subsequent results. Long-wave radiant exchange between the surface of a building and its external environment is influenced in the main by the absolute temperatures of the sky, ground, surrounding buildings and landscape features together with their corresponding dimensions. Expanding equation (2.9) to define the long-wave radiation balance $L^*(\delta)$ on an external building surface of temperature T_{sur} and inclination δ, in view of the sky, ground and surrounding buildings gives:

$$L^*(\delta) = \varepsilon\sigma\left[\left(F_{sky}T_{sky}^4 + F_{grd}T_{grd}^4 + F_{bld}T_{bld}^4\right) - T_{sur}^4\right] \qquad (2.27)$$

Representative values of the view factors can be obtained from the literature [27] or can be determined from view factor algebra. The ground temperature and surrounding building

surface temperatures may only be determined accurately by carrying-out heat balance calculations at each surface, an obviously impractical option due to the number of surfaces involved. A compromise is that surrounding building surfaces possess temperatures similar to the corresponding surfaces of the building being analysed. The CIBSE guide [28] provides a formula for estimating the ground long-wave radiation based on external air temperature and global horizontal solar irradiation, $(I_d + I_h)$,:

$$\sigma T_{grd}^4 = L_g = \sigma\left[0.98T_{ao} + 0.037\left(1-\rho_g\right)\left(I_d + I_h\right)\right]^4 \tag{2.28}$$

The same appendix of the CIBSE guide provides an external long-wave radiation expression but does not include a long-wave component for surrounding buildings. It also assumes that the external surface temperature T_{sur}, of the building being simulated, is equal to the corresponding sol-air temperature of the surface. Such an assumption may cause a substantial error in the surface's long-wave radiation value due to the fourth power exponent of the surface's emissive power.

Sky radiation originates mainly from water vapour and carbon dioxide within the atmosphere. Clouds are found to be strong emitters of long-wave radiation. Normally there is a net long-wave radiation loss to the sky vault; the loss peaks under nocturnal clear sky conditions. Cloud cover increases the incoming atmospheric radiation hence reducing the net long-wave radiation loss. A formulation for estimating the sky and ground long-wave radiation was developed by Cole [29] from measurements of net radiation R_N, incident solar radiation I and surface temperature T_S for a number of building façades with grass and tarmac frontages, under overcast and clear sky conditions. Measurements of screen air temperature, surface solar reflectivity ρ_S, surface long-wave reflectivity ρ_L and surface emissivity ε was also recorded. The sky and ground long-wave radiation R, was then determined by taking a radiation heat balance at the building's surface:

$$R_N = I - \rho_S I + R - \rho_L R - \varepsilon\sigma T_S^4 \tag{2.29}$$

It was found that long-wave radiation R, obtained from equation (2.29), correlated quite well with screen air temperature t_a and fractional cloud cover C. It followed that long-wave radiation R could be defined by linear correlations of the form [29]:

For a grass frontage $$R = 281 + 5.25t_a + \left(20 + 0.45t_a\right)C \tag{2.30}$$

For a tarmac frontage $$R = 284 + 5.92t_a + \left(20 - 0.20t_a\right)C \tag{2.31}$$

General expressions were then derived for the sky and ground radiation:

$$R_{sky} = \cos^2(\delta/2)\left[222 + 4.9t_a + (65 + 1.39t_a)C\right] + 0.09\left[1 - C(0.7067 + 0.00822t_a)\right]K_3\sigma T_a^4 \quad (2.32)$$

$$R_G = \varepsilon_g \sigma T_g^4 \sin^2(\delta/2) \quad (2.33)$$

Values of K_3, as a function of surface inclination angle δ, are given by Cole [29]; alternatively, the CIBSE guide [28] provides the following formula for evaluating K_3:

$$K_3 = 0.7629(0.01\delta)^4 - 2.2215(0.01\delta)^3 + 1.7483(0.01\delta)^2 + 0.054(0.01\delta) \quad (2.34)$$

For a vertical surface $K_3 = 0.3457$. The advantage of equation (2.32) is that it relies solely on obtaining screen air temperature, fractional cloud cover and surface inclination angle. Equation (2.33) requires determining the ground temperature, which may be difficult to obtain or calculate. Alternatively, ground temperature may be approximated using equation (2.28), which is less problematic due to relying on available meteorological data.

2.1.9 External air temperature model

Normally, measured values of air temperature are available from local met offices or representative values are provided in national engineering guides similar to the North American ASHRAE or UK's CIBSE [26] publications. Simple simulation models can be found in the literature, for example reference [30] provides the following expression for determining external air temperature at time θ given the air temperature at 15.00 h t_{15} and the diurnal range D, the difference between the mean daily maximum and minimum temperatures.

$$t_\theta = t_{15} - \frac{D}{2}\left(1 - \sin\frac{\theta\pi - 9\pi}{12}\right) \quad (2.35)$$

2.2 Thermal relationship between the models and the transfer of errors

Within a building dynamic thermal model, some of the physical models described above can be set-up independently of the other physical models and only export results to particular physical models. In comparison, other physical models are thermally inter-linked due to import, or exchanges of results. The conduction model requires numerical results from almost all the models. In the relationship between the internal radiant exchange and conduction models, there is a continuous exchange of results. Figure 2.2 illustrates the

thermal relationship between the models. Level 1 models are independent of imports from any model. Level 2 models receive imports from level 1 models and exchange results with level 3 models but do not exchange information with each other. Model levels 1 and 2 can be described as physical models that contribute to the space's heat gains. Level 3 models define the modes of heat transfer influencing the inside environment; they are not the sources of any heat gains but are the only group of physical models that exchange information with each other. They receive results from level 1 models and exchange

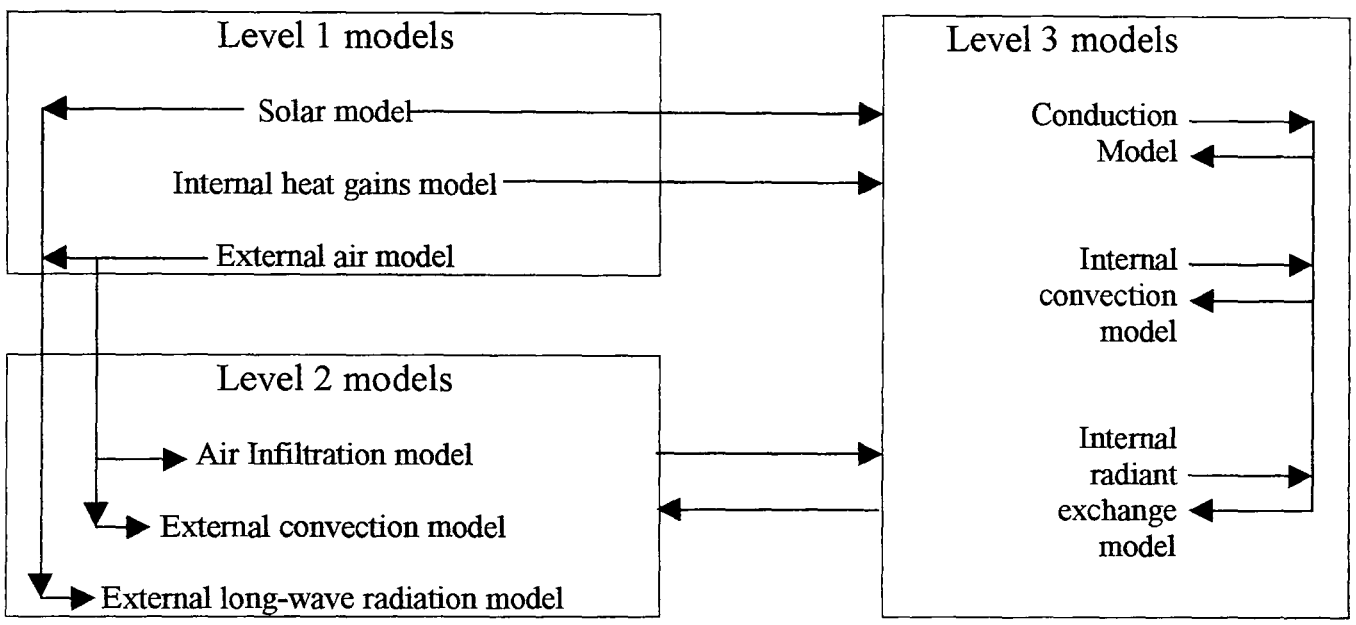

Figure 2.2 Physical model levels

results with level two models. Errors, due to inaccuracies in the physical models, will also be transmitted and in the case of model levels 2 and 3, errors are compounded. Therefore the ability of building dynamic thermal model to accurately simulate building thermal behaviour is related to the accuracy of each physical model and the thermal relationship between the physical models. Many of the difficulties and uncertainties regarding precise modelling of the physical phenomena associated with building heat transfer is associated with level 1 and 2 physical models. Due to this factor, improvements in the accuracy of level 3 physical models may not pay any dividends until improvements have been achieved in the precision of some of the lower level models. Of concern is the dominant influential position in the hierarchy of levels that the internal gains hold. It of all the thermal excitations has the greatest uncertainties associated with its assessment. The uncertainties increase in the case of speculative building projects. Although the internal

gains are a significant contributor to the total heat gains, the convective and radiant heat transfers due to its sources are not determined using analytical or empirical expressions. The precision of the physical models may be used to rank the performance of building dynamic thermal models. A building dynamic thermal model containing accurate physical models should potentially pass all test cell type, validation tests and be ranked as a prediction "class A" model. The survey of current status of the physical models in this thesis reveals that prediction "class A", dynamic thermal models are not available at the moment. In a guide concerning the validation of dynamic thermal models by Lomas [1b], it was recommended that uncertainties in the input parameters required by the thermal model and in the measurements should be taken into account in order to carry out a fair validation process. Although this guide relates to the late 1990's, its validation criteria may be deemed too stringent considering that the uncertainties that exist with many of the physical models are not merely in the physical properties defining their mathematical expressions.

Chapter III

3.0 MATHEMATICAL THERMAL SIMULATION TECHNIQUES

3.1 Introduction

Mathematical simulation techniques were adopted or developed to provide solutions to the differential equation defining the conduction of heat in solids. Frequency domain, thermal response factor and finite difference methods are the main techniques employed. Practical application of the response factor and finite difference methods had to await the advent of the digital computer, although the fundamentals behind these techniques, electrical circuit theory and numerical methods, were derived much earlier. The frequency domain and thermal response factor methods are specific analytical techniques whilst finite difference methods are usually described as numerical approximation techniques. However, when these techniques are applied to a dynamic thermal model, the subsequent precision demonstrated by each method may not correlate with the perceived meanings of accuracy conveyed by the words analytical and approximate.

3.1.1 Frequency Domain Method

The frequency domain method was the earliest of the methods to be developed. The method is composed of two parts: a procedure to calculate the mean thermal response and another to calculate the fluctuating thermal response. The total thermal response is represented by the sum of the two components. The mean thermal response is determined by a steady state analysis of the space, using only mean values of the thermal excitations and the steady state thermal transmittances (U-values) of the structural elements. Essentially, the frequency domain method is the procedure used to calculate the fluctuating component, which accounts for the dynamic heat transfer processes taking place. The frequency domain method is based on the amalgamation of three analytical techniques, i.e., periodic heat transfer, frequency analysis and the matrix method. Periodic heat transfer is the kernel of the technique, providing an analytical solution to heat conduction through homogeneous elements due to sinusoidal excitations. Fourier analysis allows real periodic thermal excitations to be decomposed into a discrete series of sinusoidal thermal excitations, each to be applied to the periodic conduction equation. Invoking the principle of superposition, the resulting series of sinusoidal thermal responses are summed to produce the total fluctuating response. The matrix method transforms the periodic conduction equation into a thermal

transmission matrix that defines the thermal behaviour of a homogeneous material element and the relationship between the surface temperatures and heat fluxes. The purpose of the matrix formulation is that it allows homogeneous thermal transmission matrices to be combined in series or in parallel to form an overall thermal transmission matrix with associated surface temperatures and heat fluxes. The significant advantage of the matrix method is that the thermal characteristics of a zone, floor of a building or entire building can be encapsulated within a single four-element thermal transmission matrix. A further important factor is that, because the matrix formulation characterises the relationship between the thermophysical properties, surface temperatures and heat fluxes, thermal analysis of spaces and buildings can also be carried-out without the need for thermal simulation.

The application of the frequency domain method to building thermal analysis has its origins in a paper by Alford *et al* [32] (1939) although the authors make reference to an earlier paper [33] (1935) regarding the derivation of the mathematical technique used. The fundamental component of the frequency domain technique, periodic heat transfer, is attributed to earlier researchers. Gröber [34] gives a good account of this early work, describing the derivations of the solution equations to periodic heat transfer and heat storage, in semi-infinite and finite plates. Alone, periodic heat transfer has limited application because the thermal excitation must be defined by a sinusoidal expression, which can only approximate a real thermal excitation. The significant feature of Alford *et al* paper [32], was the combination of a discrete Fourier analysis technique with periodic heat transfer to simulate real thermal excitations and subsequent thermal behaviour of homogeneous walls. Further contributions to the development of the frequency domain technique were made by Mackey and Wright [36, 37] but still dealt with homogeneous building elements. Following these publications, Mackey and Wright presented a paper [38] (1946) dealing with composite building elements but the proposed technique is based on determining an equivalent homogeneous construction. Davies [39] has clearly pointed out that defining the thermal behaviour of a distributed resistance/capacitance system by an equivalent 'lumped one' may only be justifiable in the case of thin elements. A precise treatment of composite constructions had to await a paper by Van Gorcum [40] (1950) which introduced the matrix method for defining thermal behaviour within building elements. Van Gorcum showed that the close analogy between AC electrical circuits and periodic heat transfer could be used to systematically solve heat conduction problems.

Drawing on electrical circuit theory, Van Gorcum showed that the relationship between the temperatures and heat fluxes at each surface of a homogeneous building element can be modelled by a two by two thermal transmission matrix whose four elements define the thermal behaviour of the building element. The significant contribution of Van Gorcum's paper, showed that the matrix formulation could be extended to model compound building elements by matrix multiplication of the transmission matrices defining the individual elements of the compound construction. To a certain extent, Pipes [41] (1957) reiterated Van Gorcan's paper but included a matrix procedure for combining parallel building elements into a single transmission matrix. With Pipes paper, the essential components of the frequency domain method, periodic heat transfer, frequency analysis and the matrix method, had been formulated.

3.1.2 Response Factor Method

The development of the response factor method can be attributed to a paper by Brisken and Reque [42] (1956) which clearly describes the fundamentals of the method, drawing analogies with the impulse-voltage and subsequent current-response of an electrical circuit. They used 2- lumped thermal models of building elements to generate hourly thermal response factors due to a unit temperature pulse. Based on a linear relationship between the thermal excitation and response, the hourly response to any magnitude of temperature pulse is simply the product of the pre-calculated hourly response factors and the temperature pulse. Hence, the thermal response to a diurnal excitation could be determined by decomposing the excitation into a time-series of unit pulses and then invoking the principle of superposition to sum-up the thermal response to each pulse at each hour. Although the method could be adopted for manual calculations, it was one of the first methods proposed for use on digital computers. Improvements in the accuracy of the method were introduced by Mitalas and Stephenson [43] (1967). A triangular unit pulse replaced Brisken and Reque's rectangular unit pulse to represent a smooth excitation function more precisely. An analytical solution was used to generate the response factors, in contrast to Brisken and Reque's approximate 2-lumped thermal network model. The space long-wave radiation and convection processes were treated separately in contrast to the approximate method using a combined surface radiation and convection coefficient employed by Brisken and Reque. A companion paper by Stephenson and Mitalas [44] described the application of the response factor method to a cooling load calculation procedure. As with the frequency domain

method, the response factor technique can employ the matrix method to model the thermal response of compound building elements. Alternatively, the response factors of the individual homogeneous elements can be combined using the procedure described by Mitalas and Stephenson [43]. In 1971 Stephenson and Mitalas introduced the Z-transform [45] method which gave results (response factors) identical to those given by the response factor method but with about a five-fold reduction in the number of arithmetic operations. Although refinements to the method followed in later years, Mitalas and Stephenson paper of 1967 [43] established the fundamentals of the response factor method.

3.1.3 Finite Difference Methods

The finite difference methods are numerical approximation methods based on representing derivatives by a truncated Taylor series. In the case of building heat transfer, the derivatives of the partial differential diffusion equation, governing one-dimensional heat conduction, are replaced by finite difference approximations. Discretisation of space and time is used to divide the region of interest into discrete elements defined by nodal points. If all room surfaces are assumed to be isothermal, about 40 nodes are required per room. The finite difference equations are derived by setting-up energy balances at all the nodes. The solution of the difference equations provides the temperatures at the nodes. Finite difference techniques may employ explicit, implicit or mixed discretisation schemes. When using finite difference methods, a preconditioning period is required before accurate results can be obtained. The length of the preconditioning period depends on the thermal response of the space or building being modelled. For a mediumweight construction, a preconditioning period of about 18.5 days is required [93].

Whilst the frequency domain and response factor techniques were solely developed to simulate dynamic heat transfer in buildings, the finite difference techniques were in existence for many years prior to their adaptation to building heat transfer. Gröber [46] attributes a German paper by Binder [35] (1910) as the first to provide a solution to Fourier's equation of heat conduction for unsteady heat flow in an infinite plate, using the finite difference technique. Gröber also states the main advantage of the finite difference technique: its application to non-linear heat transfer problems that cannot be solved analytically. This is still the main argument used by current promoters of computer simulation programs based on finite difference techniques. However, practical application and the potentials of the finite difference technique, to the building heat transfer problem,

had to await the introduction of powerful digital computers. Mitalas and Stephenson [44] stated that finite difference techniques 'involved far more arithmetic calculations than the response factor method'. This implied an interest in finite difference techniques at time of publication (1967) but insufficient computer power was available to demonstrate the technique's capabilities. From about the mid-1970's, increasing computer power allowed the development of a number of finite difference based computer simulation programs [47]. Two forms of finite difference based programs have evolved, those based on the explicit finite difference formulation (e.g. SERI-RES and HTB2 programs) and those based on the implicit finite difference formulation (e.g. ESP and DEROB programs) [47]. Since the mid-1970's, progress in the development of finite difference based programs has correlated with increasing computer power. As a consequence confidence in the simulation capabilities of the ESP program has resulted in its research version, ESP-r, being selected as the European reference simulation program for passive solar systems and buildings [48].

3.1.4 Application of the simulation techniques to the physical models

On examining the state of the art physical models it was evident that none can be claimed as precise models of the thermal processes taking place. Some of the physical models, for instance the conduction model, require a mathematical technique to simulate the dynamic energy flows defined by it. The purpose of this section is to identify the additional errors incurred due to applying the mathematical simulation techniques to the physical models.

3.1.4.1 Frequency Domain and Response Factor Methods

The frequency domain and response factor methods are analytical techniques dependant upon the principle of superposition which requires that thermal responses are linearly related to the thermal excitations taking place, and that invariability also applies to the relationship between the thermal excitations and responses. This implies that the frequency domain and response factor methods cannot be used to simulate the dynamic heat flow processes defined by non-linear physical models. In practice, this limitation is overcome by linearizing the non-linear physical models. Assuming constant thermophysical properties, constant air infiltration rates and constant convection heat transfer coefficients are typical measures taken to linearize the non-linear heat transfer processes. An extreme case of linearization is where the surface convection and long-wave radiant exchange processes are combined into a single process using combined convection/radiation coefficient. Mitalas

[49] examined the common assumptions justifying linearization and concluded that except for the combined convective/radiant model, linearizing the physical processes does not incur significant errors in estimating cooling loads and space temperatures. Long-wave radiation is a function of temperature to the fourth power whilst convection can be shown to be a function of temperature differences to the power of about 1.3. Convection processes can therefore be described as mildly non-linear compared to long-wave radiation processes. This suggests that the degree of non-linearity of the physical model is an important factor influencing the magnitude of the error incurred due to model linearisation.

Since the frequency domain method relies on periodic heat transfer, the thermal response is based on a repeating thermal excitation cycle, which is not precisely representative of real weather and internal heat gain profiles over a number of days. When predicting the air-conditioning cooling load, it is usually assumed that the maximum load will occur after a period of hot sunny days and results based on a repeating daily heat gain cycle are normally acceptable. Also, the profile of internal gains are more likely to be similar over a number of days and in well insulated modern office buildings with low façade glazing ratios, the internal gains tend to dominate. If this is not the case, a significant error in the prediction of the thermal response is likely. It can be shown that the simulation process becomes more accurate as longer periods of daily weather and internal gain profiles are used. The required number of harmonics in the discrete Fourier series equals half the number of simulation hours less one [94], 11 harmonics for a 24-hour period and 83 harmonics for 7 days, for example. As the simulation period increases, computer power starts to become the limiting factor. However, reasonably accurate results may be obtained by using fewer harmonics.

3.1.4.2 Finite Difference Method

In contrast to the analytical methods, the finite difference techniques can model non-linear processes and account for temperature-dependant properties. This does not mean that linearizing is not considered when using finite difference techniques. Linearizing may be worth incurring an acceptable level of error if there is a gain in computing speed and time. Rounding and discretisation errors are the main types of error associated with finite difference techniques. Rounding errors occur because computed values are processed using a fixed number of significant digits. Rounding errors can be controlled if the computer is set to process calculations with double-precision arithmetic. However, if the finite difference method is unstable, the error grows exponentially. Discretisation errors are due

to replacing derivatives of the partial differential equations with finite difference approximations, which involves expressing the derivatives by a truncated Taylor series and hence these errors are unavoidable. Discretisation results in a lumped resistance/capacitance thermal model and the magnitude of the error depends on the size of the space and time increments chosen. Generally, discretisation involves dividing a building element, such as the inner block leaf of an external wall, into three slices, a central slice of half the element thickness and two surface slices of a quarter element thickness. In the case of explicit finite difference methods, the maximum time step is limited by stability criteria based on the size of space increment and boundary conditions. Hence, for explicit finite difference methods, the maximum dicretisation error is limited by stability criteria but the probability of a resulting small time step can be costly in terms of computing time. Implicit finite difference formulations do not suffer from such numerical instabilities but large space and time steps can result in significant errors. Alternatively, small space and time steps incur penalties in terms of computational speed with consequent costs in time. A compromise is usually met between accuracy and computational speed/time. Clark [50] compares the effects of space and time discretisation for implicit finite difference formulations and concludes that using three temperature nodes per homogeneous element and time-steps not exceeding one hour, should result in dicretisation schemes meeting an acceptable level of accuracy. Further, in order to solve differential equations efficiently, the time increment can be varied to maintain an acceptable level of accuracy. Hence, with implicit finite difference methods, computational efficiency is the main factor influencing the magnitude of the discretisation error.

3.1.5 Influence of errors on the results

A building and its spaces may be modelled as a complex coupling of a large number of thermal sub-circuits. Due to interaction of this large complex system, it is difficult to assess the effects due to the accumulation of errors. Within a single space, with seven major surfaces, there are a significant number of heat transfer processes being modelled and it is unlikely that all the errors are positive or negative, rather a mixture of both resulting in a degree of error cancellation. It is also possible that for a particular thermal process, the associated error swings from positive to negative over the simulation period tending to reduce the mean error. When determining the total simultaneous cooling load for a floor of inter-linked spaces with different cooling load profiles, a greater degree of error

cancellation probably takes place. The size and complexity of the building thermal network tends to dissipate the effect of model inaccuracies and as a consequence it is difficult to grade the performance of the mathematical simulation techniques when they are applied in practice to actual buildings. To a certain extent, the reduction of the total error due to this error cancellation process, seems beneficial, but does not instil confidence in the use of the thermal simulation programs. Single cell validation methods would seem to be the best option available but unless it is vigorously carried-out with validated measured data, error cancellation between the physical models and the mathematical simulation techniques can go unnoticed. In consideration, sub-model validation should precede whole model validation. Sub-model validation should also help to identify human errors associated with writing the corresponding algorithms and computer programs.

Chapter IV

4.0 DESIGN COOLING LOAD CALCULATION METHODS

4.1 Objectives

The current CIBSE and ASHRAE cooling load methods are examined with the purpose of establishing criteria for developing an improved design thermal analysis method. To achieve this goal, it is necessary to examine the calculation procedures of the methods in detail to determine how each method models the building heat transfer processes. An analytical comparison with the precise physical models will follow. The assumptions adopted, by each method, to justify simplifying the building thermal model, will be examined and compared. The outcome of this analysis should reveal the attributes and deficiencies of the methods and where efficient improvements can be made.

4.2 Background

The main tasks of the design cooling load methods is to estimate design day space peak and building simultaneous loads in order to determine the capacities of local and central air-conditioning plant, and to size system components such as ductwork and pipework distribution systems. The CIBSE Admittance Method [51] and, the ASHRAE Heat Balance and Radiant Time Series Methods [52] are the recommended thermal design tools presented to U.K. and North American Engineers respectively. Whilst the Heat Balance and Radiant Time Series Method are primarily used to determine space cooling loads, the Admittance Method also includes a procedure for predicting peak environmental or dry-resultant temperatures. The CIBSE peak temperature procedure is employed to establish whether there is a risk of overheating and hence a need for air-conditioning or mechanical ventilation. Whilst the Heat balance and Radiant Time Series Methods are used to calculate the cooling load based on air temperature control, the Admittance Method provides the options of calculating the cooling load due to air or dry-resultant temperature control.
The development of the Admittance Method is attributed to Danter [53] (1960), who presented a calculation procedure for estimating the cooling load due to heat flow through a homogeneous element caused by a sol-air thermal excitation. Danter based his method on an approximate method proposed by Mackey and Wright [37] (1944). Danter's cooling load formula expresses the heat flow in terms of the fundamental decrement factor and associated time lag of the Fourier series and the steady state transmittance (U-value).

Loudon [54] (1968) made a substantial contribution to the development of the Admittance Method by presenting a calculation procedure for predicting peak environmental temperatures in buildings without air-conditioning. Environmental temperature replaced the air temperature as an index of thermal comfort. Thermal admittances and solar gain factors were derived to account for heat storage effects and transmitted solar gains to the environmental node respectively. Essentially, the procedure is similar to the current procedure with the exception of specific factors being introduced to convert peak environmental temperature to peak dry-resultant temperature.

The Heat Balance [55] and Radiant Time Series Methods [56] are the latest methods, introduced by ASHRAE, to replace the Transfer Function, CLTD/SCL/CLF and TETD/TA methods [12]. The new methods were the outcome of an ASHRAE funded research project titled, Advanced Methods for Calculating Peak Cooling Loads (1996). The CLTD/SCL/CLF method is a reduced version of the Transfer Function Method and was ASHRAE's simplified cooling load calculation method. ASHRAE's new simplified method, the Radiant Time Series Method, is based on the Response Factor Method. Response factors relate the current value of the cooling load to the current and past values of the heat gains. Transfer functions are similar to response factors but they relate the current value of the cooling load to the current and past values of the heat gains and the past values of the cooling loads. A disadvantage of the Transfer Function based methods is that iteration is required over a number of days before reaching a steady periodic condition, which also requires checking for convergence. In contrast, the Radiant Time Series response factors are generated using a 24-hour periodic excitation pulse, resulting in a series of only 24 response factors called periodic response factors. This is similar to the CIBSE admittance method, in which the resulting cooling load is due to a repeating 24-hour thermal excitation profile. A further development is that the Radiant Time Series Method uses the new concept of periodic radiant time factors to approximate the cooling load due to internal long-wave radiant exchange, internal radiant gains, and transmitted solar gains. By introducing the Heat Balance Method, ASHRAE has taken a new approach to the modelling of dynamic heat transfer in buildings. The Heat Balance Method is fundamentally different from the response factor based methods in that it only uses response factors to model heat conduction through external building elements. Hourly surface temperatures, heat fluxes, and space cooling load are determined by taking energy balances at the external and internal surfaces, and the space air node. The cooling load

produced by the Heat Balance Method is also based on a 24-hour repeating cycle of thermal excitations but it is obtained using an iterative heat balance calculation process rather than solely using periodic response factors as with the Radiant Time Series Method. Although the new ASHRAE Methods are limited in use to design day calculations for predicting peak cooling loads, the methods are found to be computationally more efficient than the transfer function methods. The CIBSE and ASHRAE methods are limited to single zone applications.

4.3 The Principles Underlying the Methods

4.3.1 CIBSE Admittance Method

The Admittance Method consists of a two-part calculation process, the calculation of a mean component and the calculation of a fluctuating component. The principle of superposition is then invoked and depending on the procedure used, the total cooling load or peak temperature is obtained. Figure 4.1, flow diagram of the peak temperature calculation procedure, illustrates this two-part calculation process. In contrast, the cooling

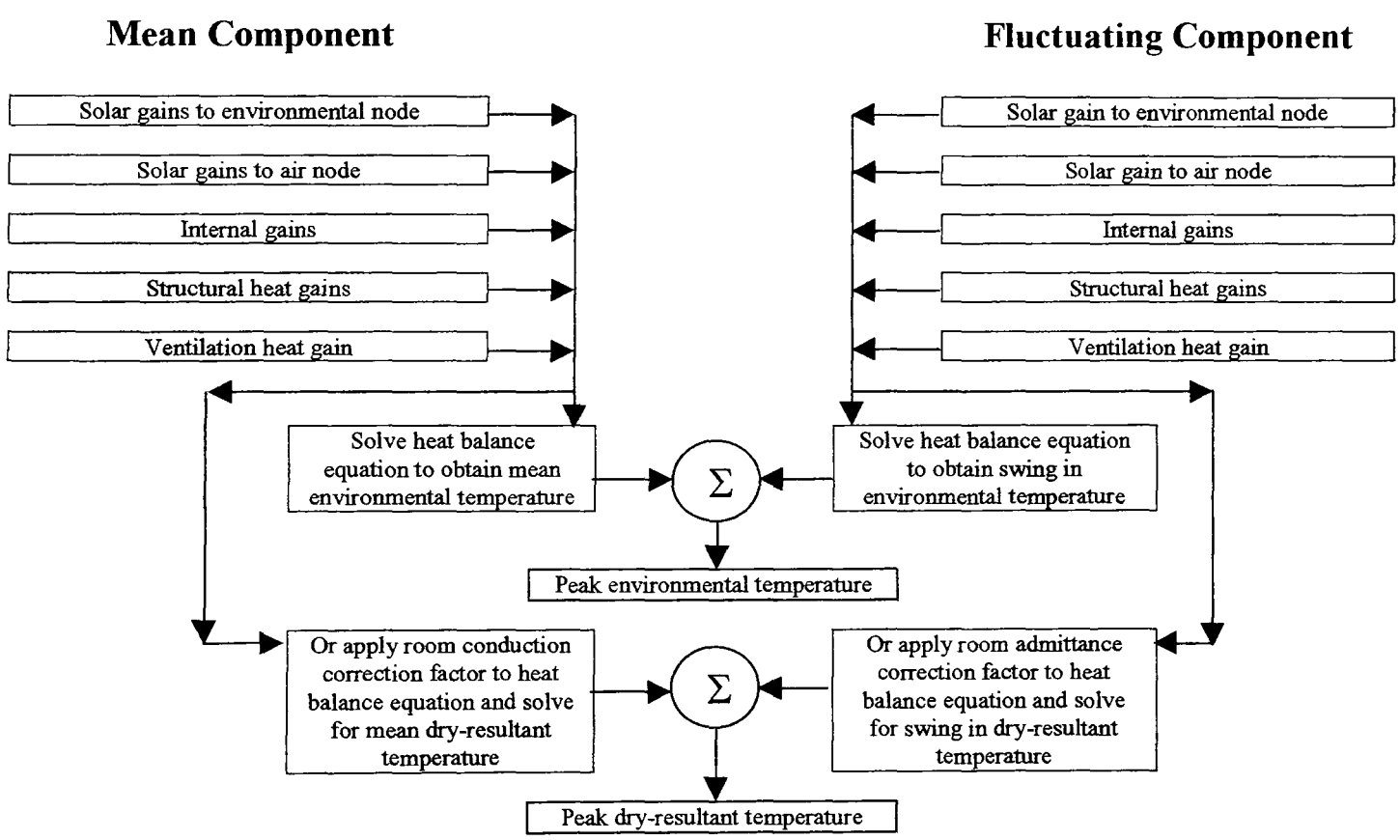

Figure 4.1. Flow diagram representation of the CIBSE Admittance peak temperature calculation procedure

load procedure, illustrated by figure 4.2, indicates a noticeable deviation from the two-part calculation process. This modification is due to simplifying the cooling load procedure for the purpose of manual calculations depending on a substantial amount of pre-calculated

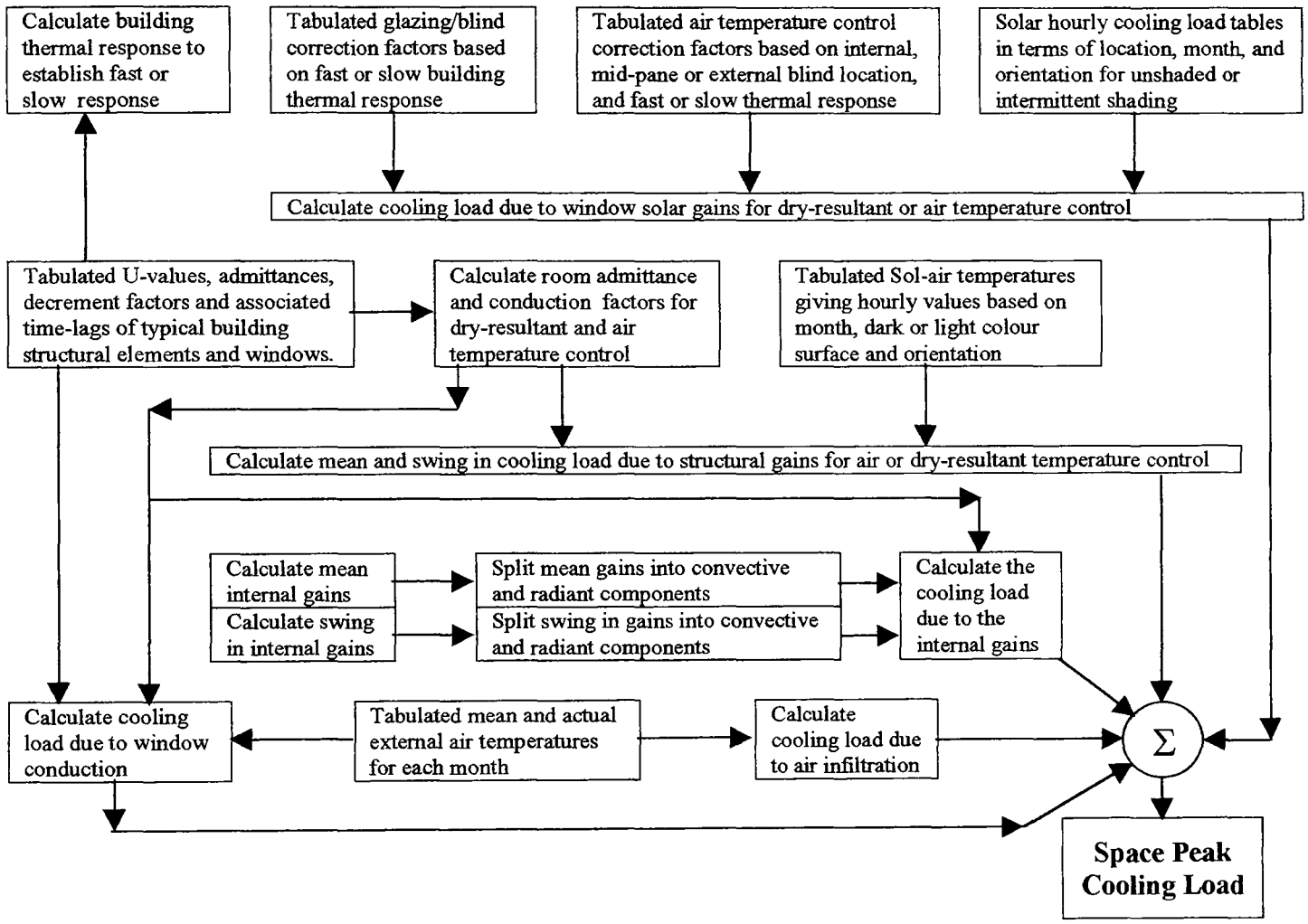

Figure 4.2. Flow diagram representation of the Admittance Method cooling load calculation procedure

tabulated data. Computerised versions of the cooling load procedure are not subject to this constraint and usually model the two-part calculation process. Historically, the Admittance Method has been developed for manual application and for this reason the calculation procedures presented in the CIBSE guide A5 [51], will be examined. Both procedures account for five distinct sources of heat gain; transient conduction through building structural elements, internal heat sources, absorbed and transmitted solar radiation due to fenestration, window conduction and air infiltration. For the cooling load procedure, the mean and fluctuating components are calculated only in the cases of transient conduction and internal heat gains. The cooling load due to transmitted solar, window conduction and

infiltration gains are each calculated using procedures that result in the corresponding total cooling load, rather than the individual mean and fluctuating component loads. In both the cooling load and peak temperature procedures, the calculation of the mean component is based on steady state heat transfer. The heat transfer formulae are expressed in terms of daily mean values of the thermal excitations and building element U-values. The fluctuating component calculation procedure is a simplified version of the Frequency Domain Method. The matrix method is used to combine homogeneous structural elements into thermal transmission matrices representing the thermal behaviour of compound structural building elements. However, only the thermal transmission matrix corresponding to the fundamental harmonic of the Fourier series is used to calculate the fundamental thermal admittances, transmittances, and associated time lags of building structural elements. Thermal transmittances are used to determine the decrement factors and time lags of external building elements. External thermal excitation profiles are not represented by a discrete Fourier series, as in the Frequency Domain Method, but the actual hourly values are formulated with the fundamental decrement factor and associated time lag in order to estimate the structural heat gains. Similarly, internal radiant gains are not transformed into a discrete Fourier series but the actual hourly values are used in estimating their contribution to the cooling load or peak temperature. For structural heat gains, daily mean and mean hourly sol-air temperatures are tabulated in terms of dark and light surfaces, and nine surface orientations per calendar month. The effects of long-wave radiant exchange are included in the calculation of the sol-air temperatures. Internal convection and long-wave radiant exchange heat transfer processes are combined into a single process by employing a combined convection/radiation surface heat transfer coefficient permitting the surfaces to exchange convective and radiant energy with a hypothetical environmental temperature node. Internal heat gains are split into convective and radiant portions, with the cooling load procedure, using specified percentage convective/radiant fractions [14], the convective portion becoming an instant contribution to the cooling load. The radiant portion of the gains is added to the environmental temperature node but because of the formulation of the environmental temperature ($t_{ei} = 2/3\ t_r + 1/3\ t_{ai}$), an implicit 2/3 radiant, 1/3 convective split results. In order to add a purely radiant gain and maintain an energy balance, an additional 50% of the radiant gain is added to the environmental node. To cancel the corresponding convective gain to the environmental node, the same 50% of the radiant gain is subtracted from the air node. In contrast, no convective/radiant split takes

place in the calculation of peak temperature; the total internal gain is added to the environmental node. To account for the influence of absorbed and transmitted solar energy due to fenestration, solar cooling load and solar irradiance tables are provided for the cooling load and peak-temperature calculation procedures respectively. Mean-hourly direct and diffuse solar irradiance and daily mean irradiance values, are tabulated for nine surface orientations per calendar month. Mean and cyclic solar gain factors, evaluated for 25 generic glazing/blind combinations are employed to process the incident solar irradiance into mean and cyclic heat gains at the air and environmental nodes. A detailed derivation of the solar gain factors is given in the CIBSE guide [58]. Environmental-node mean and cyclic solar gain factors account for heat transfer to the environmental node by convection, long-wave radiation and transmitted solar radiation due to purely glazed window systems. Environmental-node, cyclic solar gain factors have been evaluated for thermally lightweight and heavyweight buildings. Internal blinds cause additional convective gains to the air node. Mean and cyclic solar gain factors are provided to account for these gains. The tables of cooling loads have been produced for a thermally lightweight (fast response) building with constant dry-resultant temperature held by plant operating for 10 hours per day during a sunny spell of 4 to 5 days. The cooling loads are also evaluated in terms of unshaded single clear glazing and intermittently shaded single clear glazing. Correction factors for generic glazing/blind combinations evaluated in terms of thermally fast (lightweight) and slow (heavyweight) response buildings, and correction factors for air-point control are provided. The Admittance Method characterises a thermally lightweight building as: 0.8 average surface factor, de-mountable partitioning, suspended ceilings, solid or suspended floor with carpet or woodblock finish. Thermally heavyweight buildings are characterised by 0.5 average surface factor, solid internal walls and partitions, solid floors and ceilings. Surface factors are used to determine the amount of energy readmitted to a space from internal surfaces due to incident transmitted solar radiation. Surface factors are included in the calculation of the environmental-node solar gain factors. The tabulated cooling loads have been calculated using a comprehensive and detailed fenestration model that takes into account the variation of transmitted and absorbed solar radiation with glazing incident angle. The total transmitted solar radiation is assumed uniformly distributed over all space surfaces. An algorithm for the tabulated solar cooling loads and corresponding space details is provided in the CIBSE guide [59]. The product of the appropriate tabulated cooling load, glazed window area and glazing/blind correction factor

gives the solar cooling load, in respect of the dry-resultant temperature control. Alternatively, the solar cooling for air-point temperature control is obtained by multiplying the solar cooling load due to dry-resultant temperature control by an air-node correction factor. For both the cooling load and peak temperature procedures, the infiltration and window heat gain calculations are essentially steady state, using hourly temperature differences, air change rates and window U-values. In the case of the peak temperature procedure, figure 4.1 shows that all the heat gains are formulated into mean and fluctuating heat balance equations that are solved for environmental or dry-resultant temperature. The mean and fluctuating components are then summed to give either the peak environmental or dry-resultant temperature. In contrast, figure 4.2 shows that the design cooling load, using the manual calculation procedure, is not obtained by a heat balance but by simply summing the components of the cooling load. With the Admittance Methods, judgement is required to establish the times and month that the individual space peak and building simultaneous cooling loads and peak temperature will occur. This is of little concern when a computer program version is used.

4.3.2 The Heat Balance Method

Essentially, the Heat Balance Method consists of four thermally linked distinct processes as illustrated in figure 4.3. The thermal behaviour of each external building element, such as a wall, is modelled by an external surface heat balance that is thermally linked to a wall conduction process, which is linked to an inside surface heat balance with a convective connection to the zone air node. The external surface heat balance formulates the relationship between the external thermal excitations and the wall transient conduction process. Similarly, the inside heat balance describes the relationship between the wall conduction process and the internal surface thermal driving forces. The space air heat balance forms the nucleus of the thermal network, connecting all the inside surface heat balances with the casual convective and air infiltration gains, and the air-conditioning cooling load. The heat balance equations are solved for each surface per hour, but to simulate the design cooling load due to 24-hour periodic thermal excitations, an iteration process, requiring four to six surface iterations to establish convergence, is required. The iteration run incorporates a double iteration process, iteration through all the surfaces per

hour followed by iteration through the 24 hours of the day. The iterative heat balance process helps to simulate the non-linear heat transfers, such as, surface radiant exchange and surface convection. The space model can include up to twelve surfaces consisting of

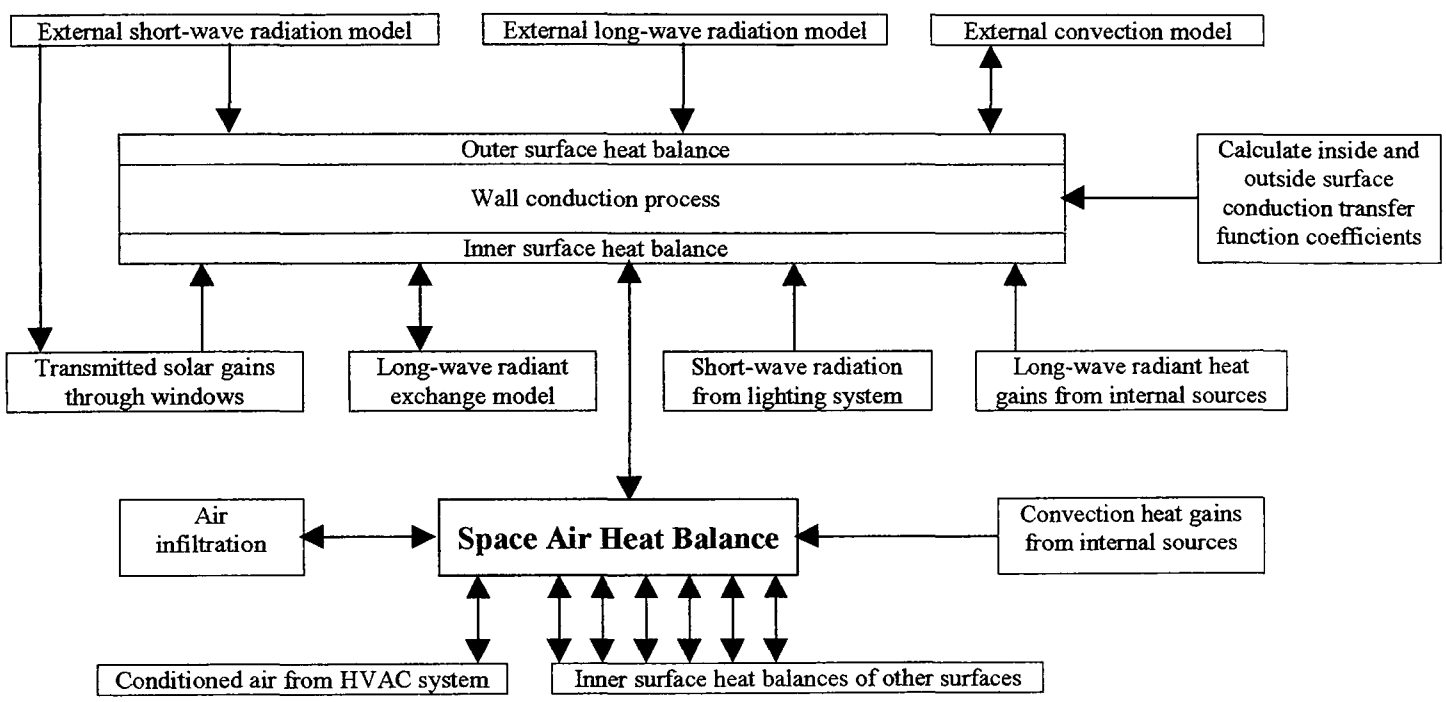

Figure 4.3. Flow diagram representation of the Heat Balance Method cooling load calculation procedure

four walls, roof or ceiling, floor and a thermal mass. Each wall may include a window, the roof, a skylight. The thermal mass can include furniture or de-mountable partitions. The area of any of the surfaces can be set to zero if it does not form an actual surface in the model. The wall conduction process is formulated using conduction transfer functions (CTF's) which relate conductive heat fluxes to current and past surface temperatures and past heat fluxes. CTF's are similar to thermal response functions and consist of a series of CTF coefficients, the total number of coefficients depending on the length of the iteration process required to establish the steady state periodic cooling load. Surface convection coefficients are not included in the calculation of the CTF's, allowing inclusion of the coefficients within the external and internal convection physical models. Figure 4.3, flow diagram of the calculation procedure, illustrates the physical models, defining the external and internal thermal excitations that are included in the surface heat balances. Although specific physical models are used in the software program, the authors do not recommend

any particular model to be used, suggesting only that accurate physical models should be adopted. Two accompanying papers describe optional external [60] and internal [61] physical models that may be used in the Heat Balance Method. Currently, the MRT/Balance procedure [61] for estimating long-wave radiant exchange between internal surfaces has been adopted. The mean radiant temperature (MRT) formulation models radiant exchange between a particular surface and a fictitious surface representing the other surfaces in view of the surface. Weighted averages of the temperatures, areas and emissivities of the other surfaces in the zone are used for the fictitious surface. This approximation incurs a radiation energy imbalance that must be redistributed uniformly over all surfaces to conserve energy and correct the error. Although the MRT/Balance is an approximation procedure, it can account for furniture and other non-structural surfaces in the radiant exchange process, which may be difficult to include in precise radiant exchange models, due to the frequent rearrangement of furniture. The internal convection physical model uses constant surface coefficients but other, more sophisticated models, may be employed. Since the conduction transfer functions governing the transient conduction processes do not include external or internal convective coefficients, variable surface coefficients can be generated and continuously updated via the iterative heat balance calculation process. Long-wave radiation from internal sources is not treated in a realistic manner, due to the practical difficulty of obtaining equipment surface temperatures. A traditional approach is taken; the internal gains are split into convective and radiant portions using fixed convective/radiant fractions. The convective portion of the gains is assumed to contribute instantaneously to the cooling load and therefore, appears as a convective flux in the space-air heat balance equation. The radiant portion of the gains is distributed uniformly over all internal surfaces and is therefore included in the surface heat balance equations. If required, other radiant flux surface distribution patterns can be adopted. Solar heat gain due to fenestration is evaluated, using solar transmittance and solar heat gain coefficients (SHGC) of the glazing system. The solar energy, absorbed by the glazing system, gives rise to convection and long-wave radiation transfer from the window surface to the zone air and other room surfaces respectively. The SHGC accounts for both the transmitted solar radiation and the inward flowing fraction caused by solar radiation absorbed by the window system. Subtracting the solar transmittance from the SHGC approximates the inward flowing fraction; multiplying this fraction by the incident solar beam, gives the inward flowing heat due to the absorbed solar beam. A similar procedure,

using diffuse parameters, gives the inward flowing heat due to diffuse solar radiation. The total inward flowing heat, due to both the absorbed beam and diffuse solar energy, is then added to the window conduction process in order to take part in the surface convection and long-wave radiation processes. The transmitted beam solar radiation is obtained from the product of the glazing system solar transmittance and the incident beam solar radiation intensity. Similarly, the transmitted diffuse solar radiation is determined using the diffuse solar transmittance and diffuse solar irradiance. The transmitted beam solar radiation is assumed incident and uniformly distributed on the floor, and the transmitted diffuse component is assumed uniformly distributed over all surfaces. If required, more sophisticated distribution patterns may be used.

4.3.3 The Radiant Time Series Method

The Radiant Time Series Method resembles the Transfer Function Method [63] in terms of calculation procedure. Figure 4.4 illustrates the Radiant Time Series calculation procedure. The calculation of the heat gains due to external and internal excitations is identical to that

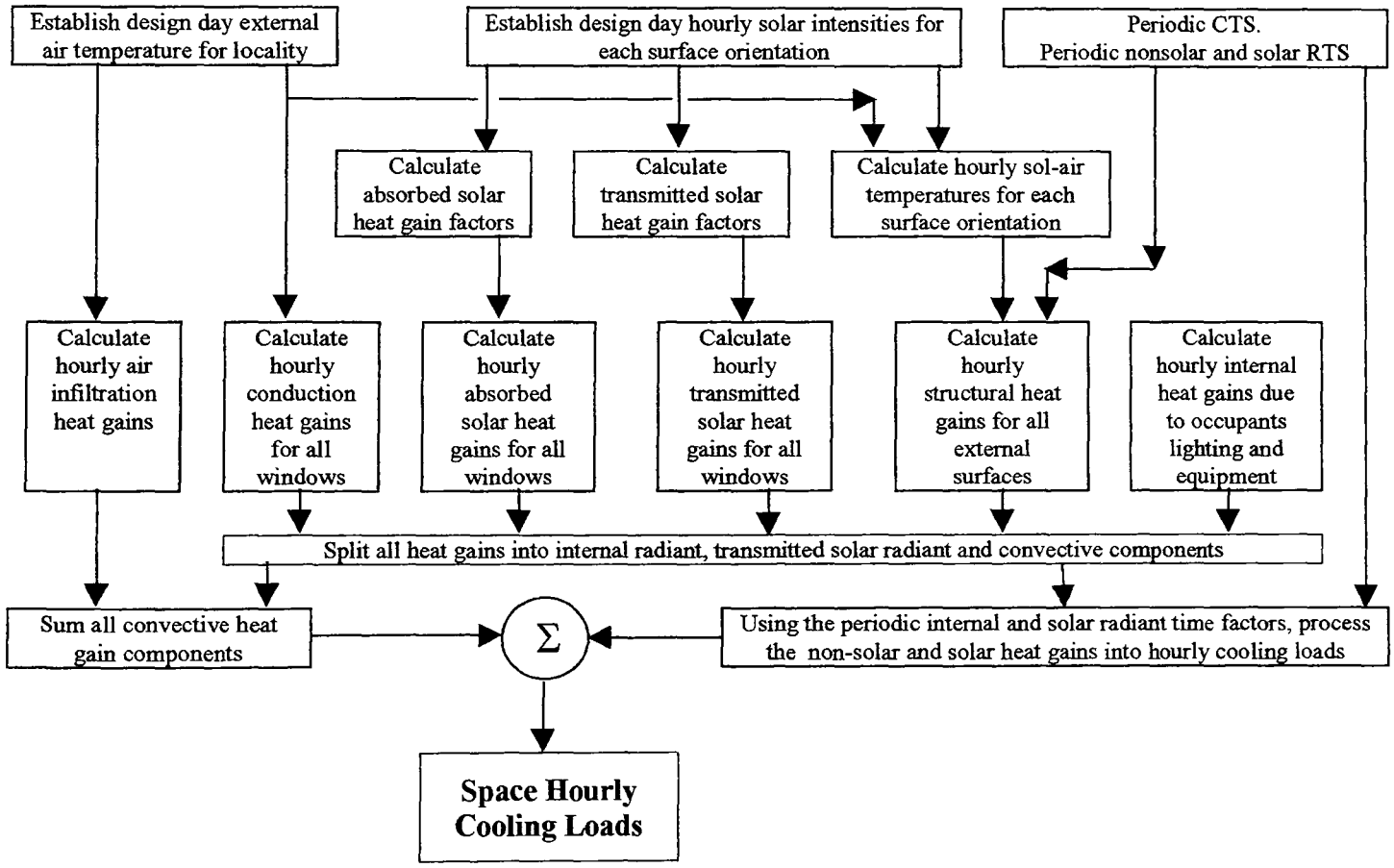

Figure 4.4. Flow diagram representation of the Radiant Time Series calculation procedure

of the Transfer Function Method, except for the calculations of gains due to heat conduction through the zone external structural elements. The other significant difference between the two methods relates to the processing of the conduction, transmitted solar and internal heat gains into convective contributions to the cooling load. For heat conduction processes, conduction time factors (CTF's), which are periodic response factors divided by the corresponding U-value of the construction, are used to compute internal surface heat gains. For a 24-hour periodic thermal excitation, there are 24 CTF's in a conduction time series (CTS). The ASHRAE Fundamentals Handbook [52] tabulates CTS for 35 wall and 19 roof standard constructions. The internal surface conductive heat gains are split into convective and radiant proportions using typical specified percentage values (ASHRAE specifies 37%/63% convective/radiant split for conductive heat gains). The convective portion of the gains is directly applied to the zone air node and therefore becomes an instantaneous cooling load. The contribution to the design cooling load due to the long-wave radiant exchange process taking place between a surface and the other space surfaces is approximated by applying radiant time factors (RTF's) to the radiant portion of the surface conductive gains. RTF's are similar to periodic response factors and are generated by thermally exciting a heat balance model of a space with a periodic unit pulse of radiant energy under adiabatic external wall conditions. A slight overestimate of the cooling load results due to the adiabatic boundary conditions. Similar to the conduction time series (CTS), there are 24 radiant time factors in a radiant time series (RTS) and their values vary with each type of zone construction and geometry. The profile of the radiant time series is also influenced by the method of distribution of the radiant flux over space surfaces. For practical purposes, only two radiant flux distribution patterns are employed. It is assumed that the solar transmitted beam is distributed uniformly over the floor. Diffuse solar radiation and internal radiant gains are assumed uniformly distributed over all the space surfaces. To generate the solar radiant time series, a periodic unit pulse of radiant energy is applied to the floor. In the case of non-solar radiant gains, a unit pulse of radiant energy is applied to all the space surfaces to produce the nonsolar radiant time series. The ASHRAE Fundamentals Handbook [52] tabulates nonsolar and solar RTS values in terms of light, medium and heavyweight construction, with and without carpet, and with 10%, 50% and 90% glazing. Similar to the conduction heat gains, internal gains are split into convective and radiant portions; the actual percentage split depending on the type of heat gain source. The convective portions become an instantaneous contribution to the design

cooling load and the radiant portions are processed using the nonsolar RTS to determine their time-lagged convective contribution to the design cooling load. The window heat gain calculation procedure accounts for transmitted and diffuse solar gains, and conduction heat gains. Solar heat gain coefficients, SHGC(θ) and $(SHGC)_D$, are used to determine the transmitted and diffuse components respectively. The direct solar radiation is processed with the SHGC(θ) to determine the transmitted solar gains. The sum of the diffuse and ground reflected solar radiation is processed with the $(SHGC)_D$ to determine the diffuse solar gains. If an internal shading device is used, the three components of the window heat gains are summed and then split into 37% convective and 63% radiant portions. The convective portion is assumed an instantaneous contribution to the cooling load. The radiant portion is processed using the nonsolar RTS to calculate its contribution to the cooling load. If there is no internal shading device, only the diffuse and conductive components of the gains are summed and their contribution to the cooling load is determined as previously described. The transmitted solar gain is assumed 100% radiant and it is processed using the solar RTS to determine the contribution to the design cooling load. The hourly air infiltration convective gains are summed with all the above corresponding hourly contributions to the cooling load to produce the periodic design cooling load profile. The main advantage of the Radiant Time Series Method is that the design cooling load can be computed without taking heat balances, or employing iterative calculation techniques.

4.4 Comparing the Methods

4.4.1 Establishing the Criteria for Comparing the Methods

The accurate performance of a prediction method depends on the sophistication of the physical models and mathematical techniques adopted, and the type of computational tool on which the method has been developed. An ideal prediction method would not compromise the accuracy of the physical models and the performance of the method would then depend solely on the accuracy of the physical models employed. In practice a compromise is usually adopted when considering which mathematical simulation technique and computational tool are to be used. The extent of the compromise is revealed by:

1. The assumptions underlying the method.

2. The recommended calculation method.
3. The simplifications of the physical models employed.

A clarification is required regarding item 3. If the prediction method is to be employed as a design tool for the purpose of plant sizing and checking peak temperatures, then some relaxation regarding the accuracy of some of the physical models may be justified. It is not essential that the solar, internal gains and external air temperature models produce exact thermal excitations that will occur on a particular day of the year. What is essential is that the models can predict thermal excitations that are representative of the type of daily thermal excitation profiles that would produce design day cooling loads and peak temperatures. However, to differentiate the thermal responses of zones with different thermal characteristics, subjected to the same thermal excitations, it is essential to accurately model the thermal behaviour of the zone. This requires accurate physical models of the modes of heat transfer, a comprehensive window model and an accurate infiltration/ventilation model.

4.4.2 The Assumptions Underlying the Methods

Common to all dynamic thermal models are the assumptions made to simplify the heat transfer processes taking place. The common assumptions made in the case of both the CIBSE and ASHRAE methods are:

1. Design cooling load calculations are performed for a single 24-hour peak design day. Previous days are identical to the peak design day. Hence, thermal excitations are periodic resulting in a periodic response.
2. The zone air is modelled as well mixed with negligible capacity and uniform temperature.
3. All surfaces are isothermal.
4. Each layer of a building element is homogeneous and its thermophysical properties are constant.
5. All surfaces are grey and diffuse with absorptivity and emissivity invariant with temperature. Emitted and reflected radiation is diffusely distributed.
6. One-dimensional heat conduction takes place.
7. Long-wave and short-wave radiation from internal sources are uniformly distributed over all internal surfaces.

8. All convective heat gains to the zone air node are assumed instantaneous contributions to cooling load.

With the Radiant Time Series Methods, internal convection is based on a set of constant coefficients. Although the Heat Balance Method uses constant coefficients, variable coefficients can be used, if a more sophisticated internal convection model is employed.

In the case of the Admittance Method, internal surface convective and long-wave radiant exchange are assumed a single process taking place between each surface and the environmental temperature node. A set of combined convective/radiant heat transfer coefficients, each with a fixed value, is used in the model.

In the Heat Balance and Radiant Time Series Methods, the transmitted direct solar beam is assumed incident and uniformly distributed on the floor while the diffuse component is assumed uniformly distributed over all the internal surfaces. In contrast, the Admittance method has both the direct and diffuse solar radiation uniformly distributed over all internal surfaces.

The Heat Balance and Radiant Time Series Methods assume that the long-wave radiant exchange process between internal surfaces is non-participating with the zone air. With the Admittance Method, the long-wave radiant exchange process participates with the environmental node, which incorporates both mean radiant and air temperatures.

4.4.3 The calculation methods

The CIBSE guide A5 [51] presents its peak temperature and cooling load methods as manual calculation procedures suitable for use with hand-held calculators. To support manual calculations, much pre-calculated tabulated data encompassing thermal excitations, compound thermophysical properties and thermal factors are available (See figure 4.2). Commercial computer software programs of the CIBSE methods are available but are essentially only computerised versions of the manual methods. In principle, ASHRAE's Radiant Time Series Method can be used for manual calculations but the use of a computer spreadsheet program is recommended due to the large volume of calculations required. The ASHRAE Fundamentals Handbook [52] includes pre-calculated conduction time series for a variety of standard wall and roof constructions. Pre-calculated nonsolar and solar radiant

time series, for a variety of zone constructions and percentage glazing, and other supporting tabulated data required for manual or computer spreadsheet application, are included. As the name suggests, the Heat Balance Method is similar in complexity to building simulation programs such as ESP and BLAST regarding the solving of sets of simultaneous heat balance equations to give surface and space air temperatures, and heat fluxes. Solar, external convection, external and internal long-wave radiation physical models are also included. Only computer program implementation of the Heat Balance Method is practical. The method is coded in the software called Hbfort [57].

4.4.4 Simplification of the Physical Models

4.4.4.1 The transient conduction model

The Heat Balance Method employs conduction transfer functions (CTF) to model heat conduction through building structural elements. Since exact analytical techniques are used to generate the CTF coefficients, the conduction process is modelled quite accurately. Due to surface convective coefficients not being included in the computation of the CTF's, a purely conduction process is modelled and the accurate prediction of surface temperatures and heat fluxes is not compromised if a variable convection model is employed rather than using fixed value coefficients. The Radiant Time Series Method employs periodic conduction time series, which are generated using the Heat Balance Method, to model transient conduction. However, to simplify the subsequent calculation of the convective and long-wave radiation processes, a combined convective/radiant surface coefficient is included in the CTF. Also, it is necessary to select the closest pre-calculated CTF's of the standard constructions to match the actual zone structural elements. Due to these factors, the Radiant Time Series conduction process is less accurate than the Heat Balance Method. Similar to the constraint imposed on the Radiant Time Series Method due to using pre-calculated CTF's, the Admittance Method uses decrement factors and associated time-lags of standard constructions to determine conductive heat flows. A further inaccuracy occurs due to using only the fundamental harmonic of thermal transmission matrices resulting in one complex decrement factor out of eleven being used to model the conduction process. A combined convective/radiant surface coefficient is included in the fundamental transmission matrix and U-value. A further deviation from the parent Frequency Domain Method is the use of actual values of sol-air temperature rather than using the corresponding Fourier series to represent the thermal driving force. In contrast, the Radiant

Time Series conduction procedure does not deviate noticeably from the Response Factor Method on which it is based. The Admittance Method's calculation of the mean component is based on steady state heat transfer, which accurately models the daily mean thermal response of a zone and is a distinct advantage of the two-part calculation method.

4.4.4.2 Internal convection and long-wave radiation models

The Heat Balance Method models the convection and long-wave radiation processes separately. Although sophisticated models can be used, only the current models adopted will be examined. A set of fixed convection coefficients is used to link all inside surface temperatures to the air-node temperature. This linearized version is therefore an approximation of the non-linear convection process. Long-wave radiant exchange between surfaces is approximated using the MRT/Balance procedure. A comparison between the MRT/Balance and the exact radiant exchange procedures [61] showed, for a range of tests, that the approximate method over predicted the peak cooling load between 6.88% and 6.97%. The conclusions also drew attention to the ability of the MRT/Balance method to account for furniture, equipment and occupants, which may significantly influence radiant exchange, but are very difficult to model using exact procedures. The accuracy of the MRT/Balance method also relies on the assumption of small differences between room surface temperatures. Window surface temperatures, especially with internal shading devises, can be at significantly higher values than the other room surface temperatures. The assumption of all solar transmitted radiation being incident on the floor seems also to invalidate the assumption of closely matching surface temperatures. Both the Admittance and Radiant Time Series Methods use combined convection and radiation coefficients but differ in the manner in which the coefficients are used to process the heat flows. The Admittance Method uses the coefficient to transfer the convective and long-wave radiation to the environmental node resulting in an implicit 2/3 radiant to 1/3 convective split of the gains. Considering accurate representation of a space's thermal behaviour, this fractional split remains constant and is therefore insensitive to the geometric and thermal characteristics of the actual space being modelled. The Radiant Time Series Methods treats inner zone surfaces gains in a similar manner to internal gains by assuming a fixed 37% convective to 63% radiant split. This convective/radiant split is similar to the Admittance Method split, but the Radiant Time Series Method goes a step further by using the nonsolar radiant time series to determine, for each hour, the time-lagged convective portion of the

long-wave radiant gain that contributes to the cooling load. Because the radiant time series values are generated in a similar way to thermal response factors, they are reasonably sensitive to the thermal characteristics of the space being modelled. However, an overestimate of the cooling load is anticipated due to the calculation of the radiant time series being based on external surface adiabatic boundary conditions.

4.4.4.3 External convection and long-wave radiation models

The Heat Balance Method models external convection quite accurately by using a convection coefficient formulation that correlates with wind speed and surface to air temperature difference. The method's approach to modelling external long-wave radiation exchange is simpler due to assuming that the sky temperature is 6 K below the external air temperature and that the ground temperature equals the air temperature. The Admittance and Radiant Time Series methods use a combined external surface coefficient to model the external convective and long-wave processes, and both methods employ sol-air temperature as the thermal excitation. While the Admittance method's sol-air temperature model includes a complex long-wave sub-model [28], the Radiant Time Series method uses a much simpler model by assuming zero long-wave radiant exchange for vertical surfaces and a constant negative value for horizontal surfaces [66].

4.4.4.4 The window model

Both the Heat Balance and Radiant Time Series methods use solar heat gain coefficients [64] to determine window solar gains. The direct and diffuse radiation solar heat gain coefficients, SHGC(θ) and $(SHGC)_D$, each account for the transmitted solar radiation and the inward flowing fraction caused by solar radiation absorbed by the window system. Absorbed solar energy raises the glazing temperature (and internal shading device if included) and the inward and outward conducted heat is driven by temperature differences. Pre-calculated SHGC's are based on specific boundary conditions and are therefore insensitive to the actual external and internal surface temperatures (generated by the surface heat balances) driving the window conduction process. The direct application of these coefficients causes an error to occur, due to the absorbed, as well as the transmitted solar energy being distributed directly onto the room surfaces. The Heat Balance Method introduces a modification to the traditional calculation process employing the solar heat gain coefficients to reduce the error. The transmitted solar energy is calculated using

glazing solar transmittance values, based on solar beam incidence angles, and a hemispherical diffuse transmittance. The absorbed solar energy is approximated, using the modified calculation procedure and the result is added to the window conduction heat gain. This approximation is carried-out for both the direct and diffuse radiation components. The coefficients are used directly without modification in the case of the Radiant Time Series Method. The method overestimates the transmitted solar radiation because the SHGC(θ) accounts for both the transmitted and inward flowing heat gain due to solar energy absorbed by the window. The absorbed solar energy contributes to the window conduction process and, in time, contributes to the window surface's convective and long-wave radiant exchange processes and should not be included with the transmitted solar radiation. All the diffuse solar radiation is assumed absorbed by the window system to compensate for the missing absorbed solar energy. This is not an accurate representation of the actual heat transfer processes taking place. The procedure adopted in the Heat Balance Method, for estimating the solar gains, could be deemed more suitable for the Radiant Time Series Method. A reconciling feature is that the solar and nonsolar time series, employed to process the solar gains into cooling loads, were generated using the Heat Balance Method and they cover a comprehensive range of space thermal characteristics. Simpler procedures for estimating the effects of solar gains were developed because of the Admittance Method's reliance on manual calculations. The tabulated hourly cooling loads were calculated for a specific thermally lightweight, building room model, with and without an internal shading device. Averaged correction factors are provided for determining the hourly cooling loads due to using other window systems and are only evaluated for lightweight and heavyweight constructions. Similarly the peak temperature procedure uses tabulated solar gain factors based on only thermally fast and slow response buildings. Long-wave and short wave radiation processes are combined and processed using a single alternating solar gain factor. The alternating solar gain factor varies considerably throughout the day [65] but values are only calculated for conditions around the time of peak gain. Air-point solar gain factors are provided for windows with internal blinds only, implying that convection due to purely glazed systems is insignificant. The peak temperature heat balance includes the total thermal admittance of the space, therefore, compared to the cooling load method, the peak temperature procedure relates more to the thermal characteristics of the space being modelled. Neither the ASHRAE or CIBSE methods account for external long-wave radiation in their window models. Glazing

temperatures in summer (and winter) are generally significantly higher than external environmental temperatures and if not taken into account, can result in significant errors.

4.4.4.5 Internal gains

The ASHRAE and CIBSE methods adopt similar procedures regarding estimation of the internal heat gains and the manner in which the heat gains are split into their convective and radiant fractions. After the convective/radiant split, each method employs a different technique in processing the heat gains into cooling loads. If used appropriately, the Heat Balance Method should product the most accurate results. The Radiant Time Series Method employs sets of nonsolar radiant time series, which are generated by the Heat Balance Method for a comprehensive range of space thermal characteristics. Results should closely match the parent method. However, external surface adiabatic boundary conditions are used in the generation of the radiant time series resulting in an overestimation of cooling load. The Admittance method processes the convective portion of the internal gains into cooling loads in a similar manner to the ASHRAE methods but uses a very simple approach when dealing with the radiant component. The radiant gains become an instant cooling load to the environmental node, without being influenced by the thermophysical properties of the space surfaces. This is in contrast to the method's treatment of solar gains, where surface factors are used to process the transmitted solar gains into cooling loads at the environmental node.

4.4.4.6 Air infiltration and ventilation

The ASHRAE and CIBSE cooling load methods all assume that the air infiltration heat gain becomes an instantaneous cooling load. A further assumption is that the summertime infiltration gain is relatively small and a constant infiltration rate is usually adopted; the Admittance method cooling load tables are based on 0.25 air changes per hour [59]. The Admittance peak temperature procedure can include for daily mean ventilation rates due to a number of window-opening options. The simplicity of the model deems that it can only be relied upon to provide indicative results when comparing design options.

Chapter V

5.0 CRITERIA FOR DEVELOPING A DESIGN THERMAL ANALYSIS METHOD

A new building thermal design method should, at a minimum, match the performance of the best of the current methods and have the potential to achieve more. To achieve this goal, it is necessary to set clear objectives by establishing criteria for developing the new method and to source a suitable calculation tool for its implementation. Assumptions regarding the application of the new method can then be drafted.

5.1 Basic criteria relating to the current cooling load design methods

Comparing the current cooling load design methods and examining the accuracy of the physical models employed by each has revealed their attributing and deficient features. Highlighting these positive and negative aspects of the current methods will help formulate the basic criteria required for developing the new design method. A new design method must, as a minimum requirement, achieve the attributes and include improvements regarding the deficiencies of the existing methods.

The CIBSE Admittance method can be employed to estimate the cooling load and peak-temperature of a space. Including these outcomes and surface temperatures should help designers to analyse in more detail thermal comfort and solutions for passively cooled buildings, mixed mode and traditional air-conditioned buildings.

A notable feature of the Radiant Time Series Method is that contributions to the cooling load can be determined explicitly, without the need for heat balances or numerical iteration procedures. The ASHRAE Heat Balance Method integrates iterative techniques with its heat balance formulations to simulate non-linear heat transfer processes. The majority of heat transfer processes taking place in buildings are moderately to highly non-linear processes. The Admittance's peak temperature procedure and the Heat Balance Method demonstrate the benefits of heat balance formulations that describe the relationship between the thermal excitations and thermal characteristics of the space. Explicit, iterative and heat balance calculation techniques all possess certain attributing features and should, where appropriate, be included in the new design method.

The developers of the ASHRAE Heat Balance Method have demonstrated that when modelling transient conduction, it is beneficial to exclude the convective heat transfer coefficients from the conduction process of structural elements in order to treat surface convection more precisely as a non-linear process. Including the convection coefficient in the overall thermal transmission matrix of a structural element, is a deficiency of the frequency domain method. The thermal transmission matrix should include only constant thermophysical properties in order to accurately model dynamic conduction processes in solids. Finite difference methods do not suffer from this problem and variable convection coefficients may be included in its heat balance formulations.

All the current cooling load methods use an approximate internal long-wave radiant exchange model. In the case of a single zone method, the employment of a more accurate long-wave radiant exchange model should be aimed for.

ASHRAE's Heat Balance Method accounts for the thermal influence of internal mass due to movable partitions, furniture, equipment etc. Such items can account for up to 10% of the internal thermal mass and should be included in the room model.

Constant internal surface convection coefficients are used in both the ASHRAE and Admittance methods. It should be possible to include a variable convection coefficient model to match the requirement for an accurate internal long-wave radiant exchange model.

The Heat Balance Method's external convection model correlates with wind speed and surface to air temperature difference. This model is the preferred option, especially in the case of window surfaces where the convection coefficients have a dominating influence on the conductive and convective heat transfer processes.

ASHRAE's Heat Balance Method models transmitted solar radiation quite accurately. None of the methods accurately model the conductive and convective processes due to absorbed solar radiation in the window system. A calculation procedure representative of the actual heat transfer processes taking place, should be aimed for.

The ASHRAE method's assumption of all transmitted solar radiation being incident on the floor, could be deemed logical, having regards to the high solar altitude angles experienced in North American climates. It is envisaged that the new design tool will be used for a wide range of climates and times of year. In particular cases, the solar-room geometric relationship may not always result in the beam being mainly incident on the floor. A number of options regarding the solar beam distribution pattern should be made available or a simple procedure for establishing solar beam position should be developed.
In modern buildings the internal heat gains may contribute significantly to the total space heat load, warranting an accurate calculation of the corresponding cooling load.
ASHRAE's Heat Balance Method accurately calculates the contribution to the cooling by including the convective and radiant portions of the internal heat gain in the air node and surface heat balance equations respectively.

Summarising these comments establishes the basic criteria for developing the new design method.

1. Include cooling load, air and surface temperature calculation procedures within a single method.
2. Use explicit type calculation procedures, where possible, to improve computational efficiency.
3. Use heat balances/iterative techniques for simulating non-linear processes.
4. Employ separate pure conduction and convection models in order to process the associated heat transfers more accurately.
5. Use accurate convection and long-wave radiant exchange models.
6. Account for internal thermal mass due to furniture etc.
7. Require accurate calculation of heat transfers due to absorbed solar radiation in window systems.
8. Adopt flexible approach regarding transmitted solar beam distribution pattern.
9. Include the convective and radiant portions of the internal heat gains in the air node and surface heat balance equations respectively, to accurately calculate the subsequent cooling load.

5.2 Additional criteria

A major factor influencing the performance of a current thermal design method is the calculation tool it has been designed for implementation on. ASHRAE's Heat Balance Method would be deemed the most accurate of the design methods due to it being coded into a computer software program. With a computer software program, only minimal parameter input is required. Calculations processed on a hand-held calculator or a computer spreadsheet program are completely under the control of the user. With both calculation tools, the user must input all formulae and parameters. ASHRAE's Radiant Time Series Method is a manual design procedure that employs a computer spreadsheet program as its calculation tool. It does not use the full potential of the tool, only employing its arithmetic functions, though at this low level of application the computer spreadsheet is far more powerful than the hand-held calculator, on which the CIBSE manual Admittance method is based. Hand-held calculators contain approximately eighty mathematical functions. A single spreadsheet cell has approximately 330 functions available to it. Each spreadsheet file contains 230 columns, and 65,536 rows, summing to over 15 million cells; i.e., 15 million calculators linked together. This arsenal of computational power allows great potential for developing a design thermal analysis method not compromised by oversimplifying the fundamentals. The full potential of spreadsheet programs for engineering design calculations has not yet been realised by the engineering community at large. Trigonometric, hyperbolic, complex numbers and matrix operation functions together with numerical iteration capability and logic functions are the important mathematical components required for dynamic thermal modelling of buildings. A suitable computer spreadsheet program possesses these mathematical components. Generally, the user cannot modify a computer simulation software program. A computer spreadsheet based design method has innate flexibility in the manner in which it can be modified or extended to suit a particular design problem. It is possible to widen the scope of application of a thermal analysis design method, using this calculation tool. Computer power and the ability of the user are the only limiting factors influencing the scope of application. The application of computer spreadsheet programs to building thermal modelling bridges the enormous gap between the performance of hand-held calculator and a building thermal simulation software program. The following additional criteria, for developing a new design method, gives an insight into the capabilities of a computer spreadsheet program for building thermal analysis.

5.2.1 Thermal comfort sub-model

The ASHRAE and CIBSE methods determine design cooling loads or peak temperatures to meet specific inside design conditions relating to a thermal comfort index; CIBSE employing dry-resultant temperature and ASHRAE using air temperature. These are inadequate thermal comfort criteria considering the current trend for a wider choice of design solutions compared to the traditional convective cooling air-conditioning solutions. The new design thermal analysis method should include a more rigorous thermal comfort analysis tool, especially in the case of designing a natural ventilated building. Surface temperatures, average space air velocity and air temperature need to be determined and provided as inputs to the thermal comfort model. With the additional parameters, a thermal comfort model, similar to Fanger's model [84], can be employed as an optional link to the building thermal model.

5.2.2 A wider choice of design solutions

The new design tool should be developed to simulate the space response due to chilled ceilings, free cooling via mechanical ventilation, natural ventilation, mixed mode cooling systems, traditional air-conditioning systems and passive thermal control devices.

5.2.3 A radiant exchange surface view factor sub-model

One of the basic criteria requires that an accurate internal long-wave radiant exchange model should be employed, an essential requirement if a chilled ceiling or other type of radiant cooling system is to be modelled. To achieve this goal, a sub-model is required to compute the space surfaces' radiant exchange view factors.

5.2.4 Levels of complexity

ASHRAE developed two new cooling load methods, a relatively complex and a less complex version, to span the range of needs of its HVAC industry. A need for a variety of design tools, offering different levels of sophistication, is also evident in the variety of commercially available software packages. An alternative means of meeting the range of needs is to develop a single design method that can be employed at a number of levels of complexity. The level adopted will depend on the level of analysis required, ranging from indicative to an accurate prediction.

5.2.5 Include for multi-zone analysis

The ASHRAE and CIBSE methods have primarily been developed for single zone models. These methods may be adequate for an airtight air-conditioned building where the majority of spaces are controlled at the same set-point temperature. Spaces in a naturally ventilated building are generally not at the same temperatures with heat transfers and ventilation exchange taking place between spaces. Multi-zone analysis is possible using a computer spreadsheet program; the number of spaces involved depending on the level of complexity adopted.

5.2.6 Model longer simulation periods

The ASHRAE and CIBSE design cooling load methods are based on a 24-hour repeating thermal cycle. In the case of a single zone, a nine-day simulation period has been successfully implemented using a computer spreadsheet program. It is envisaged that mainly 24-hour simulation periods will be employed with the option of using longer simulation periods at higher levels of complexity.

5.3 Choosing a suitable mathematical simulation technique for a computer spreadsheet program

Finite difference, response factor and frequency domain techniques can all be implemented on computer spreadsheet programs. Ease in formulating the techniques on a spreadsheet program, computational efficiency and the ability to model the non-linear heat transfer processes are the key factors to be considered in choosing the most suitable technique. Finite difference techniques require the greatest number of computations due to space and time discretisation. Explicit schemes suffer due to numerical instability requiring smaller time-steps. The modelling of a single space would require about 40 temperature nodal points and a corresponding number of heat balance equations to simulate the heat transfer processes at each time step. In addition a preconditioning period is required, its length depending on the thermal response of the space (See sec. 3.1.3). As a result, finite difference schemes would require much time and a large number of spreadsheet cells to set up, the exception being where a single temperature nodal point can be used to model an element. For example, A window glazing pane, an internal blind or space's air node. An implicit finite difference scheme can model single nodal elements and maintain numerical stability employing one-hour time steps. Single nodal finite difference schemes are

computationally very efficient for computer spreadsheet application. The ASHRAE Fundamentals Handbook [67] demonstrate the relative ease of using response factor calculation procedures using the Radiant Time Series Method. However, the response factors are generated using AHSRAE's Heat Balance Method. It may be possible to generate the response factors using a spreadsheet program, but a preconditioning period is required to simulate a periodic design day as with the finite difference technique. The response factor methods do not suffer due to space discretisation, requiring only surface nodal points and a space air node to formulate the heat transfer processes. Periodic heat transfer is the principle process on which the frequency domain technique is based. The frequency domain technique is naturally suited to simulating a periodic design day, requiring no preconditioning period, due to this. Fourier series of the thermal excitations and space element matrices can be generated directly on a suitable spreadsheet program. There are no convergence problems compared to generating the periodic response factors. For a 24-hour design period, each Fourier series will contain 11 components (See sec. 3.1.4.1) compared to 24 periodic response factors required in the Radiant Time Series Method. The frequency domain technique is ideally suited for setting-up heat balances. In the case of a rectangular shaped space with a single window, only eight heat balance equations are required to establish the space air and surface temperature profiles. Each heat balance equation can fully characterise the periodic thermal behaviour of its space element, unlike the finite difference and response factor methods. Traditionally, the frequency domain technique has only been found suitable for modelling linear heat transfer processes and it was therefore necessary to linearise the non-linear processes for implementation of the technique. It will be demonstrated that by combining the frequency domain technique with iterative techniques, non-linear as well as plant dynamic heat transfer processes can be simulated using a suitable spreadsheet program.

5.4 The Assumptions regarding the application of the new design method

The thermal modelling of building heat transfer in a detailed and comprehensive manner is complex. Certain simplifying assumptions must be made for practical design calculations to be performed in a reasonable time period. An isothermal surface condition is a typical assumption adopted in dynamic thermal models, for example. A more sophisticated thermal model would divide each room surface into a number of smaller isothermal patches, which would cause an exponential increase in the number of subsequent calculations and

computer run times. The assumptions underlying the ASHRAE and CIBSE design methods are based on a single level of modelling complexity. The new design method can be implemented at a number of levels of complexity requiring a more flexible approach to defining the assumptions. At the lower levels of complexity, the assumptions are similar to those of the existing design methods. At higher levels of complexity, the assumptions are user defined. For example, solar beam tracking is possible using a spreadsheet program and the user may wish to redefine the transmitted solar beam distribution pattern. The user must decide how the solar flux will be distributed, e.g., uniformly spread over an entire surface or a more complex distribution pattern requiring subdivision of the main room surfaces into isothermal patches. The latter option would also have implications regarding the basic assumption of isothermal surfaces. The assumptions of the Thermal Analysis Design Method are:

1. Design cooling load and hourly temperature calculations are performed for a single 24-hour peak design day. Previous days are identical to the peak design day. Thermal excitations are periodic resulting in a periodic response. Longer periods may be simulated, the number of days depending on the level of complexity adopted.
2. The zone air is modelled as a well-mixed medium with a uniform temperature.
3. All surfaces are isothermal. Minimal sub-division of room surfaces into isothermal patches is possible at higher levels of complexity.
4. Each layer of a building element is homogeneous and its thermophysical properties are treated as constants.
5. All surfaces are grey and diffuse with absorptivity and emissivity invariant with temperature. Emitted and reflected radiation is diffusely distributed.
6. One-dimensional heat conduction takes place through structural elements.
7. Long-wave and short-wave radiation from internal sources are uniformly distributed over all internal surfaces. More precise distribution patterns are possible at higher levels of modelling complexity.
8. Internal and external convection processes may be based on a set of constant heat transfer coefficients or variable coefficients generated by sophisticated convection models, depending on the level of complexity adopted.

9. An exact internal long-wave radiant exchange model shall be employed. Approximate methods, similar to the MRT/Balance method, may be used at lower levels of modelling complexity.
10. Surface convection and long-wave radiant exchange processes may be combined into a single process using a set of combined surface heat transfer coefficients, at the lowest level of complexity.
11. Window transmitted solar radiation will be uniformly distributed over all surfaces, except the window wall. Solar tracking of the direct beam is possible at a higher level of complexity but diffuse solar radiation is assumed evenly distributed.
12. A single zone is the basic room model but multi-zone models can be implemented at higher levels of complexity.
13. An airtight building is assumed and a constant infiltration rate of 0.25 air changes per hour shall be used for design cooling load calculations. Network ventilation models may be used at higher levels of complexity.
14. Sol-air temperature is the preferred external thermal excitation for determining heat gains through opaque building fabric. All external environmental thermal influences must be included when calculating the sol-air temperature. Heat gains due to external thermal excitations may be calculated separately.

Chapter VI

6.0 THE DESIGN THERMAL ANALYSIS METHOD

6.1 New concepts

The salient innovation is the combination of numerical iterative techniques with the frequency domain technique to produce a powerful thermal simulation tool for modelling non-linear heat transfer processes. The Iterative Frequency Domain Method (IFDM) and the Adiabatic Iterative Frequency Domain Method (AIFDM) are the fundamental simulation techniques on which the new thermal model is based. The following overview includes further contributions to the thermal modelling of buildings, which evolved during the development of the Design Thermal Analysis Method.

6.1.1 The non-linear convection model

In the frequency domain method, constant convection coefficients, in the form of surface resistance matrices, are combined with the overall thermal transmission matrix modelling conduction through building elements. All thermophysical properties must be invariant with time due to the matrix formulation being only suitable for modelling linear conduction heat transfer processes. This constraint limits the frequency domain method to the simulation of convection heat transfers employing constant convection coefficients. Two solutions (IFDM and AIFDM), employing variable convection coefficients in the frequency domain, have been derived. One solution method involves excluding the heat transfer coefficients from the thermal transmission matrices, the other method maintains the traditional matrix formulation but includes a calculation procedure that cancels the errors incurred due to employing the constant coefficients in the thermal transmission matrices. The methods give identical results.

6.1.2 Simplifying the convection models for design calculations

The published internal and external convection models are generally formulated with relatively complex empirical correlation expressions defining non-linear processes. The correlation expressions can be reduced to simpler expressions, within the normal range of surface-to-air temperature differences and external wind speeds encountered, for the purpose of practical design calculations. The resulting correlation expressions are computationally more efficient and perform comparable to the original correlations.

6.1.3 Internal long-wave radiant exchange model

Employing combined convective and long-wave radiative surface coefficients that are included in the thermal transmission matrices of building elements, is the traditional approach when using the frequency domain method. The ASHRAE methods approximate the long-wave radiant exchange processes. Long-wave radiant exchange is processed using an exact grey solution method in the case of the proposed model. Surface temperatures and radiant exchange view factors are computed, and an iterative heat balance method is used to establish steady state net radiant flux transfers and surface temperatures.

A new approximate method of radiant exchange is also proposed. The method exploits the dominant long-wave radiant exchange processes taking place between the major surfaces that are at significantly different temperatures.

6.1.4 Plant models

The Iterative Frequency Domain Technique allows a variety of plant options to be modelled, from convective cooling to chilled ceiling with displacement ventilation. Plant options can be modelled by setting-up suitable iterative heat balance routines which converge to a specified space set-point temperature.

6.1.5 The sol-air temperature model

Sol-air temperature has the advantage of being a single thermal excitation that accounts for all the external thermal environmental influences. Only one Fourier series and one mean value is required, a desired efficiency when using the frequency domain method. The sol-air temperature formulation given in the CIBSE guide [26] does not include radiant exchange with external buildings and the design building façade surface temperature is assumed equal to the sol-air temperature. In the ASHRAE methods, long-wave radiant exchange is not included for a vertical surface and a constant negative value is assumed for a horizontal surface [66]. The CIBSE and ASHRAE methods do not account for solar shading of the design building façade. The proposed sol-air temperature formulation is based on the concept of an external environmental model that simulates all external surface and sky temperatures, and accounts for solar shading of external surfaces. External long-wave radiant exchange view factors are also computed in respect of all modelled surfaces.

6.1.6 Window sol-air temperature model

It is necessary to compute the inner window system's surface temperature profile, to model the subsequent conductive and convective heat transfers accurately. A significant proportion of thermal energy entering and leaving a space is transferred via the window system. Transmitted solar and surface temperature profiles need to be computed. It is necessary to generate a Fourier series for each of the thermal excitations to account for the influence on inner surface temperature due to external air temperature, long-wave radiation exchange with the external environment and solar absorption. Five Fourier series are required, three of these accounting for the absorbed solar radiation in the three layers of the window system, in the case of a double glazed window with internal blind. Much computational effort is needed, especially if iterative heat balance methods are employed. This inefficiency is overcome by combining all the external excitations into a single thermal excitation that can be represented by a single Fourier series. This concept is similar to the idea of sol-air temperature but includes the influences due to absorbed solar energy within the window layers and that of the internal environment.

6.1.7 Modelling tabulated solar data

The CIBSE guide contains many pages of useful solar data required for design day calculations. This design data can be encapsulated into a small set of correlation expressions that can be employed by the solar model to generate solar irradiance profiles for surfaces at any inclination angle, azimuth angle and month.

6.1.8 Surface factors

The CIBSE admittance method employs only one type of surface factor, which is used to determine the proportion of transmitted solar gains, incident on room surfaces, and consequently convected to the space environmental node. The surface factor is derived from the thermal transmission matrix of the space structural element, one factor for each space surface. For precise thermal modelling, three types of surface factor are required and each is derived from the thermal transmission matrices of the space structural elements. These factors are:

1. **Radiant heat gain factors** are used to calculate the convective heat gain to the space air node due to radiant gains incident on the room surfaces. The radiant gains are due to internal heat gains, window solar transmitted gains or radiant exchange between room

surfaces. Two radiant gain factors are required to account for the convective heat gains due to radiant heat gains incident on the space side as well as on the neighbouring side of room structural surfaces.

2. **Surface temperature factors due to radiant heat gains** are used to determine the incremental rise in surface temperature due to the incident radiant gains. Two factors are required to determine the total incremental rise in surface temperature due to radiant heat gains incident on both sides of the room structural surfaces.
3. **Surface temperature factors due to convective heat exchange** are used to determine the incremental change in surface temperature due to convective heat exchange between the surface and space air temperature, and heat exchange between the external surface and sol-air temperature in the case of external walls and roofs. Two factors are required to determine the total change in surface temperature due to environmental temperature excitations on both sides of the structural element.

6.2 The scope of application of the method

6.2.1 Multitask method

The Design Thermal Analysis Method embodies a new approach to design day calculations. In contrast to the traditional single task methods, specifically employed to determine design day cooling load, the new method is a multitask analysis tool that can be used to:

1. Determine space cooling loads.
2. Determine space air and surface temperatures.
3. Check space thermal comfort.
4. Analyse network ventilation models.
5. Analyse design solutions based on mechanical ventilation with night-time cooling, chilled ceiling with displacement or conventional ventilation, natural ventilation and other methods of passive cooling/mixed mode systems.
6. Analyse multi-zone models.

6.2.2 Levels of modelling complexity

The new method can be implemented at a number of levels of complexity to suit the required accuracy of the design day calculations or the level of thermal analysis required. Levels of complexity can be categorised according to the complexity of modelling the

physical and plant models, whether single or multi-zone. Table 6.1, for example, shows levels of complexity in relation to the choice of surface convection and long-wave radiant exchange models. Table 6.2 illustrates levels of complexity associated with the difficulty of

Table 6.1. Levels of complexity according to surface convective and long-wave radiant exchange models

Modelling complexity of physical models	Level 1	Level 2	Level 3	Level 4	Level 5
Single zone	Yes	Yes	Yes	Yes	Yes
Variable internal convection coefficient model				Yes	Yes
Constant internal convection coefficient model		Yes	Yes		
Combined internal convection and long-wave radiation exchange model	Yes				
Approximate internal long-wave radiant exchange model.		Yes			
Accurate internal long-wave radiant exchange model.			Yes	Yes	Yes
Variable external convection coefficient model					Yes
Constant external convection coefficient model				Yes	
Combined external convection and long-wave radiation model	Yes	Yes	Yes		
Accurate external long-wave radiant exchange model.				Yes	Yes

Table 6.2. Levels of complexity according to design solutions

Modelling complexity of design solutions	Level 1	Level 2	Level 3	Level 4	Level 5	Level 6
Free-running building, constant air infiltration	✓					
Convective cooling plant			✓			
Chilled ceiling with conventional or displacement ventilation						✓
Mechanical ventilation, constant ventilation rate	✓					
Mechanical ventilation with night-time cooling		✓				
Natural ventilation – wind driven				✓		
Natural ventilation – stack effect					✓	
Natural ventilation – wind and stack effect						✓

modelling the design solutions. Table 6.3 indicates how the two categories of complexity levels are combined to establish the overall modelling complexity relating to choice of physical model and design solution. The overall levels of 1,1 and 6,5, in table 6.3, define the lowest and highest levels of modelling complexity respectively.

Table 6.3. Combining Table 1 & 2 Levels to establish overall modelling complexity

Table 2 levels of complexity	Table 1 levels of complexity				
	Level 1	**Level 2**	**Level 3**	**Level 4**	**Level 5**
Level 1	Free-running building. Combined convective & L-W radiation model				
Level 2			Mechanical ventilation with night-time cooling. Constant internal convection coefficient & accurate L-W radiation models. Combined external convection & L-W radiation model		
Level 3	Convective cooling plant. Combined convective & L-W radiation model				Convective cooling Variable convection coefficient & accurate L-W radiation model
Level 4	Natural ventilation – wind driven. Combined convective & L-W radiation model				
Level 5		Natural ventilation – stack effect. Constant internal convection coefficient & approx. L-W radiation. Combined external convection & L-W radiation model			
Level 6					Chilled ceiling. Variable convection coefficient & accurate L-W radiation model

6.3 The structure of the method

Employing a set of heat balance equations to link precisely all the space's heat transfer processes is a distinct advantage of the frequency domain technique. The inability to model non- linear heat transfer processes is a deficiency of the frequency domain technique. This limitation is overcome by integrating numerical iterative techniques with the heat balance equations in the frequency domain. Level 1,1 and 3,1 models, in table 6.3, can be run on a spreadsheet program using the traditional frequency domain technique. All other models

defined in the table, including non-linear sub-models, would require the iterative frequency domain technique (IFDT) to run them in the computer spreadsheet environment. The Design Thermal Analysis Method encompasses three thermal models, an external and an internal environmental model, and a window system model. Each model includes conduction, convection and long-wave radiation sub-models. Solar radiation and solar shadow are additional sub-models of the external environmental model. These sub-models form the basic components for simulating a free-running building. For space temperature control solutions, space cooling plant and network ventilation models are optional sub-models that can be included in the internal environmental model. Some of the sub-models comprise of further sub-models. Adjacent building façades and ground structures must be modelled, to accurately model external long-wave radiant exchange, for example. The main task of the external environmental model is to generate the sol-air temperature profile. To compute sol-air temperatures, the influence of long-wave radiant exchange, surface convection and solar shading are accounted for and estimated with greater accuracy than the current design methods. The window model simulates a sol-air temperature that can be used to compute the inner surface temperature profile of a window system, in addition to predicting the transmitted solar radiation. This new concept of window sol-air temperature combines the influences of external air temperature, long-wave radiation, and absorbed solar radiation into a single thermal excitation. The thermal relationship between all the sub-models is illustrated in the flow diagram of Figure 6.1. The flow diagram depicts a single zone with its external wall and window conduction models thermally linking the external and internal environmental models. For clarity, a single block represents the other space structural surfaces, i.e., ceiling, floor and internal partition. These surfaces are thermally linked to neighbouring spaces or in the case of further external structural elements such as external walls and roof, thermally linked to the external environmental thermal model. Internal long-wave radiant and convective heat exchange with the internal surface of the window have also been omitted for clarity. Two-way directional flow lines indicate iterative heat balance processes. The structure of the method allows for the inclusion of further sub-models or exclusion of a sub-model. The adjacent building façade model can be "switched off" in the case of a green-field site location, for example. A plant model may be switched off to simulate a free running building. A chilled ceiling is treated as another surface, thermally linked to the surface convection and long-wave thermal

models and its displacement ventilation system thermally linked to the space air temperature node.

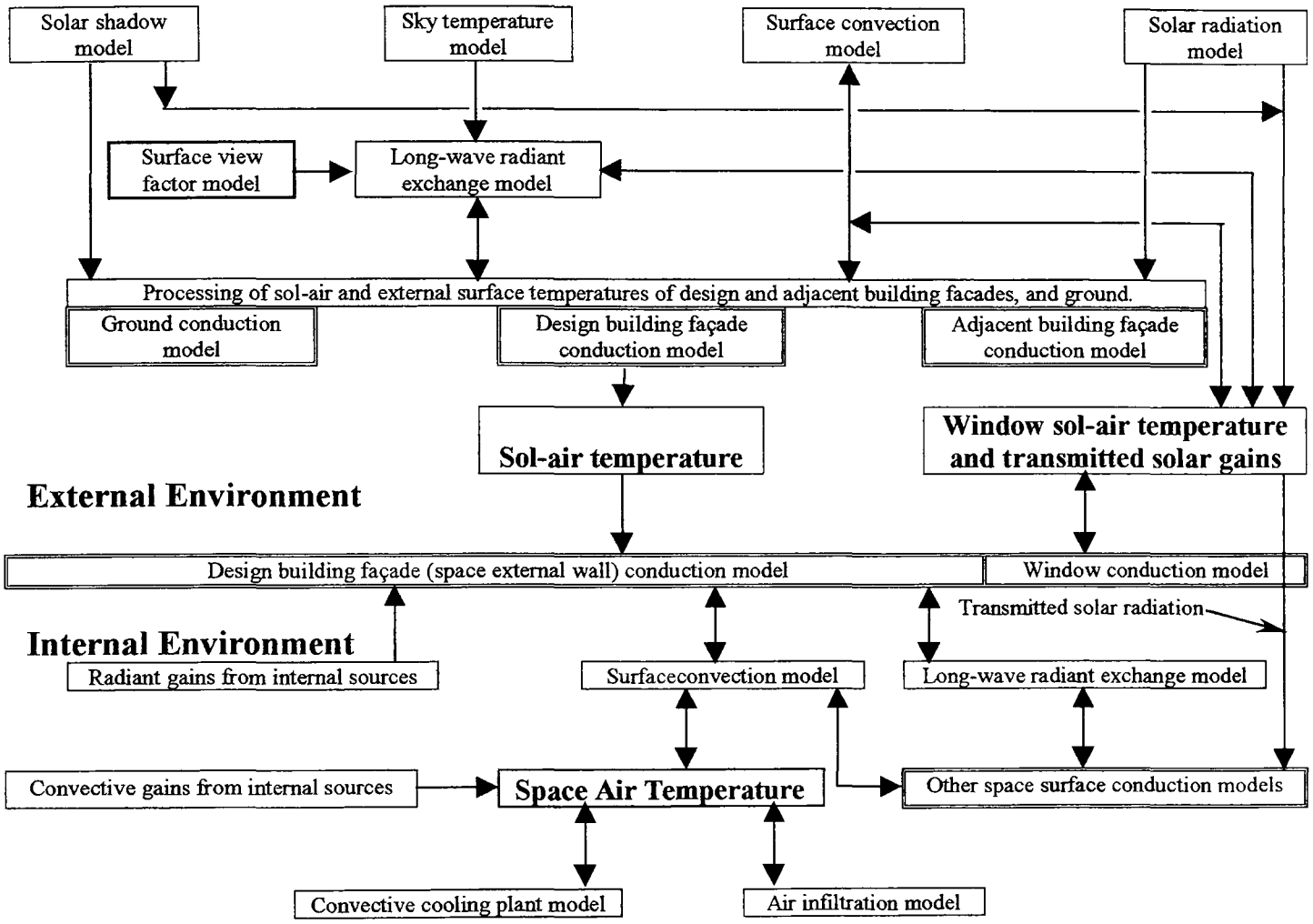

Figure 6.1. Flow diagram representing the structure of Design Thermal Analysis Method

6.4 Development of the External Environmental Thermal Model

6.4.1 Triple-surfaced representation of the external environment model

It is necessary to account for the influences of all the external thermal driving forces and the effects of solar shading, in order to predict representative values of sol-air temperature. Solar shading can significantly influence the magnitude of local surface temperatures which in turn influence external long-wave radiant exchange and the subsequent daily mean heat transfer through building facades. External buildings obstruct the view of the sky dome, reducing the amount of solar diffuse radiation incident on the design building facade. Shadow geometry and long-wave radiant exchange are difficult to model due to the

topographical features of the local buildings, ground and space in a city environment. It is possible to produce a virtual model of the local external environment using a sophisticated computer package, but much input data is required. It is not necessary to create a virtual geometric model of the local topography for the purpose of design calculations. Creating a three-surfaced model representation of the local topography, which is sensitive to the dominant external features, is a more pragmatic approach. Two long building facades separated by a road can be modelled to represent typical city or town local topographies. Figure 6.2 illustrates the three-surfaced local topographical model created within the external environmental thermal model. With this simple topographical model, average building height, total length of building facades, road width and length can be varied to represent the dominant external dimensions. The roof surface of the design building can be included as an additional surface if required. The roof surface is modelled in a similar manner to the ground surface accounting for shading and sky dome obstruction in the case of external high rise buildings. The dimensional co-ordinates of the space's external wall area are also inputted in order to locate its position on the design building façade. Its precise location on the façade is required in order to compute its long-wave radiation view factors to the facing building façade, road and sky. Its co-ordinates are also required

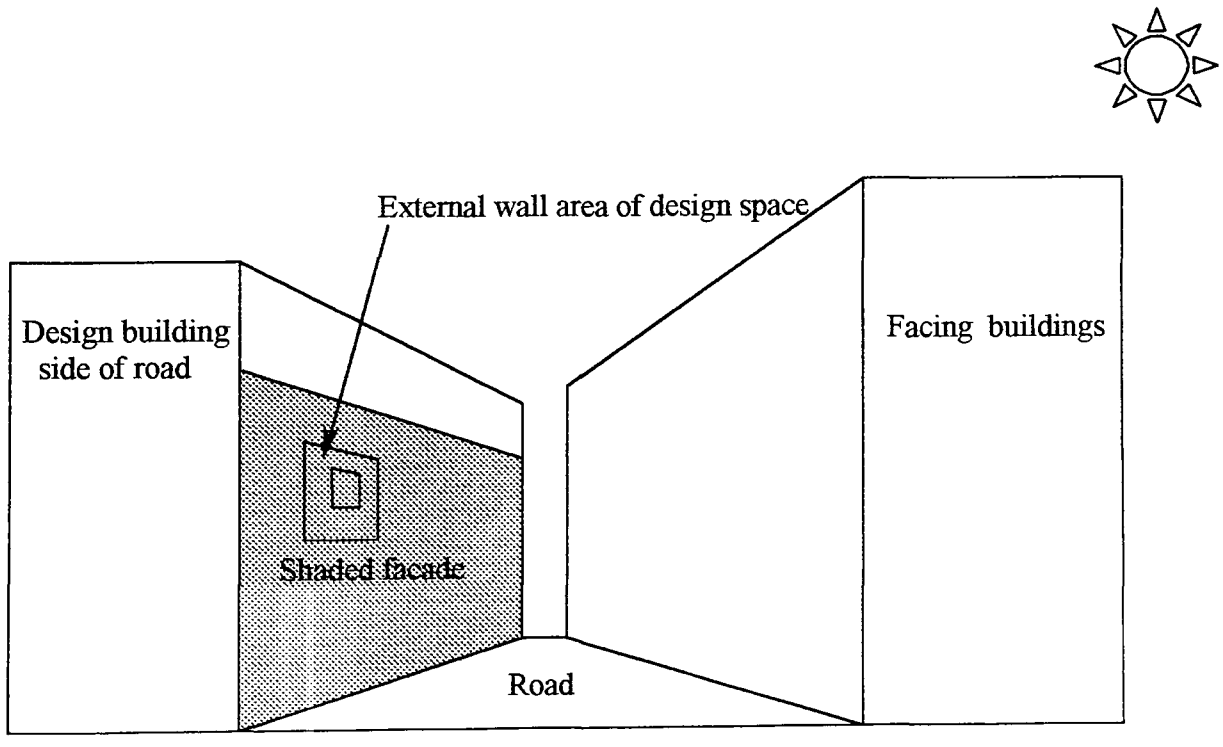

Figure 6.2. Simplified three-surface representation of city local topography

to determine the shaded portion of the elemental area throughout the day. The azimuth orientation of the three-surfaced model can be varied to suit the design building façade, azimuth angle. The significant influence of solar shading and obstruction of diffuse sky radiation is demonstrated by figure 6.3, which illustrates sol-air temperature profiles for a south-orientated façade facing taller buildings located on the opposite side of the street. The unshaded external wall is of a top floor space and the totally shaded external wall is of a lower ground floor space. The lower surfaces of the façade are always in the shadow of the taller buildings on the opposite side of the street and receive less diffuse solar radiation due the restricted view of the sky dome. The lower space's external wall will also receive less long-wave radiation from the sky compared to the upper space's external wall. The upper space's external wall receives less long-wave radiation from the ground and facing buildings compared to the lower external wall element. The differences in incident long-wave radiation is due to differences in radiation view factors from the sky and ground, to the lower and upper regions of the external wall.

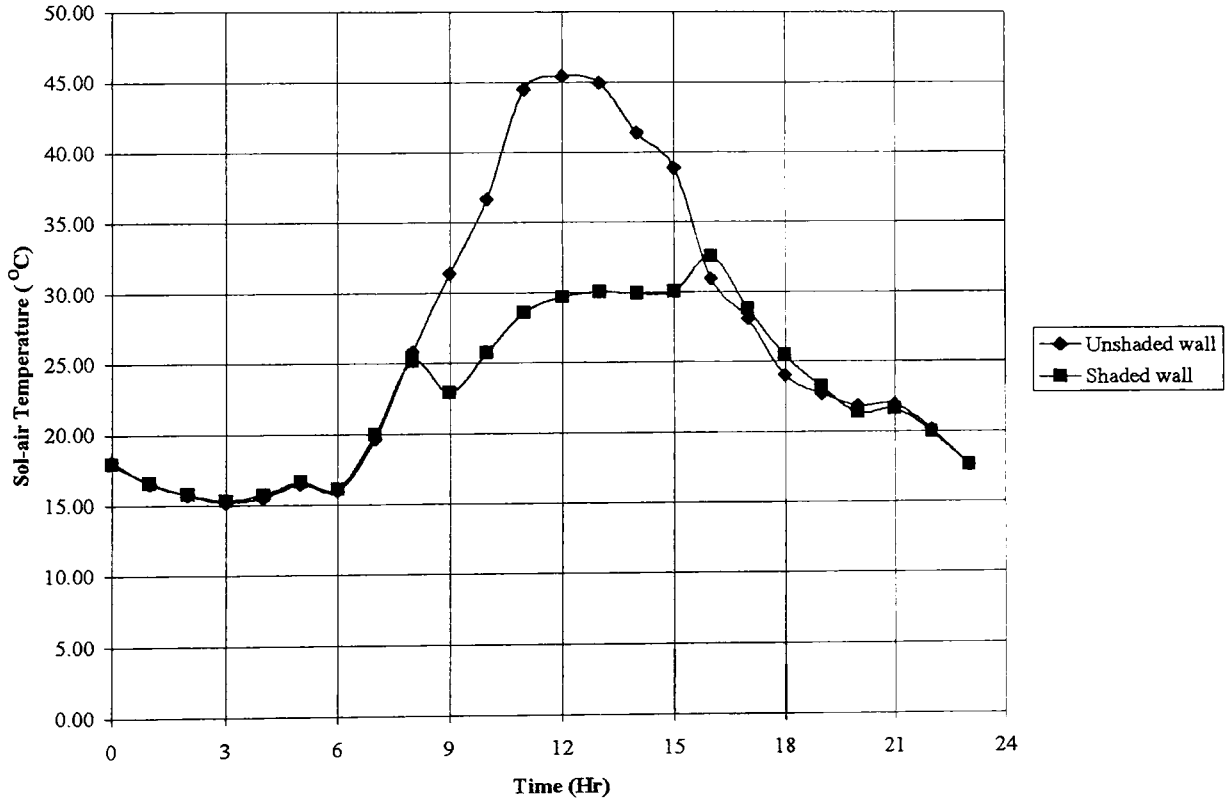

Figure 6.3. Comparison of sol-air temperature between shaded and unshaded walls

Figure 6.1 shows the main sub-models involved in developing the external environmental model. The outputs of these sub-models are used to generate the sol-air temperature profiles

of the design and facing building facades, and the ground surface between them. Sol-air temperature is defined in chapter II by equation (2.26) as:

$$T_{eo} = \left[\alpha I_G(\delta\gamma) + L^*(\delta)\right] / \bar{h}_{co} + T_{ao}$$

The total solar irradiation incident on vertical surfaces, $\alpha I_G(\delta\gamma)$, is normally taken as the sum of the direct, sky diffuse and ground reflected solar radiation. Reflected solar radiation from surrounding vertical surfaces is not normally accounted for. Reflected solar radiation from vertical surfaces is accounted for in the external environmental model. This component can be significant, compared to the magnitude of ground reflected radiation, due to the close proximity of the vertical facades within a city environment. Equation (2.26) includes the solar absorption coefficient, α, though other factors are necessary to account for solar shading and sky dome view factors. These additional factors will be included in the following detailed descriptions of the models. The net long-wave radiation on a surface, $L^*(\delta)$, is defined by:

$$L^*(\delta) = \sigma\left[\left(\varepsilon_{sky} F_{sky} T_{sky}^4 + \varepsilon_{grd} F_{grd} T_{grd}^4 + \varepsilon_{bld} F_{bld} T_{bld}^4\right) - \varepsilon_{sur} T_{sur}^4\right] \quad (6.1)$$

Conduction models are produced for each surface of the external environmental model to generate surface temperature profiles. The sky emissivity and temperature model is developed from work done by Cole [29]. The view factor model is based on typical view factor algebraic methods found in the literature. An integrated iterative heat balance model of the external environment is required due to the long-wave thermal radiation link between the external surfaces. In contrast, it will be demonstrated that the external environmental model can be formulated to simulate sol-air temperature profiles independent of the internal environmental model.

6.4.2 External conduction models

6.4.2.1 Modelling conduction in the frequency domain

A steady state conductance and a series of thermal transmission matrices define the mean and dynamic conduction processes of a particular structural surface respectively. The mean and dynamic conduction processes are employed to determine the mean and fluctuating surface temperature responses. Each thermal transmission matrix is derived from the matrix multiplication of the individual thermal transmission matrices defining a particular layer of the structural surface. Thermal excitations are represented by a Fourier series of eleven harmonic components (See sec. 3.1.4.1), in the case of a 24-hour simulation period, and

require a corresponding number of thermal transmission matrices in the series representing a particular surface. The calculation process is identical for each of the thermal transmission matrices in the series and only the fundamental thermal transmission matrix will be employed in the examples used to explain the method.

6.4.2.2 The fluctuating component

The external wall of the design façade and thermal excitations can be represented symbolically by the matrix formulation:

$$\begin{bmatrix} \tilde{t}_{eo} \\ \tilde{q}_{eo} \end{bmatrix} = \begin{bmatrix} d_{11} & d_{12} \\ d_{21} & d_{22} \end{bmatrix} \cdot \begin{bmatrix} \tilde{t}_{ai} \\ \tilde{q}_{ai} \end{bmatrix}, \tag{6.2}$$

where $\tilde{t}_{eo}$ and $\tilde{t}_{ai}$ are the sol-air and internal air temperatures respectively.

All quantities in the matrix are represented by complex numbers. The fluctuating thermal excitations and responses are defined by their corresponding complex quantities. Equation (6.1), defining long-wave radiant exchange, indicates that the complex external surface temperature of the wall $\tilde{t}_{sur}$ is required. Expanding the above thermal transmission matrix reveals the complex surface temperature and outside convective thermal resistance as follows:

$$\begin{bmatrix} \tilde{t}_{eo} \\ \tilde{q}_{eo} \end{bmatrix} = \begin{bmatrix} 1 & R_{co} \\ 0 & 1 \end{bmatrix} \cdot \begin{bmatrix} \tilde{t}_{sur} \\ \tilde{q}_{sur} \end{bmatrix} \tag{6.3a}$$

$$\begin{bmatrix} \tilde{t}_{sur} \\ \tilde{q}_{sur} \end{bmatrix} = \begin{bmatrix} d'_{11} & d'_{12} \\ d'_{21} & d'_{22} \end{bmatrix} \cdot \begin{bmatrix} \tilde{t}_{ai} \\ \tilde{q}_{ai} \end{bmatrix} \tag{6.3b}$$

Equations (6.3a) and (6.3b) shows the external surface temperature is influenced by the external and internal thermal excitations. It can be shown that the complex external surface temperature is given by:

$$\tilde{t}_{sur} = \left(1 - R_{co}\frac{d_{22}}{d_{12}}\right)\tilde{t}_{eo} + \frac{R_{co}}{d_{12}}\tilde{t}_{ai} + \frac{R_{co}R_{ci}}{d_{12}}\tilde{q}_{ri}, \tag{6.4}$$

where the additional quantities R_{ci} and $\tilde{q}_{ri}$, not shown in equation (6.3b), represent the internal surface convective resistance and incident complex radiant flux respectively. For a typical external cavity wall construction, the complex coefficients of the two inner complex excitations, $\tilde{t}_{ai}$ and $\tilde{q}_{ri}$, are relatively small in magnitude due to the high thermal storage and insulation properties of the wall. Using typical average values of surface convective

coefficients the magnitude of these complex coefficients of air temperature and radiant flux are approximately 0.003 and 0.002 respectively. Hence the fluctuating components of the inside thermal excitations have an insignificant influence on the external surface temperature of a cavity wall and for practical purposes, equation (6.4) may be reduced to:

$$\tilde{t}_{sur} = \left(1 - R_{co}\frac{d_{22}}{d_{12}}\right)\tilde{t}_{eo} \tag{6.5}$$

where d_{22}/d_{12} is the external thermal admittance of the wall.

6.4.2.3 The mean component

The mean surface temperature is obtained from a steady state analysis of the external cavity wall and it can be shown that:

$$\overline{T}_{sur} = \overline{T}_{eo} + R_{co}U\left(\overline{T}_{ai} - \overline{T}_{eo}\right) + \frac{R_{ci}R_{co}}{U}\overline{q}_{ri} \tag{6.6}$$

It can be demonstrated that for an insulated cavity wall the last two terms on the RHS of equation (6.6) are for practical purposes insignificant in magnitude compared to the mean sol-air temperature of equation (6.6). Further, the temperature difference term in equation (6.6), tends to be negative due to the mean sol-air temperature being normally higher than the inside mean air temperature. The resulting negative component will reduce further the influence of the inside mean radiant flux component. Equation (6.6) then reduces to:

$$\overline{T}_{sur} = \overline{T}_{eo} \tag{6.7}$$

6.4.2.4 Independence of the internal environmental model

The results described by equations (6.5) and (6.7) are very beneficial, allowing the external environmental model to simulate sol-air temperatures independently of the internal environmental model. Equations (6.5) and (6.7) provide a more accurate means of determining the external surface temperature for calculating external long-wave radiant exchange, and subsequently, a more precise sol-air temperature formulation. The CIBSE guide formulation for sol-air temperature assumes the surface temperature is equal to the sol-air temperature. This assumption is only plausible for the mean value of temperature. Equations (6.5) and (6.7) can also be used to determine the surface temperatures of the facing building façade and ground conduction models.

6.4.2.5 Sol-air temperature calculation procedure

The calculating procedure is illustrated by figure 6.4. A main feature is the double iteration heat balance loops. Only the iterative calculation procedure for the design space's external wall surface is shown. The facing building façade and ground conduction models have similar iterative calculation loops but for clarity are shown unexpanded at the bottom of figure 6.4. The second iterative calculations loop, shown near the bottom of figure 6.4,

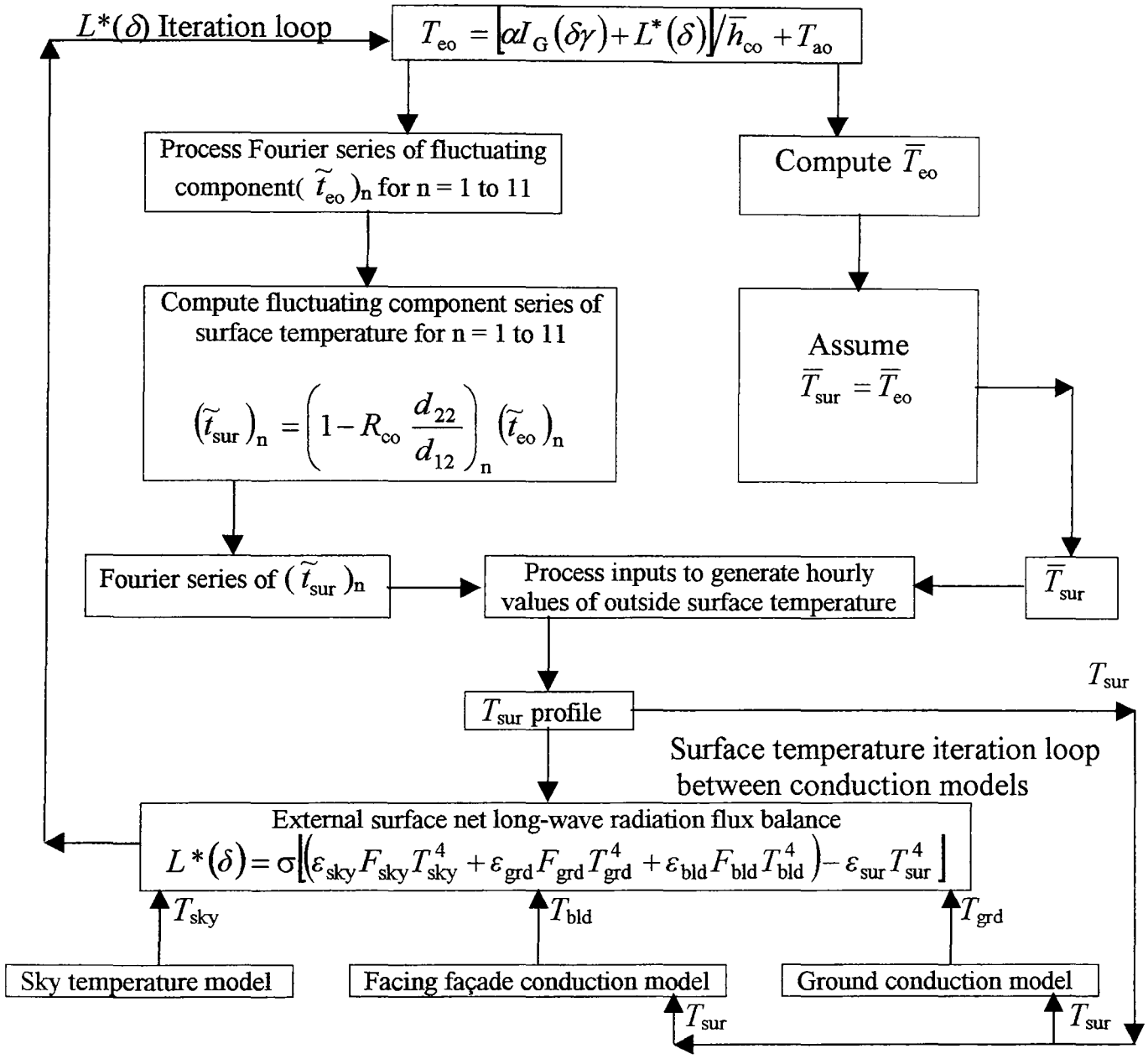

Figure 6.4. External wall sol-air and outer surface temperature calculation procedure

thermally links the three external surfaces' conduction models in order to update the surface temperature values for the long-wave radiation sub-models. Figure 6.4 is typical for each external surface's conduction model.

6.4.2.6 Correction due to constant surface heat transfer coefficients

A deficiency of the frequency domain's thermal transmission matrix formulation is that constant values of the convective surface resistances must be employed. The hourly values of external surface convective coefficients can vary significantly due to changing wind and surface temperatures. The corresponding variations in surface flux must be accounted for if an accurate prediction of the sol-air temperature profile is required. A simple modification is made to equation (2.26) that effectvely accounts for the fluctuation in the external surface convective coefficient. Equation (2.26) is recast below as equation (6.8) and includes the correction term, q_{co}.

$$T_{eo} = \left[\alpha I_G(\delta\gamma) + L^*(\delta) + q_{co}\right]/\bar{h}_{co} + T_{ao} \tag{6.8}$$

The surface convective heat flux, q_{co}, minimises the error incurred due to employing a constant convective coefficient, $\bar{h}_{co}$, in the thermal transmission matrix and in equation (6.8). If the convective fluxes due to using variable and constant coefficients are $h_{co}(T_{ao} - T_{sur})$ and $\bar{h}_{co}(T_{ao} - T_{sur})$ respectively, then the corrective heat flux is given by:

$$q_{co} = (h_{co} - \bar{h}_{co}) \cdot (T_{ao} - T_{sur}) \tag{6.9}$$

where h_{co} is the hourly value of the external convective heat transfer coefficient. Figure 6.5 illustrates the additional iterative calculation loop due to including the residual error convective correction flux, q_{co}. After a suitable number of iterations, q_{co} converges to the required value.

6.4.2.7 Roof Conduction Model

Well-insulated roofs of heavy construction possess similar thermal characteristics to insulated cavity walls and the same procedures for determining sol-air temperature and external surface temperature may be employed. Long-wave radiant exchange will only be possible with the sky and any high-rise neighbouring buildings. Excluding the ground conduction model, the calculation procedure illustrated by figure 6.5 would also be applicable to roofs.

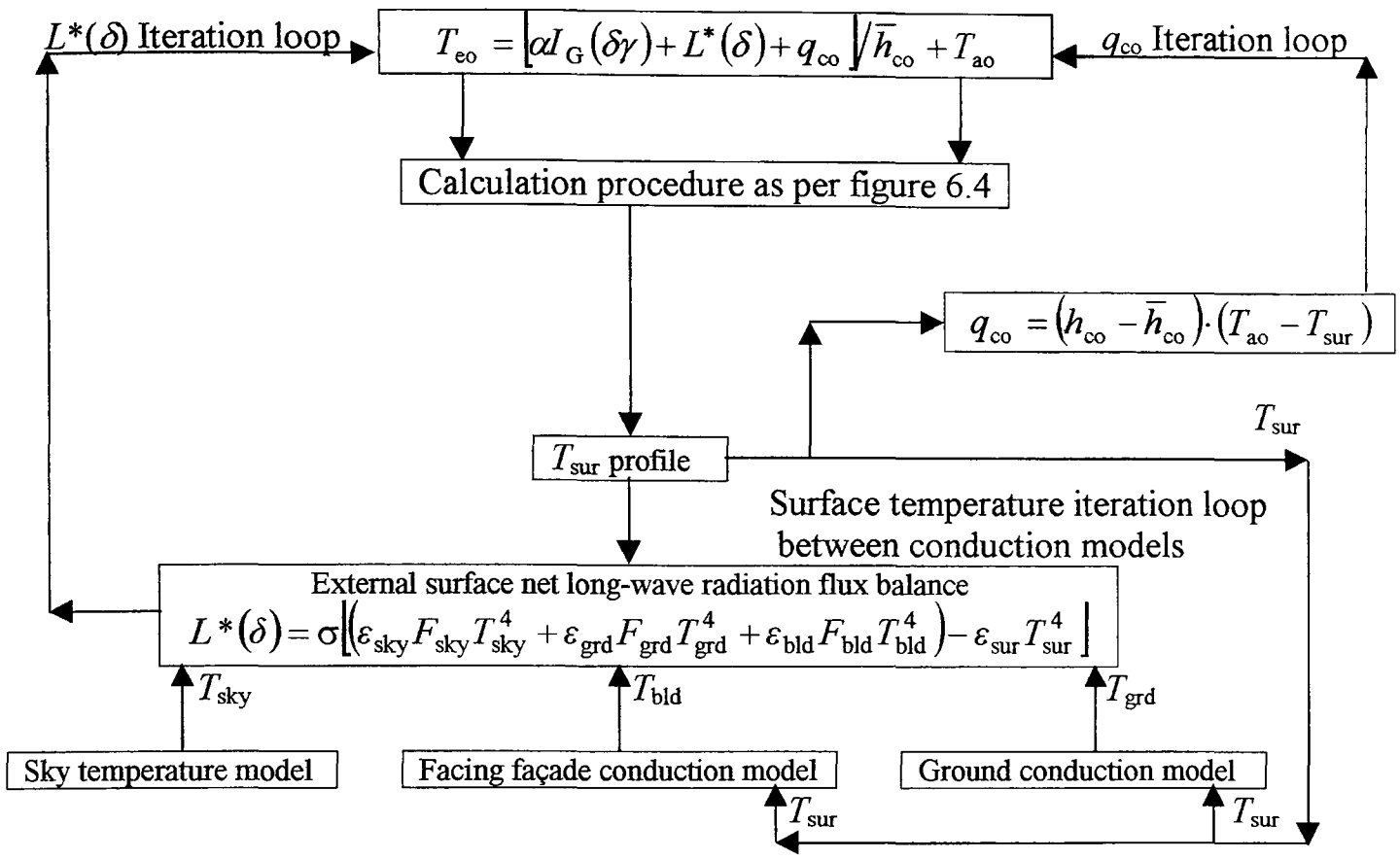

Figure 6.5. Calculation procedure as per figure 6.4 but including q_{co} iteration loop

6.4.2.8 Accuracy of the new sol-air temperature model

The objective of the external environmental model is to generate an accurate 24-hour sol-air temperature profile. It is necessary to determine external surface temperatures of all participating external surfaces and to simulate external surface convection due to variable convection coefficients in order to achieve this goal. Current models of sol-air temperature do not account for these variables in a precise manner. The flexibility of finite difference techniques allows for simulation of external surface temperatures and the use of variable heat transfer coefficients. A finite difference model was set-up to check the accuracy of the iterative frequency domain model employing the new sol-air temperature formulation defined by equation (6.8). The test involved the comparison of the external surface temperatures produced by the two simulation models. Both models were subjected to identical thermal excitations. In the finite difference model, the 24-hour thermal excitation profiles were repeated to simulate the periodic thermal excitations, which are a feature of the frequency domain model. In the finite difference model, all the thermal excitations such as solar radiation and long-wave radiant fluxes were applied separately. In the iterative frequency domain model, all the thermal excitations were combined into a sol-air

temperature using equation (6.8). A number of tests, using different thermal excitation profiles, were performed. The hourly external surface temperatures produced by both models were in agreement. Any slight discrepancies were due to the time and space descretisation of the finite difference model. The results demonstrate that identical results will be obtained if the same dynamic thermal model applies the thermal excitations separately or uses an accurate formulation of sol-air temperature.

6.4.3 The external convection model

6.4.3.1 Comparing the current methods

Any suitable convection model may be used in the external environmental model. However, the published methods have much disparity between them resulting in large differences in values of convective coefficient. The CIBSE guide uses the following empirical relationship [26] that correlates the coefficient with wind speed only.

$$h_{co} = 4 + 4v \tag{6.10}$$

The ASHRAE Heat Balance Method's use of the MoWiTT model [60], represented by equations (6.11) and (6.12), correlates the coefficient to wind speed and surface-to-air temperature difference.

Windward side of building: $$h_{co} = \sqrt{\left[0.84(\Delta T)^{1/3}\right]^2 + \left[2.38V_o^{0.89}\right]^2} \tag{6.11}$$

Leeward side of building: $$h_{co} = \sqrt{\left[0.84(\Delta T)^{1/3}\right]^2 + \left[2.86V_o^{0.617}\right]^2}\,. \tag{6.12}$$

Table 6.4 indicates that on average, the CIBSE formula produces results more than twice the magnitude of the MoWiTT windward model (See columns 3 and 4). The advantage of using equation (6.10) is due to its independence of surface temperature, allowing the hourly values to be calculated independently of the building thermal model. The magnitude of the external convection coefficient is mainly influenced by wind speed and the effect due to surface-to-air temperature difference is only significant at wind speeds below a metre per second.

6.4.3.2 Linearizing the MoWiTT convection models

The MoWiTT windward formula can be transformed, with little error incurred, to resemble the CIBSE formula. Plotting the convective coefficient, obtained from the MoWiTT

formula, against wind speed and then employing linear regression to produce the following correlation expression.

$$h_{co} = 1.4 + 1.73V_o \tag{6.13}$$

Columns 5 and 6 of table 6.4 compares the results obtained from the MoWiTT and linearized MoWiTT expressions. Column 7 gives the error in terms of the ratio of the linearized MoWiTT to the original MoWiTT expression. Overall, the linearized MoWiTT correlation performs comparable to the original MoWiTT expression. Any differences will have an insignificant influence on the inside surface temperature, in the case of standard cavity wall and roof constructions. Table 6.4, shows that the accuracy of the linearized MoWiTT correlation improves above wind speeds of 2 m/s.

Table 6.4. Comparing CIBSE, MoWiTT and linearized MoWiTT convective coefficient models

Time	ΔT (K)	Wind Speed (m/s)	CIBSE $4 + 4v$ (W/m^{2}K)	MoWiTT Windward (W/m^{2}K)	$1.4 + 1.73V_o$ windward (W/m^{2}K)	Accuracy	MoWiTT Leeward (W/m^{2}K)	$2.1V_o^{0.7} + 1.45$ Leeward (W/m^{2}K)	Accuracy
0	4.59	0.0	4.00	1.40	1.40	1.00	1.40	1.45	1.04
1	5.39	0.0	4.00	1.47	1.40	0.95	1.47	1.45	0.98
2	5.10	0.0	4.00	1.45	1.40	0.97	1.45	1.45	1.00
3	4.82	0.0	4.00	1.42	1.40	0.99	1.42	1.45	1.02
4	4.80	0.0	4.00	1.42	1.40	0.99	1.42	1.45	1.02
5	4.20	1.3	9.20	3.30	3.65	1.11	3.63	3.97	1.10
6	2.49	5.9	27.60	11.61	11.61	1.00	8.63	8.72	1.01
7	1.63	5.6	26.40	11.07	11.09	1.00	8.34	8.46	1.02
8	2.74	6.5	30.00	12.65	12.65	1.00	9.15	9.24	1.01
9	4.45	8.8	39.20	16.55	16.62	1.00	11.03	11.07	1.00
10	6.54	8.5	38.00	16.06	16.11	1.00	10.83	10.84	1.00
11	9.80	5.1	24.40	10.30	10.22	0.99	8.02	8.02	1.00
12	11.82	5.2	24.80	10.50	10.40	0.99	8.14	8.11	1.00
13	12.43	5.0	24.00	10.16	10.05	0.99	7.96	7.93	1.00
14	11.68	5.2	24.80	10.50	10.40	0.99	8.14	8.11	1.00
15	10.47	4.0	20.00	8.38	8.32	0.99	6.97	6.99	1.00
16	7.49	5.5	26.00	10.98	10.92	0.99	8.35	8.38	1.00
17	5.26	3.8	19.20	7.94	7.97	1.00	6.68	6.80	1.02
18	3.87	6.9	31.60	13.34	13.34	1.00	9.51	9.57	1.01
19	3.07	7.1	32.40	13.68	13.68	1.00	9.66	9.73	1.01
20	3.37	5.9	27.60	11.62	11.61	1.00	8.64	8.72	1.01
21	4.35	0.1	4.40	1.41	1.57	1.12	1.54	1.87	1.22
22	4.86	0.6	6.40	2.07	2.44	1.18	2.53	2.92	1.16
23	4.18	2.0	12.00	4.61	4.86	1.05	4.59	4.86	1.06

6.4.3.3 Linearizing other convection models

A much earlier model by McAdams' [5] is given by equation (6.14). Table 6.5 provides values of its coefficients and exponents. It is similar to the CIBSE recommended model in terms of correlating the convective coefficient with wind speed only.

$$h_{co} = 5.678\left[a + b\left(\frac{v_{pf}}{0.3048}\right)^{n}\right] \tag{6.14}$$

where v_{pf} is the parallel flow velocity.

Table 6.5 Values of coefficient for equation (6)

Nature of surface	v_{pf}<4.88 m s^{-1}			4.88≤v_{pf}<30.48 m s^{-1}		
	a	*b*	*n*	*a*	*b*	*n*
Smooth	0.99	0.21	1	0	0.5	0.78
Rough	1.09	0.23	1	0	0.53	0.78

The parallel flow velocity v_{pf} is approximately related to wind speed, v, as follows

Windward side: If $v > 2$ m s^{-1} then $v_{pf} = 0.25\ v$, otherwise $v_{pf} = 0.5$.

Leeward side: $v_{pf} = 0.3 + 0.05\ v$.

McAdam's windward convection model can also be reduced to a linear correlation, which gives almost identical results to the original expression. The linearized formulations are

For smooth surfaces: $h_{co} = 5.62 + 3.91 v_{pf}$ (6.15)

For rough surfaces: $h_{co} = 6.19 + 4.29\ v_{pf}$ (6.16)

Note that the constants and coefficients of equations (6.15) and (6.16) are of similar magnitude when compared to those of the CIBSE expression defined by equation (6.10). The definitions of wind speed given by the two models may lead to significantly different results; i.e., parallel wind velocity, v_{pf}, used the in McAdam's model compared to just wind speed in used in the CIBSE expression. The relationships between parallel wind velocity v_{pf} and wind speed v, shown below table 6.5, provides an indication of the difference in magnitude to be expected.

The DOE-2 convection model combines the velocity component of the MoWiTT model with a surface-air temperature component and a surface roughness multiplier R_f [60]. For vertical surfaces the DOE-2 model is described by the expressions:

Windward: $$h_{co} = 1.31(|\Delta T|)^{1/3}(1 - R_f) + R_f\sqrt{[1.31(|\Delta T|)^{1/3}]^2 + (2.38V_o^{0.89})^2} \quad (6.17)$$

Leeward: $$h_{co} = 1.31(|\Delta T|)^{1/3}(1 - R_f) + R_f\sqrt{[1.31(|\Delta T|)^{1/3}]^2 + (2.86V_o^{0.617})^2} \quad (6.18)$$

Again equations (6.17) and (6.18) can be reduced to simpler expressions that correlate with wind speed only. Employing a roughness multiplier of 1.67 for brick, equation (6.17) can be simplified to:

$$h_{co} = 1.85 + 2.76V_o \quad (6.19)$$

The relationship between convective coefficient and wind speed is mildly non-linear, in the case of leeward surfaces. It can be shown that a strong linear relationship exists between the convective coefficient and wind speed to the power of 0.7. The MoWiTT leeward convection model, expressed by equation (6.12), can be reduced to the form:

$$2.1V_o^{0.7} + 1.45 \quad (6.20)$$

The last three columns of Table 6.4 compare the accuracy of equation (6.20) with the actual MoWiTT leeward convection model.

6.4.3.4 Similarity between the Convection Models

An examination of the convective models has revealed that, although of different origin, the models can be reduced to similar, simpler relationships that correlate the convection coefficient with wind speed only and that for practical purposes the influence of surface-to-air temperature difference may be neglected. The windward convection models can be represented by a linear relationship of the form:

$$h_{co} = c + m.v \quad (6.21)$$

and the leeward convection models by a correlation of the form:

$$h_{co} = c + m.v^{0.7} \quad (6.22)$$

This similarity indicates that the convection models are, to a certain extent, in agreement and appear to follow the same fundamental law. The remaining task is to establish representative values for the constant, c and coefficient, m, of equation (6.22). A

satisfactory solution to this problem can only be obtained from further validation tests of the convection models. For the time being, an investigation into the factors influencing the magnitude of the convection coefficients of each model may provide provisional values for practical design calculations.

6.4.3.5 Factors influencing the magnitude of the convection coefficients

If roughness multipliers are used with the MowiTT model, similar results to the DOE-2 model are produced. In the case of McAdam's model, Table 6.5 shows that there is little difference between the values of coefficients and exponents for smooth and rough surfaces. In contrast, DOE-2's model uses roughness multipliers of 1.00 and 1.67 for glass and brick respectively. Using a corresponding ratio of rough to smooth multipliers for the "*b*" coefficient in Table 6.5, the McAdams model produces closer results to the MoWiTT and DOE-2 models. The CIBSE guide specifies the velocity in equation (6.10) as the wind speed. If as with the McAdams model, the parallel surface velocity is used, equation (6.10) gives comparable results to the other three convective models. It seems that if the same values of roughness coefficient are used in each model and the parallel surface velocity is used in the CIBSE recommended model, then all four models tend to give comparable results.

6.4.3.6 Establishing a convection model for design calculations

Following the reasoning outlined in 6.4.3.5 above, the MoWiTT convection model was modified to include surface roughness multipliers to give similar results to the DOE-2 model. The following coefficients and constants in table 6.6 were then established for the correlation equations (6.21) and (6.22).

Table 6.6. Coefficient *m* for equations (6.21) and (6.22)

Surface material:	Stucco	Brick	Concrete	Clear pine	Smooth plaster	Glass
Windward *m*	3.9	2.9	2.6	1.9	1.85	1.7
Leeward *m*	4.8	3.6	3.2	2.3	2.25	2

For both windward and leeward cases a value of 2 for the constant *c* was found to give satisfactory results. The value of the constant *c* is influenced by the surface-to-air

temperature difference and only becomes significant at wind speeds less than a metre per second. At zero wind speed, the MoWiTT and DOE-2 convection models tend to give values of convection coefficient below and above the value of 2 respectively.

6.4.3.7 Performance of the linearized convection model

Figure 6.6 gives a comparison of results between the approximate linear correlation and the MoWiTT and DOE-2 convection models. Note that for the sample of weather data used, the wind speed was zero for the first four hours of the day resulting in minimum convection coefficients corresponding to surface-to-air temperature differences only. Within these hours, the approximate method gives results between those of the MoWiTT and DOE-2 models. Overall, the simplified correlation model performs comparable to the MoWiTT and DOE models. Note that the same roughness factor for brick was applied to both the MoWiTT and DOE models. The original MoWiTT model, as defined in the literature, does not include roughness factors.

6.4.3.8 Range of application of the linearized convection model

Over a wide range of wind speeds (e.g., 0 to 30 m/s), all the convection models show greater non-linearity with velocity. The external design data in the CIBSE guide [69] shows that for London, Manchester and Edinburgh, the percentage frequency of wind speeds under 10 m/s are 99.3%, 97.7% and 95.7% respectively. For the same locations the percentage frequency of wind speeds above 2 m/s are 73.4%, 81.5% and 79.5% respectively. The weather data relates to the period 1975 to 1994. These statistics indicate that representative weather data, for design purposes, should include wind speeds between 2 m/s and10 m/s. Within this range there is a strong linear relationship between the convective coefficient and velocity, and relatively negligible influence on the magnitude of the coefficient due to surface-to-air temperature difference. The correlation formulae represented by equations (6.21) and (6.22) are of comparable accuracy to the contemporary convection models within the 2 m/s to10 m/s range of wind speeds. Considering the disparity in performance that exists between the current convection models, the results of the linearized model lie within the band of results produced by the current models.

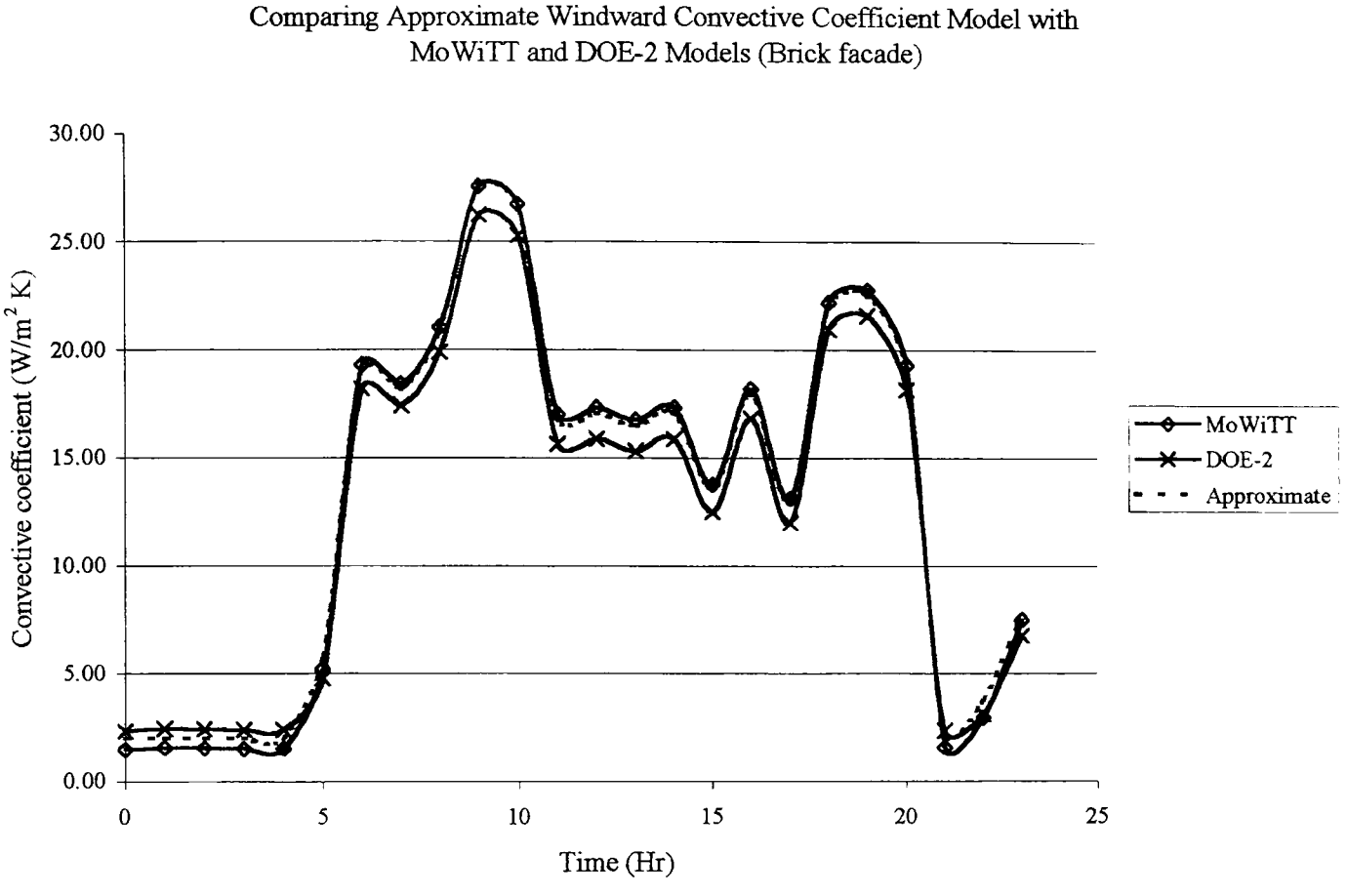

Figure 6.6. Comparing the approximate convective model with the MoWiTT and DOE-2 models

6.4.3.9 Correction for height

Mean wind speeds are measured at a height of 10 metres above sea level and must be corrected for locations above this reference height. The CIBSE guide provides the following relationship [69].

$$v_z = v_{\text{ref}} C_{\text{R}}(z) C_{\text{T}} \tag{6.23}$$

Supporting data is included in order to establish values for the roughness coefficient, C_{R}, at height z and the topography coefficient, C_{T}. The corrected wind speed v_z is then used in equations (6.21) and (6.22).

6.4.4 External long-wave radiant exchange model

6.4.4.1 View factor sub-model

The net long-wave radiation on a surface can be expressed by equation (6.1) as follows

$$L^*(\delta) = \sigma\left[\left(\varepsilon_{\text{sky}} F_{\text{sky}} T_{\text{sky}}^4 + \varepsilon_{\text{grd}} F_{\text{grd}} T_{\text{grd}}^4 + \varepsilon_{\text{bld}} F_{\text{bld}} T_{\text{bld}}^4\right) - \varepsilon_{\text{sur}} T_{\text{sur}}^4\right].$$

The abbreviations grd, bld and sur define ground, facing building and design building surfaces respectively. Figure 6.2 illustrates the three-surfaced model of external building topography, which defines surface dimensions for the purpose of estimating the long-wave radiant exchange between the three external surfaces and sky. In the case of a green field site, the adjacent building can be excluded from the model. The topography model forms part of the radiant exchange, view factor sub-model. The view factor model is based on well established view factor algebraic methods described in the literature. The geometry of the local topography requires using the view factor formulations for parallel and perpendicular surfaces only and the corresponding formulae given in the CIBSE guide [70] are employed in the model. View factor models have been set up for each of the three surfaces. For a particular surface, the view factors to the other two facing surfaces are computed. Using the view factor summation rule (which states that the sum of all view factors from a particular surface to all facing surfaces equals one), subtracting these two view factors from one gives the view factor from the particular surface to the sky.

6.4.4.2 Design side building's view factor sub-model

The design building façade forms one of the building facades on its side of the street. The ground and facing building facades will exchange long-wave radiant energy with all the building facades on the design building side of the street, including the design building. All the design side building surfaces must be taken into account in order to simulate the facing buildings and ground surface temperatures more realistically. An average height and total length of façades approximates the influence of the design side buildings for view factor calculations.

6.4.4.3 Design façade view factor sub-model

For more precise thermal simulation, the model is set up to compute view factors from elemental areas of the design building façade, the external wall of a single office or window for example. The elemental area can be located anywhere on the building façade in order to analyse the variation of view factors to the ground, facing buildings and sky, as well as the influence of shading, and reflected solar radiation from the sky and facing buildings. The elemental surface area can be varied in size, from a single window to the entire design building façade. Hence, four view factor models are required, one for each external surface and the fourth for the design façade elemental surface area. The function of the facing

building and ground view factor models is to facilitate realistic long-wave radiant exchange with the design façade elemental area. In addition, all the external facades, ground and sky models will participate in long-wave radiant exchange with each other.

6.4.4.4 Surface temperatures

Equation 6.1 defines the net radiant flux for the design façade, elemental surface area. Another three equations, similar to equation (6.1), defining the net radiant flux for the design side building facades, the facing building facades and the ground, are required. Figure 6.5 shows that the surface temperature results from the conduction models are inputted into the long-wave radiation models and the net long-wave radiant fluxes responses become inputs to the conduction models. This iteration process continues until the surface temperatures converge to steady state values. The sky temperature model is independent of all external surfaces and an iteration process is not required to establish its temperature.

6.4.4.5 Sky temperature for vertical surfaces

Cole [29] gives the following expression for estimating the sky long-wave radiation on a surface inclined at angle δ to the horizontal and extent of cloud cover C.

$$R_{\text{sky}} = K_1\left[222 + 4.9t_{\text{ao}} + (65 + 1.39t_{\text{ao}})C\right] + 0.09\left[1 - C(0.7067 + 0.00822t_{\text{ao}})\right]K_3\sigma T_{\text{ao}}^4 \quad (6.24)$$

where $K_3 = 0.7629(0.01\delta)^4 - 2.2215(0.01\delta)^3 + 1.7483(0.01\delta)^2 + 0.054(0.01\delta)$

and $K_1 = \cos^2(\delta/2)$

Cloud cover C may be estimated using the following expression, which correlates cloud cover with horizontal direct and diffuse solar radiation, I_{d} and I_{h} respectively.

$$C = 1 - I_{\text{d}}/(I_{\text{d}} + I_{\text{h}}) \quad (6.25)$$

As cloud cover increases, C increases to a maximum value of one.

Equation (6.24) accounts for sky long-wave radiation due to an unobstructed sky dome, in the case of a vertical surface receiving sky radiation. K_1 is the sky view factor and for a vertical surface becomes 0.5. The view factor will be less for an obstructed sky dome. The effective sky temperature may be estimated using the following expression, based on the emissive power of the sky, in the case of a vertical surface receiving sky radiation:

$$K_1 \varepsilon_{sky} \sigma T_{sky}^4 = R_{sky} \tag{6.26}$$

From which $$T_{sky} = \left[R_{sky} / \left(K_1 \varepsilon_{sky} \sigma\right)\right]^{0.25} \tag{6.27}$$

Cole [29] provides expressions that can be used to derive the following relationship for estimating the sky emissivity, which correlates sky emissivity with cloud cover and external air temperature.

$$\varepsilon_{sky} = (1 - 0.84C)\{0.527 + 0.161 \exp[8.45(1 - 273/T_{ao})]\} + 0.85C \tag{6.28}$$

The actual sky view factor corresponding to the vertical surface of interest is obtained from the surface's view factor model. The values of effective sky temperature, emissivity and view factor are then inputted into equation (6.1).

6.4.4.6 Sky temperature for horizontal surfaces

In the case of the ground or a roof surface, the inclination angle δ becomes zero and equation (6.24) reduces to:

$$R_{sky} = [222 + 4.9 t_{ao} + (65 + 1.39 t_{ao})C] \tag{6.29}$$

The effective sky temperature can be estimated using equation (6.27). For a horizontal surface $K_1 = 1$. The actual sky view factor for the ground is obtained from its view factor model. The effective sky temperature, emissivity and view factor can then be inputted into equation (6.1) formulated for a ground surface or roof.

The hourly values of effective sky temperature estimated for vertical or horizontal surfaces, using equations (6.24) and (6.29) respectively, differ only by a small amount and for practical purposes, estimating the sky temperature using equation (6.29) should suffice for both vertical and horizontal surfaces.

6.4.5 Solar model

6.4.5.1 Source of solar data

The solar model can employ either meteorological solar data obtained from weather files or published solar data, as provided in the CIBSE guide [71], for example. Normally horizontal global and diffuse radiation is measured and recorded in weather files. The normal direct beam radiation can be calculated from the direct horizontal radiation and using solar geometry, the direct radiation on a surface at any inclination and orientation can then be determined. Solar data from weather files is more appropriate for simulation runs

covering a period of days or longer. The solar data provided in the CIBSE guide is more suitable for design day type calculations due to being statistically compiled from real weather data during the period 1981 to 1992. The data is representative of the local climate during warm sunny periods. The tables provide solar irradiance data for a number of locations across the U.K. Hourly solar irradiances are given for eight surface orientations and for the horizontal surface. Hourly values of the normal direct beam radiation are also provided.

6.4.5.2 Modelling with tabulated solar data

Although the solar data provided in the CIBSE guide can be used directly, a more flexible approach is to model the normal direct beam in order to compute the direct irradiation on any surface inclination angle, orientation and time of the day. In a similar manner, the horizontal diffuse irradiation can be modelled and then used with a suitable diffuse radiation model to compute diffuse irradiation on any inclined surface and orientation. The tabulated values of normal direct beam and horizontal diffuse radiation, given in Table 2.24 of the CIBSE guide, correlate very well with the sine of the solar altitude angle, a. Non-linear relationships are produced which may be curve fitted, using polynomial regression, to produce expressions of the form:

$$I = m_1 \sin^2 a + m_2 \sin a + C \tag{6.30}$$

Two correlation equations are required to fit each series of normal beam and horizontal diffuse irradiances, due to the profiles of solar altitude before and after 12.00 hours solar time, being mirror images of each other. To obtain optimum fitting curves a "split-time" is used to define the time at which the series is divided to produce the two correlations. Tables 6.7 and 6.8 provide samples of the resulting correlation coefficients and constants for

Table 6.7 Coefficients for correlation equation (6.30) normal direct beam solar radiation. Based on Table 2.24, London area, CIBSE guide

Month	Time split	m_1	m_2	C
Jun-21	Up to 13.00:	-788	1576	59
	After 13.00:	-630	1408	72
Jul-04	Up to 13.00:	-738	1449	58
	After 13.00:	-734	1439	58
Aug-04	Up to 11.00:	-454	1202	88
	After 11.00:	-317	1083	72

Table 6.8 Coefficients for correlation equation (6.30) horizontal diffuse solar radiation. Based on Table 2.24, London area, CIBSE guide

Month	Time split	m_1	m_2	C
Jun-21	Up to 14.00:	-151	280	16
	After 14.00:	-157	301	14
Jul-04	Up to 12.00:	-68	227	13
	After 12.00:	-89	250	11
Aug-04	Up to 12.00:	-94	245	20
	After 12.00:	-63	234	19

normal beam and horizontal diffuse irradiances respectively. For example, using equation (6.30), the correlation expressions for June are:

Normal direct beam:	$I = -788\sin^2 a + 1576\sin a + 59$	up to 13.00 solar time
Normal direct beam:	$I = -630\sin^2 a + 1408\sin a + 72$	after 13.00 solar time
Horizontal diffuse:	$I_h = -151\sin^2 a + 280\sin a + 16$	up to 14.00 solar time
Horizontal diffuse:	$I_h = -157\sin^2 a + 301\sin a + 14$	after 14.00 solar time

The split times of the correlation expressions are given at the RHS. For application on a computer spreadsheet program, a logic statement is used to ensure that the appropriate part of the correlation equation is employed before or after the specified split solar time. The core information required for calculating the hourly direct and diffuse solar irradiation being encapsulated in only four equations is the key advantage of using the correlation equations. The solar model is arranged to automatically generate normal beam and horizontal diffuse irradiance on inputting the appropriate latitude and month day number. The day number is the number of days counting from one on the 1st January to the day of the month specified in Table 2.24 of the CIBSE guide (e.g. see first column of table 6.7). The normal direct beam can then be used to determine the hourly values of direct solar irradiance on any inclined surface, as well as the horizontal surface, by employing equations (2.17) to (2.22), which are described in chapter II.

The diffuse solar irradiance for any surface inclination and azimuth angle is determined by employing the Perez *et al* model [20] as described in chapter II and defined by equation (2.23) as follows.

$$I_c = I_h \left[0.5(1+\cos\delta)(1-F_1') + F_1' a/c + F_2' \sin\delta\right]$$

The hourly values of horizontal diffuse irradiance I_h, required for the above equation, are obtained from the appropriate horizontal diffuse irradiance correlation defined by equation (6.30).

The solar model is arranged to automatically generate the surface direct and diffuse irradiances on inputting the appropriate surface orientation and inclination angle. The latitude and day number are also used to automatically select the appropriate correlation equations employed to generate normal beam and horizontal diffuse irradiances.

A second solar model is created for the facing building façade for the purpose of simulating external surface temperatures for input into the long-wave radiant exchange model.

6.4.5.3 Modelling solar irradiance from weather data

Horizontal global and diffuse solar radiation are normally measured and recorded in weather data files. Real solar radiation tends not to exhibit a smooth rising and descending daily profile compared to the tabulated solar irradiance profiles provided in CIBSE guide. Varying cloud cover normally produces a jagged solar profile, the exception being during cloudless or totally overcast sky conditions. Consequently, real solar irradiances do not correlate well with solar altitude angle and modelling the daily solar irradiance profile using equation (6.30) is not appropriate. Further, solar data varies from day to day and there is no benefit from correlating the data to a particular variable as with tabulated solar data. The measured data is inputted directly into the solar model. The direct horizontal solar radiation is determined from the measured values of horizontal global and diffuse solar radiation. The normal direct beam radiation is then calculated using equation (2.17). From this point on, the calculation process is identical to that for employing tabulated design data in the form of the correlation equation (6.30). The process is fully automated, on inputting the measured solar data into the solar model.

6.4.6 Solar shadow model

6.4.6.1 Shading of building facades and ground

The shadow model is used to determine the shaded fraction of the facades on the design and facing building sides of the street, and the ground surface between the buildings. Further, the shaded fraction on any elemental area of the design building façade and self-shading of glazing, due to window reveals, may be determined. The shaded fractions of the building facades on both sides of the street and the ground are required for simulating surface temperature responses, due to direct and diffuse irradiation, and for the purpose of estimating long-wave radiant exchange. Two shadow models are required, one for the design building façade and the other for the facing buildings on the opposite side of the street. Figure 6.7 shows that vertical and horizontal shadow dimensions can be determined from the solar altitude and wall-solar azimuth angles, a and n respectively. Hourly values of these angles are generated in the solar model. The plan of figure 6.7 shows that the shadow model must be arranged to automatically switch from calculating sunlit dimensions on the right hand side to the left hand side of the buildings due to the changing solar position during the day. The elevation shows that the model must be sensitive to the time when each façade faces the sun to account for partial shading due to facing buildings, and total shading due to the façade not facing the sun. The solar incident angle can be used to detect the solar position relative to a particular façade. The solar incident angle is positive when a façade is facing the sun and negative when the façade is totally in shade due to the sun being behind the building. Logic statements are included in the model to switch to the appropriate geometric formulation to suit solar position relative to the surface of interest. For each façade, ground and design façade elemental area of interest, hourly shading factors, S, are computed. Shading factors are defined as the ratio of the shaded to total surface area. The complementary term of the shading factor is the sunlit factor defined by $(1 - S)$.

6.4.6.2 Self shading of glazed areas

It is necessary to establish both the sunlit area of windows in order to determine the amount of direct beam and diffuse radiation being transmitted into a space, and the surface temperatures of the glazing which influence conductive and convective heat transfers. Results from the façade shadow model will indicate whether a window is totally shaded and partially or totally sunlit. If totally shaded, the model computes the total diffuse solar

irradiance on the window. In the case of totally or partially sunlit windows, the model computes the additional shading due to window reveals. Similar to the façade shadow

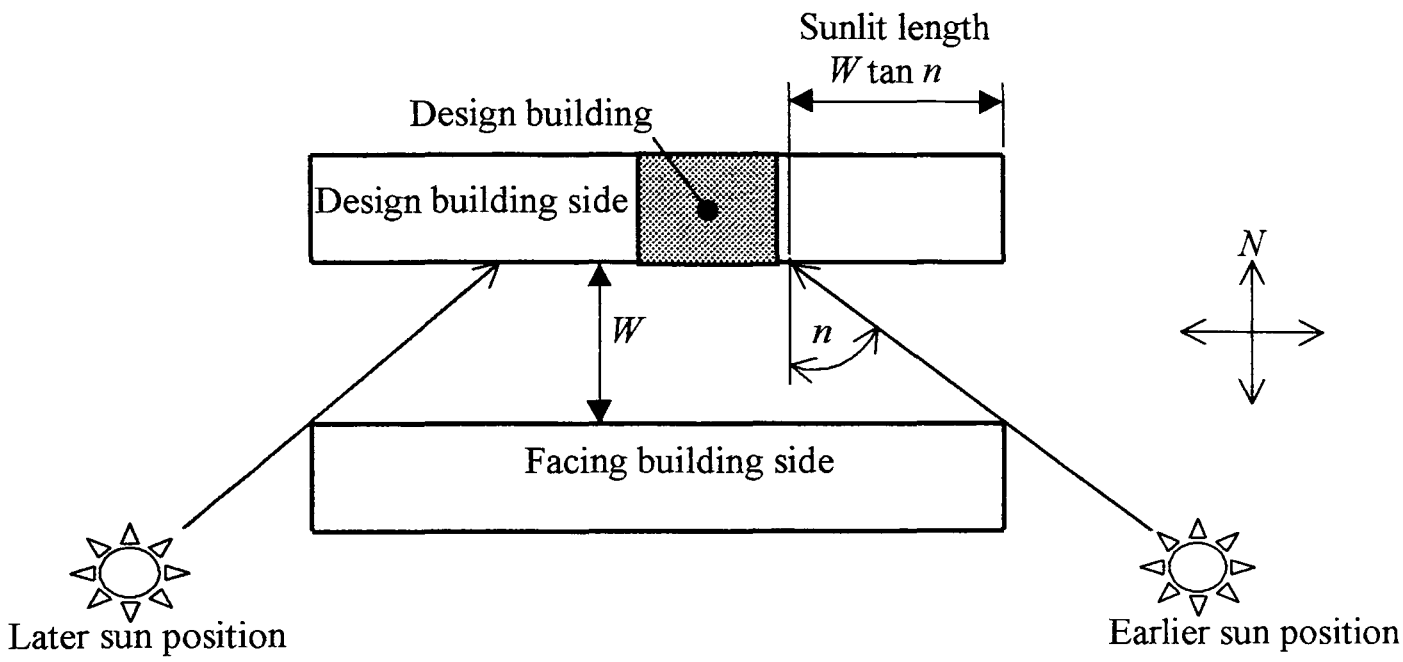

Figure 6.7. Solar geometry of three-surfaced model

model, horizontal and vertical shadow dimensions are determined using solar altitude and wall-solar azimuth angles as well as the window reveal depth and, overhang dimensions. The model then computes the total direct and diffuse irradiance on the window.

6.4.7 Solar irradiance of external surfaces

6.4.7.1 Design façade

Shaded surfaces of the design façade receive sky diffuse, facing building and ground reflected solar radiation. Sunlit surfaces also receive direct solar irradiation. As described in section 6.5.4.2, the Perez *et al* model [20] is employed for modelling diffuse irradiance on vertical surfaces. The model is based on an unobstructed sky dome and therefore the resulting value of diffuse radiation I_c must be corrected in the case of an obstructed sky dome. The view factor from the design façade area of interest to the sky F_{sky} is obtained from the radiation exchange, view factor model. In the case of a vertical surface, the view factor for an unobstructed sky is 0.5. The corrected value of diffuse irradiance is given by:

$$(I_c)_{corrected} = \frac{F_{sky}}{0.5} I_c \tag{6.31}$$

where I_c is defined by equation (2.23).

For a partially sunlit area, the direct irradiance is multiplied by the complementary term of the shading factor S_{sur}. The direct radiation incident on the sunlit area is spread over the entire façade area of interest, due to the assumption of isothermal surfaces. It is found that façade elemental areas are more frequently either totally sunlit or shaded and the overall error incurred due to assuming isothermal surfaces is small.

The ground and facing façade reflected radiation is assumed totally diffuse and the fraction received by the design façade elemental area is estimated using the same view factors employed in the long-wave radiant exchange model.

6.4.7.2 Facing building and ground

The total solar irradiance of the facing building and ground are determined in a similar manner to the design façade. However, the reflected solar radiation from the design façade to these surfaces is estimated by including the reflected solar radiation from all the design side building facades.

6.4.7.3 Reflected solar radiation

The external surfaces participate in the solar reflecting process in a similar manner to the long-wave radiant exchange process. Modelling reflected solar radiation involves iterative calculation processes due to these thermal links between the external surfaces. Reflected solar radiation from the ground and facing façade is also applied to the design façade windows.

Chapter VI

6.5 Development of the Window System Thermal Model

6.5.1 A Dominant thermal link between the external and internal environments

Significant energy exchanges occur via the window system to the extent that it may be defined as a complex bi-directional space heat exchanger with the ability to transfer energy by long and short-wave radiation, conduction and convection. The energy transfers are complicated by solar inter-reflections, absorption, and energy exchanges between the transparent layers, in the case of a double-glazed unit with internal blinds. External shading and intermittent operation of the internal blind further complicates the thermal modelling of the window system. The main objectives of thermally modelling the window system are to determine the total transmitted solar radiation and its surface temperatures. Determining surface temperatures is relatively more complex compared to determining the transmitted solar radiation when employing the frequency domain method. It is necessary to generate a Fourier series for each of the thermal excitations to establish the inner surface temperature. For a double glazed window with internal blind, five Fourier series are required; three of these account for the absorbed solar in the three layers of the window system. This approach is computationally very inefficient. The two new concepts of ***Window Solar Temperature*** and ***Window Sol-air Temperature*** have been developed to model the window heat transfers in a computationally more efficient manner. A new window performance indicator in terms of minimising the space cooling load, the ***Window Solar Gain Index***, is described. The inclusion and operation of internal window blinds increases modelling complexity due to the convective air flows that are produced and the varying inner thermal resistance due to the operation of the blinds. A window model has been developed to account for these additional thermal processes.

6.5.2 Window Solar Temperature

6.5.2.1 Combining the solar radiation absorptions of the window layers

Window solar temperature combines the effects of solar absorption within the window layers into an equivalent temperature excitation, which acts at the external boundary of the window. Figure 6.8 illustrates the tracing of a single ray of solar radiation as it undergoes the processes of transmittance, absorption and reflection through a treble glazed or double glazed window unit with internal blinds. It is assumed that the internal blinds are well

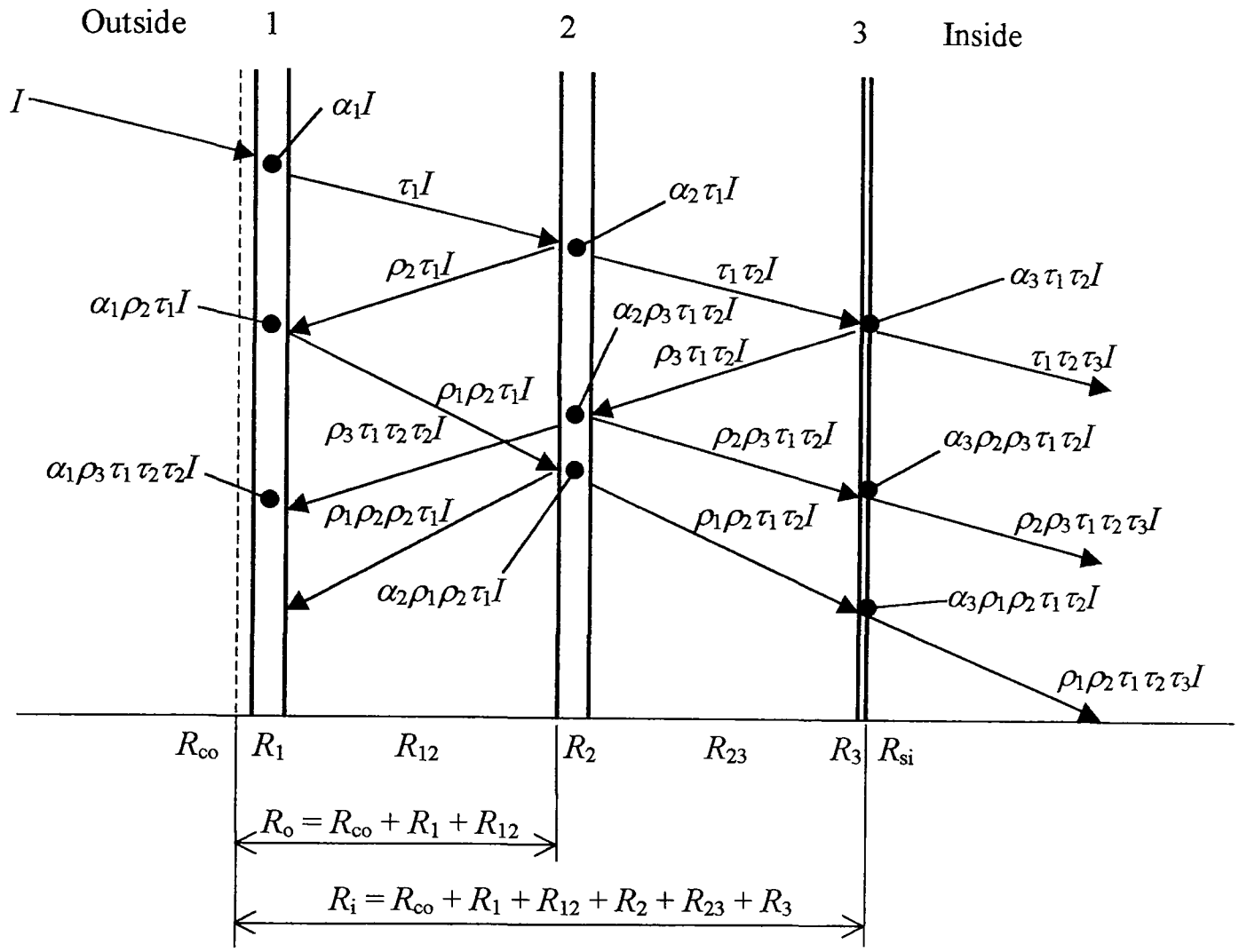

Figure 6.8. Solar absorption, transmittance and thermal resistances of window system

sealed, allowing negligible airflow between inner glazing and blind. Loose fitting blinds are addressed in section 6.5.5. The cumulative processes of solar transmittance, absorption and reflectance, defined by τ, α and ρ respectively, are shown in order to estimate the total solar radiation absorption in the layers, 1, 2 & 3, and the total solar transmittance into the space. For clarity, the accumulation process is terminated after three solar absorptions at each layer. Further ray tracing will have an insignificant influence on the results. The outside convective surface resistance, thermal resistances of each layer and the thermal resistances representing the spaces between the layers are shown at the bottom of the diagram. Heat conduction through the system is assumed purely resistive in behaviour, due to the window system having negligible thermal capacity. Referring to figure 6.8, the total solar radiation absorption at each layer is given by

$$\text{Layer 1: } IA_1 = I\alpha_1\left(1+\rho_2\tau_1+\rho_3\tau_1\tau_2^2+\rho_1\rho_2^2\tau_1\right) \tag{6.32}$$

$$\text{Layer 2: } IA_2 = I\alpha_2\tau_1\left(1+\rho_3\tau_2+\rho_1\rho_2\right) \tag{6.33}$$

$$\text{Layer 3: } IA_3 = I\alpha_3\tau_1\tau_2\left(1+\rho_2\rho_3+\rho_1\rho_2\right) \tag{6.34}$$

where I is the solar irradiance incident on the external surface of the window.

The total absorbed solar radiation is then given by

$$\textit{Total absorbed solar radiation} = I\left(A_1+A_2+A_3\right) \tag{6.35}$$

Employing the thermal resistances shown in figure 6.8, it can be shown that the window solar temperature is given by:

$$t_{ws} = I\left(R_{co}A_1+R_oA_2+R_iA_3\right) \tag{6.36}$$

Only the 24-hour mean values of thermal resistances are used in equation (6.36). A method for correcting the error, incurred due to using mean values of thermal resistances, is described in section 6.5.3. The window solar temperatures for direct and diffuse solar radiation should be determined separately, the optical properties for direct and diffuse solar radiation being different. The results are then summed to give the total window solar temperature. The direct solar optical properties vary with solar incident angle and must be calculated for each hour. The hemispherical diffuse optical properties are independent of solar incident angle and are therefore defined by single values of absorption, reflectance and transmittance.

Window solar temperature is not the external surface temperature of the window. It is analogous to sol-air temperature in terms of converting the solar radiation excitation into an equivalent temperature excitation. It can only be used to determine the inner surface temperature of the window system in order to calculate the subsequent convective heat transfers and long-wave radiant exchange with the internal environment. The validity of equation (6.36) has been fully tested against a finite difference model. Results are provided in chapter VII, Validation.

6.5.2.2 Solar shading

The shaded area of glazing, due to external buildings and window reveals, is determined using the solar shadow model described in section 6.4.6. The resulting total diffuse and direct solar radiation incident on shaded and sunlit glass respectively is distributed evenly over the total surface area of the glazing, due to isothermal surfaces being assumed. The

resulting hourly values of diffuse and direct radiation are used in equation (6.36) to compute the corresponding diffuse and direct window solar temperatures.

6.5.2.3 Operation of internal blinds

The 24-hour window solar temperature and transmitted solar radiation profiles can be generated to include the operation of internal blinds. Equation (6.36) is formulated for a double glazed window only during the period when the blinds are open, and during the time the blinds are closed the equation is formulated to include the pertinent optical and thermal properties of a three-layered window system. Logical statements are employed to switch to the appropriate formulation corresponding to a prescribed daily blind operation schedule.

6.5.2.4 Window Solar Gain Index

The correct choice of window system can have a significant influence on reducing plant cooling load or reducing the environmental temperature in the case of a naturally ventilated building. The approach is to select window systems that minimise solar transmittance and inner surface temperature. At the initial design stages of a building project, it is beneficial to select an energy efficient window system without recourse to employing a dynamic thermal simulation, software program. This approach is possible employing the findings of section 6.5.2. The thermal and optical properties enclosed within the brackets of equation (6.36) characterise the thermal behaviour of the window system in terms of the heat exchange performance of its inner surface. The window solar absorption factor, from equation (6.36) is:

$$F_{\alpha} = \left(R_{co} A_1 + R_o A_2 + R_i A_3\right) \tag{6.37}$$

Further, a solar transmittance factor, which characterises the performance of the window system in terms of transmitting solar radiation, may also be formulated. Referring to figure (6.8), the total solar transmitted radiation into the space is given by

$$q_{\tau} = I\tau_1\tau_2\left(1 + \rho_1\rho_2 + \rho_1^2\rho_2^2\right) \tag{6.38}$$

The solar transmittance factor can be extracted from equation (6.38) and expressed by

$$F_{\tau} = \tau_1\tau_2\left(1 + \rho_1\rho_2 + \rho_1^2\rho_2^2\right) \tag{6.39}$$

The window solar factors will be defined by different formulations of thermal and optical properties than those defined by equations (6.37) and (6.39) for window systems consisting of a different number of layers. Referring to equations (6.38) and (6.39) the solar

transmittance factor can be defined as the transmitted solar radiation per watt of incident solar radiation:

$$F_\tau = q_\tau / I \tag{6.40}$$

The solar absorption factor can also be recast as a specific transmitted energy factor by multiplying it by the U-value of the window layers. The U-value should include an inner combined convective and radiative surface resistance R_{si} to account for the influence of long-wave radiant exchange between the inner surface of the window system and the space surfaces. Referring to figure 6.8, the corresponding U-value is given by:

$$U_\alpha = 1/(R_i + R_{si}) \tag{6.41}$$

The approximate amount of energy transferred to the inside environment, via absorbed solar energy, per watt of incident solar radiation is then given by:

$$q_\alpha / I = F_\alpha U_\alpha \tag{6.42}$$

The window solar gain index is therefore given by the sum of equations (6.40) and (6.42) as:

$$WSGI = F_\tau + F_\alpha U_\alpha \tag{6.43}$$

It is sufficient to determine the window solar gain index using only the direct optical properties. The advantage of the window solar gain index is that it combines the effects of the convective and transmitted solar heat transfers into a single indicative measure. Window systems with low values of window solar gain index should be selected in order to minimise the space cooling load. Reading from outside to inside of a window system, for example, the *WSGI*'s of some typical window systems are: clear/clear 0.715, absorbing bronze/clear 0.488, clear/clear/blind 0.344, reflecting bronze/clear 0.151 and clear/reflecting blind/clear 0.092. Figure 6.9 illustrates the results from a study involving the examination of twenty-eight window systems. The transferred solar energy was determined for each window system and plotted against its window solar gain index. The graph shows a close correlation between transferred solar energy and the window solar gain index, the more efficient window systems appearing closer to the origin of the graph.

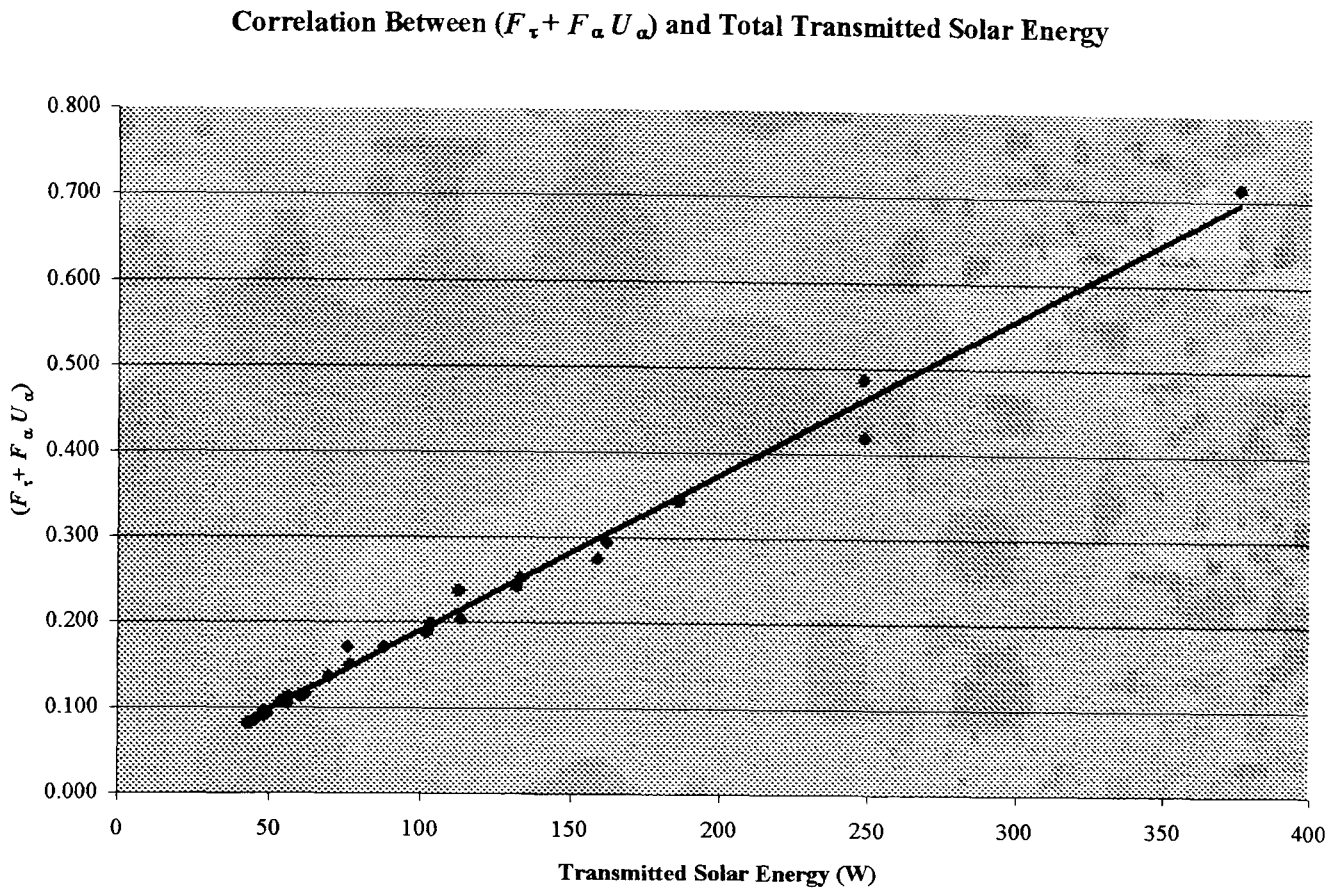

Figure 6.9. Correlation between window solar gain index and total transmitted solar energy

6.5.2.5 Glass optical properties

Glass optical properties vary with the solar beam incident angle, glass thickness and type of glazing. The solar beam incident angle is determined in the solar model. Trigonometric formulations for computing the properties are not too complex but the computational process is relatively long requiring much computer time and effort. Further, it is necessary first to establish the refractive index and extinction coefficient for each type of glass used in the window system. A more efficient computational approach is to correlate the optical properties directly with the beam incident angle. ASHRAE publish comprehensive tables of solar optical properties [64] for single and multiple layer windows in terms of incident angle. The tabulated properties of single glazing correlate accurately with the solar beam incident angle and employing polynomial regression results in the following expression.

$$P = m_1 \cos^3 i + m_2 \cos^2 i + m_3 \cos i + c \qquad (6.44)$$

where P can represent absorption, reflectance or transmittance. Table 6.9 provides values of the coefficients and constants of equation 6.44 for a sample of glass types, in order to

calculate their transmittance and absorption properties. The reflectance can be obtained by subtracting the resulting absorption and transmittance values from one, since the sum of the optical properties of a particular glass type equals one. Optical properties derived from the

Table 6.9. Transmittance and absorption coefficients and constants for equation (6.44)

Class type	Transmittance				Absorption			
	m_1	m_2	m_3	C	m_1	m_2	m_3	C
3mm CLR	1.4037	-3.5123	2.964	-0.0245	0.0284	-0.0906	0.0482	0.1039
6mm CLR	1.0533	-2.7331	2.4358	0.0241	0.2609	-0.5844	0.3596	0.1141
3mm BRZ	0.981	-2.4108	2.1069	-0.026	0.4873	-1.0697	0.6684	0.2044
6mm BRZ	0.7869	-1.8656	1.617	-0.0482	0.7439	-1.7356	1.2018	0.2504
3mm GRN	1.0435	-2.5316	2.1505	-0.0522	0.548	-1.2351	0.814	0.2033
6mm GRN	0.7537	-1.8132	1.5707	-0.0406	0.7123	-1.7154	1.2397	0.2339
3mm GRY	0.9043	-2.2892	2.0453	-0.0503	0.3756	-0.9403	0.6625	0.2329
6mm GRY	0.6793	-1.6435	1.474	-0.0498	0.7902	-1.8726	1.3185	0.254
6mm BLUGRN	0.7068	-1.7565	1.5733	-0.0333	0.7123	-1.7154	1.2397	0.2139
6mm SS on CLR 8%	-0.0784	0.0769	0.0405	0.0208	0.977	-2.3497	1.8715	0.1119
6mm SS on CLR 20%	0.2273	-0.5976	0.5363	-0.0154	1.1316	-2.6284	2.0119	0.1263

single glazing correlation can then be employed to compute the optical properties of the multiple layer window systems as defined by equation's (6.32) to (6.34) and (6.38).

6.5.3. Window Sol-Air Temperature

6.5.3.1 Combining the thermal excitations

Section 6.5.2 described a procedure for combining the absorbed solar radiation in each layer of a window system, into a single equivalent window solar temperature acting at the external boundary of the window. Combining all the window thermal excitations into a single thermal driving force that can then be represented by a single Fourier series, develops the concept further. The result is a computationally efficient process compared to representing each thermal driving force by its own Fourier series. The window sol-air temperature is defined by:

$$t_{\text{eow}} = t_{\text{ws}} + t_{\text{ao}} + \left(L_{\text{e}} - L_{\text{so}}\right)/\bar{h}_{\text{co}} + \left(\Delta t_{\text{eow}}\right)_{\text{c}} \tag{6.45}$$

Equation (6.45) is similar to the traditional sol-air temperature formulation for external structural elements but includes the additional terms of window solar temperature, t_{ws}, and a convection correction term, $(\Delta t_{\text{eow}})_{\text{c}}$. The external long-wave radiation, L_{e}, due to external buildings, sky and ground is obtained from the external long-wave radiation model

described in section 6.4.4. The external window long-wave radiation, L_{so}, depends on its external surface temperature, t_{so}, which is influenced by all the external and internal heat transfers of the window system indicating that the window sol-air temperature cannot be determined independently of the internal environment. The window sol-air temperature model must be thermally connected to the internal environmental model to simulate heat transfer with the internal window surface. Figure 6.10 illustrates a double glazed window with internal blinds showing heat transfer coefficients, surface temperatures and absorbed solar radiation. The heat transfer coefficients symbolised with a bar are the 24-hour mean values that must be employed in the thermal transmission matrix, defining the thermal behaviour of the window conduction model. The heat transfer coefficients shown below the mean values correspond to the variable hourly values. The inner and outer glass

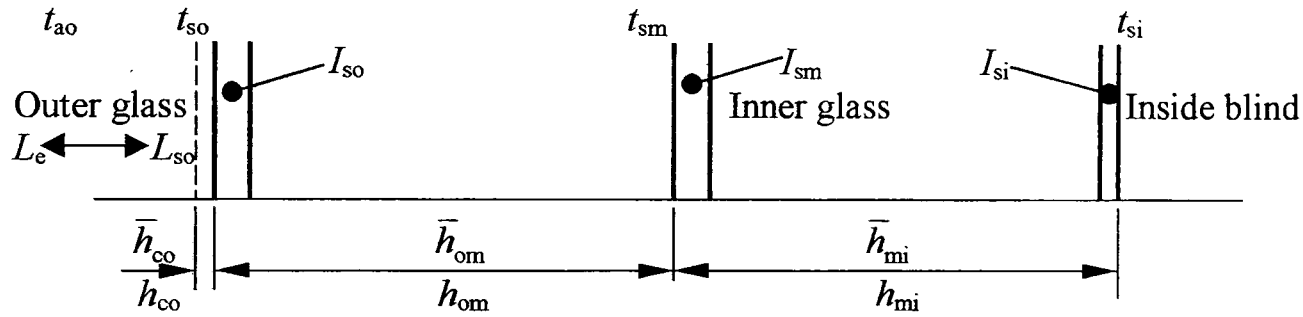

Figure 6.10. Double-glazed window system with internal blind

temperatures may be estimated, with little error incurred, by modelling solely with the heat transfer coefficients, due to the insignificant mass of the window system. The surface temperature are then given by:

$$t_{so} = \frac{(h_{om} + h_{mi})[I_{so} + (L_e - L_{so}) + h_{co} t_{ao}] + h_{om}(I_{sm} + h_{mi} t_{si})}{h_{co}(h_{om} + h_{mi}) + h_{om} h_{mi}} \tag{6.46}$$

$$t_{sm} = \frac{I_{sm} + h_{om} t_{so} + h_{mi} t_{si}}{h_{om} + h_{mi}} \tag{6.47}$$

The inner surface temperature, t_{si}, is obtained from the internal environmental model. Iterative calculation processes are required due to the dependent thermal links between the window layer surface temperatures and the window sol-air temperature. A correction must be applied to equation (6.45) to cancel the error incurred due to employing the constant mean values of heat transfer coefficients in the window thermal transmission matrix.

Referring to figure 6.10, the heat transfers between the surfaces, based on mean heat transfer coefficients, are given by

$$\bar{q}_{co} = \bar{h}_{co}(t_{ao} - t_{so}), \qquad \bar{q}_{om} = \bar{h}_{om}(t_{so} - t_{sm}) \qquad \text{and} \qquad \bar{q}_{mi} = \bar{h}_{mi}(t_{sm} - t_{si}) \tag{6.48}$$

and the heat transfers between the surfaces, based on the hourly variable heat transfer coefficients, are given by

$$q_{co} = h_{co}(t_{ao} - t_{so}), \qquad q_{om} = h_{om}(t_{so} - t_{sm}) \qquad \text{and} \qquad q_{mi} = h_{mi}(t_{sm} - t_{si}) \tag{6.49}$$

The residual heat transfer correction fluxes are then given by:

$$q_{co} - \bar{q}_{co}, \qquad q_{om} - \bar{q}_{om} \qquad \text{and} \qquad q_{mi} - \bar{q}_{mi} \tag{6.50}$$

Dividing each residual error by the corresponding mean heat transfer coefficient, results in the equivalent temperature difference corrections between each surface and hence the total window sol-air, correction term of equation (6.45) is given by:

$$(\Delta t_{eow})_c = \frac{(h_{co} - \bar{h}_{co})(t_{ao} - t_{so})}{\vec{h}_{co}} + \frac{(h_{om} - \bar{h}_{om})(t_{so} - t_{sm})}{\vec{h}_{om}} + \frac{(h_{mi} - \bar{h}_{mi})(t_{sm} - t_{si})}{\vec{h}_{mi}} \tag{6.51}$$

Only the first correction term on the RHS of equation (6.51) is required if constant coefficients between the window layers are employed. No correction term is required in equation (6.45) if the external convection coefficient is also assumed constant. Figure 6.11 illustrates the calculation process for determining the window sol-air temperature. The window sol-air temperature model has been successfully validated against a finite difference model, which applied all the thermal excitations as separate simultaneous inputs in contrast to a window sol-air temperature. Results are provided in chapter VII, Validation.

6.5.4 Window heat transfer coefficients

The heat transfer coefficients at the surfaces of the window layers play a dominant role in the thermal behaviour of the window system due to the insignificant masses and thermal resistances of the window layers. Accurate assessment of hourly values of the heat transfer coefficients is necessary, in order to model the significant influence the window system has on the internal environment. The external convective heat transfer coefficient is determined in the external convection model, as described in section 6.4.3. Section 6.6.4 describes the calculation processes involved in the internal convection model. Heat transfer between the

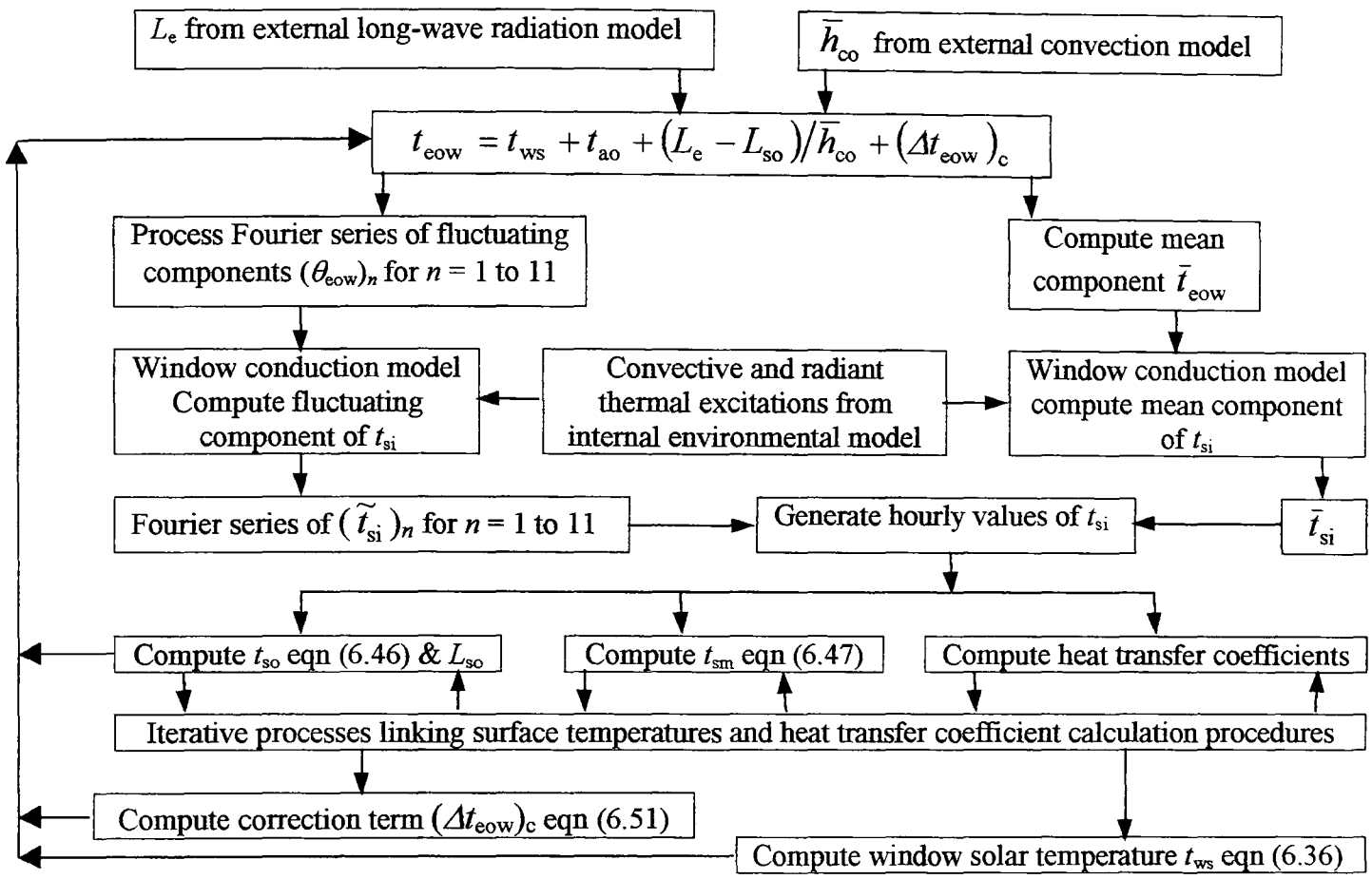

Figure 6.11. Window solar temperature calculation process

window layers is governed by long-wave radiant exchange between the surfaces as well as convection between the fill gas and window layer surfaces.

6.5.4.1 Long-wave radiant exchange between window layers

The general expression for long-wave radiant exchange between a number of surfaces is given by equation (2.8). In the case of two parallel facing surfaces of equal area, equation (2.8) simplifies to:

$$q_1 = \varepsilon_1 \left[\sigma F_{12} \left(T_1^4 - T_2^4 \right) + F_{12} \left(1/\varepsilon_2 - 1 \right) q_2 \right] \tag{6.52}$$

For two parallel window surfaces $q_1 = -q_2$ and equation (6.52) reduces to

$$q_1 = F_r \sigma \left(T_1^4 - T_2^4 \right) \tag{6.53}$$

where the radiant exchange coefficient $F_r = \left[\dfrac{1}{1/\varepsilon_1 + F_{12}(1/\varepsilon_2 - 1)} \right] F_{12}$

The view factor, F_{12}, nearly equals one and may be excluded from equation (6.53), in the case of large parallel surfaces separated by a small distance. However, the results of Table

6.10 suggest that significant errors may be incurred if the view factor is permanently disregarded from equation (6.53).

Table 6.10 Radiant exchange view factors for parallel surfaces separated by 25mm

Surface dimensions (m)	2.0 × 2.0	2.0 × 1.0	1.0 × 1.0	1.0 × 0.5	0.5 × 0.5
View Factor F_{12}	0.976	0.964	0.952	0.929	0.908

A radiant exchange heat transfer coefficient can be formulated, from equation (6.53), in terms of the temperature difference between the parallel surfaces as follows

$$h_r = F_r \sigma \frac{T_1^4 - T_2^4}{t_1 - t_2} \tag{6.54}$$

The temperature difference relationship of equation (6.54), generally described as non-linear, can be shown to be quite linear over short ranges of temperature. The temperature relationship $\left(T_1^4 - T_1^4\right)/\left(t_1 - t_2\right)$ correlates almost linearly with $(t_1 + t_2)$ over the mean temperature range $0<0.5(t_1 + t_2)<35$ and temperature differences, $(t_1 - t_2)$, ranging from 5K to 50K within the specified mean temperature range. Over this range of mean temperatures and temperature differences, equation (6.54) may be simplified to:

$$h_r = F_r\left[0.0288\left(t_1 + t_2\right) + 4.6028\right] \tag{6.55}$$

The maximum difference in results between equations (6.54) and (6.55) is approximately 1% over the mean temperature and temperature difference ranges specified above. This is a much smaller error compared to the error that may be incurred due to assuming a radiant view factor of unity. The simpler formulation of equation (6.55) and its performance over the specified temperature ranges demonstrates its computational efficiency, compared to equation (6.54), for computer calculations. Similar correlation formulae to equation (6.55) may be developed to suit other temperature ranges.

6.5.4.2 Convective heat transfer between window layers

Wright [72] has proposed a procedure for determining the convective heat transfer coefficient between glazing layers. The procedure is based on the following formulation set, which correlates the heat transfer coefficient with the Nusselt number.

$$\mathrm{Nu} = 0.0673838\,\mathrm{Ra}^{1/3} \qquad \mathrm{Ra} > 5\times10^{4} \qquad (6.56a)$$

$$\mathrm{Nu} = 0.028154\,\mathrm{Ra}^{0.4134} \qquad 10^{4} < \mathrm{Ra} \le 5\times10^{4} \qquad (6.56b)$$

$$\mathrm{Nu} = 1 + 1.75967\times10^{-10}\,\mathrm{Ra}^{2.2984755} \qquad \mathrm{Ra} \le 10^{4} \qquad (6.56c)$$

where the Rayleigh number $\mathrm{Ra} = \dfrac{\rho^2 l^3 g C_p \Delta T}{\mu\lambda T_m}$

ρ, C_p, μ and λ are density, specific heat, dynamic viscosity and thermal conductivity of the fill gas respectively, and l, glazing pane spacing.

The convective heat transfer coefficient is then given by

$$h_c = \mathrm{Nu}\frac{\lambda}{l} \qquad (6.57)$$

The correlations are independent of the cross sectional aspect ratio of the glazing, thus, for a particular spacing between glazing panes and type of fill gas, the convective coefficient varies with glazing surface and mean fill gas temperatures only. The Rayleigh number must be computed at each hour in order to select the appropriate correlation expression from the equation set and a further complication is that the expressions are non-linear. It can be demonstrated that the Rayleigh number does not vary significantly with the mean gas temperature T_m. Further, the mean gas temperature can be assumed to be the mean of the glazing surface temperatures due to the insignificant mass of gas between the panes. Based on these assumptions, the convective coefficient was computed for a range of mean temperatures from zero to 50K and ΔT's from 5K to 50K, at each mean temperature. The calculations were carried out for air, argon and krypton gases, for pane spacings of 6, 9, 12, 16, 20 and 20mm. The mean convective coefficient was calculated, over the mean temperature range, for each ΔT. When the mean convective coefficients are plotted against ΔT, mildly non-linear curves, which can be approximated by two straight lines joined near the centre of the curve, are produced. For a particular fill gas and glazing spacing, the convective coefficient can then be correlated against the ΔT of the glazing panes by a linear relationship of the form:

$$h_c = m\Delta T + c \qquad (6.58)$$

Table 6.11 gives the coefficients and constants for the range of standard glazing spacings, in the case of an air filled system, and the specified ΔT temperature ranges.

Table 6.11 Correlation coefficients and constants for equation (6.58) in the case of air fill gas

Spacing (mm)	5K < ΔT <25K		25K < ΔT <50K	
	m	*c*	*m*	*c*
6	0.00007	4.3728	0.0002	4.3686
9	0.0008	2.9103	0.0026	2.864
12	0.0043	2.1582	0.014	1.9058
16	0.023	1.4921	0.0278	1.4338
20	0.0446	1.12	0.0294	1.51
25	0.0558	1.0046	0.0271	1.7091

The influence of the error, associated with the approximate convective correlation equation (6.58), is diminished when the convective and radiative coefficients are combined to produce the overall heat transfer coefficient, due to the usually higher value of radiant heat transfer coefficient.

6.5.4.3 Performance of the linearised heat transfer coefficients

Table 6.12 demonstrates the performance of the combined radiant and convective correlation equations (6.55) and (6.58), in the case of 25mm and 20mm pane spacings. The values in table 6.12 are obtained by dividing the combined linearised coefficients by the combination of the more precise coefficients defined by equations (6.54) and (6.57). Overall, the results summarised in table 6.12, confirm a high accuracy over a wide range of

Table 6.12 Accuracy of combined radiant and convective correlation equations (6.55 & 6.58) compared to combined heat transfer coefficient based on equations (6.54 & 6.57) for glazing spaced at 20mm and 25mm

ΔT (K)	Mean temperature t_m - 25mm spacing						Mean temperature t_m - 20mm spacing					
	0	10	20	30	40	50	0	10	20	30	40	50
5	1.02	1.03	1.03	1.04	1.03	1.03	0.99	1.00	1.00	1.00	0.99	0.99
10	0.96	0.98	0.99	0.99	0.98	1.00	1.00	1.01	1.02	1.02	1.00	1.02
15	0.96	0.97	0.99	0.99	0.98	1.00	0.98	0.99	1.00	1.01	0.99	1.01
20	0.97	0.99	1.00	1.01	0.99	1.01	0.98	0.99	1.00	1.01	0.99	1.01
25	0.99	1.01	1.02	1.02	1.01	1.03	0.99	1.00	1.01	1.02	1.01	1.02
30	0.97	0.99	1.00	1.01	1.00	1.02	0.98	0.99	1.00	1.01	1.00	1.02
35	0.97	0.98	0.99	1.00	0.99	1.01	0.97	0.99	1.00	1.01	1.00	1.01
40	0.98	0.99	1.00	1.00	0.99	1.01	0.97	0.99	1.00	1.01	1.00	1.02
45	0.98	0.99	1.00	1.01	1.00	1.01	0.98	0.99	1.00	1.01	1.00	1.02
50	0.99	1.00	1.01	1.02	1.01	1.02	0.98	1.00	1.01	1.02	1.01	1.02

mean temperatures and temperature differences. Note the overall improvement in accuracy with the 20mm spacing system; the accuracy improves further with smaller spacings. The performance of the correlation equations (6.55) and (6.58) demonstrates their computational efficiency when compared to the application of equations (6.54) and (6.57) to computer calculations.

6.5.5 Window with internal loose fitting blinds

Closed non-perforated roller blinds, installed in well-sealed slide rails with insignificant air gaps at top and bottom, may be assumed to be the inner pane of a multiple glazing system. The methods described in section 6.5.4, for establishing hourly values of convective and radiant heat transfer coefficients, may be employed. Loose fitting blinds, such as venetian blinds, generate thermal buoyancy forces inducing room air to circulate between the inner glazing pane and blind. A further convection path, connecting the glazing/blind air cavity and room air node, is formed in addition to convection between the inner glazing pane and

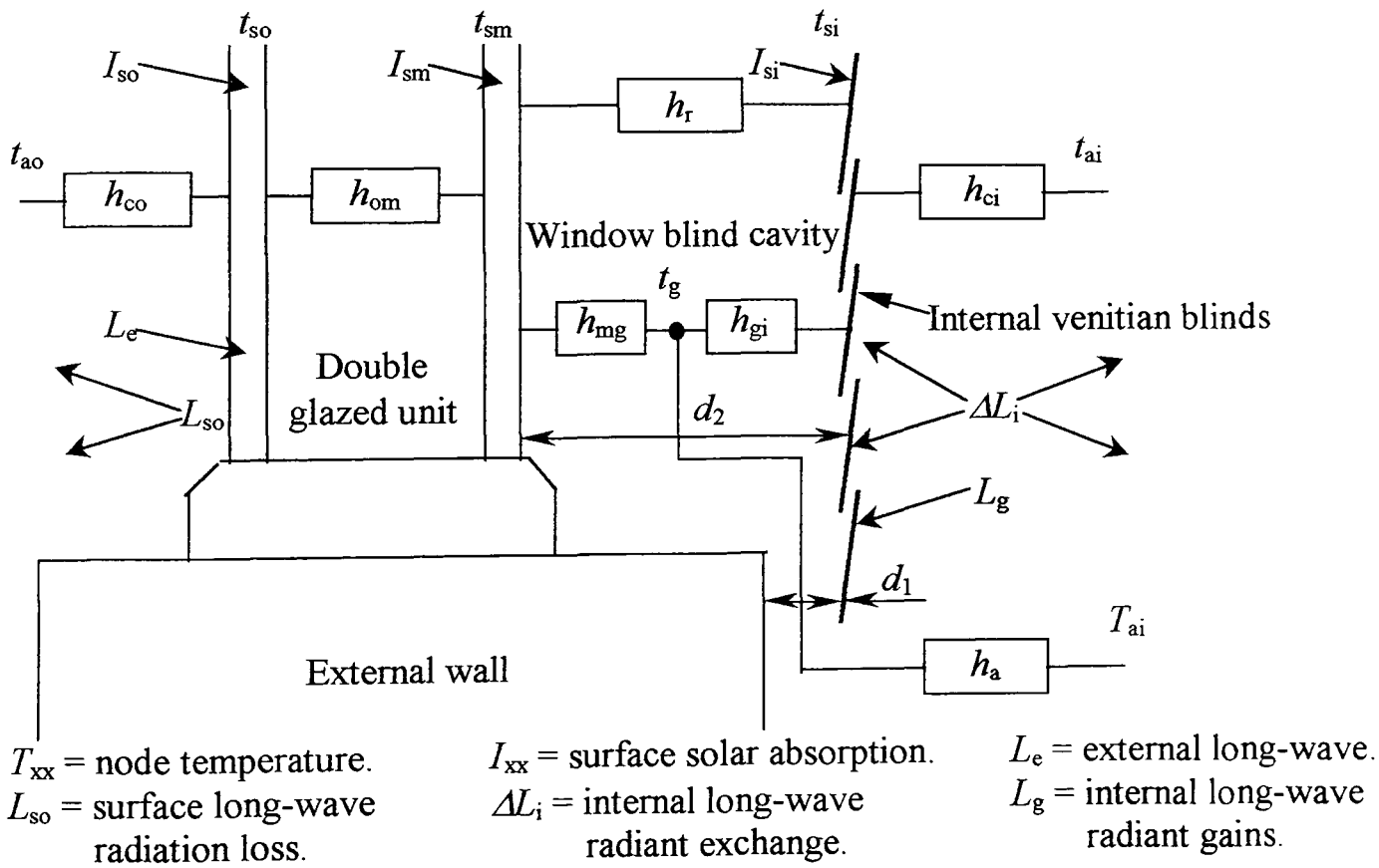

Figure 6.12. Window/blind thermal circuit

blind. Figure 6.12 illustrates the thermal circuit of the window system with the blinds closed. The thermal modelling of the window system must include for the modification of the thermal circuit when the blinds are opened, resulting in a direct thermal path between the inner glazing pane and the air node, via the heat transfer coefficient h_{ci}. The long-wave radiant exchange coefficient, h_r, depends only on surface temperatures and is determined as described in section 6.5.4.1. In the case of convective heat transfer, three interconnected thermal paths, symbolised by h_{mg}, h_{gi} and h_a, must be modelled. The convection coefficient, h_a, accounts for forced convection due to airflow through the gaps formed by the perimeter of the blinds and wall surface, and through the slots created by the loose-fitting louvres. The convective coefficients h_{mg} and h_{gi} vary with glazing surface and glazing/blind cavity temperatures as well as air velocity in the cavity. The model must be flexible to account for airflow through a variety of internal blind types. The dimensions of the airflow paths, created by the loose fitting blinds, must be treated as variables to compute the airflow discharge coefficients, in order to achieve this goal. Thus, precise modelling of the window system requires developing and integrating thermal and airflow models.

6.5.5.1 Window/blind airflow model

It is assumed that the main buoyancy force creating airflow is due to a "stack effect" caused by air density differences between the space volume and window blind cavity. The air gaps around the perimeter of the blinds are on average of similar dimensions (say 25mm). If the gaps between the blind's louvres are also of similar dimensions (say 2mm), then a neutral pressure plane is established at about the mid-height of the window blinds. When the room air is cooler than the air in the glazing/blind cavity, air enters the window cavity below the neutral plane and returns to the room above the neutral plane. When the room air is warmer than the air in the window cavity, the airflow reverses in direction about the neutral pressure plane. The pressure difference due to stack effect can be determined from [11]

$$\Delta p_s = 2680 \rho_{ai} Z \left(1/T_{ai} - 1/T_g\right) \tag{6.59}$$

Due to air entering and exiting at various heights above and below the neutral pressure plane, the vertical distance, Z, between the entering and exiting air streams is averaged over the flow paths using an area weighted calculation. In the case of air entering and exiting the window air cavity, via the blind's louvres, the average height between the flow paths is

$$Z_{louvre} = 0.5\, H \tag{6.60}$$

For the perimeter gap airflow paths, the average height is given by

$$Z_{\text{perimeter}} = \frac{HW + 0.5H^2}{H + W} \tag{6.61}$$

where H and W are the window blind's height and width respectively.

The airflow rates through each convective path is given by

$$V = C_{\text{d}} (\Delta p_{\text{s}})^n / \rho_{\text{ai}}^n \tag{6.62}$$

Reference to equation (6.59) indicates that the air density, ρ_{ai}, will be cancelled, resulting in the airflow rate being dependent on T_{ai}, T_{g}, Z and C_{d} only. Pressure losses will be mainly due to velocity pressure losses as the air enters, expands, contracts and exits the window cavity. Turbulent flow is assumed due to the short airflow path lengths between changes of direction, not allowing laminar flow patterns to be established. For turbulent flow, the power exponent, n, in equation (6.62) is normally taken as 0.5. Equating the total velocity pressure losses to the stack pressure gives

$$\Delta p_{\text{s}} = \frac{\rho_{\text{ai}} v^2}{2} \sum \zeta \tag{6.63}$$

Velocity pressure loss factors, ζ, for various flow configurations, are widely published in fluid dynamic textbooks and appropriate guides [73]. Rearranging equation (6.63) to give air velocity, v, and then multiplying by flow area, A, gives the airflow rate as follows

$$V = Av = \frac{A}{\left(0.5 \sum \zeta\right)^{0.5}} \left(\frac{\Delta p_s}{\rho_{\text{ai}}} \right)^{0.5} \tag{6.64}$$

Referring to equation (6.62) reveals the discharge coefficient of equation (6.64) as:

$$C_d = \frac{A}{\left(0.5 \sum \zeta\right)^{0.5}} \tag{6.65}$$

Velocity pressure loss factors for entry and exits are normally taken as 0.5 and 1.0 respectively. In the case of an abrupt enlargement, the velocity pressure loss factor can be determined from [73]:

$$\zeta = \left(1 - A_1 / A_2\right)^2 \tag{6.66}$$

where A_1 refers to the smaller flow area.

Figure 6.12 shows that for the perimeter airflow path, the area ratio A_1/A_2 can be taken as the ratio of the air entry gap depth and window blind cavity depth, d_1/d_2. The value of the corresponding area ratio for airflow between the blind's louvres will be relatively small (for

gaps between louvres of 1 to 2 mm), resulting in equation (6.66) giving a velocity pressure loss factor of approximately 1.0. A simple relationship, as defined by equation (6.66), is not available in the case of an abrupt contraction. The CIBSE guide [74] tabulates values of velocity pressure loss factors in terms of the flow area ratio A_2/A_1, A_2 referring to the smaller flow area. A correlation equation, for an abrupt contraction, can be fitted to this tabulated data to produce the following relationship

$$\zeta = -0.6242\left(A_2/A_1\right)+0.5315 \tag{6.67}$$

The area ratio A_2/A_1 will be relatively small, in the case of airflow through the abrupt contraction before exiting between the blind's louvres, resulting in equation (6.67) giving a value approximately equal to 0.5. For airflow undergoing an abrupt contraction at the perimeter of the blinds, figure 6.12 shows that the area ratio of equation (6.67) corresponds with the ratio d_1/d_2. Expanding equation (6.65), the window blind's perimeter airflow discharge coefficient is then given by

$$\left(C_{\mathrm{d}}\right)_{\mathrm{perimeter}} = \frac{A_{\mathrm{perimeter}}}{\left\{0.5\left[1.5+\left(1-d_1/d_2\right)^2+\left(-0.6242\,d_1/d_2+0.5315\right)\right]\right\}^{0.5}} \tag{6.68}$$

where 1.5 equals the sum of the entry and exit velocity pressure loss factors.

In the case of airflow between the blind's louvres, the sum of the velocity pressure loss factors is 3.0. For N number of louvres the number of parallel entering and exiting airflow paths is 0.5 N and equation (6.65) reduces to

$$\left(C_{\mathrm{d}}\right)_{\mathrm{louvre}} = NA_{\mathrm{louvre}}/6^{0.5} \qquad \text{or} \qquad \left(C_{\mathrm{d}}\right)_{\mathrm{louvre}} = NA_{\mathrm{louvre}}/2.45 \tag{6.69}$$

Referring to equations (6.59) and (6.62), the total air flow rate through the blinds is given by

$$V_{\mathrm{a}} = \left[\left(C_{\mathrm{d}}Z^{0.5}\right)_{\mathrm{perimeter}}+\left(C_{\mathrm{d}}Z^{0.5}\right)_{\mathrm{louvres}}\right]\cdot\left[2680\left(1/T_{\mathrm{ai}}-1/T_{\mathrm{g}}\right)\right]^{0.5} \tag{6.70}$$

The heat transfer between the window cavity and space air nodes, per square metre of window area, is then given by

$$Q_{\mathrm{a}} = V_{\mathrm{a}}\rho_{\mathrm{ai}}c_{\mathrm{ai}}\left(T_{\mathrm{g}}-T_{\mathrm{ai}}\right)/A_{\mathrm{w}} \tag{6.71}$$

where c_{ai} is the specific heat of humid air.

Finally, from equation (6.71) the airflow heat transfer coefficient is given by

$$h_{\mathrm{a}} = V_{\mathrm{a}}\rho_{\mathrm{ai}}c_{\mathrm{ai}}/A_{\mathrm{w}} \tag{6.72}$$

6.5.5.2 Window blind cavity convective heat transfer coefficients h_{mg} & h_{gi}

With air flowing through the window blind cavity, the convective heat transfer coefficients h_{mg} and h_{gi} will vary with the parallel air velocity as well as surface to cavity air temperatures. McAdams expression for forced convection, given by equation (6.14), is based on a copper plate experiment using a parallel airflow at a reference temperature of 294.26 K. In the case of a smooth surface, the velocity dependent term of McAdams expression is given by

$$h = 3.91\frac{T_{ref}}{T_g}v \tag{6.73}$$

where T_{ref} is the experimental air reference temperature of 294.26 K.

However, McAdams expression does not include a term that defines the convection component due to temperature difference. The following MoWiTT external convection model [60] includes the two components but the velocity used is defined as wind speed at standard conditions.

$$h = \sqrt{\left[0.84\left(|\Delta T|\right)^{1/3}\right]^2 + \left(2.38v^{0.89}\right)^2} \tag{6.74}$$

Since the airflow in the window blind cavity is essentially parallel, it would be appropriate to substitute the velocity component in the MoWiTT expression for the McAdams velocity component. Referring to figure 6.12, the convection coefficients can then be estimated using

$$h_{mg} = \sqrt{\left[0.84\left(|T_{sm} - T_g|\right)^{1/3}\right]^2 + \left(3.91\frac{T_{ref}}{T_g}v_c\right)^2} \tag{6.75}$$

$$h_{gi} = \sqrt{\left[0.84\left(|T_{si} - T_g|\right)^{1/3}\right]^2 + \left(3.91\frac{T_{ref}}{T_g}v_c\right)^2} \tag{6.76}$$

where v_c is the window blind cavity parallel air velocity which is obtained by dividing the total cavity airflow rate, V_a, by the cross sectional area of the cavity at the neutral pressure plane. Under low airflow conditions, the heat transfer coefficients are not allowed to drop in value below the value corresponding to pure thermal conductance of stagnant air. When this lower limit is reached by either of the coefficients, its value is set to equal the conductivity of the air divided by half the window blind cavity depth.

Table 6.13 provides simulation results of heat transfer coefficients based on the window system of figure 6.12 exposed to an east orientation in July. The window blind cavity depth, perimeter airflow gap and gap between the blind louvres were set at 150 mm, 12 mm and 1mm respectively. Note the relatively higher values of the airflow convective coefficient, h_a, indicating a significant contribution to the window convective heat transfers.

Table 6.13. Comparison of window heat transfer coefficients relating to figure 6.12

Time	h_{om}	h_r	h_{mg}	h_{gi}	h_a	h_{ci}	Time	h_{om}	h_r	h_{mg}	h_{gi}	h_a	h_{ci}
1	5.24	4.20	0.61	0.81	2.44	1.22	13	6.05	4.29	1.24	0.97	4.70	2.11
2	5.23	4.19	0.35	0.77	2.10	0.91	14	6.08	4.29	1.27	0.95	4.65	2.14
3	5.22	4.18	0.58	0.84	2.47	1.20	15	6.14	4.30	1.32	0.89	4.77	2.21
4	6.05	4.27	1.21	0.40	4.06	2.03	16	6.13	4.31	1.33	0.92	4.84	2.23
5	6.17	4.37	1.28	0.53	4.41	2.14	17	6.14	4.29	1.32	0.74	4.66	2.20
6	6.48	4.76	1.56	1.77	7.58	2.94	18	6.06	4.26	1.23	0.68	4.27	2.07
7	6.67	4.91	1.73	1.85	8.22	3.08	19	6.00	4.26	0.98	0.48	3.12	1.68
8	6.68	4.88	1.99	1.98	9.63	3.29	20	6.01	4.29	0.48	0.47	0.89	0.81
9	6.63	4.83	1.95	1.91	9.29	3.20	21	6.01	4.27	0.85	0.61	2.67	1.48
10	6.50	4.70	1.84	1.76	8.47	2.97	22	5.28	4.26	0.56	0.54	1.70	1.05
11	6.30	4.52	1.65	1.49	7.08	2.56	23	5.28	4.23	0.45	0.79	2.25	1.05
12	6.13	4.39	1.41	1.27	5.78	2.23	24	5.28	4.22	0.35	0.71	1.82	0.80

6.5.5.3 Window blind combination inside thermal admittance

It is necessary to determine all surface admittances connected to the space air node to model accurately the internal environmental model. The window system inside admittance is obtained from the thermal transmission matrix of the window system given by

$$\begin{bmatrix} \tilde{t}_{ai} \\ \tilde{q}_{ai} \end{bmatrix} = \begin{bmatrix} w_{11} & w_{12} \\ w_{21} & w_{22} \end{bmatrix} \cdot \begin{bmatrix} \tilde{t}_{eo} \\ \tilde{q}_{eo} \end{bmatrix} \tag{6.77}$$

which is derived from the matrix multiplication of the thermal transmission matrices of its individual components as follows

$$\begin{bmatrix} \tilde{t}_{ai} \\ \tilde{q}_{ai} \end{bmatrix} = \begin{bmatrix} 1 & \overline{R}_{eq} \\ 0 & 1 \end{bmatrix} \cdot \begin{bmatrix} g_{11} & g_{12} \\ g_{21} & g_{22} \end{bmatrix} \cdot \begin{bmatrix} 1 & \overline{R}_{om} \\ 0 & 1 \end{bmatrix} \cdot \begin{bmatrix} g_{11} & g_{12} \\ g_{21} & g_{22} \end{bmatrix} \cdot \begin{bmatrix} 1 & \overline{R}_{co} \\ 0 & 1 \end{bmatrix} \cdot \begin{bmatrix} \tilde{t}_{eo} \\ \tilde{q}_{eo} \end{bmatrix} \tag{6.78}$$

The thermal resistances, $\overline{R}_{om}$ and $\overline{R}_{co}$ are the reciprocals of the corresponding heat transfer coefficients shown in figure 6.12 and the "g_{xx}" representing the matrix components of the glazing panes. The thermal resistance $\overline{R}_{eq}$ is the equivalent thermal resistance between the inner glazing pane and the space air node. To determine $\overline{R}_{eq}$, heat balances must be set-up

at the window cavity temperature node t_g and the blind surface. From the two heat balance equations, the following expression, giving the equivalent heat transfer coefficient in terms of known heat transfer coefficients, is derived.

$$h_{eq} = \frac{\frac{h_a}{b}\left(\frac{h_{gi}h_r}{a} + h_{mg}\right) + \frac{h_{ci}}{a}\left(\frac{h_{gi}h_{mg}}{b} + h_r\right)}{1 - h_{gi}^2/ab} \tag{6.79}$$

where $a = h_r + h_{gi} + h_{ci}$ and $b = h_{mg} + h_{gi} + h_a$

Figure 6.12 shows that when the blinds are open, $h_{eq} = h_{ci}$ which requires a logic statement to be included in order to switch to the appropriate relationship for h_{eq}. The daily average of the equivalent heat transfer coefficient is then computed and its reciprocal, $\overline{R}_{eq}$, inserted in the appropriate matrix of equation (6.78).

6.5.5.4 Window layer surface temperatures

Depending on the blind operating schedule, either the blind or inner glazing surface is exposed to the internal environment and as a result the corresponding surface temperature must be determined. The external glazing surface temperature is also required to compute its long-wave radiation flux diffusion to the external environment. Determining the window layer temperatures involves setting up heat balances at each surface and the window cavity temperature node, t_g, to compute the subsequent heat transfers. Equation (6.79) is a relatively lengthy expression derived from two heat balance equations, including real numbers only. In the case of determining surface temperatures, two further heat balance equations, which include complex quantities defining the thermal behaviour of the glazing panes, are required. Compared to equation (6.79), longer expressions containing a mixture of real and complex numbers are derived for each surface and must be evaluated per hour of simulation. In addition, expressions for correcting the errors due to using 24-hour mean thermal resistances in the air-film, thermal transmission matrices must be derived for each surface. Further iteration loops are then required for processing the residual error until convergence is obtained. Employing an implicit finite difference model of the window system for computing surface temperature profiles is computationally a far more efficient approach. For a lumped capacitance model, the error is small when the corresponding Biot number, $Bi < 0.1$. For a 6mm thick pane of glass with a thermal conductivity 1.05 $Wm^{-1}K^{-1}$ and a convective heat transfer coefficient of 30 $Wm^{-2}K^{-1}$, the value of the Biot number is

$$Bi = \frac{h_c l}{2\lambda} = \frac{30 \times 0.006}{2 \times 1.05} = 0.086$$

Normally lower heat transfer coefficients will be encountered for external surfaces and, certainly, much lower in the case of internal surfaces. This result indicates an approximately flat temperature gradient through the glazing layer. Therefore, only a small error will be incurred by modelling each glass layer as a lumped rather than a distributed thermal resistive and capacitance system. One temperature node point representing each 6mm pane of glass is required. The window cavity and blind surface temperature nodes are assumed to have negligible mass. The solutions to the set of implicit finite difference equations can be processed by iteration rather than by matrices, using a suitable spreadsheet program. Referring to figure 6.12, the resulting set of implicit equations, arranged for iterative processing is:

$$T_{so}^{i+1} = \left(I_{so}^{i+1} + L_e^{i+1} - L_{so}^{i+1} + h_{co}^{i+1} T_{ao}^{i+1} + h_{om}^{i+1} T_{sm}^{i+1} + \frac{\Delta x \rho c}{\Delta t} T_{so}^{i} \right) \Big/ \left(h_{co}^{i+1} + h_{om}^{i+1} + \frac{\Delta x \rho c}{\Delta t} \right) \qquad (6.80)$$

$$T_{sm}^{i+1} = \left(I_{sm}^{i+1} + h_{om}^{i+1} T_{so}^{i+1} + h_r^{i+1} T_{si}^{i+1} + h_{mg}^{i+1} T_g^{i+1} + \frac{\Delta x \rho c}{\Delta t} T_{sm}^{i} \right) \Big/ \left(h_{om}^{i+1} + h_r^{i+1} + h_{mg}^{i+1} + \frac{\Delta x \rho c}{\Delta t} \right) \qquad (6.81)$$

When the blinds are open, equation (6.81) is replaced by

$$T_{sm}^{i+1} = \left(I_{sm}^{i+1} + \Delta L_i^{i+1} + L_g^{i+1} + h_{om}^{i+1} T_{so}^{i+1} + h_{ci}^{i+1} T_{ai}^{i+1} + \frac{\Delta x \rho c}{\Delta t} T_{sm}^{i} \right) \Big/ \left(h_{om}^{i+1} + h_{ci}^{i+1} + \frac{\Delta x \rho c}{\Delta t} \right) \qquad (6.82)$$

$$T_g^{i+1} = \left(h_{gi}^{i+1} T_{si}^{i+1} + h_{mg}^{i+1} T_{sm}^{i+1} + h_a^{i+1} T_{ai}^{i+1} \right) \Big/ \left(h_{gi}^{i+1} + h_{mg}^{i+1} + h_a^{i+1} \right) \qquad (6.83)$$

$$T_{si}^{i+1} = \left(I_{si}^{i+1} + \Delta L_i^{i+1} + L_g^{i+1} + h_{gi}^{i+1} T_g^{i+1} + h_r^{i+1} T_{sm}^{i+1} + h_{ci}^{i+1} T_{ai}^{i+1} \right) \Big/ \left(h_{gi}^{i+1} + h_r^{i+1} + h_{ci}^{i+1} \right), \qquad (6.84)$$

where Δx, ρ and c are the thickness, density and specific heat of the glass respectively, and Δt the time-step.

The space air temperature, internal long-wave radiant exchange and internal radiant gains (T_{ai}, ΔL_i and L_g) given in equations (6.82) and (6.84) are inputs from the internal environmental model. Depending on the blind operating schedule, either the blind surface or inner glazing surface temperature is inputted to the internal environmental model to process the long-wave radiant exchanges among the internal surfaces. Using the one-hour time steps adopted for the frequency domain method, the finite difference iteration process

is numerically stable. This is ideal for the thermal temporal link between the two simulation methods.

6.5.5.5 Window blind convective heat transfer due to radiant gains

The inner glazing layer is a component of the window conduction model and all heat inputs to the space air, from the window conduction model, is via the window sol-air temperature described in section 6.5.3. The window blind is also a component of the window conduction model, incorporated for the purpose of deriving the complex thermal transmittances and admittances between the external and internal environments via the window system. Solar and internal long-wave radiation incident on the internal blinds subsequently cause convective gains to the space air. These convective gains are not accounted for in the window solar temperature, as is the case with the glazing layers. Further, when the blinds are open, the internal long-wave radiation incident on the internal glazing pane is not accounted for in the window sol-air temperature. It is less complicated and computationally more efficient to compute these unaccounted convective gains using an implicit finite difference scheme, as described in the previous section. When computing convective gains to the space air node in the frequency domain, isothermal boundary conditions are assumed requiring the air temperature be set to zero. Referring to figure 6.12, when the blinds are closed, the convective gains to the space are then given by

$$Q_{\mathrm{c}} = A\left(h_{\mathrm{ci}} t_{\mathrm{si}} + h_{\mathrm{a}} t_{g}\right) \tag{6.85}$$

and when the blinds are open

$$Q_{\mathrm{c}} = A h_{\mathrm{ci}} t_{\mathrm{sm}} \tag{6.86}$$

The temperatures, t_{si}, t_{g} and t_{sm}, are obtained from solving the set of finite difference equations (6.80) to (6.84). All thermal excitations must be excluded from the equations except for the solar, internal long-wave exchange and internal gains incident on the blinds. Previous temperatures, symbolised by t_{xx}^{i} in the implicit finite difference equation, must also be excluded since these are considered thermal excitations that would reside on the right hand side of the heat balance equations with the other thermal driving forces. Depending on the window blind operating schedule, the resulting convective gains profile obtained from either equation (6.85) or (6.86) is converted into a Fourier series and becomes an input to the frequency domain space model.

6.5.5.6 Window blind heat flux correction term

Section 6.3.5.1 includes a description of the procedure required to correct the error incurred by using constant values of convective and radiant thermal resistances in the thermal transmission matrices. Equation (6.51) formulates the sum of the errors in terms of a correction to the window sol-air temperature in the case of a window system incorporating three layers. Equation (6.51) is still applicable in the case of a loose fitting blind, but the last term on the R.H.S. of the equation must be replaced with a correction term incorporating the equivalent thermal heat transfer coefficient, which accounts for the operating schedule of the blinds. The revised equation is:

$$(\Delta t_{eow})_c = \frac{(h_{co} - \bar{h}_{co})(t_{ao} - t_{so})}{\vec{h}_{co}} + \frac{(h_{om} - \bar{h}_{om})(t_{so} - t_{sm})}{\vec{h}_{om}} + \frac{(h_{eq} - \bar{h}_{eq})(t_{sm} - t_{ai})}{\vec{h}_{eq}} \qquad (6.87)$$

The window system, incorporating operable internal blinds, has been validated against a finite difference model and the results are included in chapter VII, Validation.

6.5.5.7 Window frame and spacer heat transfers

Estimating the heat transfer through the window frame is complicated by the different combinations of materials used in a particular design, the different sizes, shapes and components encountered due to the multitude of available window products. The geometric aspects of the frame require two-dimensional thermal simulation techniques to predict the heat transfers, which is beyond the scope of the proposed simulation tool. The CIBSE guide [75] and ASHRAE Fundamentals Handbook [64] contain data that can be employed to estimate the frame and spacer heat transfers. Each source tabulates window frame U-values for different frame constructions, which have been determined using a two-dimensional dynamic thermal model. The tabulated U-values are daily mean values. Assuming the external and internal thermal resistances are the main variables, the mean U-value can be employed to generate a 24-hour transmittance profile by replacing the mean values of surface resistances with simulated values. Assuming the tabulated U-values are based on surfaces' resistances for normal exposure, $\bar{R}_{se} = 0.06$ and $\bar{R}_{si} = 0.12$, the hourly transmittances are given by

$$U_\varphi = 1 \Big/ \left[\frac{1}{U_{table}} - 0.18 + (R_{se} + R_{si})_\varphi \right] \qquad (6.88)$$

where R_{se} and R_{si} are the simulated hourly combined convective and radiant resistances.

The CIBSE guide provides the following formula for estimating the linear U-values of metallic and non-metallic spacers.

$$\Psi_s = \frac{(U_{gs}/U_g)C\,d_{gb}}{R_{se}+R_{si}+d_g r_g} + \phi_s \tag{6.89}$$

U_{gs} = U-value of glazing with 12 mm separation and normal exposure; typical tabulated values are provided. U_g = U-value of actual glazing used. C relates to the depth of the spacer below the edge of the frame. The average thickness of the bounding glazing panes is d_{gb}. The thickness and thermal resistivity of the glazing panes are d_g and r_g respectively. If the frame U-value exceeds 3 W m^{-2} K^{-1} $\phi_s = 0.1$, otherwise zero. Assuming negligible mass of the spacer and components, the above steady-state expressions for the spacer and glazing U-value, U_g, can be converted to more dynamic expressions by using hourly, simulated values of R_{se} and R_{si}. The tabulated values of the constant C, in terms of spacer depth D, may be curve fitted to produce the correlation

$$C = 0.002D^2 - 0.09D + 1.6 \tag{6.90}$$

The constant C can then be computed for depths up to about 10 mm, which is the maximum depth given for the tabulated values of the constant. The 24-hour, window frame and spacer thermal transmittance profiles can then be employed to simulate dynamic heat transfers between the external and internal environments. Since solar radiation is incident on the external surfaces of the window frame, a sol-air temperature excitation should be used, rather than the external air temperature. The mean value of the combined transmittances can be used in the thermal transmission matrix of the window frame and spacer in order to determine its inside admittance for incorporation into the internal environmental model.

Chapter VI

6.6 Development of the Internal Environmental Model

6.6.1 The structure of the model

The main components of the internal environmental model are illustrated in the lower portion of figure 6.1. A surface/space conduction model employing the frequency domain, thermal simulation technique forms the core of the internal environmental model. The frequency domain technique is an analytical method that can accurately simulate pure thermal conduction in solids, in which the thermophysical properties must be treated as constants. Assumptions of constant surface convective heat transfer coefficients must be made when convective boundary conditions are included. Employing surface radiant heat transfer coefficients to mimic the long-wave radiant exchange process is a further approximation. These deficiencies are overcome through the development of convective and long-wave radiant exchange sub-models which, when combined with the frequency domain technique, result in a method that can simulate non-linear heat transfer processes. Iterative calculation processes are involved in the combined simulation method. Two versions of the Iterative Frequency Domain Technique have been developed for computer spreadsheet application. The Adiabatic Iterative Frequency Domain Technique (AIFDT) excludes the surface convective coefficients from the overall thermal transmission matrix of the space's structural surfaces. The Iterative Frequency Domain Technique (IFDT) includes the surface convective coefficients in the overall thermal transmission matrix. A number of surface factors have been derived to determine the space air and surface temperature responses due to radiant gains incident on both sides of structural elements. An exact grey solution model is employed to simulate long-wave radiant exchange between the major room surfaces. A new reduced long-wave radiant exchange model that is sensitive to the dominant radiant exchange processes has been developed.

6.6.2 The frequency domain technique, core of the internal environmental model

In the frequency domain, the mean and fluctuating thermal responses are calculated separately and then summed to give the total response. Heat balance equations must be derived for the space air node and the space's structural surfaces, in the case of each component. Steady-state type heat balance equations, employing U-values and mean values of the excitation profiles, are used to determine the mean component. Discrete Fourier

analysis and periodic heat transfer are employed to calculate the fluctuating thermal response. Thermal transmission matrices model the fluctuating thermal behaviour of the structural surfaces and space air volume in periodic heat transfer. Discrete Fourier analysis is used to decompose a periodic thermal excitation time series into a series of sinusoidal excitations. Representing the sinusoidal excitations by their equivalent complex number transformations is more suitable for calculations using computer spreadsheet programs. A Fourier series of eleven sinusoidal excitation components (See sec. 3.1.4.1) together with a corresponding series of thermal transmission matrices, for each of the structural surfaces and space air volume, are required in the case of a 24-hour periodic excitation. A corresponding series of heat balance equations is required for the space air node and for each structural surface. Thermal admittances, transmittances and surface factors are derived from each series of thermal transmission matrices for input into the heat balance equations. Each series of heat balance equations is solved to produce a series of complex thermal responses. The complex thermal responses are further processed to produce the hourly fluctuating responses, which are then added to the appropriate mean responses to produce the 24-hour space air and surface temperature profiles. Convective heat transfer coefficients are used in the thermal transmission matrices rather than the combined convective and radiant heat transfer coefficients that are employed in the traditional frequency domain technique.

6.6.2.1 The thermal coefficients of the space heat balance equations

Thermal admittances, transmittances and other dynamic surface factors are derived from the thermal transmission matrices of the space's structural surfaces to form the thermal coefficients of the heat balance equations. The compound thermal transmission matrix of a structural surface is described by

$$\begin{bmatrix} \tilde{t}_a \\ \tilde{q}_a \end{bmatrix} = \begin{bmatrix} s_{11} & s_{12} \\ s_{21} & s_{22} \end{bmatrix} . \begin{bmatrix} \tilde{t}_b \\ \tilde{q}_b \end{bmatrix} \tag{6.91}$$

A series of eleven transmission matrices are required to define the thermal behaviour of the structure in the case of a 24-hour periodic thermal excitation. Only the fundamental matrix will be used in the examples, the mathematical operations being identical for each matrix in the series. All quantities in equation (6.91) are complex numbers. Adiabatic or isothermal boundary conditions must be set to match the actual boundary conditions. Isothermal

boundary conditions are specified in the case of convective heat transfers to the external and internal environments. The arrangement of equation (6.91) indicates that the thermal excitations are on its LHS. The thermal admittance and transmittance, derived from the matrix, are given by s_{22}/s_{12} and $1/s_{12}$ respectively. Multiplying the thermal admittance and transmittance by the excitation temperature gives the complex heat flows $\tilde{q}_a$ and $\tilde{q}_b$ respectively. The matrix multiplication of the individual matrices of the structural layers must be reversed to formulate the compound thermal transmission matrix due to the thermal excitations on the RHS of equation (6.91). A different compound thermal transmission matrix results. However, the reversed compound matrix may be obtained directly by just interchanging the two leading diagonal elements of the original matrix of equation (6.91) as follows.

$$\begin{bmatrix} \tilde{t}_{\mathrm{b}} \\ \tilde{q}_{\mathrm{b}} \end{bmatrix} = \begin{bmatrix} (s_{22})_{11} & s_{12} \\ s_{21} & (s_{11})_{22} \end{bmatrix} \cdot \begin{bmatrix} \tilde{t}_{\mathrm{a}} \\ \tilde{q}_{\mathrm{a}} \end{bmatrix} \tag{6.92}$$

The other two elements remain unchanged. The admittance becomes $(s_{11})_{22}/s_{12}$. The transmittance is independent of the direction of heat flow and therefore remains unchanged. Thermal admittances and transmittances are coefficients employed in the space air node, heat balance equations of the fluctuating component. The steady state transmittance, the U-value, is the only compound thermal coefficient used in the mean component's heat balance equation. Multiplying these thermal coefficients by the total surface area of the structure will give the total admittance Y, transmittance K and steady state conductance C, which are used in the space heat balance equation of section 6.6.2.3.

Two further thermal coefficients are required to account for the convective gains to the space air node caused by incident radiant gains on internal surfaces. Solar radiation, casual gains and surface long-wave radiant exchange are normally the cause of internal surface radiant gains. Equations (6.93a) and (6.93b), shown below, are produced from equation (6.91) to reveal the surface radiant flux and corresponding temperature (Shown with subscript "r"). The inverted comma matrix elements, s'_{xx}, indicates that the compound matrix of the surface structure does not include the surface resistance matrix R_{ci}, which is shown separated from the compound matrix and forming the matrix of equation (6.93a).

$$\begin{bmatrix} \widetilde{t}_r \\ \alpha_a \widetilde{q}_{ra1} \end{bmatrix} = \begin{bmatrix} 1 & R_{ci} \\ 0 & 1 \end{bmatrix} \cdot \begin{bmatrix} \widetilde{t}_a \\ \widetilde{q}_a \end{bmatrix} \qquad (6.93a). \qquad \begin{bmatrix} \widetilde{t}_r \\ \alpha_a \widetilde{q}_{ra2} \end{bmatrix} = \begin{bmatrix} s'_{11} & s'_{12} \\ s'_{21} & s'_{22} \end{bmatrix} \cdot \begin{bmatrix} \widetilde{t}_b \\ \widetilde{q}_b \end{bmatrix} \qquad (6.93b)$$

where the total incident radiant flux $\widetilde{q}_{ra} = \widetilde{q}_{ra1} + \widetilde{q}_{ra2}$

The surface radiant absorption coefficient is symbolised by α_a. Incident radiant flux produces a surface temperature rise causing heat to flow towards space "a" via the resistance R_{ci} and towards space "b" through the structure. The division of radiant flux is indicated by $\widetilde{q}_{ra1}$ and $\widetilde{q}_{ra2}$ in equations (6.93a) and (6.93b) respectively. A fraction of the radiant flux $\widetilde{q}_{ra2}$ will be stored in the structure, whereas the radiant flux $\widetilde{q}_{ra1}$ flows directly into the space. By setting isothermal boundary conditions at "a" and "b", it can be shown that the resulting convective heat flows are given by

$$\widetilde{q}_a = \alpha_a \widetilde{q}_{ra}(s'_{12}/s_{12}) \quad \text{or alternatively} \quad \widetilde{q}_a = \alpha_a \widetilde{q}_{ra}(1 - R_{ci} s_{22}/s_{12}) \qquad (6.94)$$

$$\widetilde{q}_b = \alpha_a \widetilde{q}_{ra}(R_{ci}/s_{12}) \qquad (6.95)$$

Note that only the matrix element s'_{12} of equation (6.94) excludes the surface resistance. The alternative formulation of equation (6.94), including both surface resistances, is more convenient to use. The total fluctuating convective gain to the space air node is obtained by multiplying the results of equations (6.94) and (6.95) by the total surface area of the structure. Radiant flux incident on the opposite side of the structure is treated in a similar manner. The matrix element s_{12} is identical for either direction of heat flow. This may not be the case for matrix element s'_{12}, due to the possible differences in surface resistance either side of the structure. Only equation (6.94) is applicable in the case of exterior structural surfaces, e.g., roof, due to external radiant fluxes being accounted for in the sol-air temperature.

Convective gains due to the mean radiant gains must also be accounted for and included in the mean component, space air node heat balance equation. The resulting expressions, shown below, are similar in appearance to the fluctuating component equations.

$$\overline{q}_a = \alpha_a \overline{q}_{ra}(R'/R) \qquad \text{or} \qquad \overline{q}_a = \alpha_a \overline{q}_{ra}(1 - R_{ci}/R) \qquad (6.96)$$

$$\overline{q}_b = \alpha_a \overline{q}_{ra}(R_{ci}/R) \qquad (6.97)$$

where the resistance $R' = R - R_{ci}$, and R = total structural thermal resistance.

The total mean convective gain to the space air node is obtained by multiplying the results of equations (6.96) and (6.97) by total surface area of the structure. The fluctuating convective gains from each surface are summed and represented in the space air node, heat balance equation, given in section 6.6.2.3, by $\widetilde{Q}_{\mathrm{KR}}$. The mean convective gains are summed and represented by $\overline{Q}_{\mathrm{KR}}$ in the mean component, heat balance equation.

6.6.2.2 The thermal coefficients of the surface heat balance equations

Internal surface temperatures are influenced by the environmental temperatures and net radiant heat fluxes on both sides of the structure. Surface factors may be derived from the compound matrix equations and used for determining incremental surface temperature fluctuations due to radiant gains and changes in environmental temperatures. The matrix equations for radiant flux incident on the "a" and "b" sides of a partition may be obtained by recasting equations (6.93a) and (6.93b) in terms of the partition as follows:

$$\begin{bmatrix} \widetilde{t}_{\mathrm{ra}} \\ \alpha_{\mathrm{a}}\widetilde{q}_{\mathrm{ra1}} \end{bmatrix} = \begin{bmatrix} 1 & R_{\mathrm{cia}} \\ 0 & 1 \end{bmatrix} \cdot \begin{bmatrix} \widetilde{t}_{\mathrm{a}} \\ \widetilde{q}_{\mathrm{a}} \end{bmatrix} \quad (6.98a), \qquad \begin{bmatrix} \widetilde{t}_{\mathrm{ra}} \\ \alpha_{\mathrm{a}}\widetilde{q}_{\mathrm{ra2}} \end{bmatrix} = \begin{bmatrix} p'_{11\mathrm{a}} & p'_{12\mathrm{a}} \\ p'_{21\mathrm{a}} & p'_{22\mathrm{a}} \end{bmatrix} \cdot \begin{bmatrix} \widetilde{t}_{\mathrm{b}} \\ \widetilde{q}_{\mathrm{b}} \end{bmatrix} \quad (6.98b)$$

where the total incident radiant flux $\widetilde{q}_{\mathrm{ra}} = \widetilde{q}_{\mathrm{ra1}} + \widetilde{q}_{\mathrm{ra2}}$

$$\begin{bmatrix} \widetilde{t}_{\mathrm{rb}} \\ \alpha_{\mathrm{b}}\widetilde{q}_{\mathrm{rb1}} \end{bmatrix} = \begin{bmatrix} 1 & R_{\mathrm{cib}} \\ 0 & 1 \end{bmatrix} \cdot \begin{bmatrix} \widetilde{t}_{\mathrm{b}} \\ \widetilde{q}_{\mathrm{b}} \end{bmatrix} \quad (6.99a), \qquad \begin{bmatrix} \widetilde{t}_{\mathrm{rb}} \\ \alpha_{\mathrm{b}}\widetilde{q}_{\mathrm{rb2}} \end{bmatrix} = \begin{bmatrix} p'_{11\mathrm{b}} & p'_{12\mathrm{b}} \\ p'_{21\mathrm{b}} & p'_{22\mathrm{b}} \end{bmatrix} \cdot \begin{bmatrix} \widetilde{t}_{\mathrm{a}} \\ \widetilde{q}_{\mathrm{a}} \end{bmatrix} \quad (6.99b)$$

where the total incident radiant flux $\widetilde{q}_{\mathrm{rb}} = \widetilde{q}_{\mathrm{rb1}} + \widetilde{q}_{\mathrm{rb2}}$

The complex surface temperature responses due to the incident radiant gains on both sides are derived individually from these matrix formulations. Invoking the principle of superposition, the total temperature response on each surface is then given by

$$\widetilde{t}_{\mathrm{ra}} = (R_{\mathrm{cia}}\, p'_{12\mathrm{a}}/p_{12})\alpha_{\mathrm{a}}\widetilde{q}_{\mathrm{ra}} + (R_{\mathrm{cia}}R_{\mathrm{cib}}/p_{12})\alpha_{\mathrm{b}}\widetilde{q}_{\mathrm{rb}} \quad (6.100)$$

and $$\widetilde{t}_{\mathrm{rb}} = (R_{\mathrm{cib}}\, p'_{12\mathrm{b}}/p_{12})\alpha_{\mathrm{b}}\widetilde{q}_{\mathrm{rb}} + (R_{\mathrm{cia}}R_{\mathrm{cib}}/p_{12})\alpha_{\mathrm{a}}\widetilde{q}_{\mathrm{ra}} \quad (6.101)$$

Equations (6.98a) and (6.99b) are rearranged as follows to derive the surface temperature responses due to space air temperature excitations.

$$\begin{bmatrix}\tilde{t}_a\\ \tilde{q}_a\end{bmatrix}=\begin{bmatrix}1 & R_{cia}\\ 0 & 1\end{bmatrix}\cdot\begin{bmatrix}\tilde{t}_{sa}\\ \tilde{q}_{sa}\end{bmatrix} \quad (6.102a), \qquad \begin{bmatrix}\tilde{t}_{sa}\\ \tilde{q}_{sa}\end{bmatrix}=\begin{bmatrix}p'_{11a} & p'_{12a}\\ p'_{21a} & p'_{22a}\end{bmatrix}\cdot\begin{bmatrix}\tilde{t}_b\\ \tilde{q}_b\end{bmatrix} \quad (6.102b)$$

$$\begin{bmatrix}\tilde{t}_b\\ \tilde{q}_b\end{bmatrix}=\begin{bmatrix}1 & R_{cib}\\ 0 & 1\end{bmatrix}\cdot\begin{bmatrix}\tilde{t}_{sb}\\ \tilde{q}_{sb}\end{bmatrix} \quad (6.103a), \qquad \begin{bmatrix}\tilde{t}_{sb}\\ \tilde{q}_{sb}\end{bmatrix}=\begin{bmatrix}p'_{11b} & p'_{12b}\\ p'_{21b} & p'_{22b}\end{bmatrix}\cdot\begin{bmatrix}\tilde{t}_a\\ \tilde{q}_a\end{bmatrix} \quad (6.103b)$$

It can be shown that the total surface temperature responses due to air temperature excitations on both sides of the partition are given by:

$$\tilde{t}_{sa}=(p'_{12a}/p_{12})\tilde{t}_a+(R_{cia}/p_{12})\tilde{t}_b \quad (6.104)$$

$$\tilde{t}_{sb}=(p'_{12b}/p_{12})\tilde{t}_b+(R_{cib}/p_{12})\tilde{t}_a \quad (6.105)$$

The total surface temperature heat balance equation for surface "a" is obtained by summing equations (6.100) and (6.104). The total surface temperature heat balance equation for surface "b" is given by summing equations (6.101) and (6.105). A series of eleven heat balance equations per surface are required to correspond to the eleven thermal transmission matrices defining the thermal behaviour of the structural surface. Hence, the total thermal response of a surface is defined by a series of eleven complex temperature components. A further process transforms the series of complex surface temperature components into a 24-hour periodic fluctuating surface temperature profile.

An advantage of the frequency domain method is that the heat balance equations for the fluctuating and mean component appear very similar in format. Either heat balance equation can be formulated from an inspection of the other. Thus the mean component surface temperatures are given by:

$$\bar{t}_{ra}+\bar{t}_{sa}=(R_{cia}R'_a/R)\alpha_a\bar{q}_{ra}+(R_{cia}R_{cib}/R)\alpha_b\bar{q}_{rb}+(R'_a/R)\bar{t}_a+(R_{cia}/R)\bar{t}_b \quad (6.106)$$

$$\bar{t}_{rb}+\bar{t}_{sb}=(R_{cib}R'_b/R)\alpha_b\bar{q}_{rb}+(R_{cia}R_{cib}/R)\alpha_a\bar{q}_{ra}+(R'_b/R)\bar{t}_b+(R_{cib}/R)\bar{t}_a \quad (6.107)$$

The total surface temperature profile is obtained by superimposing the fluctuating temperature profile onto the mean temperature component.

6.6.2.3 The heat balance equations

A significant advantage of the frequency domain method is that discretisation of structural elements is not required allowing the dynamic thermal behaviour of an entire element to be

described by a single thermal transmission matrix. While the mathematical process is divided into a mean and fluctuating procedure, each is very similar. The method also allows systematic formulation of the heat balance equations for computer spreadsheet implementation. Figure 6.13 illustrates four rooms of an intermediate floor of a building. The RHS of figure 6.13 shows space 'A' in more detail, illustrating connecting thermal conductances, temperatures and space convective heat gains. By inspection of figure 6.13, the space air node mean component heat balance equation can be systematically formulated as follows:

$$(C_W + C_N + C_G + C_P + C_R + C_F + C_C + C_V)\bar{t}_{Aai} - (C_P\bar{t}_{Bai} + C_R\bar{t}_{Cai} + C_C\bar{t}_{Uai} + C_F\bar{t}_{Lai}) = \bar{Q}_K + \bar{Q}_{KR} + C_W\bar{t}_{Weo} + C_N\bar{t}_{Neo} + (C_G + C_V)\bar{t}_{ao} \qquad (6.108)$$

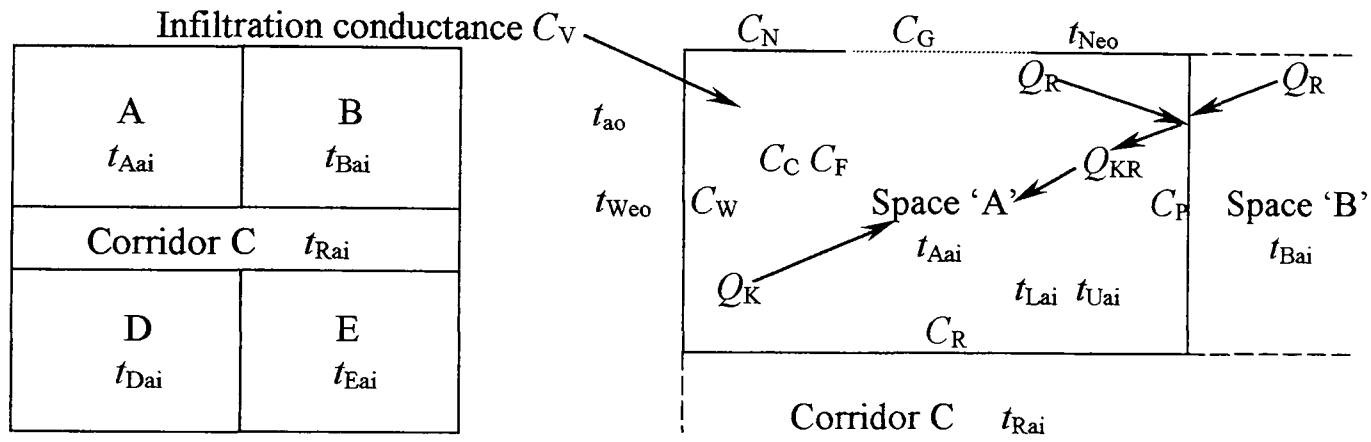

Except for the ventilation conductance, C_V, thermal conductances C = Area × U-value and the subscipts N, W, C, F, G, P, R mean north, west, ceiling, floor, partition and corridor partition respectively. For sol-air temperatures (e.g. t_{Weo}) the first subscript letter denotes north, east, etc. Q_K is casual convective gains and Q_{KR} is the convective gain to the air node due to radiant heat gains incident on the internal surfaces. The space air temperatures, t_{Lai} and t_{Uai}, denote lower and upper space air temperatures respectively.

Figure 6.13 Space 'A' air node mean component heat balance quantities

An inspection of the groupings in equation (6.108) shows that the heat balance equation may be condensed to the general form:

$$\sum(C)_S\bar{t}_{Sai} - \sum(C_X\bar{t}_{Yai}) = \sum(\bar{Q})_{Gains} \qquad (6.109)$$

Sum of space's thermal conductances times the mean space air temperature	–	Sum of the neighbouring space's mean air temperatures times the connecting conductances	=	Sum of the space mean heat gains

With some care, the heat balance equation for the fluctuating component may be obtained by substituting the conductances in equation (6.108) with the appropriate dynamic thermal coefficients, temperatures and thermal excitations thus:

$$\left(Y_{\mathrm{W}}+Y_{\mathrm{N}}+Y_{\mathrm{G}}+Y_{\mathrm{P}}+Y_{\mathrm{R}}+Y_{\mathrm{F}}+Y_{\mathrm{C}}+Y_{\mathrm{V}}+Y_{\mathrm{A}}+Y_{\mathrm{f}}\right)\tilde{t}_{\mathrm{Aai}}-\left(K_{\mathrm{P}}\tilde{t}_{\mathrm{Bai}}+K_{\mathrm{R}}\tilde{t}_{\mathrm{Cai}}+K_{\mathrm{C}}\tilde{t}_{\mathrm{Uai}}+K_{\mathrm{F}}\tilde{t}_{\mathrm{Lai}}\right)$$

$$=\tilde{Q}_{\mathrm{K}}+\tilde{Q}_{\mathrm{KR}}+K_{\mathrm{W}}\tilde{t}_{\mathrm{Weo}}+K_{\mathrm{N}}\tilde{t}_{\mathrm{Neo}}+\left(K_{\mathrm{G}}+K_{\mathrm{V}}\right)\tilde{t}_{\mathrm{ao}} \qquad (6.110)$$

All items in the above heat balance equation are complex quantities. Inspection of equation (6.110) shows that the first group of total space conductances in equation (6.108) is replaced by the total of the space admittances. The space air and furniture admittances, Y_{A} and Y_{f} respectively are included to account for their influence on the internal environment. The remaining conductances in equation (6.108) are replaced by dynamic thermal transmittances, K_{X}. Note that each of the thermal admittances and transmittances, given in equation (6.110), represents total surface quantities, as defined for the thermal conductances given in the footnote of figure 6.13. Equation (6.110) may be condensed into the following general format.

$$\sum\left(Y\right)_{\mathrm{S}}\tilde{t}_{\mathrm{Sai}}-\sum\left(K_{\mathrm{X}}\tilde{t}_{\mathrm{Yai}}\right)=\sum\left(\tilde{Q}\right)_{\mathrm{Gains}} \qquad (6.111)$$

Sum of space's thermal admittances times the space air temperature	–	Sum of the neighbouring space's fluctuating air temperatures times the connecting transmittances	=	Sum of the fluctuating space heat gains

Eleven fluctuating heat balance equations must be generated for each space to correspond to a Fourier series representing a 24-hour periodic excitation. The mean and fluctuating component heat balance equations may be systematically written down, in the case of the four spaces shown in figure 6.13, by employing the general expressions described by equations (6.109) and (6.111). Further heat balance equations can be produced for upper and lower spaces. If the spaces above and below are assumed to have the same air temperature as the intermediate space, then adiabatic boundary conditions at ceiling and floor level can be introduced into the heat balance equations. In the case of space 'A' this is achieved by substituting t_{Aai} for t_{Lai} and t_{Uai} in equations (6.108) and (6.110). To model a single zone linked to other zones with similar environmental conditions, all neighbouring

space temperatures should be set to the zone temperature of interest. For example, to simulate space "A" as a single zone, only its heat balance equations are required and all the space air temperatures in equations (6.108) and (6.109) are set to the appropriate mean and fluctuating temperature of space "A" only.

6.6.2.4 Solving the heat balance equations

The mean component, heat balance equations can be solved using a suitable spreadsheet program that includes matrix inversion and multiplication functions. Since only arithmetic operations are required to solve the equation set, computational time is fast and a large number of spaces can be arranged into a thermal network model in order to determine the mean air temperature of each space. The fluctuating component, heat balance equations are formulated with complex quantities. A computer spreadsheet is not usually programmed to solve a set of complex simultaneous equations. It is possible to set-up a procedure to solve the complex equation set by employing Gaussian elimination using the in-built complex number functions. However, the procedure becomes more difficult to set-up due to the number of terms required in the Gaussian elimination procedure increasing exponentially with each additional equation. An alternative and simpler approach to solving the set of complex simultaneous equations is by numerical iteration. The equation set for the four spaces and corridor, illustrated in figure 6.13, is given by:

$$\sum (Y)_A \tilde{t}_{\mathrm{Aai}} - \left(K_{\mathrm{P}} \tilde{t}_{\mathrm{Bai}} + K_{\mathrm{R}} \tilde{t}_{\mathrm{Cai}} + K_{\mathrm{C}} \tilde{t}_{\mathrm{UAai}} + K_{\mathrm{F}} \tilde{t}_{\mathrm{LAai}}\right) = \sum \left(\tilde{Q}\right)_{\mathrm{A\ gains}} \tag{6.112}$$

$$\sum (Y)_{\mathrm{B}} \tilde{t}_{\mathrm{Bai}} - \left(K_{\mathrm{P}} \tilde{t}_{\mathrm{Aai}} + K_{\mathrm{R}} \tilde{t}_{\mathrm{Cai}} + K_{\mathrm{C}} \tilde{t}_{\mathrm{UBai}} + K_{\mathrm{F}} \tilde{t}_{\mathrm{LBai}}\right) = \sum \left(\tilde{Q}\right)_{\mathrm{B\ gains}} \tag{6.113}$$

$$\sum (Y)_{\mathrm{C}} \tilde{t}_{\mathrm{Cai}} - \left[K_{\mathrm{R}} \left(\tilde{t}_{\mathrm{Aai}} + \tilde{t}_{\mathrm{Bai}} + \tilde{t}_{\mathrm{Dai}} + \tilde{t}_{\mathrm{Eai}}\right) + \left(K_{\mathrm{C}} \tilde{t}_{\mathrm{UCai}} + K_{\mathrm{F}} \tilde{t}_{\mathrm{LCai}}\right)\right] = \sum \left(\tilde{Q}\right)_{\mathrm{C\ gains}} \tag{6.114}$$

$$\sum (Y)_{\mathrm{D}} \tilde{t}_{\mathrm{Dai}} - \left(K_{\mathrm{P}} \tilde{t}_{\mathrm{Eai}} + K_{\mathrm{R}} \tilde{t}_{\mathrm{Cai}} + K_{\mathrm{C}} \tilde{t}_{\mathrm{UDai}} + K_{\mathrm{F}} \tilde{t}_{\mathrm{LDai}}\right) = \sum \left(\tilde{Q}\right)_{\mathrm{D\ gains}} \tag{6.115}$$

$$\sum (Y)_{\mathrm{E}} \tilde{t}_{\mathrm{Eai}} - \left(K_{\mathrm{P}} \tilde{t}_{\mathrm{Dai}} + K_{\mathrm{R}} \tilde{t}_{\mathrm{Cai}} + K_{\mathrm{C}} \tilde{t}_{\mathrm{UEai}} + K_{\mathrm{F}} \tilde{t}_{\mathrm{LEai}}\right) = \sum \left(\tilde{Q}\right)_{\mathrm{E\ gains}} \tag{6.116}$$

Spaces above and below spaces "A to E" are assumed at the same temperature as the intermediate spaces, effectively eliminating ten equations. This also implies that the upper and lower space temperatures (with subscript U or L) must be set equal to the space's air temperature defined on the LHS of each equation. To start the iteration process, initial

conditions are established by assuming all the temperatures in each equation are equal to the space's air temperature shown on the LHS of each equation. This effectively sets up adiabatic boundaries around each space, enabling each equation to be solved explicitly. Each space is modelled as a single zone resulting in a good approximation of the complex air temperature for each space. The approximate space air temperatures are then inputted into their appropriate locations within each equation. The space air temperature, on the LHS of each equation, is set to zero and each equation is solved explicitly to produce the revised space air temperature. The iteration process continues until satisfactory convergence of each space air temperature has been obtained. Only four to five iterations are required, due to the initial adiabatic approximation.

6.6.2.5 Processing the periodic space air and surface temperature profiles

A series of eleven complex temperature components results from solving the series of eleven heat balance equations representing the fluctuating air temperature of a particular space. If the series of complex temperature components is given by

$$(A + jB)_1, (A + jB)_2, (A + jB)_3, \ldots\ldots\ldots (A + jB)_{11}, \tag{6.117}$$

the fluctuating space air temperature, at each time increment, is then given by the real part of the sum of the following complex series, which results from the product of the complex time coefficient and complex temperature

$$\tilde{\theta}_\phi = \text{Real} \sum_{n=1}^{11} \left[\left(C_\phi + jD_\phi \right)_n (A + jB)_n \right] \tag{6.118}$$

$$\text{The complex time coefficient } \left(C_\phi + jD_\phi \right)_n = \cos(\omega_n \phi) + j \sin(\omega_n \phi), \tag{6.119}$$

where $\omega_n = 2\pi n/P$, $n = 1$ to 11, P = periodic time and ϕ = time from 1 to 24 in the case of a 24-hour periodic formulation.

The resulting fluctuating space temperature profile is then superimposed onto the mean component to produce the 24-hour periodic air temperature response. Surface temperatures are processed in the same manner.

The complex time coefficients need only be evaluated once, using equation (6.119), and the stored values may be used repeatedly for any periodic frequency domain formulation using the same periodic time P and time discretisation. The complex time coefficients may be

formed into a matrix of N rows by (N/2-1) columns, which is representative of N discrete thermal excitation values and Fourier series of (N/2-1) terms.

6.6.2.6 Generating the complex thermal excitations

In the frequency domain, periodic thermal excitation profiles must be transformed into a discrete Fourier series prior to being included in the heat balance equations. The thermal excitation profile is decomposed into a mean value and a fluctuating profile. Fourier coefficients and phase angles are generated from the discrete values of the fluctuating profile. The Fourier series is usually generated using the following trigonometric procedure

$$F_n = \sqrt{C_n^2 + S_n^2} \quad \text{and} \quad \gamma_n = \tan^{-1}(S_n / C_n) \tag{6.120}$$

where F_n and γ_n are the Fourier coefficient and phase angle respectively,

$C_n = (2/N)\sum_{m=1}^{N}[E_m \cos(n\omega\phi_m)]$, $S_n = (2/N)\sum_{m=1}^{N}[E_m \sin(n\omega\phi_m)]$, N is the number of discrete thermal excitation values, E_m is the fluctuating component at time ϕ_m, n is the number of terms in the Fourier series, $\omega = 2\pi/P$, P is the periodic time.

The Fourier series, including the mean value can then be expressed by:

$$\bar{F} + \sum_{n=1}^{N/2-1}[F_n \cos(n\omega\phi - \gamma_n)] \tag{6.121}$$

A complex number transformation of the Fourier series is preferred to the trigonometric formulation of equation (6.121), due to the fluctuating component heat balance equations being defined by complex quantities. The following *complex Fourier coefficient* replaces the Fourier coefficient and phase angle.

$$(F_{\text{complex}})_n = \frac{2}{N}\sum_{m=1}^{N} E_m f_{m,n} \quad \text{for } n = 1 \text{ to } N/2 - 1, \tag{6.122}$$

where $f_{m,n} = (c - js)_{m,n} = \cos(n\omega\phi_m) - j\sin(n\omega\phi_m)$

The complex quantities, $f_{m,n}$, remain constant for a particular periodic time P and N discrete values representing the fluctuating excitation profile. When evaluated, these complex constants may be formed into a complex Fourier matrix of N-rows by (N/2-1) columns. The

matrix can be employed repeatedly for processing thermal excitations, defined by the same P and N profiles, into complex Fourier coefficients. Expanding equation (6.122) in the case of $n = 1$ gives the first complex Fourier coefficient of the series, for example.

$$\left(F_{\text{complex}}\right)_{n=1} = 2\left(E_1 f_{11} + E_2 f_{21} + E_3 f_{31} + \ldots\ldots + E_N f_{N1}\right)/N \tag{6.123}$$

The second complex Fourier coefficient, $\left(F_{\text{complex}}\right)_{n=2}$, is obtained by substituting the second column of complex elements (f_{12} to f_{N2}) from the complex Fourier matrix into equation (6.123). Subsequent complex Fourier coefficients are obtained in the same manner. The complex Fourier series is then given by:

$$\overline{F} + \sum_{n=1}^{N/2-1} \left(F_{\text{complex}}\right)_n \tag{6.124}$$

The generating of the Fourier series reduces to a systematic process when employing the complex Fourier matrix.

6.6.3 The long-wave radiant exchange model

Representing the long-wave radiant exchange process via a radiative surface resistance is the traditional approach taken, when employing the frequency domain technique. The radiative and convective resistances are combined, and included in the thermal transmission matrix of the structural element. In the proposed method, long-wave radiant exchange is processed, in a more precise manner, as a thermal excitation. The thermal excitation is in the form of the net radiant flux incident upon each surface. In the case of a rectangular shaped space with a single window, seven thermal excitation profiles are generated. A sub-model is used to establish the radiation view factors between the surfaces. The net radiant flux is computed for each surface and then the fluctuating component is transformed into a complex Fourier series to be inputted into the appropriate surface heat balance equations. The mean component of the net radiant flux is inputted into the mean component's surface heat balance equation. The subsequent convective gains, due to the radiant fluxes, are computed and inputted into the space air node's mean and fluctuating component, heat balance equations (see section 6.6.21). The long-wave radiant exchange model is linked via a software switch to the frequency domain model. Initially, the switch is set to zero, and no net radiant fluxes are inputted to the heat balance equations. Surface temperatures are

inputted to the long-wave exchange model to generate the initial net surface flux profiles per surface. Each surface flux profile is then transformed into a Fourier series. Setting the switch to one initiates the radiant exchange process, causing each Fourier series to be inputted into the appropriate surface heat balance equation. The subsequent convective fluxes are calculated and inputted into the space air, heat balance equations. In response, the frequency domain model recalculates all surface temperatures and the space air node temperature. The updated surface temperatures are inputted into the radiant exchange model to recalculate the net surface fluxes and subsequent Fourier series. The iteration process continues until satisfactory steady state conditions of space air and surface temperatures are established. Figure 6.14 illustrates the calculation process. The iteration process may become unstable, tending to diverge rather than converge. Figure 6.14 illustrates a stability routine that controls the iteration process towards convergence. A sub-routine is arranged to store the surfaces' net radiant flux values per iteration; identified as "previous flux value" in figure 6.14. A fraction of the revised net radiant flux value is then added to a fraction of the previous net radiant flux value. Both fractions must sum to unity,

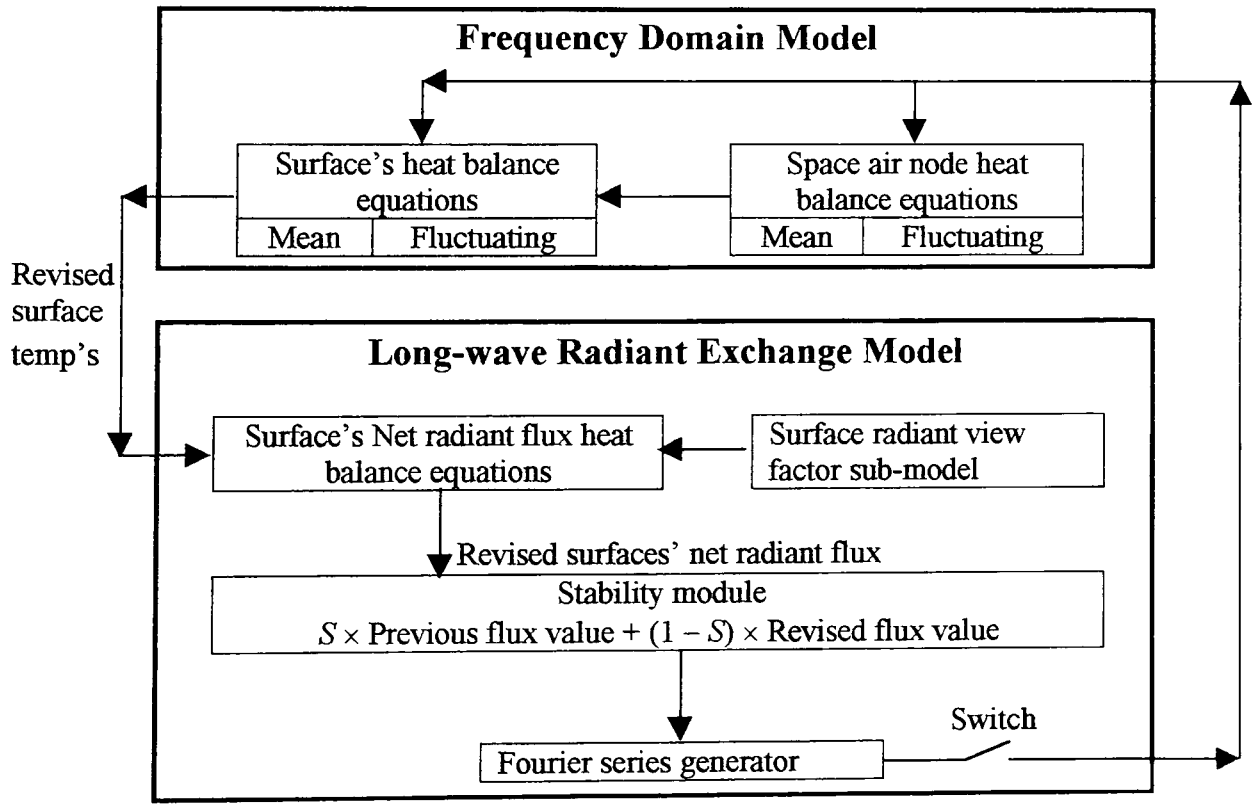

Figure 6.14 Long-wave radiant exchange iterative calculation procedure

values of 0.1 and 0.9 are employed with the larger fraction being applied to the previous net radiant flux value.

6.6.3.1 Response factor method of calculating long-wave radiant exchange

A suitable expression for calculating long-wave radiant exchange is given by equation (2.8), which can be rearranged as follows for solution by matrices.

$$q_i/\varepsilon_i - \sum_{j=1}^{N} F_{ij}\left(\frac{1}{\varepsilon_j} - 1\right) q_j = \left[\sigma \sum_{j=1}^{N} F_{ij}\left(T_i^4 - T_j^4\right)\right] \tag{6.125}$$

The net radiant flux for each surface is symbolised by q. The subscript i represents the single surface that is exchanging radiant flux with the other room surfaces, identified by subscript j, which are in view of it. Solution by matrices or an appropriate iteration process may be used to determine the net surface radiant fluxes. A procedure employing a *total grey interchange factor* to compute the net radiant exchange per surface is an alternative solution method. The procedure, which is attributed to Hottel and Sarofin [76], is described in a review of long-wave radiation models [61]. The total grey interchange factors are similar to response factors, linearly relating the net radiant flux on a particular surface to the emissive power excitations of all the surfaces. The idea takes advantage of the fixed geometrical relationship between the major surfaces of a room. The total grey interchange factors need only to be computed once, resulting in each surface radiant exchange equation being solved explicitly. Hottel and Sarofin's derivation of the interchange factors were based on a radiosity formulation of the radiant exchange process. Equation (6.125) gives the net radiant fluxes directly in terms of surface temperatures, rather than radiosities. Applying Hottel and Sarofin's idea to equation (6.125) results in a systematic approach to deriving the interchange factors. A two-stage procedure is employed to determine the interchange factors. Responses to emissive power excitations on each surface are determined. The emissive power responses are then employed to obtain the total grey interchange factors. All surface temperatures, except one, are set to absolute zero and the thermal responses of all the surfaces are calculated. This process is repeated until each of the room surfaces has acted as the non-zero temperature surface. As a result, a thermal response has been recorded, for each surface, due to an emissive power excitation on the other room surfaces. In the case of a rectangular room with a window, equation (6.125) produces a set of seven simultaneous equations. The equation set can be solved sequentially to determine the emissive power responses due to a non-zero emissive power excitation on

each surface in turn. If an excitation emissive power value of unity is used for the non-zero surface, then the resulting net radiation fluxes are the corresponding thermal responses of the surfaces due to a unity emissive power excitation. Alternatively the unity emissive power responses can be obtained directly from the radiation view factors. Assume for a particular rectangular room with a window that the radiation view factors are as per the view factor matrix shown in table 6.14. Note that the sum of the view factors of a particular surface is unity. The window is located in the south wall, resulting in the view factor between these two surfaces being zero. The emissive power responses are obtained directly from an inspection of the view factor matrix of table 6.14. The resulting unity emissive power responses are given in table 6.15; the diagonal of ones, corresponding to the unity emissive power excitations, replaces the diagonal of zeros in table 6.14. The emissive power responses are obtained by changing the view factors to negative values. Note that the resulting matrix of table 6.15 represents the surfaces' heat balance, summing to zero in the RHS column. The ceiling values in the top row of table 6.15 indicates that the ceiling is the non-zero surface on which unity emissive power excitation is applied and all the other

Table 6.14 Radiation view factors for rectangular room with a window

Surface		Ceiling	Floor	N-Wall	S-Wall	W-Part	E-Part	Window	$\Sigma(F_{i-j})$
Ceiling	F_{i-j}	0.000	0.342	0.200	0.157	0.130	0.130	0.042	1.000
Floor	F_{i-j}	0.342	0.000	0.200	0.157	0.130	0.130	0.042	1.000
N-Wall	F_{i-j}	0.266	0.266	0.000	0.157	0.131	0.131	0.048	1.000
S-Wall	F_{i-j}	0.262	0.262	0.196	0.000	0.140	0.140	0.000	1.000
W-Part	F_{i-j}	0.259	0.259	0.197	0.168	0.000	0.087	0.029	1.000
E-Part	F_{i-j}	0.259	0.259	0.197	0.168	0.087	0.000	0.029	1.000
Window	F_{i-j}	0.283	0.283	0.239	0.000	0.097	0.097	0.000	1.000

Table 6.15 Emissive power responses to a unity emissive power excitation

Surface		Ceiling	Floor	N-Wall	S-Wall	W-Part	E-Part	Window	$\Sigma(E_{i-j})$
Ceiling	E_{i-j}	1.000	-0.342	-0.200	-0.157	-0.130	-0.130	-0.042	000
Floor	E_{i-j}	-0.342	1.000	-0.200	-0.157	-0.130	-0.130	-0.042	000
N-Wall	E_{i-j}	-0.266	-0.266	1.000	-0.157	-0.131	-0.131	-0.048	000
S-Wall	E_{i-j}	-0.262	-0.262	-0.196	1.000	-0.140	-0.140	0.000	000
W-Part	E_{i-j}	-0.259	-0.259	-0.197	-0.168	1.000	-0.087	-0.029	000
E-Part	E_{i-j}	-0.259	-0.259	-0.197	-0.168	-0.087	1.000	-0.029	000
Window	E_{i-j}	-0.283	-0.283	-0.239	0.000	-0.097	-0.097	1.000	000

values, shown in the row, are the corresponding emissivity power responses on the other surfaces. The emissive power responses of a particular surface are given in the surface's column of responses.

If each of these surface columns represents an excitation vector of equation (6.125) then the corresponding solutions are the total grey interchange factors. Equation (6.126), given below, shows the coefficient matrix of equation (6.125) and the ceiling's excitation vector obtained from table 6.15.

$$\begin{bmatrix} 1.111 & -0.038 & -0.200 & -0.017 & -0.014 & -0.014 & -0.008 \\ -0.038 & 1.111 & -0.200 & -0.017 & -0.014 & -0.014 & -0.008 \\ -0.030 & -0.030 & 2.000 & -0.017 & -0.015 & -0.015 & -0.009 \\ -0.029 & -0.029 & -0.196 & 1.111 & -0.016 & -0.016 & 0.000 \\ -0.029 & -0.029 & -0.197 & -0.019 & 1.111 & -0.010 & -0.006 \\ -0.029 & -0.029 & -0.197 & -0.019 & -0.010 & 1.111 & -0.006 \\ -0.031 & -0.031 & -0.239 & 0.000 & -0.011 & -0.011 & 1.190 \end{bmatrix} \cdot \begin{bmatrix} q_1 \\ q_2 \\ q_3 \\ q_4 \\ q_5 \\ q_6 \\ q_7 \end{bmatrix} = \begin{bmatrix} 1.000 \\ -0.342 \\ -0.266 \\ -0.262 \\ -0.259 \\ -0.259 \\ -0.283 \end{bmatrix} \quad (6.126)$$

Emissivity values of 0.9 and 0.84 were used for the opaque surfaces and window respectively. The solution of equation (6.126) to the ceiling excitation vector is given in table 6.16 and the solution to all the surface excitation vectors is given in table 6.17. Each

Table 6.16 Solution to equation (6.126) to the ceiling excitation vector

Surface	Ceiling	Floor	N-Wall	S-Wall	W-Part	E-Part	Window
	q_1	q_2	q_3	q_4	q_5	q_6	q_7
Net surface radiant flux (W/m^2)	0.853	-0.314	-0.132	-0.252	-0.250	-0.250	-0.255

Table 6.17 Solution to equation (6.126) to all surface excitation vectors (W/m^2)
The total grey interchange factors

Surface	Ceiling	Floor	N-Wall	S-Wall	W-Part	E-Part	Window
Surface	q_1	q_2	q_3	q_4	q_5	q_6	q_7
Ceiling	0.853	-0.314	-0.132	-0.252	-0.250	-0.250	-0.255
Floor	-0.314	0.853	-0.132	-0.252	-0.250	-0.250	-0.255
N-Wall	-0.099	-0.099	0.494	-0.097	-0.098	-0.098	-0.109
S-Wall	-0.151	-0.151	-0.078	0.874	-0.160	-0.160	-0.027
W-Part	-0.125	-0.125	-0.065	-0.133	0.878	-0.092	-0.094
E-Part	-0.125	-0.125	-0.065	-0.133	-0.092	0.878	-0.094
Window	-0.038	-0.038	-0.022	-0.007	-0.028	-0.028	0.833

column of table 6.17 gives the total grey interchange factors of the pertinent surface. The total grey interchange factors are linearly related to the emissive powers of all the surfaces. As a result, the net radiant flux, on a particular surface, is determined from a response factor expression. The net radiant flux, in the case of the ceiling, is given by:

$$q_1 = 0.853E_1 - 0.314E_2 - 0.099E_3 - 0.151E_4 - 0.125E_5 - 0.125E_6 - 0.038E_7 \qquad (6.127)$$

where E_s is the actual emissive power (σT_s) of surface "s" at a particular time.
The general form of the expression is given by

$$q_i = \sum_{j=1}^{N} R_{ij} E_j \qquad (6.128)$$

The subscripts *ij* refer to total grey interchange factors at the intersection of column *i* and row *j* of table 6.17. E_j is the emissive power of the surface designating row "*j*".
The set of seven long-wave radiation equations must be solved for each hour of the simulation period. Equation (6.128) is solved explicitly, resulting in a computationally more efficient solution process compared to solving equation (6.125) by matrices or iteration.

6.6.3.2 Linearizing surface emissive powers

The emissive powers of a space's surfaces dominate the radiant exchange process. Due to this factor, equation (6.125) tends to be reduced to the form:

$$q_i = \left[\sigma \sum_{j=1}^{N} F_{ij} \left(T_i^4 - T_j^4 \right) \right] \qquad (6.129)$$

A widely used linearized version of equation (6.129) is given by

$$q_i = \sum_{j=1}^{N} h_{r_i} \left(T_i - T_j \right) \qquad (6.130)$$

where the radiative heat transfer coefficient $h_{r_i} = 4\sigma F_{ij} T_{avg_i}^3$ and T_{avg} is the average of the participating surface temperatures.
For accurate simulation, the radiative heat transfer coefficient, h_r, of each surface, must be updated frequently. A disadvantage of the approximation is that the third power exponent of the average temperature must still be computed for each surface for each hour of simulation. Further, equation (6.130) is derived from equation (6.129), which is a reduced formulation of equation (6.125).

The emissive power, σT^4, displays a close linear relationship with temperature, in degrees Celsius, over the typical range of temperatures experienced in rooms. A process of linear regression results in the following linear expressions of emissive power, for example.

Temperature range 0°C to 25°C: $$E_i = \sigma T^4 \cong 5.2944 t_i + 313.35 \qquad (6.131)$$

Temperature range 25°C to 50°C: $$E_i = \sigma T^4 \cong 6.8081 t_i + 275.13 \qquad (6.132)$$

The maximum errors incurred by employing equations (6.131) and (6.132) are 0.72 % and 0.61 % respectively. The corresponding average errors are 0.43 % and 0.35 % respectively. The percentage absolute error was calculated from 100% × absolute $(E_{\text{exact}} - E_{\text{linear}})/ E_{\text{exact}}$. The range of temperatures normally exhibited by the structural room surfaces is smaller, 25°C to 36°C for example. The accuracy of the linear correlation improves with decreasing temperature range. The inner surface of a window blind exhibits a wider range of temperatures, 23°C to 50°C for example. In the internal environmental model, two linear expressions are employed, one represents the window's emissive power, with its wider range of surface temperatures, and the other represents the room structural surface emissive powers. The gradient and constant of each expression are revised after each iteration step in order to maintain precision of the radiant exchange process. If the general linear expression is given by $E = m \times t + c$, then the gradient m and constant c are obtained employing the following linear regressions.

$$m = \sigma \left(T_{\max}^4 - T_{\min}^4\right) / \left(t_{\max} - t_{\min}\right) \qquad (6.133)$$

and $$c = \sigma T_{\min}^4 - m t_{\min} \qquad (6.134)$$

where T and t represent the absolute and corresponding Celsius surface temperatures respectively. Only two emissive powers are computed per iteration in the case of the six opaque room surfaces compared to the 144 emissive power evaluations required using equation (6.129). The two surface emissive powers and corresponding temperature are then used to calculate the gradient and slope of equations (6.133) and (6.134). If the maximum and minimum surface temperatures are rounded to the nearest whole number, the gradient m and constant c are made less sensitive to small changes in the actual maximum and minimum surface temperatures. After a number of iterations, changes in m and c occurs less frequently, eventually becoming constant during the remaining iteration process. Results

between the exact and linear emissive power calculation methods are compared in table 6.18. Maximum and average absolute errors for the window are 0.80 % and 0.35 % respectively. For the ceiling, the maximum and average absolute errors are 0.24 % and 0.16 % respectively. The other room surfaces produced errors slightly below that of the ceiling.

Table 6.18 Comparing exact and linearized calculations of emissive power (Wm^{-2})

Window surface

Time	Exact	Linearized	% Error
0	453	454	0.31
2	444	445	0.16
4	439	439	0.07
6	434	434	0.04
8	440	440	0.11
10	457	459	0.44
12	475	478	0.64
14	561	565	0.65
16	623	624	0.06
18	588	590	0.47
20	525	529	0.80
22	463	466	0.46
		Maximum error = 0.80 %	
		Average error = 0.35 %	

Ceiling surface

Time	Exact	Linearized	% Error
0	467	468	0.18
2	462	462	0.13
4	458	458	0.08
6	456	457	0.07
8	458	458	0.09
10	471	472	0.20
12	481	482	0.23
14	491	492	0.21
16	505	506	0.11
18	495	496	0.18
20	485	486	0.24
22	474	475	0.22
		Maximum error = 0.24 %	
		Average error = 0.16 %	

The corresponding maximum and average errors in the space's mean surface temperature was 0.09 % and 0.06 % respectively. The maximum and average errors in the space's air temperature was 0.06 % and 0.04 % respectively. A lightweight space construction was used with three air changes per hour and plant switched off. Table 6.19 compares the space's cooling load between using the exact and liearized emissive power methods.

Table 6.19 Comparing space cooling load between exact and linearized emissive power formulations (W)

Time	8	9	10	11	12	13	14	15	16	17	18
Exact	510	593	1272	1189	1340	1315	1599	1733	1971	1324	987
Linearized	513	594	1273	1190	1342	1315	1600	1734	1972	1324	992
% Error	0.64	0.25	0.05	0.11	0.20	0.03	0.11	0.04	0.05	0.06	0.48

The error at the peak cooling load is 0.05% and the maximum and average errors are 0.64 % and 0.22 % respectively. Table 6.19 shows that, except for two results, there is a difference of a watt only between the methods.

6.6.3.3 Polynomial correlation of surface emissive power

The accuracy of the linearized emissive power expressions described in the previous section is sufficient for practical design calculations. If greater accuracy is required, the following polynomial expression, correlating emissive power with temperature over the temperature range 0°C to 50°C may be employed.

$$E = \sigma T^4 \cong 0.0303t^2 + 4.5273t + 315.9387 \qquad (6.135)$$

The maximum and average absolute errors in emissive power are 0.1 % and 0.04 % respectively. Applying polynomial regression over an appropriate temperature range, specific to a particular simulation run, will result in a more precise polynomial correlation. Polynomial correlation for the window, with its relatively wider surface temperature range, should improve overall accuracy. If greater overall accuracy is required then polynomial emissive power expressions can be employed for all the surfaces.

6.6.3.4 Approximating the long-wave radiant exchange process

The total grey interchange factor method, defined by equation (6.128), is used at the highest level of complexity. Sections 6.6.3.3 and 6.6.3.2 described the development of emissive power correlations that can provide high precision approximations of the emissive power terms of equation (6.128). A lower level in model complexity is obtained by approximating the radiant exchange view factors and reducing the number of radiant exchange paths between the space's surfaces. The process of reducing the number of long-wave radiant exchange paths has already occurred, due to the assumption of isothermal room surfaces being made. A number of approximation methods have been developed, which are primarily different versions of the *Mean Radiant Temperature Method* (MRT) [61]. ASHRAE's Heat Balance Procedure, for Calculating Cooling Loads, employs an MRT method. In the MRT models each surface radiates to a hypothetical surface, whose area, temperature and emissivity are weighted averages of the space's surfaces. The accuracy of this two-surfaced model relies on the assumption of the hypothetical surface temperature being a representative mean of all the surfaces. The internal surface temperature of a window, with closed internal blinds or solar absorptive glazing, can be significantly higher than the room surfaces. In the cooler months the inner glazing surface can be much lower than the other room surfaces. In these cases, the influence of window surface temperature is diminished when included in the hypothetical mean surface temperature and the significant

radiant exchanges taking place between the window and individual room surfaces is not fully accounted for. The accuracy of a reduced path radiant exchange model is improved by grouping surfaces with similar temperature profiles. Surfaces with significantly different temperature profiles should not be grouped. The accuracy of the reduced model further improves as the difference in temperatures between the hypothetical mean surfaces of each group or single surface increases. In well-insulated buildings, the temperature profiles of a space's structural surfaces are similar but quite different from that of the window surface. In poorly insulated buildings, the internal temperature profiles of external structural surfaces, such as a façade or roof, can be quite different from that of the internal surface. A new reduced path long-wave radiant exchange model has been developed, which is more sensitive to the diversity in internal surface temperatures, and thus, accounts for the dominant radiant exchanges taking place between the room surfaces. The model is based on a well-insulated building, in which the dominant radiant exchange process takes place between the inner window surface and the other room surfaces. Radiant exchange is modelled between the window surface and a hypothetical mean surface representing the internal structural surfaces, excluding the window wall. The distribution of the window's net radiant flux to the opaque room surfaces is achieved using approximate area weighted view factors. Radiant exchange is modelled between each room surface and a hypothetical mean surface representing the other room surfaces, excluding the window surface. An area weighted view factor between the surface and the hypothetical mean surface is employed. The net radiant exchange, on each room surface, is then the sum of the net surface fluxes obtained from the two sets of calculations. As the temperature difference between the window and hypothetical surface increases, the precision of the model improves. This sensitivity in thermal response is important when estimating peak space temperatures and cooling loads. When the window temperature approaches that of the hypothetical surface temperature, less radiant exchange takes place. When all the surface temperatures, including the window, are relatively close in value, the small amount of radiant exchange taking place has little effect on internal environmental conditions. In the MRT methods radiant exchange is modelled between the window and the hypothetical mean room surface, which accounts for the total window net radiant exchange, but the distribution of this radiant exchange flux to the individual room surfaces is neglected. When the net radiant flux is estimated for the individual room surfaces, the significant influence of the window

surface temperature is reduced due to including the window surface with the other room surfaces to form the hypothetical surface.

In the case of radiant exchange between an individual surface i and a hypothetical surface m, equation (6.125) reduces to

$$q_i = \varepsilon_i F_{im} \left[\sigma \left(T_m^4 - T_i^4 \right) + \left(1/\varepsilon_m - 1 \right) q_m \right] \tag{6.136}$$

For a heat balance $A_m q_m = -A_i q_i$, giving $q_m = (A_m / A_i) q_i$. Substituting for q_m results in

$$q_i = \left(F_{im} \right)_{\text{eff}} \sigma \left(T_m^4 - T_i^4 \right), \tag{6.137}$$

where: the effective view factor $\left(F_{im} \right)_{\text{eff}} = A_m F_{im} / \left(A_m / \varepsilon_i + F_{im} A_i / \varepsilon_m - F_{im} A_i \right)$;

$A_m = A_t - A_i - A_w$. Subscripts t and w correspond to total and window respectively.

The approximate area weighted view factor, from the surface i to the hypothetical surface area m, is given by $F_{im} = 1 - A_w / (A_t - A_i)$

In the case of the window surface, the subscript i in equation (6.137) is replaced by w and the corresponding view factor from the window to the hypothetical surface (not including the window wall) is given by $F_{wm} = 1$. The resulting net radiant flux q_w is distributed to the individual room surfaces using the approximate area weighted view factor $F_{wi} = A_i / (A_t - A_{ww})$ where A_{ww} is the window wall area, including the window. The total net radiant flux on an individual room surface is then given by

$$\left(Q_i \right)_{total} = A_i q_i - F_{wi} A_w q_w \tag{6.138}$$

Equation (6.137) will produce a negative net flux for the window, its surface temperature being higher than the hypothetical surface temperature. The negative sign in equation (6.138) will then cause the corresponding distribution of flux to be added to the opaque surfaces. The total net flux on the solid window wall will only consist of q_i. Exact, linearized or polynomial emissive powers may be used in equation (6.137). Exact view factors may be used in equation (6.137), but this tends to defeat the purpose of deriving a simpler formulation of the radiant exchange process. Table 6.19 compares results between the exact method as per equation (6.128) incorporating exact emissive powers, and the approximate radiant exchange model, employing linearized emissive powers. The space dimensions are 6m length façade by 4m depth by 3m high with a window area 20 % of the façade surface area. Simulation runs were carried out for east and west orientations of the space's façade, and for light and heavyweight constructions. Table 6.20 summarises the

results in terms of the percentage absolute errors at the peak temperatures, maximum and average temperatures. The errors were calculated using the expression 100% × absolute $(t_{exact} - t_{approx})/ t_{exact}$. The simulations were carried out for a free running building with internal blinds in operation to reduce the transmitted solar radiation at the appropriate times. Overall, there is little difference in results between the exact and approximate methods.

Table 6.20 Comparing space mean surface and air temperatures between exact and approximate long-wave radiant exchange models - July

Simulation in July	East orientation				West orientation			
	Lightweight construction		Heavyweight construction		Lightweight construction		Heavyweight construction	
	Mean surface	Air	Mean surface	Air	Mean surface	Air	Mean surface	Air
% Error at peak temperature	0.12	0.08	0.35	0.24	0.34	0.23	0.39	0.25
Maximum % error	0.86	0.67	0.41	0.30	0.49	0.41	0.43	0.36
Average % error	0.40	0.35	0.33	0.26	0.35	0.27	0.34	0.26

Table 6.21 gives results for the same space but in relation to cooling load. The space air set point temperature is 22 °C and the infiltration rate is 0.5 air changes per hour. The cooling load and the percentage errors are tabulated for the plant operating hours only. The approximate method slightly under predicts the cooling load compared to the exact method. The peak cooling load (shown in bold text) is used to determine local and central plant sizes and associated components, such as ductwork and pipework. In practice, a system is usually oversized due to plant and components being manufactured to standard sizes. It is unlikely that the small errors in peak load, shown in table 6.21, will lead to the selection of different

Table 6.21 Comparing cooling load between exact and approximate long-wave radiant exchange models

Time	East orientation						West orientation					
	Lightweight construction			Heavyweight construction			Lightweight construction			Heavyweight construction		
	Exact	Approx	%Error	Exact	Approx	%Error	Exact	Approx	%Error	Exact	Approx	%Error
8	1506	1465	2.71	1197	1171	2.17	510	500	1.88	648	628	2.96
9	1122	1097	2.27	1123	1100	2.05	593	586	1.24	686	674	1.82
10	**1846**	**1816**	**1.64**	**1738**	**1713**	**1.44**	1271	1262	0.72	1304	1291	1.00
11	1406	1388	1.29	1473	1451	1.49	1188	1182	0.52	1222	1211	0.93
12	1539	1521	1.19	1564	1543	1.34	1340	1331	0.65	1346	1333	0.93
13	1263	1251	0.97	1364	1347	1.25	1315	1304	0.87	1327	1314	1.02
14	1517	1502	0.98	1516	1498	1.19	1599	1580	1.17	1565	1549	1.02
15	1293	1282	0.91	1371	1355	1.17	1732	1709	1.34	1632	1616	0.94
16	1556	1541	0.93	1526	1510	1.05	**1970**	**1942**	**1.43**	**1821**	**1804**	**0.93**
17	724	714	1.37	864	849	1.74	1323	1296	2.05	1263	1241	1.75
18	656	645	1.68	782	767	1.92	991	965	2.59	1059	1037	2.03

sized components. Similarly, the hourly differences in cooling load between the two methods should not result in different system control strategies being formulated.
The performance of an approximate method should be based on accuracy achieved and computational effort [77]. Less computational effort is associated with the approximate method due to using area weighted view factors, reducing the number of radiant exchange paths, and employing an explicit solution method. The cost in accuracy is small and should not influence the final sizing of system components. In the case of a naturally ventilated building, the small differences in internal temperatures, indicated by the errors shown in table 6.20, should not result in different assessments regarding thermal comfort.

6.6.4 The internal convection model

Variable surface convection coefficients are generated to simulate convection between the surfaces and space air node, at the highest level of complexity. In response, the surfaces' and space air temperatures change and the resulting values are inputted to the internal convection model in order to generate new values of surface convection coefficient. The iteration process continues until satisfactory convergence of the surfaces' and space air node temperatures have been established. The iterative long-wave radiant exchange process is also operating in parallel with the iterative convection process. A software switch links the internal convection model to the frequency domain model. The switch provides the options of running the model with constant or variable convection coefficients. The mean value of the 24-hour convection coefficient profile of each surface is inputted to the thermal transmission matrices representing the space structural surfaces. The mean value is also used in mean component's heat balance equations. Errors in the hourly convection heat fluxes occur due to using mean values of convection coefficient in the thermal transmission matrices. Corrective surface flux profiles are calculated in the internal convection model and transformed into complex Fourier series. The corrective surface flux profiles are also used to correct the convection error to the air node. The complex Fourier series for each surface and the space air node are then inputted to the core frequency domain model to cancel the error. This corrective iteration process continues in parallel with the convection coefficient and radiant exchange iterative processes until satisfactorily converged temperatures have been established. To minimise the number of Fourier series being regenerated per iteration, the corrected convection flux profiles for the space surfaces are combined with the corresponding net long-wave radiant flux profiles. Similarly, the

corrected convection flux profile is combined with the plant's cooling load profile, in order to input into the space air node's heat balance equation.

6.6.4.1 Generating the convection coefficients

Clarke [78] has summarised a wide range of internal convection models, covering free and forced convection, and including combinations of the two convection modes. A number of convection models can be included in the internal convection model, due to the innate flexibility of the computer spreadsheet program. Software switches can be employed to thermally link each convection model to the frequency domain model. The following correlations, by Alamdari and Hammond [4], are used in the internal convection model, to compute the internal surface convection coefficients.

Vertical surface:
$$h_c = \left\{ \left[1.5 \left(\frac{|(t_{ai} - t_s)|}{H} \right)^{1/4} \right]^6 + \left[1.23 \left(|(t_{ai} - t_s)| \right)^{1/3} \right]^6 \right\}^{1/6} \tag{6.139}$$

Horizontal surface, upward heat flow:
$$h_c = \left\{ \left[1.4 \left(\frac{|(t_{ai} - t_s)|}{4A/P} \right)^{1/4} \right]^6 + \left[1.63 \left(|(t_{ai} - t_s)| \right)^{1/3} \right]^6 \right\}^{1/6} \tag{6.140}$$

Horizontal surface, downward heat flow:
$$h_c = 0.6 \left(\frac{|(t_{ai} - t_s)|}{(4A/P)^2} \right)^{1/5} \tag{6.141}$$

where H, A and P are the space height, floor area and perimeter respectively.

The set of correlation expressions is used to model free convection in rooms. Clark [78] presents a set of mixed buoyancy models, combining Alamdari and Hammond's correlations with mechanically driven, forced convection expressions for modelling mechanically ventilated spaces. Logic statements are used, in the internal environmental model, to switch to the appropriate correlation for downward or upward heat flow, in the case of horizontal surfaces. This is an important feature regarding the accuracy of the model, the upward convective heat transfer coefficient can on average be approximately four times that of the downward convective heat transfer coefficient. The number of exponents in Alamdari and Hammond's correlations results in much computational effort. The maximum difference between the surface temperatures and the space air temperature

usually occurs when the space is being air-conditioned. Typical temperature differences are 5°K and 20°K between the air and structural surfaces, and the air and window blind respectively. Over a temperature difference range of 1°K to 20°K, Alamdari and Hammond's correlations can be simplified to the form:

$$h_c = m(|\Delta t|)^n \tag{6.142}$$

The coefficients and exponents are summarised in table 6.22. The coefficients and exponents remain as constants throughout the simulation run, for a particular room size. It was found that for upward heat flow, the convective heat transfer coefficient was relatively insensitive to changes in room dimensions above a floor area of 9 m^2. The reason for this insensitivity is due to the second component of equation (6.140), i.e. $1.63(|(t_{ai} - t_s)|)^{1/3}$, having a dominating influence on the magnitude of the result. Equation (6.140) displays a sensitivity to changes in room size below a floor area of 9 m^2, which is below normal room sizes. As a result, the ratio A/P, which appears in equation (6.140), was excluded from the reduced correlation, as indicated by its coefficient and exponent given in table 6.22.

Table 6.22 Coefficients and exponents of equation (6.142)

Direction of heat flow	***m***	***n***	**Alandari and Hammond correlation**
Horizontal	$0.00588H^2$-0.0737H+1.50107	-0.00069H^2-0.01037H+0.28762	Equation (6.139)
Upward	1.64	0.331	Equation (6.140)
Downward	0.3446 $(A/P)^{-0.4}$	0.2	Equation (6.141)

The simpler correlations give maximum and average differences of 0.6 % and 0.25 % respectively, when compared to the exact convection models. Table 6.23 compares the

Table 6.23 Comparing space cooling load between using exact and approximate Alamdari and Hammond correlations (W)

Time	8	9	10	11	12	13	14	15	16	17	18
Exact	-510	-593	-1272	-1189	-1340	-1315	-1599	-1733	-1971	-1324	-987
Approximate	-512	-594	-1272	-1190	-1341	-1316	-1600	-1733	-1971	-1324	-992
% Error	0.53	0.19	0.01	0.04	0.11	0.05	0.09	0.00	0.01	0.04	0.46

cooling loads resulting due to using the exact and approximate correlations. The difference in results between the two correlations is insignificant.

6.6.4.2 Minimising the error due to using constant surface resistances

Equation (6.143a) and (6.143b), shown below, represents the thermal transmission matrices for an external wall. The matrix elements w'_{XX} of equation (6.143b) indicates that the combined thermal transmission matrix of the wall excludes the internal surface thermal resistance, which is modelled by equation (6.143a). The convective error due to using a constant surface thermal resistance must be minimised, to simulate realistic convection, employing variable convective heat transfer coefficients. This is achieved by adding a corrected convective flux q_i to the surface's and air node heat balance equations.

$$\begin{bmatrix} \tilde{t}_{ai} \\ \tilde{q}_{ai} \end{bmatrix} = \begin{bmatrix} 1 & R_{ci} \\ 0 & 1 \end{bmatrix} \cdot \begin{bmatrix} \tilde{t}_{s} \\ \tilde{q}_{s} \end{bmatrix} \qquad (6.143a)$$

$$\begin{bmatrix} \tilde{t}_{s} \\ \tilde{q}_{s} \end{bmatrix} = \begin{bmatrix} w'_{11} & w'_{12} \\ w'_{21} & w'_{22} \end{bmatrix} \cdot \begin{bmatrix} \tilde{t}_{eo} \\ \tilde{q}_{eo} \end{bmatrix} \qquad (6.143b)$$

Figure 6.15 illustrates the correction process. Surface air node temperatures are obtained from the heat balance equations of the frequency domain model. The surfaces to air temperature differences are calculated within the internal convection model. A stability process is required to ensure convergence of the iterative process (Usually S is set to 0.9). The temperature differences then become inputs to the appropriate convection expressions to generate the convective heat transfer coefficients. The mean values of the surface thermal resistances are computed from the convective coefficient profiles and inputted to the appropriate thermal transmission matrices and the mean component heat balance equations. In parallel with this process, the convection coefficients are used with the corresponding surface to air temperature differences to calculate the errors in convective flux for each surface. The negative sum of the convective flux errors is also computed for input to the air node heat balance equation. The convection error profiles for each surface and air node are then transformed into Fourier series for
input to the surfaces' and space air heat balance equations of the frequency domain model. With the revised surface and air node temperatures, the next iterative cycle is initiated. The iteration process continues until steady state conditions have been established. The software

switch shown in figure 6.15 enables the model to employ constant or variable convective heat transfer coefficients.

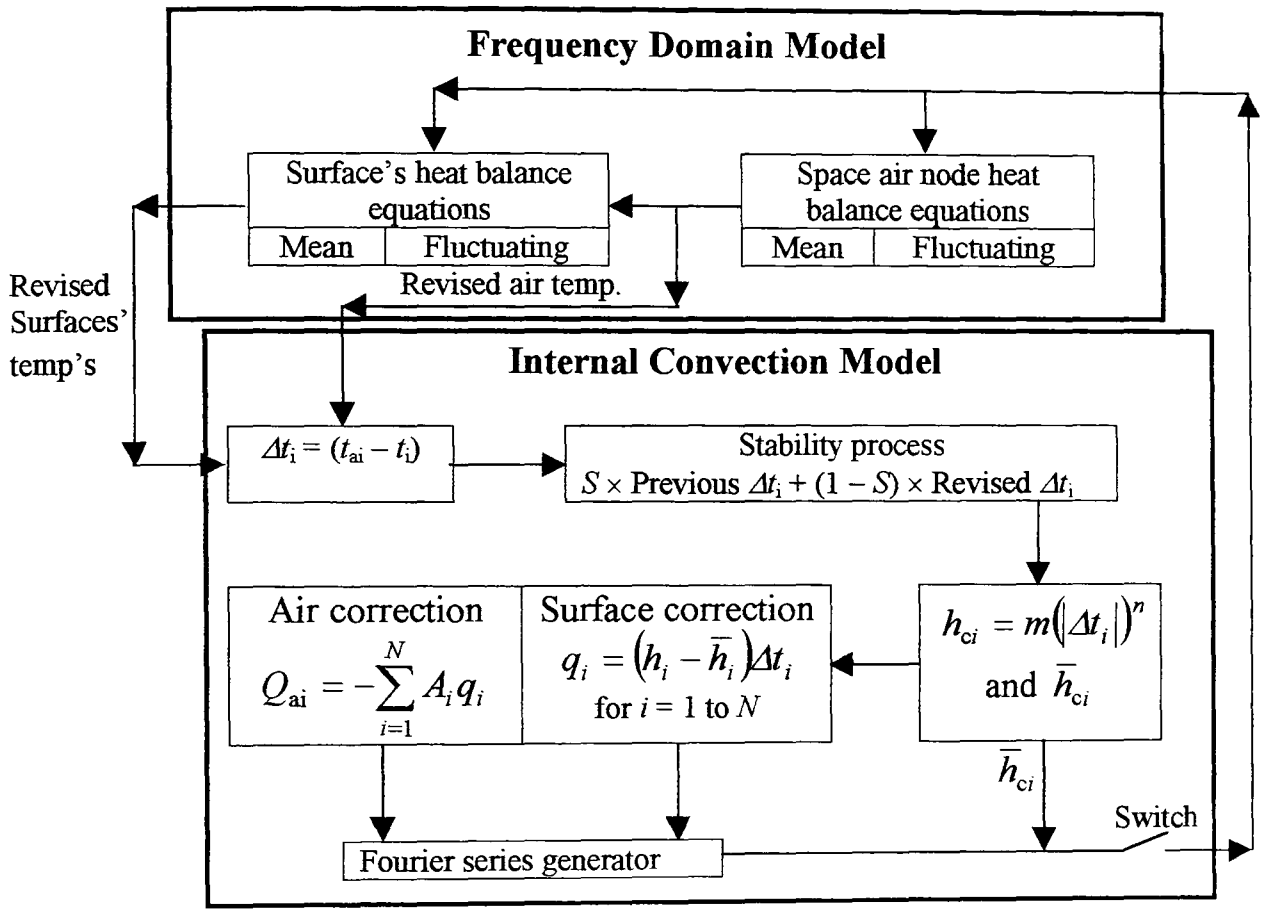

Figure 6.15. The internal convection model

6.6.5 The Adiabatic Iterative Frequency Domain Method (AIFDM)

The Iterative Frequency Domain Method includes the options of employing constant or variable convective heat transfer coefficients. If only variable convection coefficients are to be employed, then a more appropriate and computationally efficient approach is to exclude the convection coefficients from the thermal transmission matrices. As a result, a linear conduction model results, which can be accurately modelled in the frequency domain. The convective and radiant excitations, acting at the surfaces of the matrix, can be combined into a single Fourier series, which is a further advantage. The convection and long-wave radiation models, described in previous sections, are still employed. No correction to the surface convection processes are required, another beneficial result. The surface temperatures due to the incident surface fluxes are computed and become inputs to the

convection and long-wave radiation models to revise the heat fluxes. The iteration process continues until satisfactory converged conditions have been established. Adiabatic compared to isothermal boundary conditions must be used for the thermal transmission matrices. This is a significant difference by comparison with the traditional manner of setting-up the thermal transmission matrix based on convective boundary conditions. Only thermal excitations, in the form of heat fluxes, can be applied at adiabatic boundaries. A surface temperature change is the response to the incident heat flux. Revised surface heat fluxes due to the change in surface temperatures are generated in the convection and radiant exchange models. The space air node heat balance equation does not have to be modelled in the frequency domain, due to thermal transmission matrices having no convective boundaries directly linking them to the space air volume. It is computationally more efficient to use an implicit finite difference model of the space air-node for computer spreadsheet application. An hour time-step, as used in the frequency domain model, can be employed in the implicit finite difference, heat balance equation without numerical instability occurring. The window is modelled by an implicit finite difference formulation, for reasons of computational efficiency. Each layer of a window system requires only one temperature node to model it with sufficient accuracy. Only the mass of the window is accounted for in the heat balance equations, due to the insignificant thermal resistance of the glazing panes. External surfaces of structural elements can be treated as adiabatic surfaces, with the incident heat fluxes being computed in the external environmental model. However, it is more convenient to use sol-air excitation that includes all external thermal excitations. In this case, external isothermal boundary conditions are required for the external surface of the thermal transmission matrix. The Adiabatic Iterative Frequency Domain Method combines the salient features of the two thermal simulation techniques; accurate modelling of structural elements in the frequency domain, which does not require dimensional discretisation, computationally efficient finite difference modelling of the space air node and window layers using single temperature node representation.

The calculation of the mean component surface temperatures for the structural surfaces is identical to that of the Iterative Frequency Domain Method. There is no requirement to calculate the mean temperatures of the space air node and window system separately, these being modelled by finite difference simulation techniques.

6.6.5.1 The adiabatic surface heat balance equations

The adiabatic thermal transmission matrix for an internal structure, including thermal excitations and responses, is defined by:

$$\begin{bmatrix} \widetilde{t}_a \\ \widetilde{q}_a \end{bmatrix} = \begin{bmatrix} p''_{11} & p''_{12} \\ p''_{21} & p''_{22} \end{bmatrix} \cdot \begin{bmatrix} \widetilde{t}_b \\ \widetilde{q}_b = 0 \end{bmatrix} \tag{6.144}$$

The double dashed matrix elements symbolise the exclusion of both surface convective coefficients. An adiabatic boundary is defined by the heat flux equalling zero. It can be shown that the surface temperatures, due to the "a-side" heat flux excitation on the LHS of the matrix, are given by:

$$\widetilde{t}_a = (p''_{11}/p''_{21})\widetilde{q}_a \qquad \text{and} \qquad \widetilde{t}_b = \widetilde{q}_a/p''_{21}$$

In the case of thermal excitation flux on the opposite surface, the matrix must be rearranged as follows:

$$\begin{bmatrix} \widetilde{t}_b \\ \widetilde{q}_b \end{bmatrix} = \begin{bmatrix} (p''_{22})_{11} & p''_{12} \\ p''_{21} & (p''_{11})_{22} \end{bmatrix} \cdot \begin{bmatrix} \widetilde{t}_a \\ \widetilde{q}_a = 0 \end{bmatrix} \tag{6.145}$$

Interchanging the two leading diagonal matrix elements obtains the correct thermal matrix, without having to re-calculate the overall matrix. The values of the other two elements remain unchanged. Note that for a symmetrical structure, the matrix elements are identical for both thermal excitation orientations. The surface temperatures due to the "b-side" heat flux excitation is given by:

$$\widetilde{t}_b = [(p''_{22})_{11}/p''_{21}]\widetilde{q}_b \qquad \text{and} \qquad \widetilde{t}_a = \widetilde{q}_b/p''_{21}$$

The total surface temperatures are then:

$$(\widetilde{t}_a)_{total} = (p''_{11}/p''_{21})\widetilde{q}_a + \widetilde{q}_b/p''_{21} \tag{6.146}$$

$$(\widetilde{t}_b)_{total} = [(p''_{22})_{11}/p''_{21}]\widetilde{q}_b + \widetilde{q}_a/p''_{21} \tag{6.147}$$

The heat fluxes represent the total fluxes due to all the radiation sources and surface convection. Equations (6.146) and (6.147) can be employed to calculate the surface temperatures of internal structures such as partition and ceilings/floors. In the case of structural surfaces with an external surface, only the internal surface temperature is required. If adiabatic surfaces are assumed on both sides of the external structure, equation (6.146) can be employed with the "b-heat flux" representing all the external thermal flux excitations. If sol-air temperature is used, then the matrix must have an external isothermal

boundary, to account for the convective surface, and an internal adiabatic boundary. The corresponding matrix formulations are represented by:

$$\begin{bmatrix} \tilde{t}_a \\ \tilde{q}_a \end{bmatrix} = \begin{bmatrix} w'_{11} & w'_{12} \\ w'_{21} & w'_{22} \end{bmatrix} \cdot \begin{bmatrix} \tilde{t}_{eo} = 0 \\ \tilde{q}_{eo} \end{bmatrix} \tag{6.148}$$

$$\begin{bmatrix} \tilde{t}_{eo} \\ \tilde{q}_{eo} \end{bmatrix} = \begin{bmatrix} (w'_{22})_{11} & w'_{12} \\ w'_{21} & (w'_{11})_{22} \end{bmatrix} \cdot \begin{bmatrix} \tilde{t}_a \\ \tilde{q}_a = 0 \end{bmatrix} \tag{6.149}$$

The single dashed matrix elements indicate that the matrix excludes only the internal convective boundary. The temperature equalling zero defines the external isothermal boundary, in the case of internal surface excitation of the structure. Equation (6.149) shows the matrix arrangement with an internal adiabatic boundary and the external sol-air excitation. From these matrix formulations the inside surface temperature is given by:

$$\tilde{t}_a = (w'_{12}/w'_{22})\tilde{q}_a + \tilde{t}_{eo}/(w'_{22})_{11} \tag{6.150}$$

Equation (6.150) can also be used to calculate the internal surface temperature of a roof.

6.6.5.2 Stabilising the temperature fluctuations of lightweight structures

When modelling iterative calculation processes on a spreadsheet, a stability sub-routine is usually required to ensure convergence of the numerical process. With the Adiabatic Iterative Frequency Domain Method, a further problem of instability arises when modelling thermally lightweight structures such as stud partitions with material thickness in the order of 12mm. At the beginning of an iteration process, the initial calculated incident heat fluxes are much greater than the final converged values. The subsequent thermal response of the lightweight structures is very large compared to the response of heavyweight structures. This large temperature response eventually causes divergence of the numerical process. To ensure convergence, a stability sub-routine is incorporated into the model. Figure 6.15 illustrates the calculation process including the stability module. In this case a stud partition, represented by its thermal transmission matrix, is the lightweight structure causing instability of the numerical process. Some of the heavyweight structural elements such as ceiling and floor are also shown. The air node is represented by its finite difference heat balance formulation, where q_{ai} defines all the heat gains to the air node. External structural surfaces and the window system are not shown, for the purpose of clarity. The sub-model represents the convective and long-wave radiation exchange models, which also incorporate the process of summing all the surface heat flux excitations, including

excitations to the space air node. Figure 6.16 shows that computed surface temperatures become inputs to the sub-models and the air node, for processing the

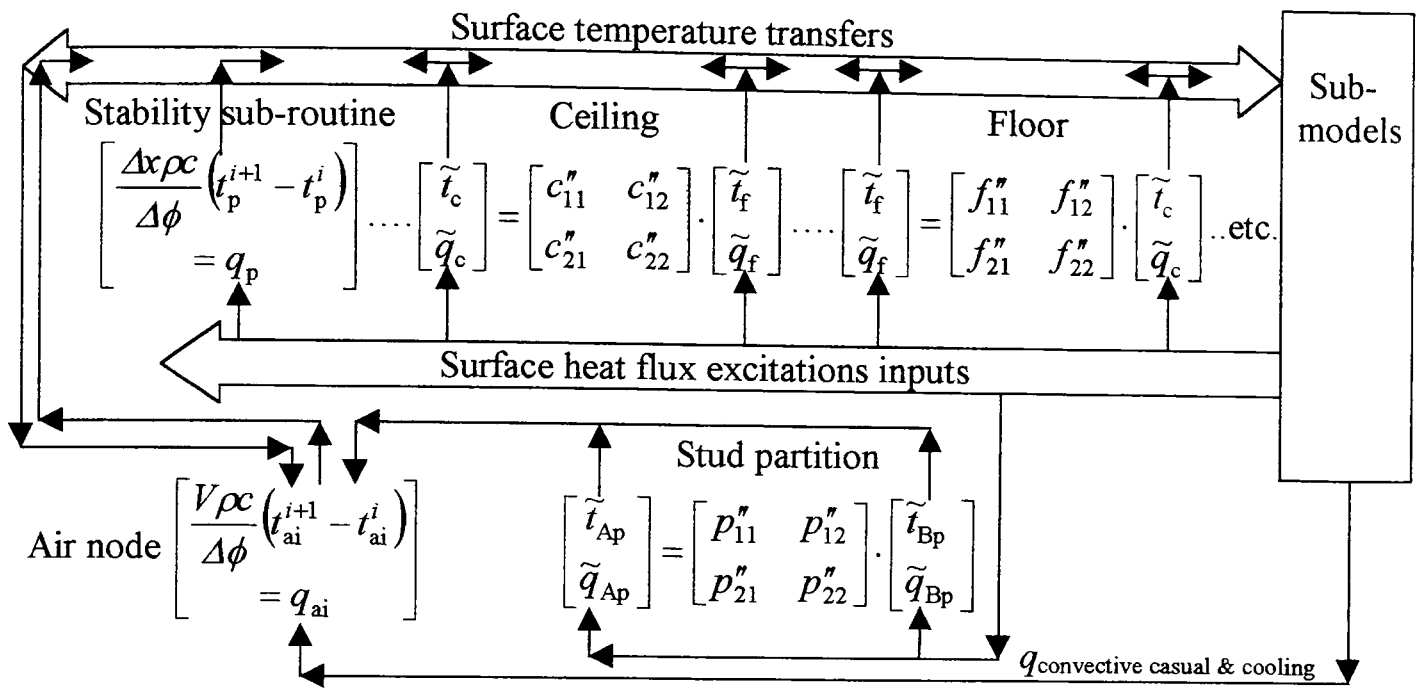

Figure 6.16. Adiabatic Iterative Frequency Domain Method incorporating stability module for lightweight partitions

appropriate responses. At the next iteration step, total surface fluxes from the sub-models become inputs to the surface heat balance equations. The stability module is an implicit finite difference model of the stud partition. A single temperature node is sufficient to represent each thin surface leaf of the partition, minimising discretisation. The thermal resistance of each leaf is negligible. The implicit finite difference formulation is numerically stable, when thermally linked and participating with the other surfaces and space air node. It approximates closely the temperature response of the partition when checked against the Iterative Frequency Domain Method. The stability module helps to simulate the partitions surface heat flux excitations, which are then used as inputs to the thermal matrix formulation of the partition's surface heat balance equation. The partition's thermal matrix heat balance equation does not participate with the other surfaces. It only receives surface flux excitation from the sub-models, but its surface temperature response becomes an input to the space air node heat balance equation. The space air node, temperature response is inputted to the stability module' surface heat balance equation. The stability module's temperature response is inputted to the sub-models and not to the space air node, as indicated by the one directional arrow, above the module. It is possible to

represent the stud partition by the implicit finite difference formulation only. However, the formulation does not include the thermal resistance of the partition whilst the thermal matrix formulation completely models the thermal behaviour of the partition. Inputting the surface temperature response of the thermal matrix version, rather than the implicit version, into the space air node improves overall accuracy. This factor was checked using the Iterative Frequency Domain Method.

In the case of solid partitions, the stability module is not required.

6.6.6. Air infiltration and natural ventilation model

A quarter to half an air change rate is a common assumption made for estimating a space's cooling load. For a more precise analysis, or the thermal design of a naturally ventilated building, a network ventilation model [79] is required. Section 2.1.5 describes such a model. The purpose of the model is to estimate the bulk transfer of air between spaces rather than analyse the characteristics of the airflow patterns within a space. Only flow path conductances and pressures are involved in the calculation process. The main difficulty involves maintaining stability of the numerical process to ensure convergence. The fundamental principle underpinning the network ventilation model is the conservation of mass. For a single space, i, the network ventilation model may be described by an expression of the form:

$$\sum_{j=1}^{N} Q_j = \sum_{j=1}^{N} \left[C_j \left(p_j + \Delta p_{ij} - p_i \right)^{n_j} \right] = 0 \qquad (6.151)$$

The total flow path conductance C_j is determined from the flow coefficients of all the air leakage paths, j, to the neighbouring spaces at pressure p_j. In the case of leakage paths to the external environment, p_j is the external wind pressure. Δp_{ij} is the difference in stack pressure due to difference in air densities between the space and a neighbouring space or external environment. Usually, matrices are used to solve the set of simultaneous equations, generated from equation (6.151). In the thesis, a purely iterative solution process was developed to solve the equations. Figure 6.17 illustrates the iteration process in the case of a single zone with all its facades exposed to the external environment. Initially, the internal pressure p_i is set to a value similar in magnitude to the external pressure. The flow rates and directions of the façade are determined, positive values indicating inward flow. The flow rates are summed to determine the residual flow error, ΔQ_e; a solution is established when a

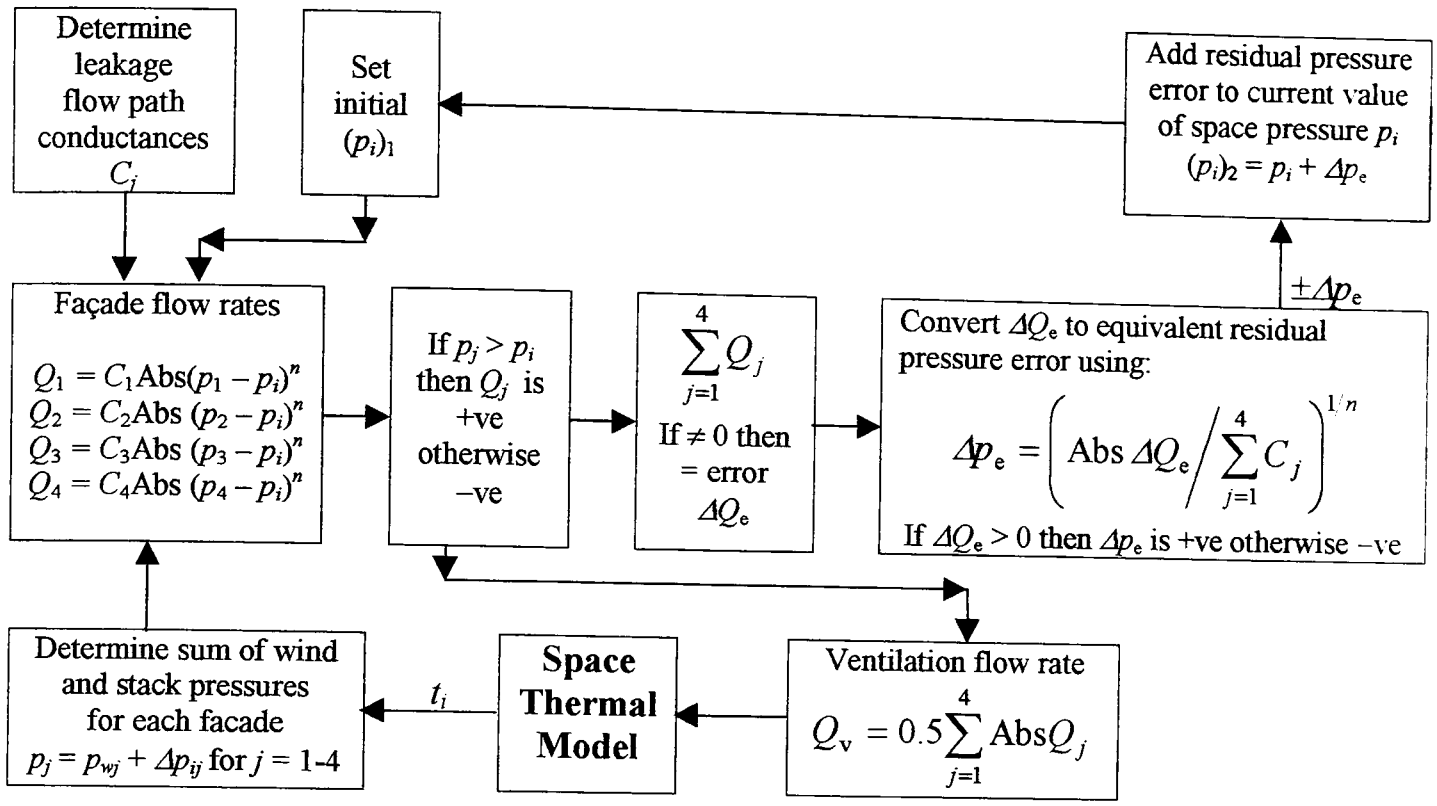

Figure 6.17 Ventilation network iteration process

sum of zero is registered. The initial pressure must be increased or decreased by a residual pressure error, Δp_e, which is proportional to the residual flow error, ΔQ_e, in order to achieve an air flow balance. The residual pressure error, Δp_e is approximated from a recasting of the flow balance equation (6.151) as follows.

$$\Delta p_e = \left(\text{Abs}\, \Delta Q_e \Big/ \sum_{j=1}^{4} C_j \right)^{1/n} \tag{6.152}$$

A positive value of ΔQ_e, indicates a positive value of Δp_e. The residual pressure error is then added to the current value of internal pressure to generate the revised value, given by $(p_i)_2$. The iteration process continues until the residual flow error is insignificant. Figure 6.17 show that at each iteration step, the ventilation flow rate is inputted to the space thermal model and the subsequent revised space temperature is inputted, from the space thermal model, to the ventilation model in order to revise the stack pressure. The ventilation flow rate is equal to half the sum of the absolute flow rates, as a result of the sum of the inward flow rates equalling the sum of the outward flow rates.

Multi-zone ventilation networks are produced by inter-linking the appropriate pressure nodes of its single zone ventilation networks. The individual zone flow balance equations are connected via the appropriate neighbouring internal pressures. Effectively, the iteration processes of the individual zone runs in tandem with the multi-zone process and steady state conditions are reached when the sum of the flow rates in each zone equals zero or is insignificant in magnitude. The sum of the flow rates through the external surfaces of the multi-zone network, or building facades, must also reduce to zero. If analysis of ventilation due to wind pressure only is required, then it is not necessary to link the ventilation network to the building thermal model. In this case, the iteration process is very rapid, establishing convergence of the numerical process in a relatively short period.

6.6.7. The assessment of internal convective and radiant heat gains

The internal heat gains may contribute a significant fraction of a space's total heat gain, in modern buildings with thermally well insulated envelopes, smaller glazing façade ratios and solar control devices. It is important to minimise the internal heat gains in naturally ventilated buildings and to achieve this requirement, a precise estimate of the internal gains is essential. A building thermal analysis method should include a procedure formulated to encourage a detailed investigation into the sources of the heat gains and help to provide a precise estimate of the associated heat gains. Assessment of the internal heat gains is difficult due to the wide range of equipment types, associated electrical power consumption and usage patterns, and the probabilistic nature of building occupancy. A statistical approach is usually followed. The CIBSE guide [14] and ASHRAE Fundamentals handbook [80] provides data and guidance towards estimating the internal heat gains. Convective and radiant fractions, in terms of the type heat sources, are also provided. Section 2.1.6 gives further details concerning the contents of the guides. Utilising this information, calculation templates may be produced in a computer spreadsheet program in order to generate internal convective and radiant gain profiles, specific to a building's function. Linear and polynomial regression may be employed to derive correlation expressions from suitable tabulated data and graphs, presented in the guides or other texts, in order to automate the calculation processes. It is possible to use more precise methods to estimate particular heat gains, e.g., electric lighting. The Lumen Method Equation should be used to determine the total number of installed lamps N, if the luminaire model is known.

$$N = \frac{E \times A}{F \times UF \times MF} \tag{6.153}$$

where E, A, F, UF and MF are the illuminance, floor area, lamp flux, utilisation factor and maintenance factor respectively. The total power demand is then given by:

$$Total\ Power\ Demand = D \times (1 + \%\ power\ of\ control\ gear/100) \times N \times Lamp\ wattage \tag{6.154}$$

The downward distribution of the lighting heat gain, D, may be obtained from the manufacturer, or an estimate obtained from the CIBSE guide [81].

6.6.8. The distribution of solar and internal radiant gains

A sensitivity analysis of space cooling load [61] concluded that, different distribution patterns of short or long-wave radiation do not have a significant influence on the subsequent cooling load. However, the proposed method, being designed for computer spreadsheet application, allows the user the flexibility of selecting appropriate distribution patterns. A pragmatic approach was taken in preparing simulation runs for the thesis. It is assumed that good thermal design practice will result in the recommendation of internal shading devices or special glazing to significantly reduce the solar beam. As a result, the transmitted solar energy should be totally diffused and distributed over all internal surfaces in view of the window. The distribution of the solar radiation can be based on an area-weighted method, or more precisely, on radiation view factors. The internal gain due to electric lighting is assumed incident on the walls and floor and is distributed by an area-weighted method. The long-wave radiation due to electrical office equipment and occupants is assumed evenly distributed over all the room surfaces.

6.6.9. The thermal comfort model

The CIBSE recommends the dry-resultant temperature as the thermal index of comfort. The dry-resultant temperature is equal to half the sum of the space's mean radiant and air temperatures, in the case of indoor air velocities below 0.1 ms^{-1}. The mean radiant temperature is usually approximated as the mean room surface temperature. Recommended ranges of dry-resultant temperature are specified in the CIBSE guide, for different types of indoor environments, for summer and winter [82]. The analysis of thermal comfort is complex, involving many physical parameters and personal influences. A single parameter index of comfort, although very convenient, is insufficient to assess satisfactorily the level of thermal comfort within a given set of environmental conditions. The CIBSE guide gives

a comprehensive account of the main environmental and personal factors influencing the level of thermal comfort [83]. Fanger's thermal comfort model [84] takes account of many of these factors. Fanger derived a thermal comfort equation [85] that correlates the predicted mean vote (PMV) with the influential environmental and personal factors, i.e., clothing, metabolic rate, external work, air temperature, mean radiant temperature, relative air velocity, percentage saturation and surface temperature of clothing. The predicted mean vote is used to determine the predicted percentage dissatisfied (PPD) of the occupants. For example, a PMV of ±0.5 would give a PPD of 10%, i.e., the possibility of 10% of the occupants being dissatisfied with the environmental conditions. The CIBSE guide recommends a PMV of ±0.25, which may be widened to ±0.5 if acceptable. The PMV may also be compared with the following thermal sensation scale.

PMV:	−3	−2	−1	0	+1	+2	+3
Thermal sensation:	Cold	Cool	Slightly cool	Neutral	Slightly warm	Warm	Hot

Fanger's thermal comfort equations may be produced on the computer spreadsheet program, as a sub-model, and linked to the space's thermal model for the purpose of a detailed thermal comfort analysis. Such an analysis may reveal that a set of environmental conditions, deemed unsuitable by the dry-resultant temperature index, is found acceptable utilising Fanger's comfort criteria. This would be beneficial in the case of assessing thermal comfort in naturally ventilated buildings, which experience larger swings in environmental conditions compared to air-conditioned buildings.

It has been found [86] that the thermal penetration coefficient "b", given by $(\lambda\rho c)^{0.5}$, relates the influence of a room surface's thermophysical properties to thermal comfort. Reference to the penetration coefficient's relationship with thermal comfort has been expressed in a more recent publication, on the optimisation of building thermal design [87]. The higher the value of the thermophysical product of a material ($\lambda\rho c$ = thermal conductivity × density × specific heat), the lower the surface temperature and corresponding mean radiant temperature of the space. The space air temperature is also reduced due to the surface's thermal admittance, which is directly influenced by the thermophysical product of the surface material. It is not a well-known compound property, but it appears (sometimes obscured) in many solutions to heat transfer in solids, especially relating to problems in periodic heat transfer. The thermophysical product gives a measure of a material's ability to

transfer and store thermal energy. Davies [88] gives a similar definition of the thermophysical product and describes how it relates to the solutions in periodic heat transfer. Heavyweight concrete has one of the highest thermophysical products and is therefore an ideal material for absorbing and storing heat. Maximising the exposure of a space's concrete surfaces is a recommended approach in the thermal design of naturally ventilated buildings,. This design strategy is also beneficial, where mechanical ventilation with night-time sub-cooling, is a solution.

Chapter VI

6.7 Modelling Design Solutions for the Thermal Environment

6.7.1 The integrated design approach

The computer spreadsheet is a flexible and powerful computational tool. Passive or mechanical plant, thermal models may be simulated in the spreadsheet environment and connected to the space thermal model. The majority of the plant simulation processes involve numerical iterative techniques. The stability of the numerical process is the main concern, in order to achieve convergence in a reasonable a time. An alternative exact solution method, for determining the convective cooling load, will also be presented.

6.7.2 Passive thermal design solutions

Any of the thermophysical properties and dimensions of the building structural elements may be varied to obtain the optimum thermal design. The window model parameters can be varied to minimise the solar gains. The external environmental model includes solar irradiation and shadow sub-models that can be used to analyse the influence of shadows and building orientation. The ventilation network model can be employed to analyse natural ventilation strategies. A multi-zone ventilation network needs no connection to the thermal model, if only wind effect investigations are required. Disconnecting the ventilation network model from the thermal model allows a much larger network of spaces to be modelled, in order to determine air infiltration or ventilation rates.

6.7.3 Mechanical ventilation

Mechanical ventilation, with night-time cooling, may form a solution if passive measures are insufficient to maintain thermal comfort. Figure 6.18 illustrates the iteration process of the ventilation model. When the external temperature is greater than the internal temperature (i.e. $\Delta t > 0$), mechanical cooling is not feasible and a zero Δt is used to effectively cancel any subsequent heating of the space air volume. Constant or variable ventilation rates can be set for each hour; the highest rate during daytime hours being limited by considerations of comfort. The model can be used for daytime ventilation only, if night-time cooling is not required. Figure 6.18 illustrates the Iterative Frequency Domain

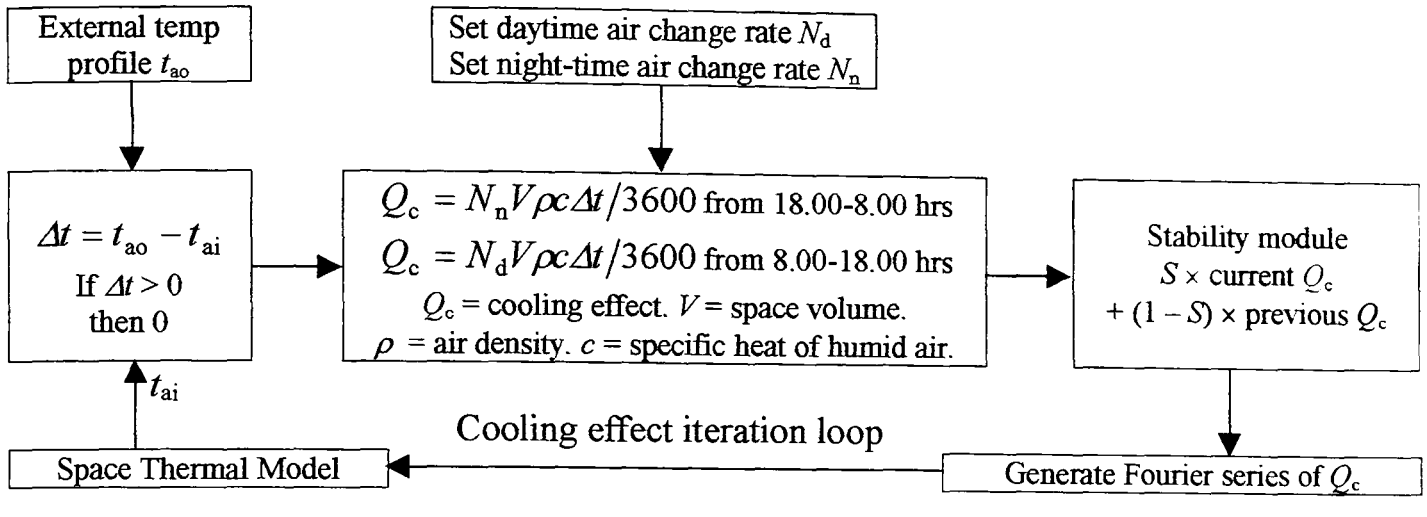

Figure 6.18 Calculation process of mechanical ventilation with night time cooling

(IFDM) version of the space thermal model. The iteration process is simpler for the Adiabatic Iterative Frequency Domain (AIFDM) option, the space air node being modelled by an implicit finite difference scheme. There are no problems of instability and generating a Fourier series of the ventilation cooling effect is not required. The hourly ventilation rates and external air temperatures become direct inputs to the space air implicit finite difference, heat balance equation. A ventilation iteration loop is not required.

6.7.4 Natural ventilation due to single side window

Window ventilation may be modelled purely as a stack effect, assuming negligible wind pressure during a hot summer's day. In this model the air change rate is a function of:

1. The window opening discharge coefficient, C_d
2. The top and bottom window opening areas, A_{top} and A_{bottom}
3. The height between the openings, h
4. The difference between the external and internal air temperatures

In the case of the IFDM version of the space thermal model, Figure 6.19 indicates that the calculation process is very similar to the mechanical ventilation process. The difference is the additional air flow iteration loop required for computing the air change rate via the stack effect formula. The calculation process is more complex due to both the air change rate and cooling effect being functions of the internal temperature and visa versa. Adjusting the window opening areas and the height between the window openings varies the

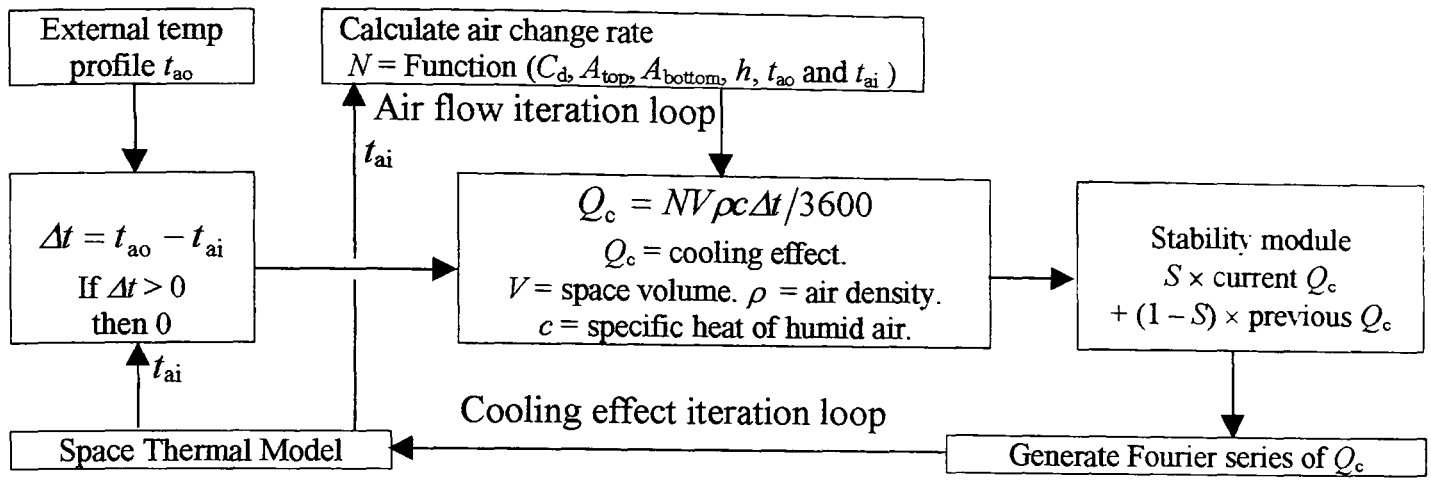

Figure 6.19 Calculation process of ventilation due to single side window opening

ventilation rate. The window dimensions may be varied for analysing the influence on ventilation due to window height and width. Night-time cooling can be simulated by using larger window opening areas during the unoccupied hours, if security is not an issue. The calculation process is simpler for the AIFDM version of the space thermal model. Only the iteration loop between the space thermal model and the window stack effect model is required to revise the air change rate N. The revised air change rate is then inputted to the space air's implicit finite difference heat balance equation.

Space cooling options may be mixed-mode, mechanical sub-cooling at night and natural ventilation during the day, for example. This option can be implemented on the spreadsheet by connecting the two ventilation models with the thermal model.

6.7.5 Convective cooling air-conditioning plant

Figure 6.20 illustrates the procedure for calculating the space cooling load. A suitable space air control temperature, t_{ps}, is set for the plant on time period. Initially the residual cooling load is overestimated and if not controlled, instability of the numerical process results eventually. A modulator, S, is used to control the iterative process and to establish convergence in the shortest possible time. Initially S is set to about 0.33 and automatically adjusted in proportion to the magnitude of the subsequent residual cooling loads. Close to convergence, when the residual cooling load is small, $S = 1.0$. As the numerical process

converges, the hourly residual cooling loads gradually oscillate from positive to negative. The final cooling load equals the sum of all the previous residual cooling loads. If heating is required, a positive result is registered. The space air set-point temperature may be scheduled at different values throughout the plant operating period, to reduce the peak cooling load. The set-point temperature can be adjusted in proportion to the cooling load, from 22°C at the minimum cooling load to 25°C at the peak, for example. Transformation of cooling load profile into a Fourier series is not required in the case of the AIFDM version of the thermal model, due to the air node being modelled by a finite difference scheme.

The calculated cooling load is a theoretical load, not characterised by any particular type of air-conditioning system. In the case of a constant volume system (CAV) the space design flow rate may be determined using a suitable air supply temperature. The design flow rate can then be used to establish the partial cooling load supply air temperatures. For a variable air volume system (VAV), the constant supply air temperature can be used to determine the design airflow rate of the VAV terminal unit. The partial cooling load airflow rates may be determined using the same constant supply temperature to check the turndown ratio and hence, the suitability of the VAV system. In the case of a fan-coil system, the required duty of the fan-coil unit is obtained by subtracting the cooling effect of the space fresh air supply (via the central air-handling unit) from the space cooling load.

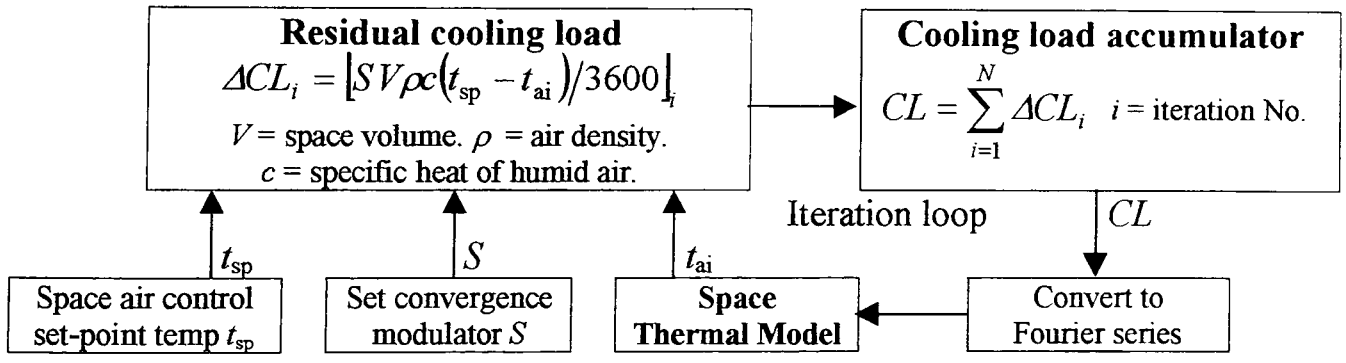

Figure 6.20 Calculation process of convective cooling air-conditioning plant

6.7.6 Chilled ceiling with displacement ventilation

A displacement ventilation system may be combined with a chilled ceiling. The displacement ventilation system usually delivers a constant volume of approximately two to three air changes per hour, two to three degrees below the room air, set-point temperature.

In this case a constant ventilation cooling effect is assumed. The chilled ceiling cools the space by long-wave radiant exchange with the room surfaces and by convection with the room air. If the chilled ceiling is used to control the space air to a particular set-point temperature, then its surface temperature must be modulated to obtain the required radiant and convective energy balances of the space. Generally, the following type of equation is employed to model convective exchange between a chilled ceiling surface and space air.

$$Q_c = A_{ch} K (t_{ai} - t_{ch})^n \tag{6.155}$$

A_{ch} is the chilled ceiling surface area exposed to the space air. K and n are the chilled ceiling characteristic coefficient and exponent respectively. If the chilled ceiling temperature is used to control the space condition, then the air temperature in equation (6.155) becomes the air set-point temperature t_{sp}. The space cooling load, CL, equals Q_c and the corresponding chilled ceiling temperature is given by the following rearrangement of equation (6.155).

$$t_{ch} = t_{sp} - [CL/(KA_{ch})]^{1/n} \tag{6.156}$$

Figure 6.21 demonstrates that the accumulated space cooling load is determined in an identical manner to that of figure 6.20. When the cooling effect of the displacement ventilation air is added to the accumulated cooling load, it is accounted for in the revised cooling load. The chilled ceiling temperature is inputted to the space thermal model subject,

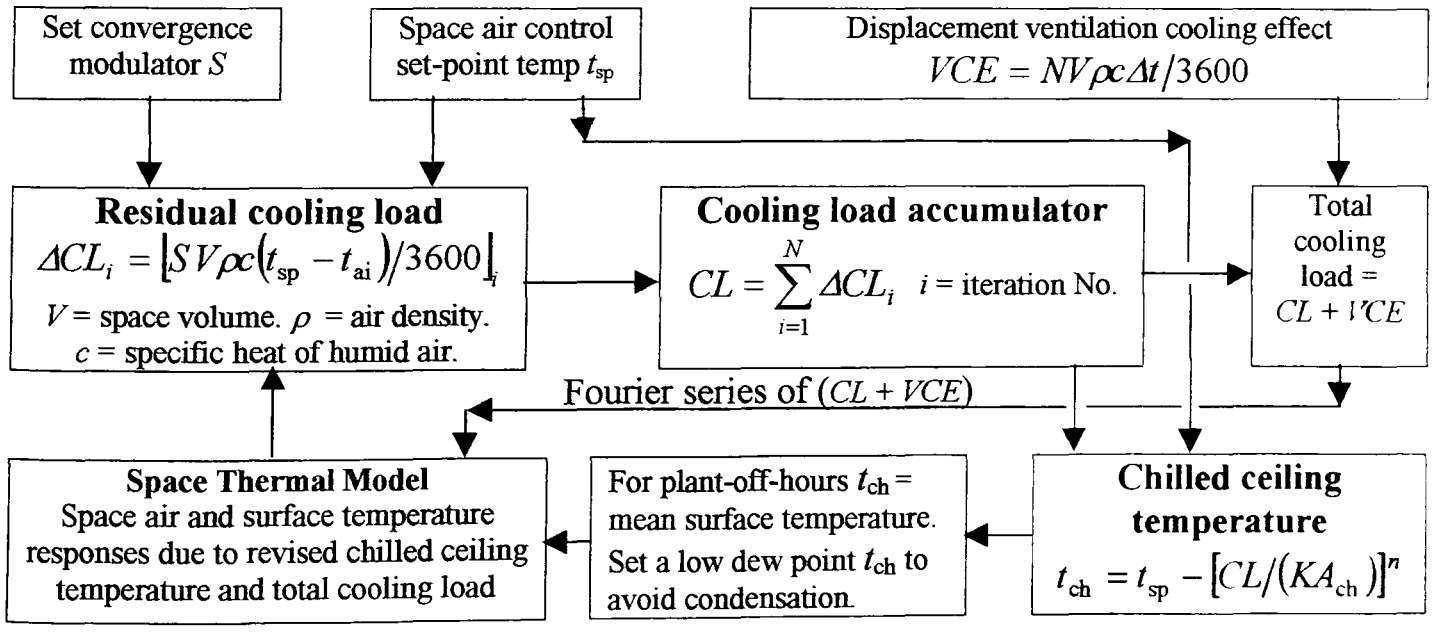

Figure 6.21 Calculation process of chilled ceiling with displacement ventilation

to a dew-point low limit temperature setting, in order to avoid surface condensation. In response to the revised total cooling load and chilled ceiling temperature, the space thermal model recalculates all energy exchanges for the next iteration cycle. Although a number of iteration loops are operating in tandem, the overall process is stable and convergence is eventually established. The chilled ceiling replaces the actual ceiling in the space thermal model, in order to participate thermally with the space surfaces and air volume. The radiant absorption duty of the chilled ceiling can then be obtained from the long-wave radiant exchange model. The accumulated cooling load, *CL* in figure 6.21, gives the convective duty of the chilled ceiling. The base cooling duty, provided by the displacement ventilation system, is given by *VCE* in figure 6.21. The chilled ceiling temperature is assumed to settle to the mean surface temperature of the structural surfaces, during the plant off period. This mean surface temperature excludes the chilled ceiling and window surfaces, as these are at significantly different temperatures. The mean surface temperature is also assumed as the temperature of the uncovered portion of the ceiling. The plant calculation processes are identical for the AIFDM version of the space thermal model, except that the transformation of the cooling load into a Fourier series is not required.

6.7.7 Convective cooling load by the response function method

In sections 6.6.5 and 6.6.6, the space cooling load is obtained by employing iterative techniques. A more elegant technique, which gives a direct solution to the cooling load, has been developed in the thesis. A space's air temperature response can be produced by inputting a convective heat flux excitation profile into its air node heat balance equation. If a unit watt convective pulse becomes an input, instead of the thermal excitation profile, a 24-hour discrete temperature response function is obtained. By invoking the principle of superposition, the response function can be utilised to determine a space's cooling load. Linearity and invariability are prerequisites of the principle of superposition. Considering invariability, identical air temperature response functions are obtained no matter what time the convective unit pulse is applied. Applying the concept of linearity, the response is linearly related to the excitation. Linearity also applies to the reverse of the relationship; i.e., the excitation is proportional to the response. Discrete hourly values of the response function (response factors) can be appropriately arranged to form the coefficient matrix representing a set of 24 response factor, cooling load equations, which can be solved to give the space's cooling load. In the case of a 24-hour periodic thermal model, a 24 by 24

array represents the full matrix of response factor coefficients. If the cooling plant operates from 8.00 to 18.00 hours, only the corresponding hourly coefficients and associated temperatures are required in the solution matrices. In this case the matrix formulation of the cooling load equations is represented by:

$$\begin{vmatrix} t_{8,8} & t_{8,9} & t_{8,10} & \cdots & t_{8,18} \\ t_{9,8} & t_{9,9} & t_{9,10} & \cdots & t_{9,18} \\ \vdots & \vdots & \vdots & & \vdots \\ t_{18,8} & t_{18,9} & t_{18,10} & \cdots & t_{18,18} \end{vmatrix} \cdot \begin{vmatrix} CL_8 \\ CL_9 \\ \vdots \\ CL_{18} \end{vmatrix} = \begin{vmatrix} t_{sp} - t_{ai8} \\ t_{sp} - t_{ai9} \\ \vdots \\ t_{sp} - t_{ai18} \end{vmatrix} \tag{6.157}$$

The space's set-point to air temperature differences are obtained by running the thermal model of the space, in a free-running building mode (no plant in operation), using the actual thermal excitations. The resulting air temperatures, corresponding to the plant operating hours, are then inputted into equation (6.157). Pre-multiplying the temperature difference column matrix by the matrix inverse of the coefficient matrix results in the cooling load solution matrix.

Once the method is arranged on a computer spreadsheet, it can be copied and used repeatedly. The response factor coefficient matrix can be revised automatically for any space thermal model by inputting the corresponding air temperature, thermal response function. The air temperature, thermal response function may be obtained without replacing the actual thermal excitations with a unit pulse excitation. Applying all the thermal excitations, obtain and record the air temperature response profile. Add one watt to the first hour of the convective gain profile. Run the model again and record the air temperature response profile. The space's thermal response function is the difference between the recorded space air temperature profiles.

In the case of a simple thermal model, in which constant convective coefficient are employed and long-wave radiant exchange is neglected (i.e. a linear thermal model), the cooling load profile is obtained directly by inputting the space's set-point to air temperature differences into the column matrix of equation (6.157). The space's air temperatures change to the set-point temperature, in response to inputting the cooling load profile. In a space thermal model incorporating variable convective coefficients and long-wave radiant exchange (i.e. a non-linear thermal model), the inputted cooling load profile upsets the

energy balances and revised space air and surface temperature energy balances must be established. The resulting space air temperatures are usually below the set-point temperature, resulting in a residual temperature difference error. Inputting the residual error profile into equation (6.157) results in a cooling load correction profile, which is added to the initial cooling load. The revised cooling load profile is very close to the exact solution. An almost exact solution is obtained in response to inputting the revised cooling load profile into the space thermal model. Table 6.24 and 6.25 give the results of the cooling load response function method for thermally lightweight and heavyweight spaces. The thermal model of the space included the influences of variable convection coefficients and long-wave radiant exchange. The 1^{st} Δt column gives the cooling load based on the initial set-point to air temperature difference. The next two columns give the revised cooling loads determined by adding the corrections due to the second and third set-point to air temperature difference residuals, 2^{nd} Δt and 3^{rd} Δt. The last two columns give the corresponding percentage errors after including the corrections to the initial cooling load. Using the first iterative cooling load should suffice, considering that the small error involved should not result in selecting a different plant size from the range of standardized manufactured sizes. The peak cooling loads are overestimate by 1.33 % and 0.4 % for the thermally lightweight and heavyweight spaces respectively.

Table 6.24 Cooling load response function method – results for thermally lightweight space

Time	Cooling loads (Watts)				% error 1^{st} iteration		% error 2^{nd} iteration
	1^{st} Δt	1^{st} Δt + 2^{nd} Δt	1^{st} Δt + 2^{nd} Δt + 3^{rd} Δt	Exact	1^{st} Δt	1^{st} Δt + 2^{nd} Δt	1^{st} Δt + 2^{nd} Δt + 3^{rd} Δt
8	1359	1428	1432	1432	5.09	0.30	0.03
9	1260	1281	1276	1275	1.20	0.45	0.09
10	**1814**	**1710**	**1691**	**1688**	**7.45**	**1.33**	**0.18**
11	1639	1529	1514	1512	8.35	1.10	0.12
12	1545	1439	1428	1427	8.26	0.87	0.10
13	1468	1381	1373	1372	6.94	0.62	0.07
14	1479	1410	1404	1403	5.39	0.51	0.08
15	1485	1411	1405	1403	5.78	0.55	0.08
16	1498	1437	1431	1431	4.69	0.42	0.06
17	805	855	860	860	6.38	0.56	0.03
18	543	584	585	585	7.06	0.15	0.02

Table 6.25 Cooling load response function method – results for thermally heavyweight space

Time	Cooling loads (Watts)				% error 1st iteration		% error 2nd iteration
	1st Δt	1st Δt + 2nd Δt	1st Δt + 2nd Δt + 3rd Δt	Exact	1st Δt	1st Δt + 2nd Δt	1st Δt + 2nd Δt + 3rd Δt
8	1037	1166	1180	1183	12.32	1.43	0.23
9	1135	1199	1207	1209	6.08	0.75	0.11
10	**1667**	**1633**	**1628**	**1627**	**2.48**	**0.40**	**0.08**
11	1591	1535	1525	1523	4.47	0.77	0.14
12	1545	1477	1466	1464	5.53	0.87	0.14
13	1511	1435	1423	1422	6.29	0.93	0.14
14	1521	1445	1433	1431	6.26	0.93	0.13
15	1527	1449	1437	1435	6.41	0.95	0.13
16	1531	1453	1441	1439	6.35	0.92	0.12
17	907	927	926	926	2.09	0.14	0.01
18	668	712	715	715	6.64	0.42	0.10

An advantage of the method is that once the space's thermal response function and its corresponding coefficient matrix, equation (6.157), have been generated, they remain as constant formulations in the thermal model of the space and can be used to determine the cooling load due to any air set-point temperature. At lower levels of modelling complexity, where much pre-calculated data is employed, thermal response function coefficient matrices may be pre-calculated in respect of a range of standard zone sizes and thermal weights. At higher levels of complexity the procedure may be set-up as a sub-model to automatically generate the thermal response function matrices of space thermal models.

Chapter VII

7.0 VALIDATION

7.1 Validation methods

In the ANSI/ASHRAE Standard 140-2001 [92], three levels of validation, empirical validation, analytical verification, comparative testing, are recommended in order to evaluate a building dynamic thermal model. This approach to validation was implemented in the thesis to test the Thermal Analysis Design Method (TADM), its sub-models and subroutines. The ANSI/ASHRAE Standard includes, within the analytical verification methods, the testing of the model against a generally accepted numerical method for isolated heat transfer mechanisms. This form of analytical verification was adopted throughout the development of the TADM method. The frequency domain and finite difference methods are mathematically significantly different simulation techniques, and as a result, are ideal checkers of each other's solution process. As each heat transfer process was thermally modelled in the frequency domain, a finite difference checker model was created, on the spreadsheet, to verify the solution process. An explicit finite difference technique was employed using standard 3-node representation of homogeneous structural elements and a temporal discretisation of 300-second time steps. In the case of testing the window thermal sub-model, 60-second time steps were used. The Iterative Frequency Domain and the Adiabatic Frequency Domain methods have been thoroughly tested against finite difference checker models. Each new development and addition to the frequency domain model had a finite difference checker model set-up in parallel. The Iterative Frequency Domain Method was developed prior to the inception of Adiabatic Iterative Frequency Domain Method. Although each method is based on the same mathematical simulation technique, their solution processes are quite different. As a result, both finite difference and Iterative Frequency Domain Methods were employed to validate the Adiabatic Iterative Frequency Domain Method. The more precise formulation of sol-air temperature and the new concepts of window solar temperature and window sol-air temperature were verified using finite difference checker models created in the spreadsheet. The results of these particular tests are provided in the following sections as examples of the analytical verification process carried out. Parallel to testing the solution processes involved in these particular examples, the corresponding new concepts are also verified. In the comparative testing, the overall performance of the TADM method is compared with

that of the ASHRAE Heat Balance Method and the CIBSE Admittance method. In this particular test, the space cooling load profiles of the methods are compared based on similar physical models being used in each model. In addition, the surface temperature profiles of the TADM and ASHRAE Heat Balance methods are compared; it is not possible to determine surface temperatures using the CIBSE Admittance method. In empirical validation tests, the thermal model simulates a test cell environment over a number of days employing actual weather data. The Thermal Design Analysis Method can be employed to simulate longer periods than a single design day, deeming it suitable for empirical validation. The empirical validation of the TADM method involved modelling a test cell using an experimental data-set from the University of Westminster direct gain test cell facility, which is located in central England, on the south-west side of Peterborough. [89]. The final section of the chapter summarises test results of correlation equations and reduced calculation methods that have been developed in the thesis.

7.2 Analytical verification

7.2.1 Sol-air temperature

The improved accuracy of the sol-air temperature concept, described by equation (6.8), is due to a more precise prediction of the external surface temperature and the inclusion of the heat transfer coefficient correction term, q_{co}. The external surface temperature is used to determine the net long-wave radiation on the surface and the heat transfer coefficient correction term cancels the error due to using a constant value of heat transfer coefficient in the thermal transmission matrix defining the thermal behaviour of the external wall. A single leaf wall, with an adiabatic internal surface, is modelled in the iterative frequency domain method and in the finite difference checker model. The external surface temperature profile is simulated by each method and compared. All the external thermal excitations were applied simultaneously but as separate thermal driving forces in the finite difference method. In the frequency domain, all the external excitations are combined into the sol-air temperature, described by equation (6.8) and then applied to the wall to simulate the external surface temperature profile. Figure 7.1 illustrates the results of testing equation (6.8), in the frequency domain, against the finite difference checker model. These results are also compared with results employing the CIBSE and ASHRAE formulations of sol-air temperature. In the CIBSE expression, the external surface temperature is assumed equal to the sol-air temperature and a constant surface heat transfer coefficient is employed. The

ASHRAE sol-air temperature is further simplified by neglecting the long-wave radiant exchange process (for vertical surfaces only). The external temperature of the wall was calculated using these simpler formulations of sol-air temperature. The results relating to equation (6.8), and the finite difference checker model almost coincide, whilst the surface temperature profiles corresponding to the CIBSE and ASHRAE formulations of sol-air temperature appear to correlate with the degree of simplification adopted.

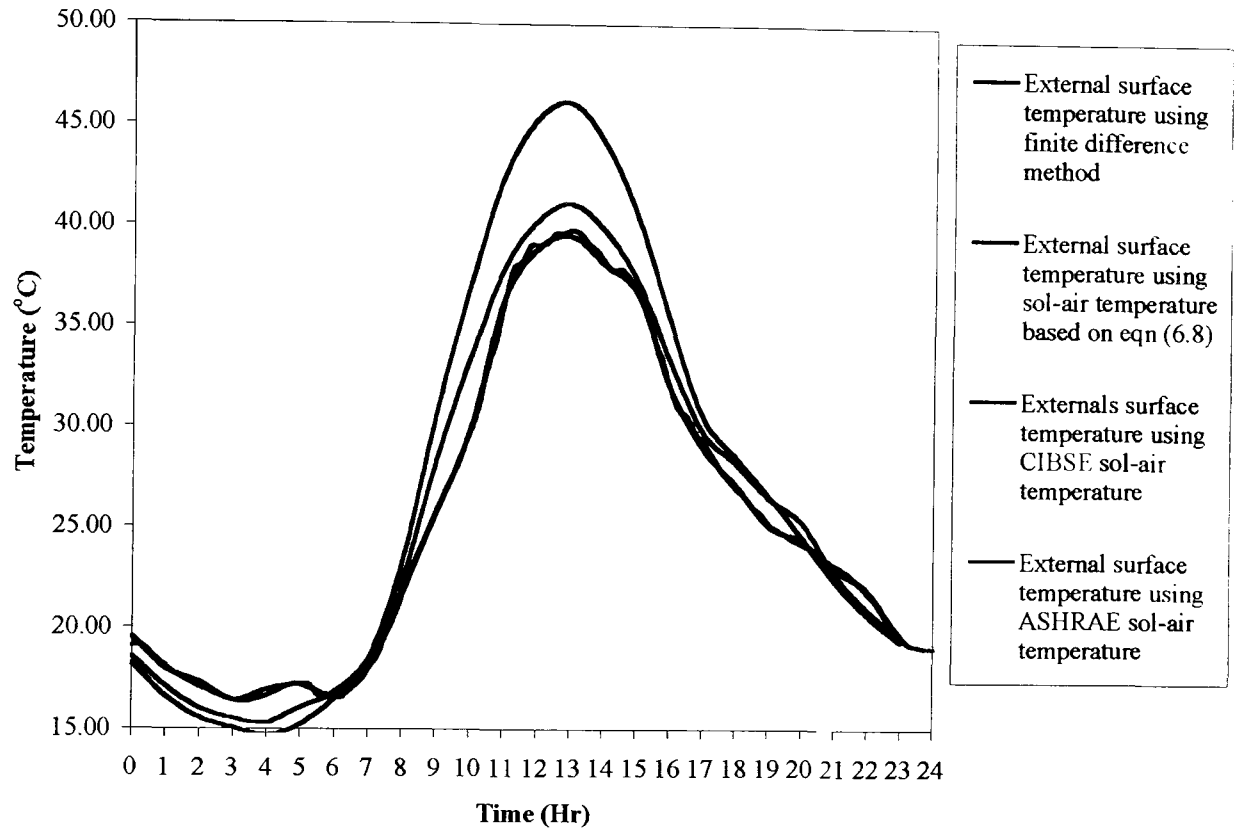

Figure 7.1 Comparing external surface temperature results between sol-air temperature models and finite difference checker model

7.2.2 Window solar temperature

The window solar temperature, described by equation (6.36), combines the influences of solar radiation absorption, in each layer of a window system, into a single thermal excitation, which acts at the external surface of the window. A double-glazed unit, with internal blinds linked to an internal air mass, was modelled in the frequency domain and in a finite difference checker model, in order to verify this new concept. Window solar temperature was used as the thermal excitation in the frequency domain model whilst the corresponding absorbed solar radiation was modelled as separate and simultaneous thermal excitations in the finite difference model. Internal surface and air node temperatures were

calculated in each model. Figure 7.2 illustrates the almost coincident results of each method. The corresponding window solar temperature is included. Clear glazing and an east window orientation were used for this particular test. Similar satisfactory results were obtained for other glazing types and window orientations.

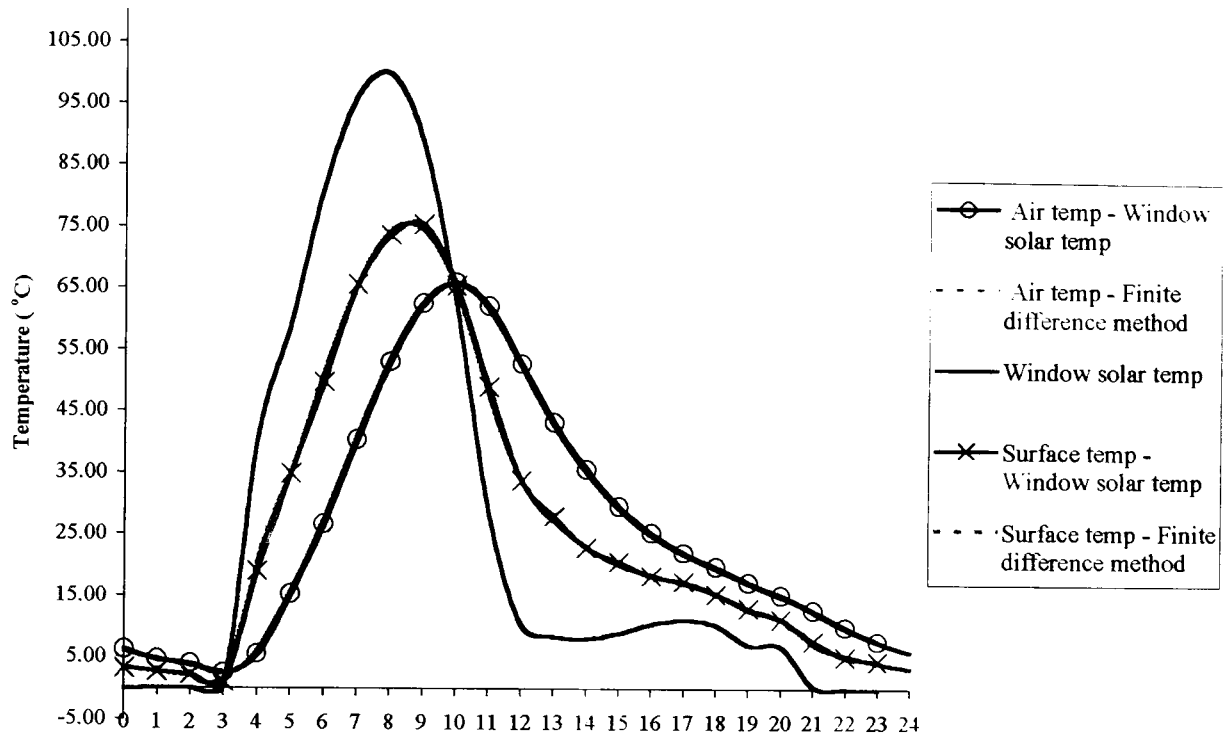

Figure 7.2 Comparing internal surface and air temperature results, using window solar temperature, with results using finite difference checker model

7.2.3 Window sol-air temperature

The new concept of window sol-air temperature, described by equation (6.45) extends the idea of window solar temperature by combining all the external and internal thermal excitations into a single thermal excitation. It also includes a correction term, described by equation (6.51), that cancels the total error incurred due to employing constant external and interlayer heat transfer coefficients in the thermal transmission matrices defining the thermal behaviour between the window layers. A similar test model, to that employed for testing the validity of window solar temperature, was used but expanded to include all the external thermal influences to simulate the window sol-air temperature in the frequency domain method. All the thermal excitations were applied as separate but simultaneous driving forces in the finite difference model. Figure 7.3 illustrates the results, indicating

agreement between the two methods. Similar satisfactory results were obtained for other glazing types and window orientations.

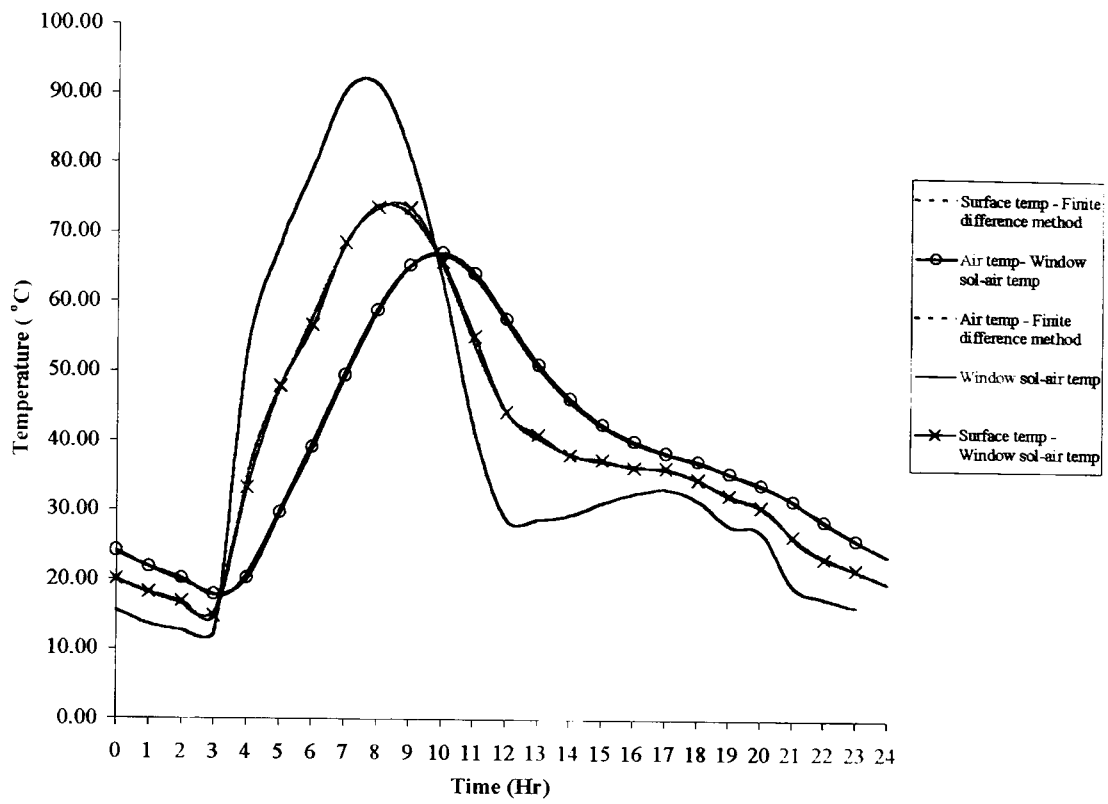

Figure 7.3 Comparing internal surface and air temperature results, using window sol-air temperature, with results using finite difference checker model

7.2.4 Window with internal loose fitting blinds test results

The modelling of this window system is described in section 6.5.5 and its thermal circuit is illustrated in figure 6.12. An airflow model is combined with a thermal model in order to simulate the thermal behaviour of the window system. Integrating iterative frequency domain and implicit finite difference techniques was found to be a computationally efficient means of implementing the model on a computer spreadsheet. The window sol-air temperature profile also accounts for the influence of the internal blind operating schedule but excludes the influence of absorbed solar radiation in the blinds. The convective gains to the internal air node, due to the absorbed solar radiation in the blinds, are simulated by an implicit finite difference formulation. All window surface temperature profiles are simulated by another implicit finite difference formulation. The window sol-air temperature heat transfer coefficient correction term must also account for the change in the window system thermal resistance due to the internal blind operation (see equation 6.87). An

explicit finite difference checker model, with time increments of 60 seconds, was set-up to check the precision of the window system model. To ensure maximum sensitivity

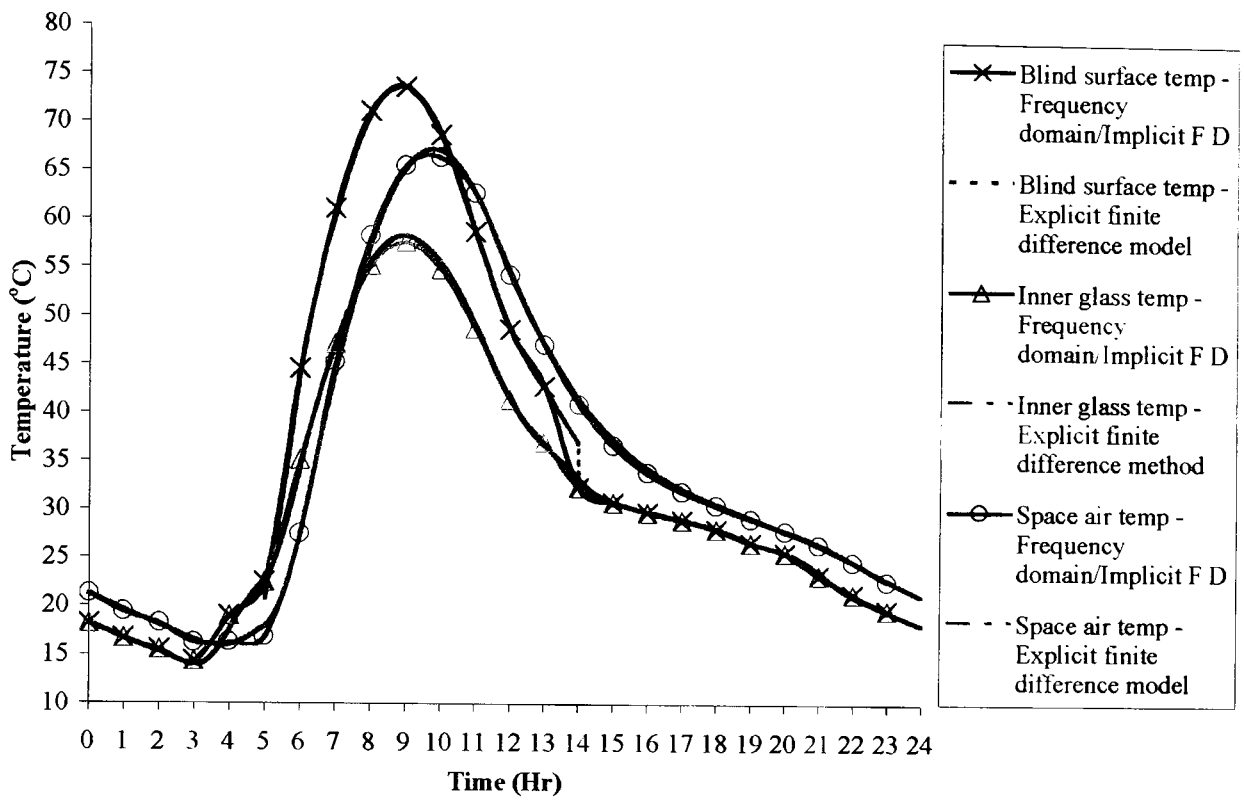

Figure 7.4 Comparing results between iterative frequency domain/implicit finite difference model and explicit finite difference checker model

in temperature responses, only an internal air mass was connected to the window system resulting in the transmitted solar energy being neglected. Figure 7.4 illustrates results in terms of blind surface, inner glass surface and air node temperatures. The window is east facing requiring the blinds to be closed between 05.00 and 14.00 hours. This feature may be observed in figure 7.4; when the blind and inner glass temperature profiles coincide, the blinds are open, otherwise, the blinds are closed. The two sets of corresponding results, from each simulation method, almost coincide. Some differences in blind surface temperature are indicated in figure 7.4 when the blind is opened at 14.00 hours. This is due to the difference in time discretisation of the two methods, one hour for the frequency domain/implicit finite difference method and 60 seconds for the explicit finite difference checker model. A logic statement of the form: when time is less than 14.00 hours, the blinds are closed, is used in both methods. This causes the change to take place over a one-

hour interval in the frequency domain/implicit finite difference method but only 60 seconds in the finite difference checker model (see vertical drop in blind surface temperature profile at 14.00 hours in figure 7.4).

7.3 Comparative testing

Intermodel comparisons cannot reveal the accuracy of the models involved unless one of the models has been fully validated as an accurate dynamic thermal model. No such model exists. However, some satisfaction may be derived if there is similarity in results between different models. Since the 1940's ASHRAE has employed an example of a single story, single zone building to compare the performance of its cooling load methods, including the latest Heat Balance Method [55]. A complete description, providing all details to thermally model the building, is provided in the 1993 SI edition of the ASHRAE Fundamental Handbook [90]. This example was used in the thesis to compare the performance of the Thermal Analysis Design Method (TADM) with the ASHRAE Heat Balance Method (HBM) and the CIBSE Admittance Method. Figure 7.5 illustrates a plan of the building and summarises the major structural details. Nine isothermal surfaces, including the north and south windows, must be modelled in order to simulate the surface convective and radiant heat exchanges taking place. Profiles of the external thermal excitations are provided in the

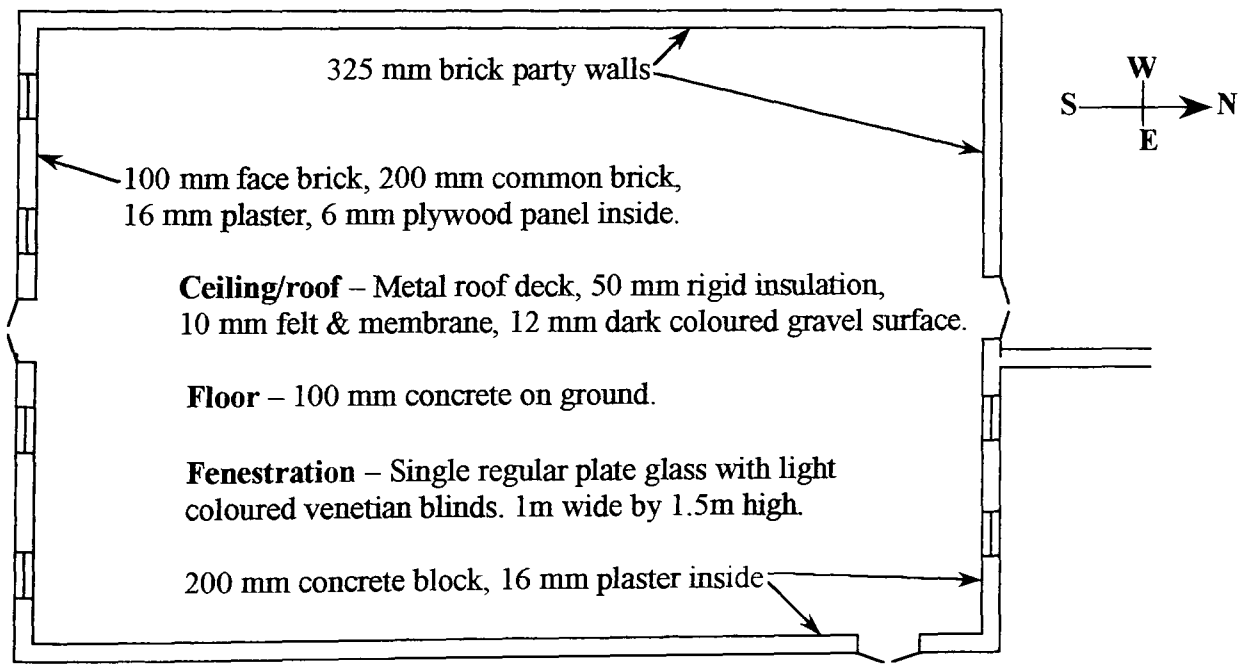

Figure 7.5 Plan of building, example 6, ASHRAE Fundamental Handbook, 1993.

ASHRAE example. Thus, the performance of the integrated conduction, convection and radiant exchange models, of each method, become the main focus of the comparison test. The space air temperature is to be maintained at 24°C for 24 hours per day. The ASHRAE Heat Balance Method's results, in the form of the sensible cooling load and surface temperatures are provided in the publication describing the development of the method [55]. Figure 7.6 illustrates the space cooling load results of the three methods. The results demonstrate a close similarity in cooling load profiles of the TADM and ASHRAE HBM methods, whilst the CIBSE cooling load profile exhibits a significant difference.

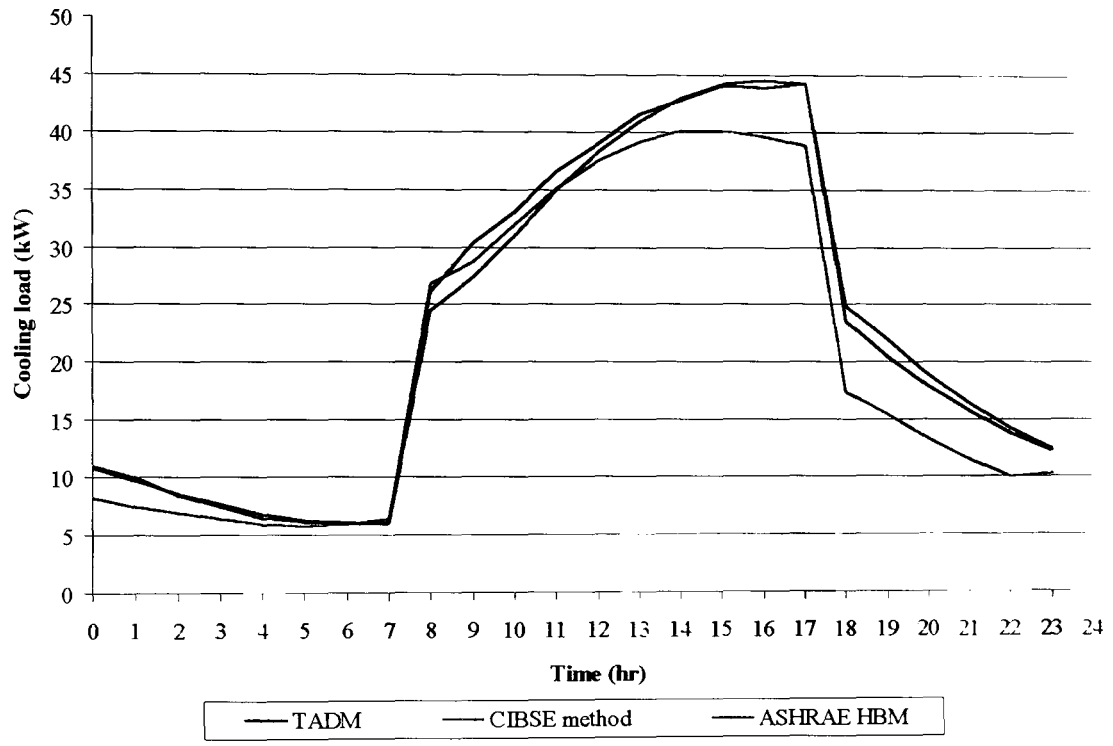

Figure 7.6 Comparison of space cooling load results

Table 7.1 gives the hourly cooling loads and the ratio of the results given by the ASHRAE and TADM methods.

The CIBSE Admittance method cannot be employed to calculate surface temperatures. Figures 7.7 to 7.10 compares the surface temperature results between the ASHRAE and TADM methods. Only the temperatures of four of the space's surfaces are compared, as these are the only surface temperature results provided in the paper describing the development of the Heat Balance Method. Table 7.2 gives a summary of the results,

Table 7.1 Comparison of cooling load results between ASHRAE HBM and TADM methods

Time (Hr)	HBM (kW)	TADM (kW)	TADM/HBM
0	11.0	10.9	0.99
1	10.0	9.8	0.98
2	8.5	8.7	1.02
3	7.5	7.7	1.03
4	6.5	6.9	1.06
5	6.2	6.3	1.02
6	6.0	6.1	1.02
7	6.0	6.2	1.03
8	24.5	26.3	1.07
9	27.5	30.4	1.11
10	31.0	33.1	1.07
11	35.0	36.6	1.05

Time (Hr)	HBM (kW)	TADM (kW)	TADM/HBM
12	38.3	39.1	1.02
13	41.0	41.6	1.01
14	43.0	42.8	1.00
15	44.2	44.1	1.00
16	**44.5**	**43.9**	**0.99**
17	44.2	44.3	1.00
18	25.0	23.7	0.95
19	22.0	20.4	0.93
20	19.0	18.0	0.95
21	16.5	15.8	0.96
22	14.3	13.9	0.97
23	12.5	12.3	0.98

Peak →

indicating that overall, the temperature differences between the two methods are small. As a result, the mean surface temperature profiles calculated by each method are similar and there would be little difference in the corresponding dry resultant temperature profiles, in fact, maximum and average absolute temperature differences of 0.34 K and 0.17 K respectively.

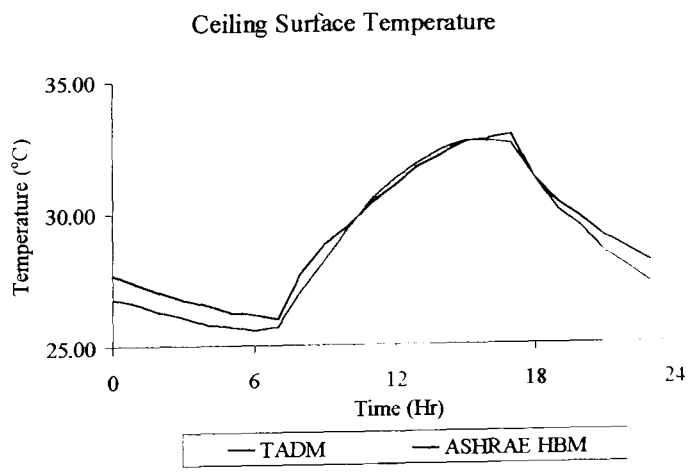

Figure 7.7 Comparison of ceiling surface temperature profiles between ASHRAE HBM and TADM methods

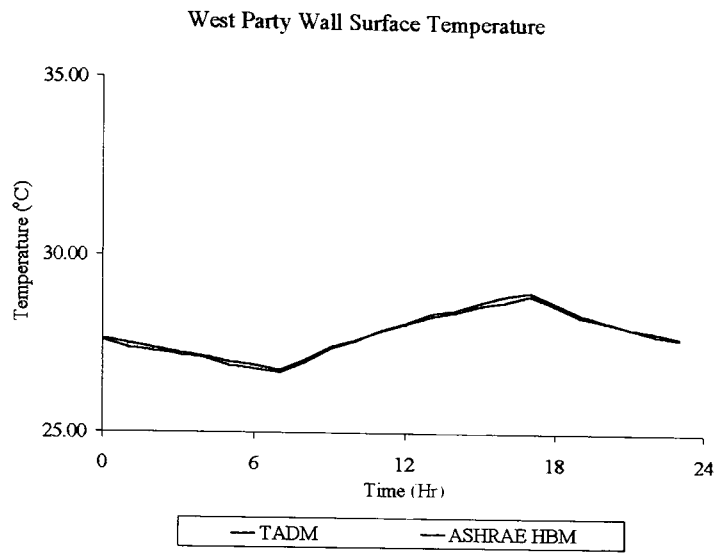

Figure 7.8 Comparison of west party wall surface temperature profiles between ASHRAE HBM and TADM methods

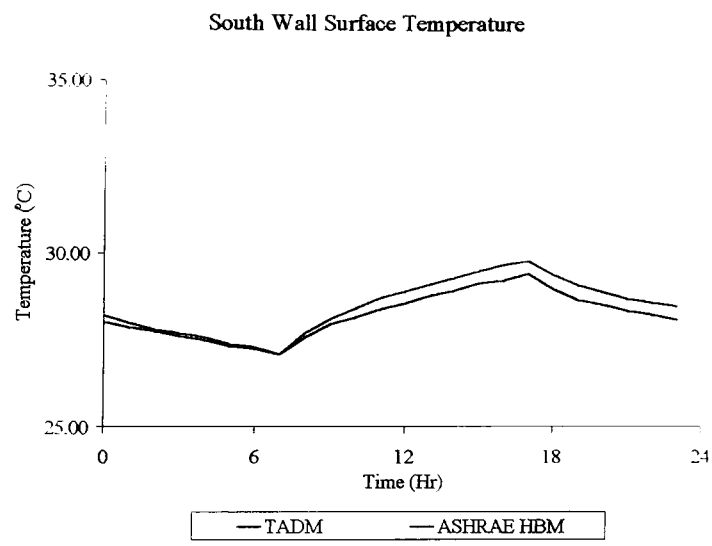

Figure 7.9 Comparison of south wall surface temperature profiles between ASHRAE HBM and TADM methods

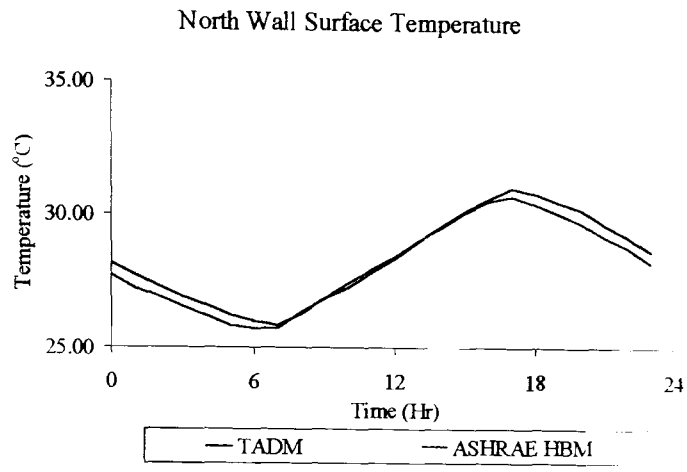

Figure 7.10 Comparison of north wall surface temperature profiles between ASHRAE HBM and TADM methods

Table 7.2 Statistical comparison of surface temperature results between ASHRAE HBM and TADM methods

Surface	Ceiling	North wall	South wall	West party wall
Absolute maximum difference (K)	0.92	0.50	0.46	0.17
Absolute average difference (K)	0.44	0.27	0.25	0.07

In the ASHRAE Heat Balance Method, constant internal surface heat transfer coefficients are used, the radiant portion of the internal heat gains are distributed evenly over the room surfaces and an approximate mean radiant temperature method (MRT) is employed to model radiant exchange between the internal surfaces [91]. Similar internal sub-models were employed in the Thermal Analysis Design Method for the purpose of obtaining similar results to that of the ASHRAE Heat Balance Method. Hence, in this comparison test, agreement in results was obtained by taking a similar thermal modelling approach to the problem rather than an accurate modelling approach. It can be shown that if a variable convection coefficient model were employed instead of the constant coefficients, there would be little change in the cooling load, but a significant change in the surface temperature profiles. In the ASRHAE example, the internal heat gains dominate the heat gains to the space. A different assumption regarding the distribution of the radiant portion of the heat gains over the room surfaces would produce different surface temperature profiles. Identical sol-air temperature profiles, to those used in the ASHRAE HBM were used in the Thermal Analysis Design Method. Sol-air temperatures are computed more

accurately in the Thermal Analysis Design Method and if used in the comparison test, would produce different results. The Thermal Design Analysis Method can be made to perform equal to the latest ASHRAE method, but can be made to perform more accurately by employing more accurate physical models. The overall accuracy of the method is then governed by the prudent choice of physical models and mathematical thermal simulation technique employed.

7.4 Empirical validation

The Thermal Analysis Method is primarily a design day, thermal simulation method, but its application can be extended to simulate longer runs. A nine-day simulation exercise was set-up to check the overall performance of the Iterative Frequency Domain version of the method. This involved modelling a test cell using an experimental data-set from the University of Westminster direct gain test cell facility, located in central England, on the south-west side of Peterborough. [89]. A handbook, containing all relevant information, for thermally modelling cells 1 and 2, and a data disk are freely available. The data disk covers the periods 25th to 4th of March and 4th to 12th May 1984. The hourly meteorological data included ambient air temperature, horizontal global and diffuse solar irradiance, south facing vertical solar irradiance, run of wind speeds in the four major compass directions and mean wind speed/direction. Test cells 1 and 2 share a common partition wall and attic space. Each cell is approximately 1580mm wide by 2160mm deep by 3050 mm high, the width dimension facing south. Interior surfaces are not exactly planar, consisting of 43 cross sections. The external side of each cell is of insulated stud construction. The partition wall between the cells is mainly constructed of 140mm of insulation material. The north wall of each cell has an internal concrete block leaf. Overall, the test cells can be described as thermally lightweight with heavily glazed south facades and highly solar driven. Test cell 2 was the primary cell modelled and the May weather data set was used. Cell 1 was modelled sufficiently to obtain the dominant thermal links between the two cells. The thermal model included the tracking of the transmitted solar beam, in order to distribute as accurately as possible the solar irradiation on the internal surfaces. Self-shading of the window frame and bars was also modelled. The Perez *et al* sky diffuse radiation model [20] was employed to predict diffuse solar radiation on vertical surfaces. Cole's model [29] for estimating sky and ground long-wave radiation was used. External surface heat transfer coefficients were based on McAdams convection model [5]. The internal convection

coefficients were generated using the Alamdari and Hammond convection model [4]. An exact long-wave radiant exchange model was employed in the internal environmental model. Figures 7.11 and 7.12 compare the simulated and measured air and window inside surface temperatures respectively. Although there are differences between the simulated and measured values, the phase relationship between the curves is

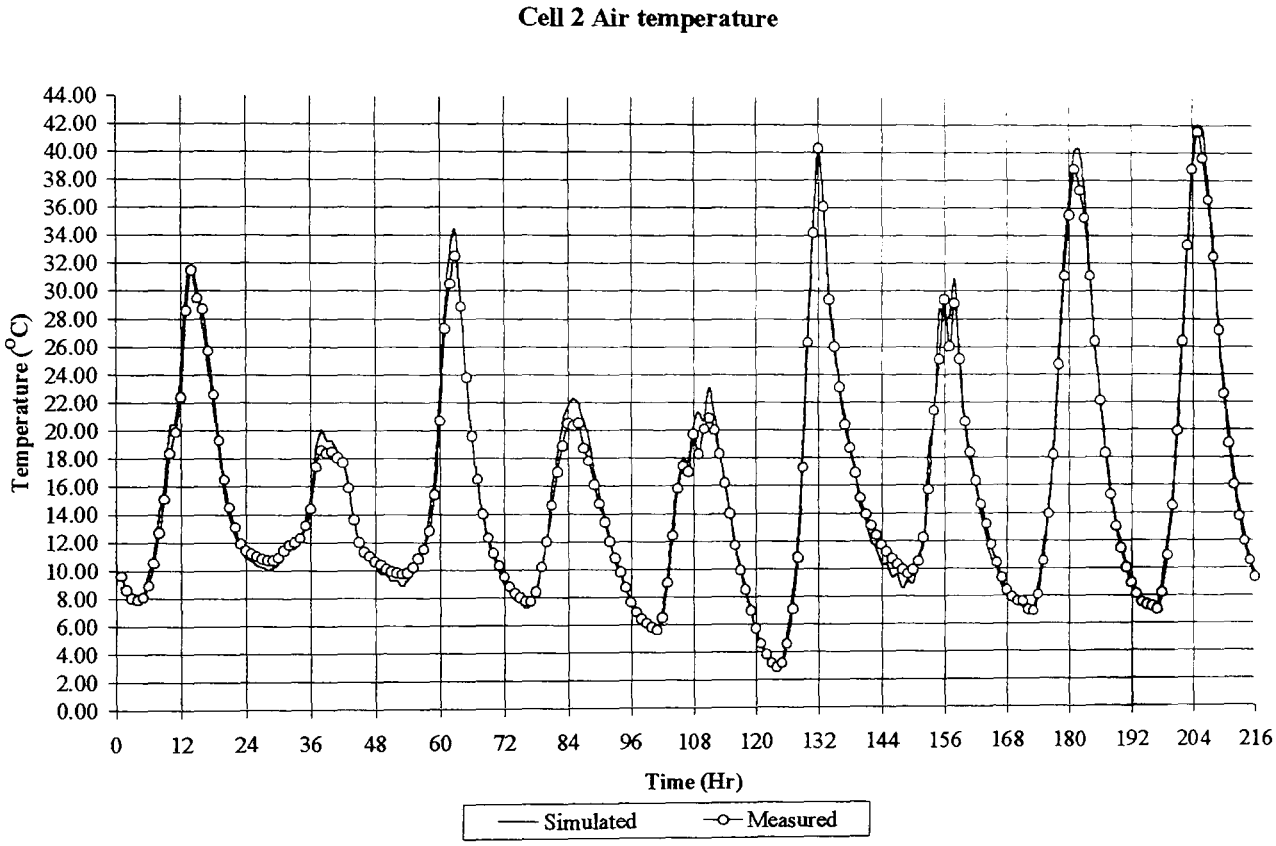

Figure 7.11 Comparing simulated and measured air temperatures

close. The results for the window compare quite well considering that it consists of a single glass pane, driven by a number of internal and external thermal influences. Table 7.3 compares the results of the Thermal Analysis Design Method (TADM) with three thermal simulation software programs that were involved in a validation exercise using the same cells and data disks. It must be emphasised that the validation took place towards the end of the 1990's and does not reflect the current performance of any of the simulation programs shown in the table. All values shown are in terms of the hourly differences between the simulated and measured values. The maximum spread is the difference between the maximum and minimum differences of the previous two columns. The mean value gives an

indication of overall performance but a more stringent indicator is the absolute mean value: the smaller the absolute mean value, the closer the overall correlation between the simulated and measured values.

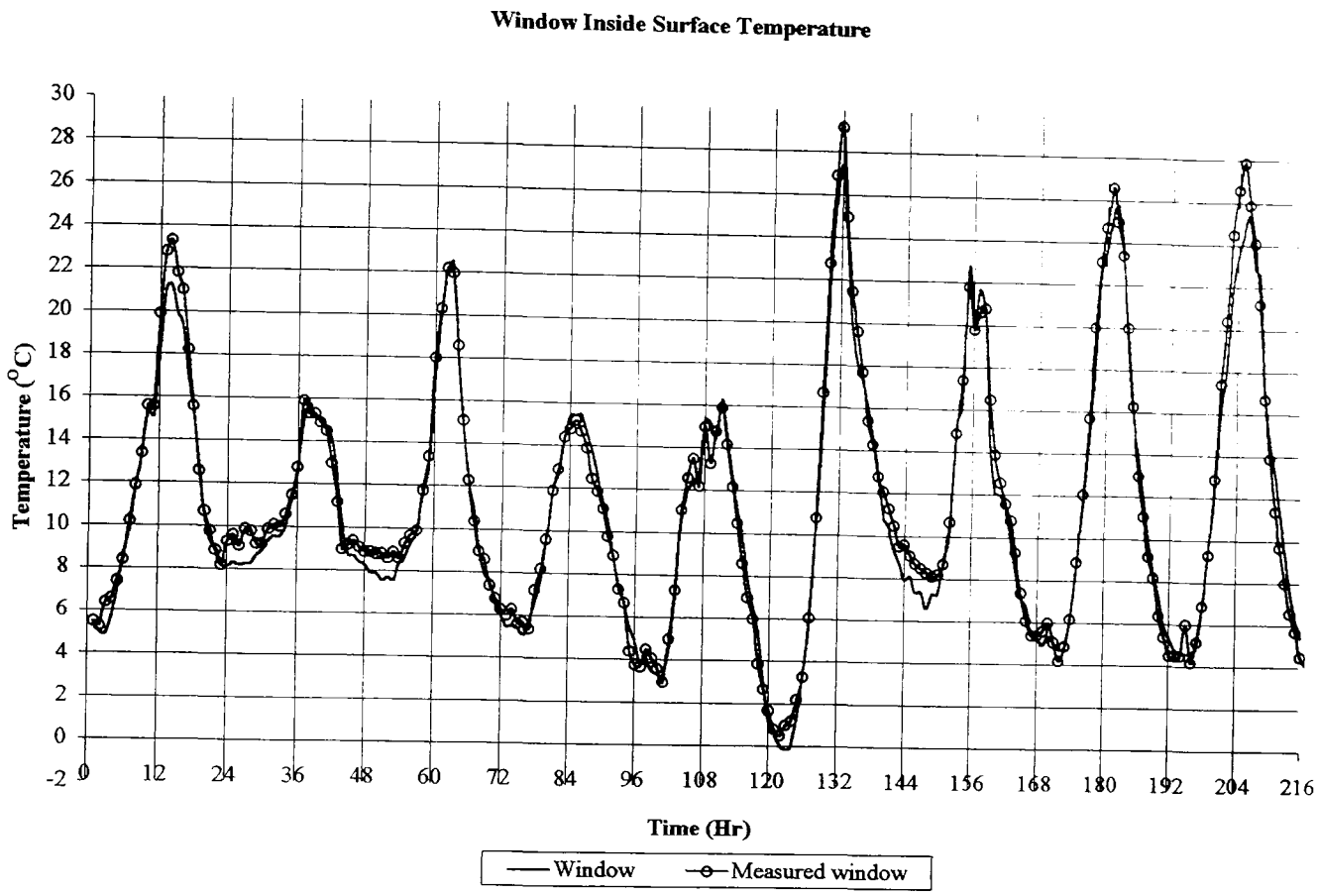

Figure 7.12 Comparing simulated and measured inside window surface temperatures

Table 7.3 demonstrates that the performance of the TADM computer spreadsheet based method compares very favourably with the building simulation software programs, confirming its capabilities as an accurate building thermal simulation method.

Table 7.3 Statistical comparison of simulated and measured cell 2 air temperatures

	Differences between measured and simulated air temperatures				
	Max. (K)	Min. (K)	Max. spread (K)	Mean (K)	Absolute mean (K)
TADM	3.6	–1.4	5.0	0.3	0.7
ESP*	7.4	–0.6	8.0	2.7	2.7
SERIRES*	2.7	–3.7	6.4	0.8	1.0
HTB2*	12.0	0.7	11.3	5.2	5.2

*** Note that these results are not current but are pre 1990.**

7.5 Verification of correlation equations and reduced calculations methods

A number of correlation equations and reduced calculations methods have been developed in the thesis in order to improve computational efficiency. Verification results regarding the majority of these ideas have been included in the relevant chapters. Reference to these and further verification results are provided in the following summary.

Reduced correlation equations of external convection models. Described by equations (6.21) and (6.22), and table 6.6. Comparison of results with current convection models are provided in table 6.4 and illustrated in figure 6.6.

Correlation equations of CIBSE tabulated solar data. Described by equation (6.30), tables 6.7 and 6.8. Results of the correlation equations can be checked against the values of solar data provided in table 2.24, CIBSE guide [26]. Table 7.4, for example, provides comparison results for June, July and August. The comparison is evaluated in terms of the ratio of the correlation equation results to the CIBSE tabulated normal beam and horizontal diffuse solar irradiation values.

Table 7.4 Ratio of correlation equation results to tabulated normal beam and horizontal diffuse solar irradiation values provided in table 2.24 of the CIBSE guide

Time	Normal beam.			Horizontal diffuse		
	June 21	July 04	August 04	June 21	July 04	August 04
03.30	0.97	0.94	0.00	1.02	1.00	0.00
04.30	1.02	1.05	0.99	0.98	1.00	1.00
05.30	1.00	0.99	1.01	1.02	1.00	1.00
06.30	1.00	1.00	1.00	0.98	1.00	1.00
07.30	0.99	1.01	0.99	1.01	0.99	1.00
08.30	1.01	1.00	1.02	1.00	1.01	1.00
09.30	1.00	1.00	1.04	0.99	1.00	1.00
10.30	0.99	1.00	1.00	1.01	1.00	1.00
11.30	1.00	1.00	1.00	1.00	1.00	1.00
12.30	1.00	1.00	1.00	1.00	1.00	1.00
13.30	1.00	0.99	1.01	1.00	1.01	0.99
14.30	0.99	1.00	0.99	1.00	0.99	1.02
15.30	1.01	1.01	1.01	1.00	1.00	0.98
16.30	1.00	0.99	1.00	1.00	1.03	1.02
17.30	1.00	1.01	1.00	0.99	0.95	0.98
18.30	0.98	0.99	1.00	1.01	1.06	1.01
19.30	1.05	1.04	1.00	0.99	0.93	1.00
20.30	0.94	0.95	0.00	1.01	1.05	0.00

Correlation equations of glass optical properties. Described by equation (6.44) and table 6.9. The correlation equations can be easily checked against the values of glass optical

properties provided in table 13, ASHRAE Fundamentals Handbook [64]. Table 7.5, for example, provides comparison results for three types of glazing. The comparison is evaluated in terms of the ratio of the correlation equation results to the tabulated solar absorption and transmittance values.

Table 7.5 Ratio of correlation equation results to tabulated solar transmittance and absorption values for glazing provided in table 13, ASHRAE Fundamentals Handbook

Solar incident angle (Deg):		0	40	50	60	70	80
6 mm clear glazing	Solar transmittance:	1.00	1.00	1.00	1.00	1.00	1.00
	Solar absorption:	1.00	0.99	1.01	1.00	1.00	1.00
6 mm bronze glazing	Solar transmittance:	1.00	1.00	1.00	1.01	0.99	1.00
	Solar absorption:	1.00	0.99	1.01	1.00	1.00	1.00
6mm grey glazing	Solar transmittance:	1.00	1.00	1.00	1.00	1.00	1.00
	Solar absorption:	1.00	1.00	1.00	1.01	1.00	1.00

Linear correlation equations of radiant and convective coefficients between window system layers. Described by equations (6.55) and (6.58), and table 6.11. Accuracy of correlation equations is demonstrated in table 6.12.

Linear correlation equation of surface emissive power. Described by equations (6.131) to (6.134). Accuracy of the equation is demonstrated in tables 6.18 and 6.19.

Polynomial correlation equation of surface emissive power. Described by equation (6.135). Accuracy of correlation equation is specified in section 6.6.3.3.

Approximate long-wave radiant exchange model. Described by equations (6.136) to (6.138). Performance of the method, compared to the exact method, is demonstrated in tables 6.20 and 6.21.

Reduced correlation equations of Alamdari and Hammond's convection models. Described by equation (6.142) and table 6.22. Accuracy of correlation equations is demonstrated in table 6.3.

Convective cooling load by the response function method. Described by equation (6.157). Accuracy of the method is demonstrated in tables 6.24 and 6.25.

Chapter VIII

8.0 CONCLUSIONS

The Thermal Analysis Design Method is a modern manual building dynamic thermal simulation method that has been designed for computer spreadsheet application. This outcome was achieved by initially establishing the design criteria and assumptions fundamental to the scope of application of the method. The major mathematical simulation techniques were investigated to find the most suitable for computer spreadsheet implementation. An integrated simulation method consisting of the frequency domain, implicit finite difference and numerical iteration techniques has resulted. The frequency domain technique is ideal for formulating the space air and surface heat balance equations in a concise and systematic manner. It forms the core simulation technique of the Thermal Analysis Design Method. Numerical iteration techniques have been specifically developed for computer spreadsheet application and are integrated with the frequency domain technique to simulate non-linear building and plant heat transfer processes. The implicit finite difference technique is computationally efficient and stable when modelling thin structural elements that can be represented by a single temperature node point and when employing a temporal dicretisation scheme of one hour.

Thermal Analysis Design Method incorporates an internal environmental model, an external environmental model and a window system model. The Iterative Frequency Domain Method (IFDM) and the Adiabatic Iterative Frequency Domain Method (AIFDM) are alternative versions of the mathematical simulation techniques that have been developed for implementation in the model. The latter option is the most elegant in terms of optimum suitability of the mathematical simulation techniques to modelling the heat transfer processes of specific space elements. The accuracy of the frequency domain technique, for example, has been enhanced due to modelling exclusively linear heat conduction processes in building structural elements. This has been achieved by excluding the surface convection coefficients from the thermal transmission matrices of the space's structural surfaces.

Further developments have ensued from examining specific building heat transfer processes, for example:

1. An accurate sol-air temperature formulation accounting for all the external environmental influences, including external long-wave radiant exchange and solar shading.
2. A window solar temperature that accounts for all the absorbed solar radiation in the window system.
3. A window sol-air temperature that accounts for all internal and external thermal influences.
4. Accurate linear correlation equations for modelling radiant and convective heat transfer coefficients between window glazing panes.
5. A window/ internal blind model that simulates the complex convective air flows due to the operating schedule of the blinds.
6. Accurate linear and polynomial expressions to determine the emissive power of a surface.
7. An accurate reduced internal long-wave radiant exchange model that is sensitive to the dominant radiant exchange processes taking place between the room surfaces.

Regarding items 1 to 3: sol-air temperature combines all the external surface excitations into a single thermal driving force requiring the generation of only one Fourier series. This is computationally very efficient when modelling in the frequency domain and when iteration is part of the solution process. The derivation of a window sol-air temperature has further developed the concept of sol-air temperature. In this case the absorbed solar radiation in the window layers and the internal environmental thermal influences are included.

Computational efficiency must be considered when creating building dynamic thermal models for computer application, particularly when employing a general purpose computer spreadsheet program. Accordingly, published physical models describing building heat transfer processes should be examined for the possibility of reducing their mathematical complexity without a corresponding significant loss in precision. The external and internal convection models, the radiative and convective heat transfer coefficients between window glazing panes, the radiative emissive powers of surfaces and the calculation of glass optical properties, are pertinent examples described in the thesis.

Solutions to building thermal problems can be successfully modelled within the computer spreadsheet environment employing passive, mechanical or mixed mode design strategies. Mechanical ventilation with night time sub-cooling, single side natural ventilation via windows, controlled convective cooling, chilled ceiling with displacement ventilation are examples presented in the thesis. This variety of solutions demonstrates the innate modular flexibility of the computer spreadsheet program, as a building thermal simulation platform on which sub-models can be created at will. Fanger's thermal comfort model is another example of a sub-model, which was set up to analyse the thermal comfort implications of particular design solutions.

Chapter VII, validation, has demonstrated that the Iterative Frequency Domain and Adiabatic Iterative Frequency Domain methods are accurate mathematical solution techniques used in the Thermal Analysis Design Method. The accuracy of a precise formulation of sol-air temperature was verified. The new concepts of window solar temperature and window sol-air temperature were successfully tested. The overall performance of the Thermal Analysis Design Method was shown to be comparable with the ASHRAE Heat Balance Method and produced satisfactory results regarding the empirical test cell exercise. In the intermodel comparison test with the ASHRAE method, close similarity in the space cooling load profiles, particularly in the region of the peak loads, resulted. A close similarity in surface temperature profiles was also demonstrated, overall, an absolute average difference of less than 0.5 K between each corresponding set of temperature profiles. Unlike empirical type validation exercises, intermodel comparisons are not suited to revealing the accuracy of dynamic thermal models. However, considering the complex problem of modelling building heat transfer, a similar performance by two distinctly different models imbues credence in the accuracy of the mathematical solution techniques employed by the methods. The empirical validation exercise demonstrated the capability of the Thermal Analysis Design Method to model the test cell over a nine-day period, employing recorded meteorological data. Its performance was shown to compare very favourably with the results of three well-known dynamic thermal models. The validation tests carried out to date are regarded as constituting the first stage in a continual validation process.

Thermal Analysis Design Method has been developed for computer spreadsheet application. Its mathematical simulation techniques and other innovations described in the thesis should also find application in building dynamic thermal simulation programs.

A comprehensive guidebook is required, explaining the fundamental theory behind the Thermal Analysis Design Method and how to apply the method in a systematic manner within a computer spreadsheet environment. The structure of the guide, its examples and supporting data must be conducive to the building services engineering industry. In this regard, the salient idea of levels of complexity inherent in the method provides an ideal learning structure to deliver its subject matter. Pre-calculated data should be provided on disk to help the novice apply the method at the lower levels of complexity. Examples of pre-calculated data are:

1. Thermal transmission matrices of standard building constructions.
2. Fourier series of external thermal excitations, such as sol-air temperature per orientation and month.
3. Fourier series of window sol-air temperature and transmitted solar radiation for different window systems, orientation and month.
4. Fourier series of internal convective and radiant heat gains to suit different building functions.

Practical examples and tutorials of the space thermal model and plant should be supplied on disk.

The development of a spreadsheet-based methodology for the modelling of moisture migration through building elements is an appropriate associated area for future research. The moisture transfer model should be integrated with the heat transfer and ventilation models. The room moisture content balance and the internal latent heat loads would also need to be addressed.

It is envisaged that the Thermal Analysis Design Method, or similar computer spreadsheet method, should in time replace the CIBSE admittance method as the recommended manual design method. The Thermal Analysis Design Method bridges the enormous gap between the traditional manual method and the current building dynamic thermal simulation programs. The method's performance is comparable to that of the dynamic thermal

simulation programs, in the case of thermally modelling a single zone. The computational speed of the computer spreadsheet program and the ability of the user are the only limitations to the level of thermal modelling that can be achieved.

REFERENCES

1a Lomas K.J., Bowman, N.T., An investigation into the analytical and empirical validation techniques for dynamic thermal models of buildings, SERC/BRE, vol. 4, Appx. 4, Site Handbook, pp. 12-13, BRE, Watford (1987)

1b Lomas K.J., Bowman, N.T., An investigation into the analytical and empirical validation techniques for dynamic thermal models of buildings, SERC/BRE, vol. 4, Appx. 10, A Guide to Validation, Watford (1987)

2. Thermal properties of building structures, CIBSE guide A3, Appendix 3.A1, Chartered Institute of Building Services Engineers, London (1999)

3. Thermal properties of building structures CIBSE guide A3, Appendix 3.A8, Chartered Institute of Building Services Engineers, London (1999).

4. Alamdari F. and Hammond G.P., Improved data correlation for buoyancy-driven convection in rooms, SME/J/83/01, Institute of Technology, Applied Energy Group, Cranfield (1983).

5. McAdams W.H., Heat Transmission, McGraw-Hill, New York (1954).

6. Thermal properties of building structures CIBSE guide A3, 3.3.9.2, Chartered Institute of Building Services Engineers, London (1999).

7. Thermal response and plant sizing, CIBSE guide A5, Appendix 5.A1, Chartered Institute of Building Services Engineers, London (1999).

8. Davies M.G., Definitions of room temperature, Building and Environment, 28, pp. 383-398 (1993).

9. Liddament M.W., Air infiltration calculation techniques –an application guide, Air Infiltration and Ventilation centre, Coventry (1986).

10. Orma M., Liddament M.W. and Wilson A., An analysis and summary of AIVC's numerical database, AVIC Technical Note 44, Air Infiltration and Ventilation centre, Coventry (1994).

11. Air infiltration and natural ventilation, CIBSE guide A4, Chartered Institute of Building Services Engineers, London (1999).

12. McQuiston F.C. and Spitler J.D., Cooling and Heating Load Calculation Manual, (ISBN 0-910110-85-9) American Society of Heating, Refrigeration and Air-conditioning Engineers Inc (1992).

13. Wilkins C.K., Kosonen R. and Laine T, An analysis of office equipment load factors, ASHRAE Journal (1991).

14. Internal heat gains, CIBSE guide A6, Chartered Institute of Building Services Engineers, London (1999).

15. Non-residential Cooling and Heating Load Calculations, ASHRAE Fundamentals Handbook, chapter 28 (ISBN 1 883413 45 1) American Society of Heating, Refrigeration and Air-conditioning Engineers, Atlanta GA (1997).

16. Fenestration, ASHRAE Fundamentals Handbook, Ch 30, p 30.16, American Society of Heating, Refrigeration and Air-conditioning Engineers, Atlanta GA (2001).

17. Jones W.P., Air Conditioning Engineering (ISBN 0 340 55637 4), Arnold, London, pp 145-149 (1994).

18. Klutcher T.M., Evaluation of Models to Predict Insolation on Tilted surfaces, Journal of Solar Energy, 23(2), pp 14-111 (1979).

19. Hay J.E., Study of Shortwave Radiation on Non-Horizontal Surfaces, Rep. 12-79, Atmospheric Environmental Service, Downsview, Ontario (1979).

20. Perez R., Seals R., Ineichen P., Stewart R. and Menicucci D., A New Simple Version of the Perez Diffuse Irradiation Model for Tilted Surfaces, Journal of Solar Energy, 39(3), pp 221-231 (1987).

21. PASSYS project (Jenson 1994)

22. Lomas K.J., Polytechnic of Central London Direct Gain test Cells, Table 14, Leicester Polytechnic (1990)

23. Thermal response and plant sizing, CIBSE guide A5, Appendix 5.A4, Chartered Institute of Building Services Engineers, London (1999).

24. Clark J.A. Energy Simulation in Building Design, Adam Hilger Ltd., Bristol and Bolton, pp 150-159 (1985).

25. Jones W.P., Air Conditioning Engineering (ISBN 0 340 55637 4), Arnold, London, pp 156-158 (1994).

26. External design data, CIBSE guide A2, Chartered Institute of Building Services Engineers, London (1999).

27. Clark J.A. Energy Simulation in Building Design, Table 5.6, Adam Hilger Ltd., Bristol and Bolton (1985).

28 External design data, CIBSE guide A2, Appendix 2.A1, Chartered Institute of Building Services Engineers, London (1999).

29. Cole R.J., The Longwave Radiation Incident upon the External Surface of Buildings, Building Services Engineering, 44, pp 195-206 (1976).

30. Jones W.P., Air Conditioning Engineering (ISBN 0 340 55637 4), Arnold, London, p 104 (1994).

31. Thermal response and plant sizing, CIBSE guide A5, Chartered Institute of Building Services Engineers, London (1999).

32. Alford J.S., Ryan J.E. and Urban F.O, Effect of Heat Storage and Variation in Outdoor Temperature and Solar Intensity on Heat Transfer Through Walls, ASHVE Transactions, American Society of Heating and Ventilating Engineers, 45 pp 369-386 (1939).

33. Stevenson Jr. and Howard A, An Advance Course in Engineering, AIEE Transactions, 54 (1935).

34. Gröber H, Erk S and Grigull, Fundamentals of Heat Transfer, McGraw-Hill, New York, pp 77-102 (1961).

35. Binder L., Über äussere Wärmeleitung und Erwärmung elektrischer Maschinen, Dissertation, München (1910).

36. Mackey C.O. and Wright L.T., Summer Comfort Factors as Influenced by The Thermal Properties of Building Materials, American Society of Heating & Ventilating Engineers Transactions, 49 p 148 (1943).

37. Mackey C.O. and Wright L.T., Periodic Heat Flow-Homogeneous Walls or Roofs, American Society of Heating & Ventilating Engineers Transactions, 50 pp 293-312 (1944).

38. Mackey C.O. and Wright L.T., Periodic Heat Flow-Composite Walls or Roofs, Heating, Piping and Air Conditioning, 18 6 pp 107-110 (1946).

39. Davies M.G., The Thermal Response of an Enclosure to Periodic Excitation: The CIBSE Approach, Building and Environment, 29 2 pp 217-235 (1994).

40. Gorcum A.H. Van., Theoretical Considerations on the Conduction of Fluctuating Heat Flow, Applied science Research, A2 pp 272-280 (1950). The Hague: Martinus Nijhoff.

41. Pipes L.A., Matrix Analysis of Heat Transfer Problems, Journal of the Franklin Institute, 625 pp 195-205 (1957).

42. Brisken W.R.and Reque S.G., Heat Load Calculations by Thermal Response, Transactions American Society of Heating & Air-Conditioning Engineers, 62 pp 391-424 (1956).

43. Mitalas G.P. and Stephenson D.G., Room Thermal Response Factors, ASHRAE Transactions, 73 1 pp 2.1-2.10 (1967).

44. Stephenson D.G. and Mitalas G.P., Cooling Load Calculations by Thermal Response

Factor Method, ASHRAE Transactions, 73 1 pp 1.1-1.7 (1967).

45. Stephenson D.G. and Mitalas G.P., Calculation of Heat Transfer Functions For Multi-Layer Slabs, ASHRAE Transactions, 77 2 pp 117-126 (1971).

46. Gröber H, Erk S and Grigull, Fundamentals of Heat Transfer, McGraw-Hill, New York, pp 102-105 (1961).

47. Clark J.A. Energy Simulation in Building Design, Adam Hilger Ltd., Bristol and Bolton, pp 17-19, Table 1.2 (1985).

48. The PASSYS Services Summary Report, The PASSYS Project, European Commission Directorate General XII for Science, Research & Development, Belgian Building Research Institute, Brussels (1994).

49. Mitalas G.P., An Assessment of Common Assumptions in Estimating Cooling Loads and Space Temperatures, ASHRAE Transactions, 71 2 pp 72-80 (1965)

50. Clark J.A. Energy Simulation in Building Design, Adam Hilger Ltd., Bristol and Bolton, pp 72-77 (1985).

51. Thermal response and plant sizing, CIBSE guide A5, Chartered Institute of Building Services Engineers, London (1999).

52 Non-residential Cooling and Heating Load Calculation Procedures, ASHRAE Fundamentals Handbook, chapter 29, American Society of Heating, Refrigeration and Air-conditioning Engineers, Atlanta GA (2001).

53. Danter E., Periodic Heat Transfer Characteristics of Simple Walls and Roof, J. Inst. Heat. Vent. Engrs., 28 pp 136-146 (1960).

54. Loudon A.G., Summertime Temperatures in Buildings Without Air-conditioning, Building Research Station Current Paper 47/68 (1968).

55. Pedersen C.O., Fisher D.E. and Liesen R.J., Development of A Heat Balance Procedure for Calculating Cooling Loads, ASHRAE Transactions, 103 2 pp 459-468 (1997).

56. Spitler J.D., Fisher D.E. and Pedersen C.O., The Radiant Time Series Cooling Load Calculation Procedure, ASHRAE Transactions, 103 2 pp 503-515 (1997).

57. Pedersen C.O., Fisher D.E., Spitler J.D. and Liesen R.J., Cooling and Heating Load Principles, ASHRAE, Atlanta (1998).

58. Thermal response and plant sizing, CIBSE guide A5, Appendix 5.A4, Chartered Institute of Building Services Engineers, London (1999).

59. Thermal response and plant sizing, CIBSE guide A5, Appendix 5.A6, Chartered

Institute of Building Services Engineers, London (1999).

60. McClellan T.M. and Pedersen C.O., Investigation of Outside Heat Balance Models for Use in a Heat Balance Cooling Load Calculation Procedure, ASHRAE Transactions, 103 2 pp 469-484 (1997).

61. Liesen R.J. and Pedersen C.O., An Evaluation of Inside Surface Heat Balance Models for Cooling Load Calculations, ASHRAE Transactions, 103 2 pp 485-502 (1997).

62. Non-residential Cooling and Heating Load Calculation Procedures, ASHRAE Fundamentals Handbook, chapter 29, pp 29.21-29.23, American Society of Heating, Refrigeration and Air-conditioning Engineers, Atlanta GA (2001).

63. Spitler J.D. and Fisher D.E., On the Relationship between the Radiant Time Series and Transfer Function Methods for Design Cooling Load Calculations, International Journal of Heating, Ventilating, Air-Conditioning and Refrigerating Research, 5 2 pp 125-138 (1999).

64. Fenestration, ASHRAE Fundamentals Handbook, chapter 30, Table 13, American Society of Heating, Refrigeration and Air-conditioning Engineers, Atlanta GA (2001).

65. Thermal response and plant sizing, CIBSE guide A5, Appendix 5.A4, Fig. 5.19, Chartered Institute of Building Services Engineers, London (1999).

66. Non-residential Cooling and Heating Load Calculation Procedures, ASHRAE Fundamentals Handbook, chapter 29, p 29.15, American Society of Heating, Refrigeration and Air-conditioning Engineers, Atlanta GA (2001).

67. Non-residential Cooling and Heating Load Calculation Procedures, ASHRAE Fundamentals Handbook, chapter 29, pp 29.29-29.37, American Society of Heating, Refrigeration and Air-conditioning Engineers, Atlanta GA (2001).

68. External design data, CIBSE guide A2, Tables 2.35 – 2.4, Chartered Institute of Building Services Engineers, London (1999).

69. External design data, CIBSE guide A2, Sec 2.8.5, Chartered Institute of Building Services Engineers, London (1999).

70. Thermal response and plant sizing, CIBSE guide A5, Appendix 5.A1, Chartered Institute of Building Services Engineers, London (1999).

71. External design data, CIBSE guide A2, Table 2.24, Chartered Institute of Building Services Engineers, London (1999).

72. Wright J.L, A Correlation to Quantify Convective Heat Transfer Between Vertical Window Glazings, ASHRAE Transactions, 102 1 pp 940-946 (1996).

73. Jones W.P., Air Conditioning Engineering (ISBN 0 340 55637 4), Arnold, London, p 409 (1994).

74. Flow of fluids in pipes and ducts, CIBSE guide C4, Table C4.35, Chartered Institute of Building Services Engineers, London (1986).

75. Thermal properties of building structures, CIBSE guide A3, sec 3.6, Chartered Institute of Building Services Engineers, London (1999)

76. Hottel, H.C. and A.F. Sarofin, Radiative transfer, chap. 3, New York: McGraw-Hill, (1967)

77. Crowley, M.E. and M.S.J. Hashmi, Evaluation of implicit numerical methods for building energy simulation, Proc Instn Mech Engrs Vol 212 Part A, p 340, (1998)

78. Clark J.A. Energy Simulation in Building Design, Butterworth-Heinemann, Oxford, pp 256-260 (2001).

79. Underwood, C.P.and F.W.H. Yik, Modelling Methods for Energy in Buildings, pp 122-126, Blackwell Publications (2004).

80. Non-residential Cooling and Heating Load Calculation Procedures, ASHRAE Fundamentals Handbook, chapter 29, pp 29.3-29.13, American Society of Heating, Refrigeration and Air-conditioning Engineers, Atlanta GA (2001).

81. Internal heat gains, CIBSE guide A6, Table 6.4, Chartered Institute of Building Services Engineers, London (1999).

82 Environmental criteria for design, CIBSE guide A1, Table 1.1, Chartered Institute of Building Services Engineers, London (1999)

83 Environmental criteria for design, CIBSE guide A1, pp 1-14, Chartered Institute of Building Services Engineers, London (1999)

84 Fanger P.O., Thermal comfort (Malabar, FL, USA: Krieger) (1982)

85 Environmental criteria for design, CIBSE guide A1, Appendix 1.1A, Chartered Institute of Building Services Engineers, London (1999)

86 Diamant R.M.E., Insulation of buildings, Iliffe, London (1965)

87 Bouchlaghem N.M., Letherman K.M., Numerical Optimization Applied to the Thermal Design of Buildings, Building and Environment, vol. 25, No. 2, pp 117-124 (1990)

88 Davies M.G., The Thermal Response of an Enclosure to Periodic Excitation: The CIBSE Approach, Building and Environment, vol. 29, No. 2, pp 217-235 (1994)

89 Lomas K.J., Bowman, N.T., An investigation into the analytical and empirical validation techniques for dynamic thermal models of buildings, SERC/BRE, vol. 4, Appx. 4, Site Handbook, BRE, Watford (1987)

90 Non-residential Cooling and Heating Load Calculations, ASHRAE Fundamentals Handbook, chapter 26, pp 26.33-26.34, (ISBN 1 883413 45 1) American Society of Heating, Refrigeration and Air-conditioning Engineers, Atlanta GA (1993).

91 Rees S.J, Spitler J.D, M.G Davies, Haves P, Qualitative Comparison of North American and U.K. Cooling Load Calculation Methods, HVAC&R Research, Vol. 6, No. 1, pp 75-99, (2000).

92 ANSI/ASHRAE Standard 140-2001. Standard Method of Test for Evaluation of Building Energy Analysis Computer Programs. American Society of Heating, Refrigeration and Air-conditioning Engineers, Atlanta GA (2001).

93 Crowley, M.E., Investigation and Development of Implicit Numerical Methods for Building Energy Simulation, Ph.D. thesis, School of Mechanical and Manufacturing Engineering, Dublin City University, Dublin (September 2005).

94 Axelsson, S.R.J., Improved Fourier Modelling of Soil Temperature Using FFT Algorithms, IEEE Transactions of Geoscience and Remote Sensing, Vol. 36, NO. 5, pp 1519-1523, (1998).